



AUTHOR:

TITLE:

YEAR:

OpenAIR citation:

This work was submitted to Robert Gordon's Institute of Technology in partial fulfilment of the following degree:

OpenAIR takedown statement:

Section 6 of the "Repository policy for OpenAIR @ RGU" (available from <http://www.rgu.ac.uk/staff-and-current-students/library/library-policies/repository-policies>) provides guidance on the criteria under which RGU will consider withdrawing material from OpenAIR. If you believe that this item is subject to any of these criteria, or for any other reason should not be held on OpenAIR, then please contact openair-help@rgu.ac.uk with the details of the item and the nature of your complaint.

This thesis is distributed under a CC _____ license.

**INTERACTIONS OF
PLATINUM COMPOUNDS
WITH HETEROCYCLIC BASES**

Lynne M Taylor (nee Prentice)

**Submitted in partial fulfilment for the requirements
of Doctor of Philosophy (CNAA)**

Robert Gordon's Institute of Technology

Aberdeen

Submitted June 1990

Interactions of Platinum Compounds with Heterocyclic Bases

Lynne M Taylor

It is generally accepted that platinum antitumour drugs bind, preferentially, to Guanine N7 in DNA. Thus the kinetics of formation and the energetics of dissociation of platinum-nitrogen bonding have been investigated, using simple model bases, namely pyridine, pyrimidine, purine and some derivatives. Six complexes of the type $\text{cis-PtCl}_2\text{L}_2$, where L is a N-heterocycle, have been successfully prepared and characterized. The kinetics of the reaction between K_2PtCl_4 and the N-heterocyclic bases in aqueous solution have been studied. This was best achieved by pre-aquating the PtCl_4^{2-} and measuring the decrease in concentration of platinum or ligand by AA or UV spectroscopy respectively. It was found that the rate of reaction is second order, the rate being dependent on the concentration of both platinum complex and the ligand. The substitution of ligand takes place by direct replacement, involving an associative $\text{S}_{\text{N}}2$ mechanism. It was found that the activation entropy and the activation energy for the reactions of platinum complexes in solution are strongly correlated.

The energetics of platinum-nitrogen bond dissociation were followed using thermogravimetric analysis. Quantitative data, which enabled calculation of the activation energy for the decomposition process involving the loss of one molecule of ligand was obtained from isothermal studies. No correlation was found between the solid state studies, involving bond breaking, and the syntheses of the complexes, probably because in solution the reaction is complicated by solvent effects.

Theoretical studies, which involved Molecular Orbital calculations on the N-heterocyclic bases themselves, were also carried out in an attempt to correlate the kinetic and energetic parameters with the electronic structure of the ligand. Several correlations were attempted but only one was found. This was the relationship between the solid state decomposition energy and the LUMO energy of the quarternized base.

Contents

	<u>Page Nr</u>
1. Introduction	
1.1 Background to the Research Programme	1
1.2 Aims and Methodology	11
2. Preparation and Characterization	
2.1 Preparation	14
2.1.1 Reagents	14
2.1.2 Synthesis of Complexes of the Type $\text{cis-Pt(L)}_2\text{Cl}_2$	15
2.2 Characterization	16
2.2.1 Equipment	16
2.2.2 Yields of Products	17
2.2.3 CHN Analysis	17
2.2.4 Thermogravimetric Analysis	18
2.2.5 Infrared Spectroscopy	21
3. Solution Studies	
3.1 Equipment	25
3.2 Choice of Experimental Method	33
3.2.1 Potentiometric Titrations	34
3.2.2 High Performance Liquid Chromatography	34
3.2.3 Spectroscopy	35
3.3 Development of Experimental Technique	37
3.3.1 Development of Atomic Absorption Method	37
3.3.1.1 Trial Experiment I	40
3.3.1.2 Trial Experiment II	42
3.3.1.3 Effect of Centrifuging on the Induction Period	43

	3.3.1.4	The Aquation of K_2PtCl_6	45
	3.3.1.5	Investigation of Aquation of K_2PtCl_6 , by UV Spectroscopy	45
	3.3.1.6	Effect of 48 Hour Aquation on Induction Period	48
	3.3.1.7	Summary of Developed Method	48
	3.3.2	Development of Ultraviolet Spectroscopic Method	49
3.4		Method of Simultaneous AA and UV Measurement	54
3.5		Results	56
	3.5.1	Initial Rate Results	57
	3.5.2	Integrated Rate Equation Results	64
	3.5.3	Summary of Kinetics of Formation Results	74
3.6		Discussion	78
4.		Solid State Studies	
	4.1	Background Theory of Isothermal Analysis	89
	4.1.1	Isothermal Analysis	94
	4.2	Background Theory of Non-isothermal Analysis	95
	4.3	Method	100
	4.4	Treatment of Data	102
	4.5	Results	108
	4.5.1	cis - Pt (2-aminopyrimidine) $_2Cl_2$	108
	4.5.2	cis - Pt (2-amino-4-methylpyrimidine) $_2Cl_2$	116
	4.5.3	cis - Pt (pyridine) $_2Cl_2$	123
	4.5.4	cis - Pt (2-aminopyridine) $_2Cl_2$	132
	4.5.5	cis - Pt (pyrimidine) $_2Cl_2$	138
	4.5.6	cis - Pt (purine) $_2Cl_2$	144
	4.5.7	Summary of Results	144
	4.6	Discussion	145
	4.7	Differential Scanning Calorimetry	147

5.	Theoretical Studies	
5.1.	Introduction	151
5.2	Introduction to Molecular Mechanics	152
5.2.1	Form of the Energy Expression used in the CHEMMOD Minimiser	155
5.3	Introduction to Molecular Orbital Theory	157
5.4	Method	159
5.5	Quantum Chemical Calculation Results	164
5.5.1	The Program	164
5.5.2	Results for Neutral Bases	166
5.5.3	Results for quaternized bases	168
6.	Discussion and Conclusion	
6.1.	Discussion	178
6.2	Conclusion	184

CHAPTER 1

Introduction

1.1 Background to the Research Programme

Cancer rates among the top three causes of death in the West and although some cancer problems have been partially solved, there still remains groups of cancers that are increasing in occurrence, for example leukemia and lung cancer. Roe⁽¹⁾ has defined cancer as a disease of multi-cellular organisms which is characterised by the seemingly uncontrollable multiplication and spread within the organism of apparently abnormal forms of the organisms own cells. The term cancer actually embodies hundreds of different types of neoplastic diseases ranging from localized skin cancers to whole body leukemias with representative cure rates being as high as 95% or as low as 0%.

Cancer is caused by carcinogens which may be defined as substances that are capable of producing tumours in any test species by any route and at any dose level. This term includes quite inert materials such as gold, silver, sodium chloride and plastics, but in general it refers to the more widely recognised carcinogens summarised in Table 1.1.

TABLE 1.1

Classification of Agents Known to Cause Cancer

<u>Chemical</u>	
Aromatic hydrocarbons and amines	Nitrosamines
Aromatic heterocyclic ring compounds	Azo compounds
4 - Nitroquinoline oxide	Urethanes
Alkylating agents	Polymers
<u>Physical</u>	<u>Others</u>
Ionizing radiation	Chromosomal abnormalities
Ultraviolet radiation	viruses

Central to the problem of curing cancer is an understanding of the ways in which normal cells and cancer cells differ. Cancer is essentially a problem of abnormal cell growth. Under the influence of chemicals in the environment, or radiation or of viruses, the DNA in normal cells may be transformed, possibly by a single alteration or by substitution of one of the constituent purine or pyrimidine bases, in such a way that the normal control mechanisms which restrict cell proliferation are removed. This process is reversible: repair enzymes can replace the altered section of DNA and restore the original structure; and the immune system of the body has a limited capacity to remove cancer cells. However, if this mechanism fails, the cancer cell may reproduce uncontrollably, invade surrounding tissue and eventually spread to different parts of the body to form secondary growths or metastases. This makes cancer a particularly difficult disease to treat.

Current drug treatment aims to control the abnormal cellular reproduction. Often by interfering with the synthesis and replication of the DNA of the cancer cells.

Structure of DNA

Deoxyribonucleic acid (DNA) is the protein material of which genes are made and carries the code for protein generation in a cell. Nucleic acids consist of nucleotides with the general formula (heterocyclic base) - (pentose sugar) - (phosphate), (Figure 1.1).

Only four principal heterocyclic bases are found in DNA, two of which are substituted pyrimidines, cytosine and thymine, and two are substituted purines, adenine and guanine (Figure 1.2).

In DNA the nucleotides are joined by condensation between the phosphate of one nucleotide and an -OH group of a pentose sugar on the next nucleotide (Figure 1.3).

A chain of nucleotides is an oligotide. The ester bonds use the 3 and 5 -OH groups of adjacent sugars and the two ends of a chain can then be described as either the 3 terminus or the 5 terminus depending on which OH group is free.

In the DNA molecule there are two oligonucleotide strands, intertwined with a right hand twist to form a double helix having the bases on the inside and the phosphates on the outside. The bases pair up by forming hydrogen bonds which hold the two strands together (Figure 1.4).

Adenine will always pair with thymine, and guanine with cytosine, so once one strand of the double helix is specified the other must also be. These two base sequences are therefore complementary. The two strands of the double helix run in opposite directions one 3 to 5 and the other 5 to 3.

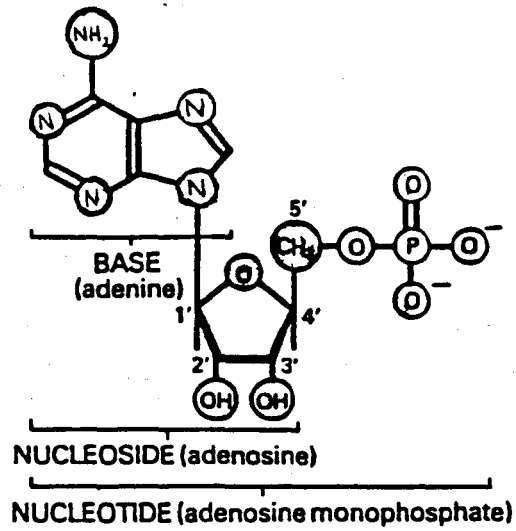


Figure 1.1 Structure of a Typical Nucleotide, AMP.

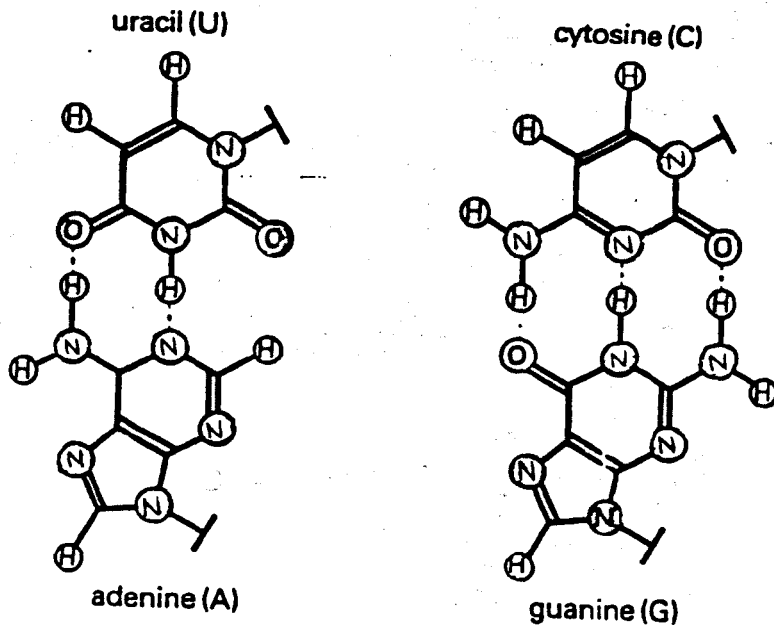


Figure 1.2 Structures of the Heterocyclic Bases of RNA.

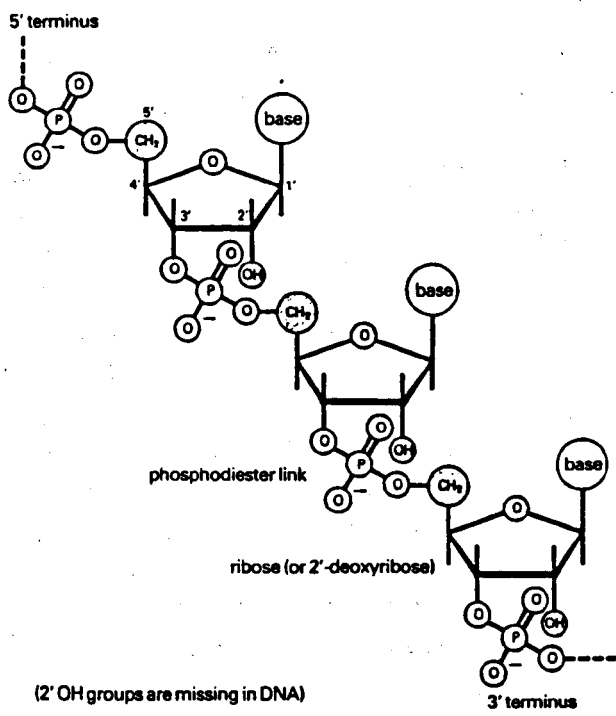


Figure 1.3 Structure of a Polynucleotide.

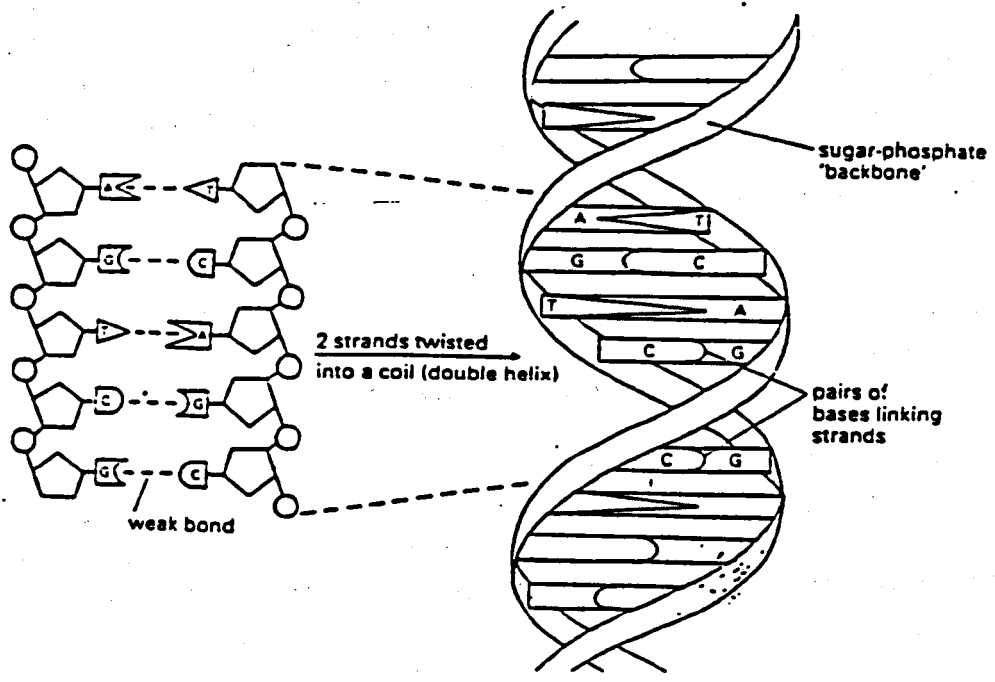


Figure 1.4 Structure of a Segment of DNA.

In DNA replication each strand of the double helix acts as a template for the biosynthesis of a new chain. The new double helices therefore contain one new and one old strand.

Chemotherapy of cancer has been practised for eighty years but has remained fairly unsuccessful until the last three decades^(2,3). Even now the treatment is not always successful and the field is beset with innumerable difficulties. The anticancer drugs can interfere with the reproduction of normal cells, particularly those which are rapidly dividing, for instance bone marrow cells and intestinal mucosa cells. This leads to poor selectivity, that is toxicity towards normal cells as well as cancerous tissue. The cancer may respond well initially to drug treatment but then develop a resistant subset of cancer cells. The drugs may either fail to penetrate a tumour, possibly because of an inadequate blood supply to the tumour or the cancer cells may change by mutation so that the cell membrane becomes impermeable to the drug.

The poor selectivity of anticancer drugs which act by inhibiting cell division reflects the relatively slow rate of division of some human cancer cells. This is one reason why some cancers are much less responsive to drug treatment than others and also complicates the use of animal tumours as models for human cancer because the former tend to divide more rapidly. Because of the problems associated with the long doubling time in the major and most refractory human cancers, such as lung cancer, intestinal cancer and breast cancer, the cancers which have responded best to chemotherapy in the past have been those where the dividing time of the cells is rapid, such as choriocarcinoma - a rare form of cancer originating in the outermost membranes surrounding the foetus - and acute childhood leukemias.

The drugs used for cancer therapy can be categorised by (i) chemical class, (ii) mode of action or (iii) origin, ie whether derived from synthetic or natural sources. Such classes include antimetabolites, antihormonal agents, alkylating agents and platinum derivatives as well as numerous others such as plant products, vincristine, vinblastine and the podophyllotoxins and the antibiotics bleomycin and adriamycin. Whilst such drugs are sometimes used as single agents, it is more usual to administer them either in combination or sequentially, to avoid the onset of resistance.

Antimetabolites are drugs with structures very similar to those of the naturally occurring molecules essential for tumour growth. The tumour mistakenly builds its new cell using the administered antimetabolite and thus hinders further growth.

Certain cancers depend on circulating steroid hormones for their growth. Specifically the female sex hormones oestrone and oestradiol in breast cancer and the male testosterone and dihydrotestosterone in prostatic cancer. Formerly these cancers were usually treated by surgery but in the 1970s the introduction of antihormonal drugs achieved the same effect by non-surgical means.

Alkylating agents were the earliest successful anticancer drugs. Although the largest category is the so called nitrogen mustards the mode of action of all members of this class is the same in their ability to cross-link opposing strands in the DNA double helix by bifunctional alkylation. The two alkylating functions react typically with the guanine bases in DNA binding opposing strands and preventing the separation needed for cell division to occur.

A relatively new and important group of drugs, drugs similar to the alkylating agents in that they act by bifunctional reaction with DNA, are those containing platinum. The parent member, cis-dichlorodiammineplatinum (II) or cisplatin (Figure 1.5), was discovered by Rosenberg in 1969⁽¹⁾ when he found that platinum electrolysis products inhibited bacterial cell growth. Further experiments showed that it was not the electric field but cis-platinum complexes, especially cisplatin, that were responsible for the effect. These species were formed by tiny amounts of platinum from the electrodes reacting with the chloride and ammonia that were present in the electrolytic medium. Only the cis and not the trans isomer appeared to be effective. Because the compounds inhibited cell division their potential as anticancer drugs was investigated.

In subsequent studies the antitumour activity of cisplatin was studied in tumours induced in animals and the promising results led to the first clinical trials in 1972⁽²⁾.

In 1978 cisplatin was officially approved as a drug in the USA and in 1983 it was that country's biggest selling antitumour drug.

Although effective against a broad spectrum of tumours, this compound is almost universally used in the treatment of testicular and ovarian cancer as well as for teratoma (tumours in foetuses). Unfortunately a major drawback of cisplatin is its severe toxicity, even in low doses, towards the kidney and nervous system. This has led to the search for new anticancer platinum drugs with higher activity and lower toxicity. Consequently this has resulted in many platinum compounds being screened for antitumour activity and these tests have identified a number of common features required for antitumour activity⁽³⁾, as follows (see also Figure 1.6).

Two cis amine groups seem to be necessary for activity, this geometric restriction is automatically answered for bidentate amines such as ethylenediamine. The compound should possess moderately strongly bound leaving groups, such as chloride. However, some readily soluble platinum compounds with relatively strongly bound anions, such as citrate, oxalate, malonate or 1,1-cyclobutanedicarboxylate, as leaving groups are also active. Compounds with either strongly bound anions (NO_2^- , SCN^- or I^-) or labile anions (NO_3^- or ClO_4^-) are not antitumour active, and the latter are highly toxic. The amine ligands should have at least one N-H group, ie the platinum-bound nitrogen should possess a hydrogen-bond donor function.

All compounds with both amine ligands lacking such a property have been found to be inactive. The role of this N-H group in the biological activity is not yet understood, it could either be kinetic or thermodynamic. However, steric effects and a role in transport through the cell wall cannot be excluded.

A rational development of a more effective analogue of a drug requires a detailed knowledge of the drug's mechanism of action at the cellular level.

Early studies^[7,9] by several groups have shown that a specific interaction of cisplatin with DNA is an important event, which may eventually lead to cell killing.

It is to be stressed that although binding to DNA is evident, these observations do not necessarily prove that this binding is the only important reaction that leads to cell killing of the tumour cell.

Although DNA has many components with lone pairs of electrons where metal ions may bind (ie the phosphate groups, the sugar oxygen atoms and the heterocyclic bases), early studies^[5,9] have made it clear that cisplatin preferentially binds at the nitrogen atoms of the nucleobases. All the bases (Figure 1.2) do have such nitrogens and have been found to co-ordinate transition metal ions. However binding at thymine can only occur after deprotonation at N3, which is not the case under physiological conditions.

To understand better the binding of cisplatin to DNA, investigations were started with studies of the binding of the nucleobases adenine (A), guanine (G) and cytosine (C). It appeared that adenine might co-ordinate to the cisplatin group through the N7 atom and through the N1 atom, whereas cytosine can co-ordinate through the N3 atom. In guanine binding is possible at N7 and, only under alkaline conditions, also at deprotonated N1. Of all these binding modes, those at the N7 atoms of guanine and adenine seem most likely in DNA, since the other sites of guanine, adenine and cytosine are involved in the base pairing of the double helix, and are less accessible for the cisplatin.

Detailed studies^[10] from about a decade ago have made clear that guanine N7 has a strong kinetic preference, and subsequent investigations^[11,12] have shown that the so formed Pt-Guanine (N7) bond is a very stable one. This has led to the generally accepted view that also in DNA, cisplatin units bind to certain guanine N7 sites.

However, the cisplatin unit has two reactive sites (the NH, ligands are not reactive enough under physiological conditions) and after binding to one guanine N7, a second reaction has to be expected. Therefore, because of the bifunctional nature of cisplatin, several types of DNA adducts can be found (these are shown schematically in Figure 1.7):

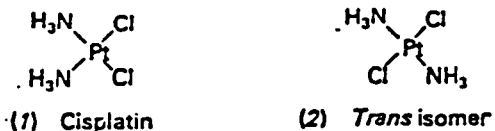
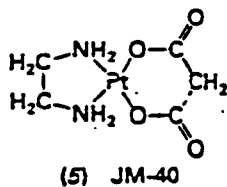
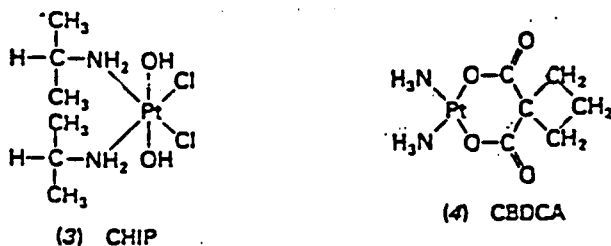
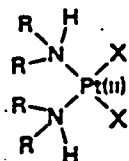


Figure 1.5 Structure of diamminedichloroplatinum (II)

Some promising 'second generation' drugs



Basic requirements for activity



(6) X = leaving group such as Cl⁻, ½SO₄²⁻ or ½ malonate

Figure 1.6 Basic Requirements for Activity and some Promising "Second Generation" Drugs.

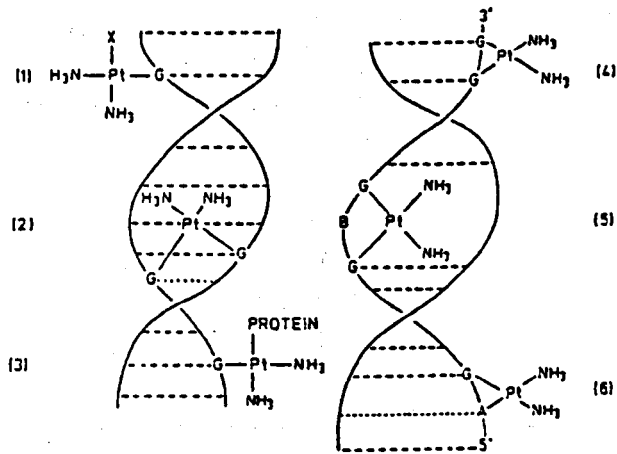


Figure 1.7 Schematic Representation of Cisplatin Bonding to DNA.

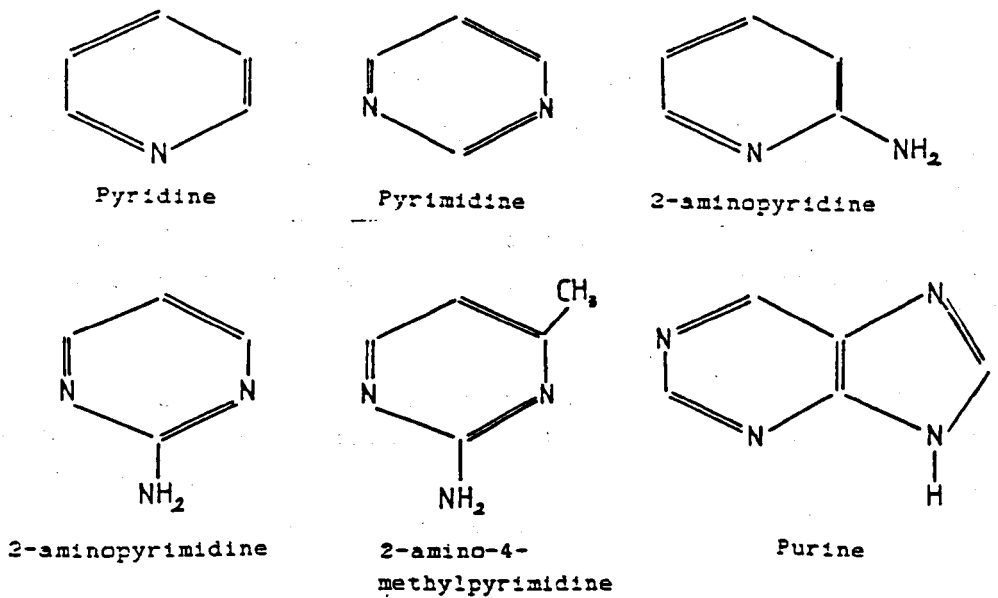


Figure 1.8 Structures of the Heterocyclic Bases under Investigation.

- stabilization of the monofunctional binding through hydrogen bonding of the amine ligands and/or H₂O or Cl
- chelation to a base in the opposite strand of double helical DNA, which may be a guanine or another base (interstrand cross-linking)
- chelation to a neighbouring guanine N7 in the same DNA strand (intrastrand cross-linking)
- chelation to a guanine in the same DNA strand (not a next neighbour)
- chelation to another base next to the guanine in the same strand, likely candidates are adenine (N7 or N1), and cytosine (N3)
- chelation to a protein side chain residue.

Since Rosenburg's discovery that certain platinum complexes exhibit antitumour activity widescale research has been carried out on the synthesis of complexes of the type cis-PtL₂Cl₂. Both the antitumour activity and the mutagenicity associated with these platinum complexes is derived from the ability of the heterocyclic bases to bind to the metal⁽¹⁹⁾. These bases represent natural multi-site ligands, but questions regarding the selectivity of base site, the identity of the type of attachment and the possible existence of isomeric forms of the metal-base complexes remain unanswered. In addition a clear pattern has yet to emerge which relates the structure and the physico-chemical properties of the various platinum anticancer drugs to their potency.

In order to gain more insight into the interactions of platinum with nucleic acids much work has gone into isolating and characterising the products formed by the reactions of platinum complexes with simpler model or natural heterocyclic bases^(14,15).

Since it is generally accepted that the platinum anticancer drugs bind, preferentially, to guanine N7 in DNA, the plan in the research described here has been to investigate the kinetics and energetics of platinum-nitrogen bonding. In order to achieve this the reaction between K₂PtCl₄ and very simple model bases, namely pyridine, pyrimidine, purine and some derivatives (Figure 1.8) have been studied. The product materials, which are cis - platinum complexes of the form PtL₂Cl₂, where L is a nitrogen heterocycle, have been subjected to thermo-analytical studies. Complementary work using theoretical chemical techniques has been carried out on the nitrogen heterocycles themselves.

The aim of the studies is to elucidate the factors which govern the rate of formation and stability of Pt-N bonds in such complexes. The information gained could be useful in the design of better anti-cancer platinum drugs.

1.2 Aims and Methodology

Square planar platinum (II) complexes, such as PtCl_4^{2-} , generally undergo nucleophilic substitution reactions, the rate of which often depends upon the nature of the group in the trans position. This concept is known as the trans effect and has been used, with considerable success, as a guide in the synthesis of desired isomeric platinum complexes. (The trans effect is discussed more fully in Chapter 3.6).

There is a large amount of kinetic data on substitution reactions of platinum square planar complexes, all of which are best explained in terms of a bimolecular displacement mechanism. For reactions such as:



in aqueous solution a two term rate law:

$$\text{Rate} = k_1[\text{PtA}_2\text{X}^{2-}] + k_2[\text{PtA}_2\text{X}^{2-}][\text{Y}^-]$$

is generally followed^(16,17), where k_1 and k_2 are the first order and second order rate constant respectively. Under pseudo-first order conditions containing excess Y, the experimental first order rate constant K_{obs} is related to the individual rate constants as shown by the equation:

$$K_{\text{obs}} = k_1 + k_2[\text{Y}^-]$$

This requires that a plot of k_{obs} versus $[\text{Y}^-]$ be linear with an intercept of k_1 for the reagent-independent path and a slope of k_2 for the reagent path. Plots of this type are common for substitution reactions of square planar complexes. Such a plot is shown in Figure 1.9 for the reaction of $\text{Pt}(\text{py})_2\text{Cl}_2$ with a wide variety of reagents.

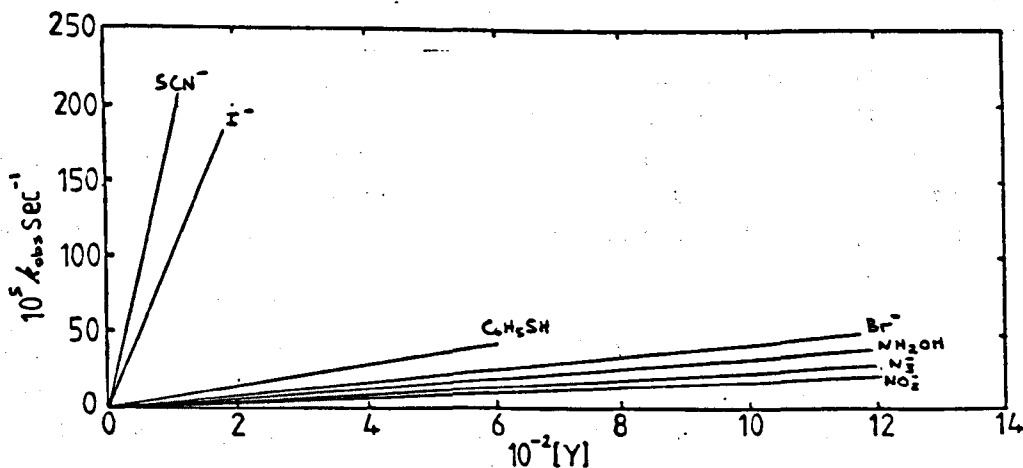


Figure 1.9 Rates of Reaction of $\text{trans-Pt}(\text{py})_2\text{Cl}_2$ in Methanol at 30° as a Function of the Concentrations of Different Nucleophiles.⁽¹⁸⁾

In this study of the kinetics of substitution between K_2PtCl_4 and N-heterocyclic bases initial preparative work was carried out. K_2PtCl_4 was reacted with various ligands in aqueous solution using a method described by Kong and Rochon⁽¹⁹⁾, who found that reactions of pyridine derivatives with K_2PtCl_4 were accompanied by precipitation of sparingly soluble compounds. The use of reactions having this characteristic allowed development of methods to monitor the concentration of reactants remaining in solution as a reaction proceeds without any interference from the solid product.

Kukushkin et al⁽²⁰⁾ carried out kinetic analysis on reactions between K_2PtCl_4 and pyridine derivatives using a potentiometric method. They established that all reactions were of second order overall, ie first order with respect to the platinum-containing ion, and first order with respect to the pyridine. The rate determining step in all instances was assumed to be the introduction of the first molecule of pyridine. In this present study several different methods were investigated in order to find the most amenable for determining the kinetics of formation of complexes of the type PtL_2Cl_2 , where L is a N-heterocyclic base. Initial studies were carried out on the reaction between K_2PtCl_4 and 2-aminopyridine. Once a technique had been developed which was found to be consistent and reproducible reactions between K_2PtCl_4 and other ligands were studied with a view to determining any possible structure-activity relationships.

In addition to investigating the kinetics of formation of complexes of the type PtL_2Cl_2 , the energetics of Pt-N bond dissociation was also studied using thermogravimetric analysis. Thermal analysis involves heating a known weight of complex with a linear heating program. As the temperature increases weight loss is observed, either as a single stage process or possibly as a multistage process. The percentage weight losses occurring at each stage can be determined and compared with theoretical weight losses and hence one can identify the removal of a particular ligand. The temperature of ligand loss and the order of ligand loss can give an insight into the relative stabilities of the Pt-ligand bonds.

More quantitative data can be obtained from isothermal studies. this involves heating the complex at a constant temperature and studying the decomposition of the samples as a function of time. Several experiments needed to be carried out at a series of different but constant temperatures. By studying the variation of weight of reactant with time for each individual experiment rate constants can be derived from appropriate rate equations. Comparison of the rate constants obtained for each isothermal condition will give an estimation of the Arrhenius parameters⁽²¹⁾ (this is discussed further in Chapter 4).

Theoretical studies on the N-heterocycles themselves have been carried out in an attempt to correlate the kinetic parameters with the electronic structure of the ligand. The trans substitution effect is known to depend on charge distribution. Information on the mechanism of substitution can sometimes be provided by the effect of charge on the complex on its rate

of reaction. Thus if a reaction involves primarily a separation of charge, as in a dissociative process, then for an analogous series of complexes the rate will decrease with a decrease of the charge of the complex. However, if the reaction is largely associative in type, the charge neutralisation process requires that an increase in positive charge on the complex be accompanied by an increase in rate of reaction. For a bimolecular displacement process, where dissociation and neutralisation are of comparable importance, there would be opposing effects and the rate of reaction would not be expected to change very much with changes of the charge on the complex⁽²²⁾.

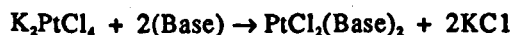
CHAPTER 2

Preparation and Characterisation of Complexes of the Type Cis-Pt L₂ Cl₂

2.1 Preparation

In order to find out about the kinetics and energetics of platinum - nitrogen bond formation investigations have been carried out using simple models of the bases of DNA. The model systems chosen were required to mimic the *in vivo* complexation of platinum with the heterocyclic bases of DNA. Suitable analogues of the DNA bases, particularly cytosine and guanine, were considered to be variously substituted forms of pyridine, pyrimidine and purine which like the natural nucleobases are multi-site ligands.

The reaction between metal and base can be studied by looking at the rate of formation of complexation when a simple platinum complex, such as K₂PtCl₄, interacts with a model base in aqueous solution according to the equation:



One criterion for the choice of base was that it had to be soluble in some solvent, preferably aqueous solution.

The solubility of several heterocyclic bases were investigated in aqueous solution, mixed aqueous/alcohol solution, alcohol solution and acetonitril. It was found that pyridine, pyrimidine, 2-aminopyridine, 2-aminopyrimidine, 2-amino, 4-methylpyrimidine and purine were all soluble in aqueous solution and thus amenable to the type of investigation envisaged. However other bases such as 4-methyl, 2-thiouracil, 4,6-dihydroxypyrimidine, 4-amino, 2,6-dihydroxypyrimidine and 2,4,6-triaminopyrimidine were insoluble in all the above solvents and so rejected as possible model systems.

2.1.1 Reagents

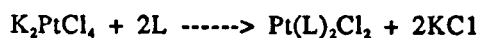
Reagents used in the preparation of the platinum-base complexes were obtained commercially as follows:

Potassium tetrachloroplatinate (II)	(K ₂ PtCl ₄)	Johnson Matthey
2-aminopyridine	(2AP)	Fluka Chemicals Ltd
2-aminopyrimidine	(2APm)	Aldrich Chemicals Co Inc
pyridine	(Py)	Aldrich Chemicals Co Inc
pyrimidine	(Pm)	Aldrich Chemicals Co Inc
2-amino, 4-methyl-pyrimidine	(AMPm)	Aldrich Chemical Co Inc
purine	(Pu)	Aldrich Chemical Co Inc

Since all reagents were at least 97% pure they were all used direct from the manufacturer without any further purification.

2.1.2 Synthesis of Complexes of the Type cis-Pt(L)₂Cl₂

The complexes were all prepared using the method described by Kong and Rochon.^[19]



In the typical case of the 2-aminopyridine ligand, to an aqueous solution of K₂PtCl₄ (0.415 g in 10 cm³ of water) an aqueous solution of 2-aminopyridine (0.141 g in 5 cm³ of water) was added. The resultant solution was left to stand at room temperature for five hours. The green precipitate was filtered and washed with water, methanol, and ether and then dried at 353 K in a vacuum oven overnight.

The concentrations of K₂PtCl₄ and 2-aminopyridine used in the above reaction are non-stoichiometric, the molar ratio being 1 : 3 respectively. In order to implement the elementary rate laws for kinetic analysis of this reaction it was considered preferable to have a quantitative relationship between the reactants and the products. Consequently the above preparative method was repeated but this time using stoichiometric quantities, ie a molar ratio of 1 (K₂PtCl₄) : 2 (2AP) to ascertain that the same product would result in the kinetic studies.

X-ray power diffraction patterns were obtained for the products obtained both non-stoichiometrically and stoichiometrically. These were found to be identical to one another but different from the X-ray diffraction patterns of both K₂PtCl₄ and 2-aminopyridine. This indicated that both preparative methods gave rise to the same product.

K₂PtCl₄ was reacted with the five other ligands, 2-aminopyrimidine, pyridine, pyrimidine, 2-amino, 4-methyl-pyrimidine and purine, using stoichiometric quantities. The amounts of reagent used for each reaction are given in Table 2.1.

TABLE 2.1**Weight and Concentration of Each Reagent**

Complex	Amt K_2PtCl_6 /g	Molarity K_2PtCl_6	Amt Ligand/g	Molarity ligand
$Pt(2AP)_2Cl_2$	0.415	0.1 M	0.188	0.2 M
$Pt(2APm)_2Cl_2$	0.415	0.1 M	0.190	0.2 M
$Pt(Py)_2Cl_2$	0.415	0.1 M	0.158	0.2 M
$Pt(Pm)_2Cl_2$	0.415	0.1 M	0.160	0.2 M
$Pt(AMPm)_2Cl_2$	0.415	0.1 M	0.218	0.2 M
$Pt(Pu)_2Cl_2$	0.415	0.1 M	0.240	0.2 M

2.2 Characterisation

The products from the reactions between K_2PtCl_6 and ligand were characterised by thermogravimetric analysis, CHN analysis, infrared spectroscopy. The information obtained from these techniques would demonstrate characteristics of the product such as the empirical formula and whether it was present in the cis- or trans-configuration.

2.2.1 Equipment**Infrared Spectroscopy:**

Perkin Elmer 683 IR spectrophotometer

Caesium iodide discs in range $4\ 000\ cm^{-1}$ - $200\ cm^{-1}$

Thermogravimetric Analysis:

CIE microbalance and a Stanton Recroft heating programmer linked to a furnace using platinum/platinum, 13% rhodium thermocouple. Both microbalance and heating programmer were linked to a JJ Instruments CR 6525 twin pen recorder.

CHN Analysis:

This was carried out courtesy of the Micro-Analytical Laboratory, Department of Chemistry, the University of Manchester.

2.2.2 Yields of Products

The percentage yield in five hours of reaction time was calculated for each product and the results are summarised in Table 2.2.

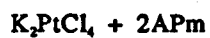
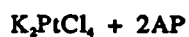
TABLE 2.2

Colour and Percentage Yield of Each Product

Product	Colour	%age yield
Pt(2AP) ₂ Cl ₂	green	53
Pt(2APm) ₂ Cl ₂	bright yellow	59
Pt(Py) ₂ Cl ₂	pale yellow	63
Pt(Pm) ₂ Cl ₂	bright yellow	64
Pt(AMPm) ₂ Cl ₂	brown	51
Pt(Pu) ₂ Cl ₂	pale yellow	65

2.2.3 CHN Analysis

CHN analysis was carried out on the products obtained from the following three reactions:



The results are listed in Table 2.3.

TABLE 2.3

Comparison of Theoretical and Experimental Percentage Yields

Pt(2AP) ₂ Cl ₂		Pt(2APm) ₂ Cl ₂		Pt(AMPm) ₂ Cl ₂	
Calculated	Found	Calculated	Found	Calculated	Found
%	%	%	%	%	%
C 26.2	26.4	21.0	21.1	24.8	25.4
H 2.45	2.6	2.2	2.2	2.9	2.9
N 12.6	12.3	18.6	18.4	17.4	17.0
Cl 15.8	15.6	15.95	15.6	14.75	14.7

These results suggest that the molecular formula of the product is of the form PtL_2Cl_2 .

2.2.4 Thermogravimetric Analysis

The technique involved the continuous weighing of a sample whilst heating using a linear temperature rise recording the weight loss as a function of temperature.

Procedure

Thermogravimetric analysis was carried out in a static air atmosphere and a platinum/platinum, 13% rhodium thermocouple. Approximately 10 mg of the product was heated on a CIE microbalance using a linear heating rate up to a maximum temperature of 653 K. The cold junction was also measured.

The temperature was obtained from chart paper by measuring the emf of the thermocouple and consulting a calibration table of emf and the corresponding temperature making due allowance for the cold junction.

Results

Thermogravimetric analysis showed that the products decomposed in a stepwise manner. The decomposition curve for the platinum - 2-aminopyridine complex is shown in Figure 2.1 and the percentage weight losses are given in Table 2.4. The theoretically calculated percentages of Pt, 2AP and Cl in a complex of molecular formula $Pt(2AP)_2Cl_2$ are also listed.

TABLE 2.4

Comparison of Theoretical and Experimental Weight Loss
from cis-Pt (2-amino pyridine)₂ Cl₂

Process	Temperature Range/K	Percentage Weight Loss	
		Theoretical	Experimental
Loss of 1 mole of 2AP and 1 mole of Cl	483-568	28.52	29.44 in 1st step of TG curve
Loss of 1 mole of 2AP and 1 mole of Cl	568-673	28.52	26.67 in 2nd step of TG curve
Loss of all Ligands leaving metallic Pt	> 673	56.11	57.04 total weight loss

As can be seen from these results thermogravimetric analysis indicated that the molecular formula of the complex is $\text{Pt}(\text{2AP})_2\text{Cl}_2$. The first two steps of the decomposition process involve the loss of the two ligands along with the loss of the two chlorine atoms, so that all that remains after 673 K corresponds to the theoretical percentage of platinum. X-ray power diffraction was carried out on the residue and confirmed it to be platinum. Table 2.5 lists the main d spacings and relative intensities of the residues diffraction pattern along with those obtained for platinum from the ASTM power diffraction file.

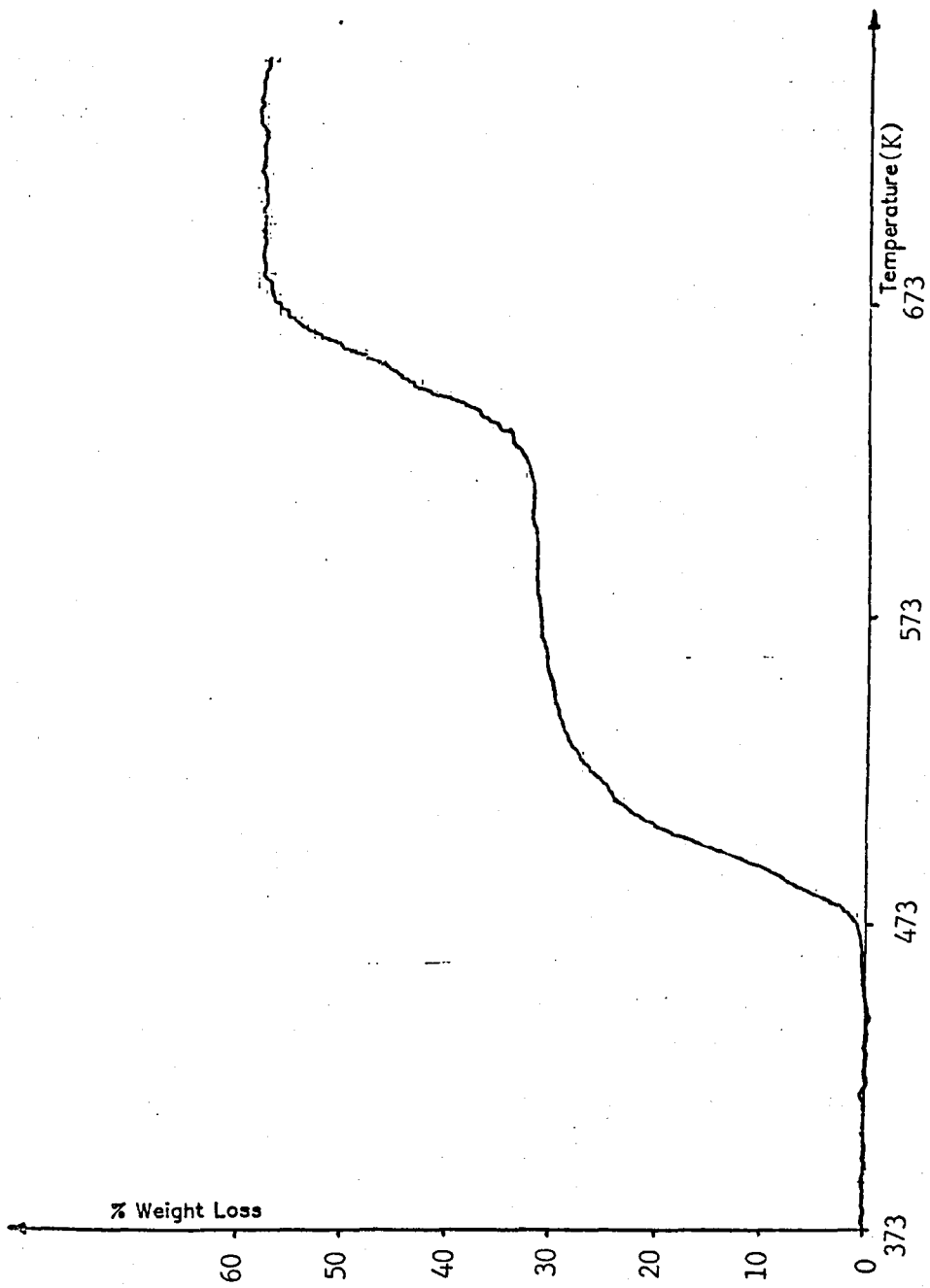


Figure 2.1 Non-isothermal Decomposition of Pt (2AP)₂ Cl₂

TABLE 2.5

Comparison of the Main d spacings obtained from the Residue and the ASTM Powder Diffraction File for Platinum

Relative intensity I/I_1	d spacings	
	ASTM file	Residue pattern
100	2.265	2.25
53	1.962	1.95
31	1.387	1.38
33	1.1826	1.18
39	0.8008	0.79

Similar stepwise decomposition curves were obtained for the other five products indicating that the molecular formula after complexation between K_2PtCl_4 and ligand is $Pt(L)_2Cl_2$. Apart from merely characterising the formula of the reaction product these results were also useful as a pre-study to thermogravimetric analysis which was considered to be kinetically important and was subsequently investigated more thoroughly.

2.2.5 Infrared Spectroscopy

Infrared spectra were obtained for each of the ligands and the corresponding complex formed by the reaction with K_2PtCl_4 . Comparisons could then be made between the two corresponding spectra and predictions made as to how the platinum binds to the ligand. A band of particular interest in the spectra is the metal - ligand stretching band. This band is likely to be due to the Pt - N bond since in these complexes it is thought that the metal binds to the ligand through a cyclic nitrogen atom. This band should arise around the region of 490 nm. Changes in the position of the N-H and C-H stretching frequencies are also expected.

An IR spectrum of K_2PtCl_4 was also obtained in order to find the position of the Pt-Cl stretching frequency. This was found to appear in the region of 330 nm.

Tables 2.5 to 2.10 list the bands of importance for each ligand and its corresponding reaction product. The assignments were made by comparison with published data. ^(19, 23, 24)

TABLE 2.5

IR Absorption Frequencies of 2-aminopyridine and its Complex

Band frequencies (cm ⁻¹)		Assignments
2-aminopyridine	Complex	
3 410	3 440	N-H str
3 300	3 310	N-H str
3 160	3 060	aromatic
3 060	3 060	C-H str
1 625	1 635	N-H str
1 595	1 590	aromatic
1 555	1 560	aromatic
1 485	1 490	aromatic
1 160	1 150	C-N str
-	450	Pt-N
-	330	Pt-Cl

TABLE 2.6

IR Absorption Frequencies of 2-aminopyrimidine and its Complex

Band frequencies (cm ⁻¹)		Assignments
2-aminopyridine	Complex	
2 320	3 420	N-H str
3 270	3 310	N-H str
3 120	3 160	aromatic
2 960	3 080	C-H str
1 620	1 645	N-H str
1 580	1 580	aromatic
1 560	1 565	aromatic
1 475	1 475	aromatic
1 130	1 125	C-N str
-	450	Pt-N
-	330	Pt-Cl

TABLE 2.7

IR Absorption Frequencies of Pyridine and its Complex

Band frequencies (cm ⁻¹)		Assignments
Pyridine	Complex	
3 680	3 700	N-H str
3 410	3 490	N-H str
3 120	3 120	aromatic
3 080	3 085	C-H str
1 630	1 627	N-h str
1 000	1 605	aromatic
1 580	1 570	aromatic
1 480	1 480	aromatic
1 160	1 155	C-N str
-	450	Pt-N
-	330	Pt-Cl

TABLE 2.8

IR Absorption Frequencies of Pyrimidine and its Complex

Band frequencies (cm ⁻¹)		Assignments
2-amino-4-methylpyrimidine	Complex	
3 410	3 470	N-H str
3 280	3 360	N-H str
3 000	2 980	aromatic
2 920	2 900	C-H str
1 585	1 610	N-H str
1 565	1 550	aromatic
1 475	1 460	aromatic
1 140	1 150	C-N str
-	440	Pt-N
-	335	Pt-Cl

TABLE 2.10

IR Absorption Frequencies of Purine and its Complex

Band frequencies (cm ⁻¹)		Assignments
Purine	Complex	
3 420	3 500	N-H str
3 075	3 090	N-H str
2 910	2 910	aromatic
2 850	2 800	C-H str
1 615	1 620	N-H str
1 570	1 570	aromatic
1 500	1 485	aromatic
1 460	1 420	aromatic
1 140	1 155	C-N str
-	450	Pt-N
-	330	Pt-Cl

Generally the IR spectrum of the ligand was very similar to that of the corresponding complex. However, in all six cases there is evidence of additional bands in the regions of 450 cm⁻¹ and 330 cm⁻¹. These bands have been assigned Pt-N and Pt-Cl respectively, thus indicating that platinum and chloride are both present after complexation and that the platinum binds to the ligand through a nitrogen atom. In addition the observation that the IR spectra of the synthesised platinum complex showed absorption in the region around 450 cm⁻¹ indicated, according to Osa et al,^[24] that the complex is present in its cis configuration.

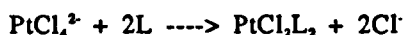
In the IR spectra of the three complexes which have an amino side group present it was observed that the N-H stretching frequency shifted to a higher frequency after complexation, indicating that the amino group is not involved in the bonding.

CHAPTER 3

Solution Studies

3.1 Introduction

Kinetic studies were carried out in aqueous solution, the aim being to determine the form of the rate equation and values for the rate constants for the reactions:



The activation energy could then be calculated for the formation of complexes of the type PtL_2Cl_2 .

In order to measure the rate of a chemical reaction it is necessary to follow the change in concentration of reactant and/or product with time by a convenient method. Numerous methods are available and the choice of a suitable technique depends on the nature of the reactants and products and the length of the half life of the reaction. Because the reactions under investigation had a reasonably long half life coupled with the fact that both reactants were soluble and the product precipitates out of solution, it was deemed satisfactory to develop an incremental method involving the withdrawal of samples of the solution for analysis at various time intervals.

Several techniques were investigated in order to study the platinum or base concentration in the complexation studies, these included potentiometric titrations of Cl^- , High Performance Liquid Chromatography (HPLC) determination of peak area of the reacting ligand, ultraviolet spectroscopic (UV) measurement of the absorbance of ligand and atomic absorption spectroscopy (AA) for measurement of platinum absorbance.

Once a consistent and reproducible method had been developed the rate equation and rate constant could then be determined in one of two ways, either by a differential or by an integral method. A differential method is a direct one since the values of $d(\text{conc})/d(\text{time})$ are determined directly from plots of concentration vs time, the tangents to the curve at any time, t , giving the rate at that time. Graphs of concentration against time are plotted for a number of initial concentrations, C_1, C_2, C_3 , etc and the tangents at the start of that reaction are drawn as in Figure 3.1a. This corresponds to the initial rate for that particular concentration. When the rate is measured at the start of a reaction it can be assumed that complications caused by the presence of secondary reactions do not occur. The logarithms of the initial rate is plotted against the logarithm of the initial concentration as in Figure 3.1b and the rate constant and order determined from the intercept and slope respectively.

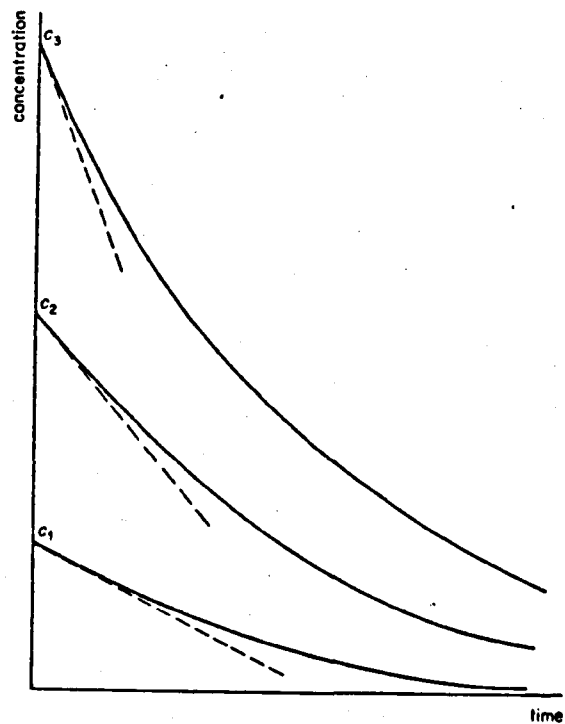


Figure 3.1a Concentration Time Curve for Different Initial Concentrations

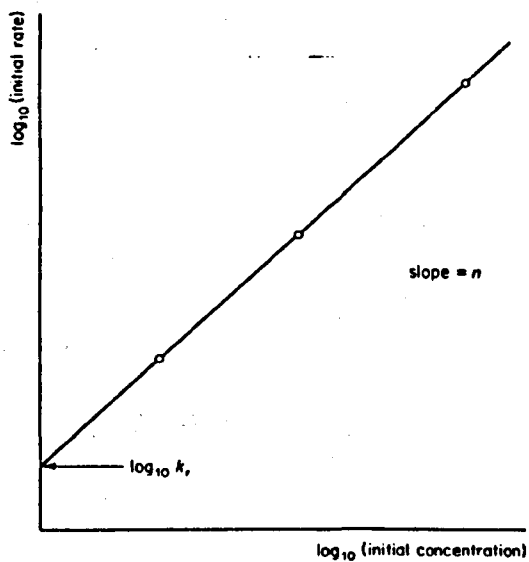


Figure 3.1b Plot of $\text{Log}_{10}(\text{initial rate})$ against $\text{Log}_{10}(\text{initial concentration})$

One advantage of this method over integration methods is that it is not dependent on a knowledge of the order of reaction.

For integration methods the experimental variation of concentration with time at constant temperature is compared to one of the integrated rate equations:

Zero Order

$$-\frac{dC}{dt} = k$$

where C = the concentration
t = time
k = the rate constant

Integrating:

$$-\int_{C_0}^{C_t} dC = \int_0^t dt$$

where C_0 = the initial concentration
 C_t = the concentration at time t
 $C_t = C_0 - kt$

First Order

$$-\frac{dC}{dt} = kC$$

Integration gives:

$$\ln(C) = \ln(C_0) - kt$$

This equation can also be expressed in other forms:

by antilogging the above equation gives exponential decay

$$C_t = C_0 e^{-kt}$$

or in the terms of extent of reaction, α , where $(1 - \alpha)$ is equal to the fraction remaining:

$$1 - \alpha = \frac{C_t}{C_0}$$

but $\ln \frac{C_0}{C_t} = kt$ therefore $-\ln \frac{C_t}{C_0} = kt$

$$-\ln(1 - \alpha) = kt$$

or if $a =$ initial concentration
 $x =$ decrease in concentration

then $a - x =$ concentration at time t

$$\ln \frac{C_0}{C_t} = kt$$

$$\ln \frac{a}{a - x} = kt$$

Second Order

$$-\frac{dC}{dt} = kC^2$$

integrating gives:

$$\frac{1}{C_t} - \frac{1}{C_0} = kt$$

Therefore a plot of C versus t, lnC, versus t or 1/C, versus t will be linear if the reaction follows zero, first or second order rate laws respectively. The rate constant can be determined from the slope of the linear graph in each case.

Once the rate constant has been determined at two or more temperatures the activation energy can be calculated using the Arrhenius equation ⁽²⁴⁾. Arrhenius found that the rate constant is related to the temperature by an equation of the form:

$$d(\ln k)/dT = E/RT^2 \quad \text{Equation 3.1}$$

where k = rate constant
T = temperature
E = activation energy
R = universal gas constant

Equation 3.1 integrates to:

$$\ln k = E/RT + \text{Const} \quad \text{Equation 3.2}$$

provided E is independent of temperature.

Equation 3.2 may be rewritten as:

$$k = Ae^{-E/RT}$$

where A is a constant known as the pre-exponential factor for the reaction

$e^{-E/RT}$ is recognised as the Boltzman distribution factor.

Therefore to determine the activation energy the value of the rate constant (k) must be evaluated at various temperatures, then from equation 3.2 a plot of lnk versus 1/T should yield a straight line of slope -E/R from which E can be calculated.

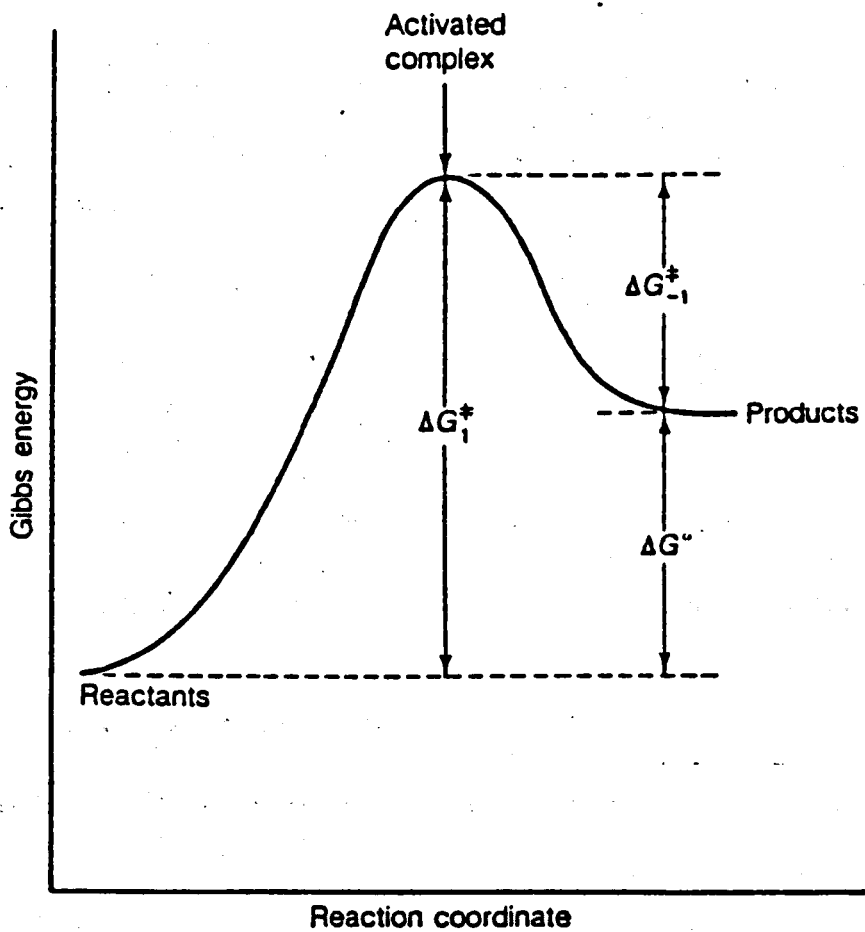


Figure 3.2 Gibbs Energy Diagram for a Reaction

Transition State Theory

According to the Arrhenius equation the rate of reaction at a given temperature is controlled entirely by the two quantities E (the activation energy) and A (the pre-exponential factor). First attempts at calculating the pre-exponential factor were based on the kinetic theory of collisions. However, the use of the hard-sphere kinetic theory led to many discrepancies and in 1935 Henry Eyring^[26] presented a much more satisfactory treatment of calculating the pre-exponential factor.

Eyring proposed what is now known as the theory of absolute reaction rate in which statistical thermodynamics is applied to the formation of the transition state. Absolute rate theory postulates that the rate of a chemical reaction is given by the rate of passage of the activated complex through the transition state. It is assumed that, although the transition state is mechanically unstable, it can be treated as a thermodynamically identifiable entity.

The theory is based on an equilibrium hypothesis. The transition state being made up of complexes that were previously either reactants or products. Equilibria therefore exists between the reactants A and B and the activated complex and between the products C and D and the activated complex X^* .



It is possible to define K^* as the equilibrium constant for the equilibrium between the reactants and the activated complex X^* .

The Gibbs free energy, ΔG , of such a system can be regarded as the difference between two terms, one of which exercises the sole control over the reaction in the forward reaction and the other in the reverse direction (Figure 3.2).

In going to the final state a reaction system must pass over Gibbs energy barrier and once at the top of this barrier the reaction can proceed without the expenditure of any additional Gibbs energy. The reaction from left to right will, therefore, depend solely on ΔG_{\rightarrow} , and that from right to left solely on ΔG_{\leftarrow} .

The equilibrium constant, k , for a chemical reaction is related to the Gibbs free energy change, ΔG by:

$$\ln(k) = - \frac{\Delta G}{RT} \qquad \text{Equation 3.3}$$

This equilibrium constant k is the ratio of the forward and reverse rate constants k_1/k_{-1} and therefore:

$$\ln(K_1) - \ln(K_{-1}) = - \frac{\Delta G}{RT} \quad \text{Equation 3.4}$$

$$= - \frac{\Delta G^*_1}{RT} + \frac{\Delta G^*_{-1}}{RT} \quad \text{Equation 3.5}$$

This latter equation may be split into two separate equations:

$$\ln(k_1) = \ln(v) - \frac{\Delta G^*_1}{RT} \quad \text{Equation 3.6}$$

$$\ln(k_{-1}) = \ln(v) - \frac{\Delta G^*_{-1}}{RT} \quad \text{Equation 3.7}$$

where v = a constant

Equation 3.6 may be written as

$$k_1 = v e^{-\Delta G^*_1/RT} \quad \text{Equation 3.8}$$

Since Gibbs energy change may be expressed in terms of enthalpy and entropy change, $\Delta G = \Delta H - T\Delta S$, then equation (3.8) may be written as

$$k_1 = v e^{\Delta S^*_1/R} e^{-\Delta H^*_1/RT} \quad \text{Equation 3.9}$$

Eyring found, by use of statistical thermodynamics, that the constant v is equal to kT/h where k is the Boltzman constant and h is Planck's constant. The Eyring equation is therefore:

$$k = \frac{kT}{h} e^{\Delta S^*_1/R} e^{-\Delta H^*_1/RT} \quad \text{Equation 3.10}$$

Another convenient form of this equation is:

$$k = \frac{kT}{h} K^* \quad \text{Equation 3.11}$$

where K^* = the equilibrium constant for the equilibrium between the ground state and the activated state.

Comparison of the Eyring equation:

$$\ln(k) = \ln \left(\frac{kT}{h} \right) + \frac{\Delta S}{R} - \frac{\Delta H}{RT} \quad \text{Equation 3.12}$$

with the Arrhenius equation

$$\ln(k) = \ln(A) - E/RT \quad \text{Equation 3.13}$$

where $\ln(A)$ = the intercept of a plot of $\ln(k)$ versus $1/T$, it can be seen that the enthalpy of activation, ΔS , can be calculated from the intercept of the Arrhenius plot.

Since from equations (3.11) and (3.12)

$$\ln(A) = \ln \frac{kT}{h} + \frac{\Delta S}{R}$$

$$\Delta S = R [\ln(A) - \ln(kT/h)]$$

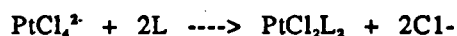
3.2 Choice of Experimental Method

Preliminary investigations were carried out into the use of potentiometric titrations, HPLC, UV and AA spectroscopy in order to determine the best method to monitor the kinetics of formation in solution conditions. Since the method which was to be developed would depend on the removal of the constituent to be analysed then, at specific time intervals, an aliquot would have to be withdrawn. This immediately leads to problems - a reaction will proceed at the same rate in the

test sample as it will in the original reaction medium. As the analysis procedure takes a certain amount of time, if a true measurement is to be obtained, then it is necessary to inhibit or quench the reaction and to ensure that the separation will not be accompanied by a modification in the properties of the constituents present. This was achieved by diluting the sample to such an extent that changes in its concentration could be considered negligible. This quenching of the reaction was an important factor when it came to deciding upon the most feasible method.

3.2.1 Potentiometric Titrations

In the reaction:



the rate of reaction might be measured by the rate of production of Cl^- , since $[\text{Cl}^-]$ can be easily measured by AgNO_3 titration using an Ag/AgCl electrode. Such a potentiometric method seemed feasible and had been used by Kukuskin et al ^[20].

The cell used was:



As incremental methods involve the removal of aliquots, with subsequent dilution the technique implemented must be able to consistently and reproducibly measure very low concentrations of the atom involved. However, preliminary results, involving the titration of low concentrations of NaCl with AgNO_3 , indicated that the Ag/AgCl electrode was not sensitive enough to detect small changes in chloride concentration as the reaction proceeded. This led to problems in trying to decide a suitable dilution factor and it was concluded that large quantities of K_2PtCl_6 would have to be used in order to obtain any meaningful results. Consequently the potentiometric titration method was rejected as being impractical.

3.2.2 High Performance Liquid Chromatography (HPLC)

Reverse phase HPLC was also assessed as a possible method of monitoring the ligand concentration in the reaction mixture and hence the kinetics of the reaction. Peak area in HPLC is proportional to concentration. Hence the reaction can be followed by measuring the decrease

in peak area as a function of time. The HPLC analysis was carried out using a Spectra Physics Liquid chromatogram. The components of the system consisted of an applied chromatography system linked to a Pye Unicam LC-3 variable wavelength UV detector. The chromatographic column (150 mm by 5 mm ID) was slurry packed at 200 bar with 5 m ODS Hypersil. Before this technique could be implemented, a number of experimental parameters had to be optimised, these included choosing the most suitable mobile phase, sensitivity range and wavelength. Using a solution of 2-aminopyridine it was finally decided to use the following operating conditions:

Mobile Phase	:	90% H ₂ O : 10% methanol
Wavelength	:	286 nm
Range	:	10 mv
Sensitivity Range	:	0.08

Several sample solutions of 2-aminopyridine (2AP) were injected and the retention time of the resultant peak measured. In each case the retention time was found to be 3.425 ± 0.01 minutes.

Having optimised the operating conditions and knowing the retention time of 2AP, a trial run was carried out monitoring the reaction between K₂PtCl₆ and 2AP. It was found that the peak area due to 2AP did decrease with time but when peak area was plotted against time there was a wide scatter of points making it impossible to apply any of the rate laws. The experiment was repeated using exactly the same parameters and again the plot of peak area versus time was meaningless. It was thought that these inconsistencies could be due to the sampling technique, so it was decided to measure the peak area of a solution of 2AP over a period of time. The results obtained indicated that it was difficult to get reproducible result using HPLC. Since kinetic analysis relies totally on reproducibility and consistency it was decided to reject HPLC as a plausible method. In addition, for each ligand investigated, the operating parameters such as the mobile phase and wavelength would have to be reoptimised.

3.2.3 Spectroscopy

Atomic Absorption Spectroscopy

Atomic absorption (AA) spectroscopy works on the principle that materials can be atomised in high temperature flames. If radiation of an atom's specific resonance wavelength is passed through the flame containing the atom in question then part of the light will be absorbed, the absorption being proportional to the number of ground state atoms present in the flame. Provided the system obeys the Beer - Lambert law then this absorbance will be proportional to the concentration of atoms in the flame and hence to the concentration of material in any solution being sprayed at a constant rate into the flame (the source of atoms).

The Beer - Lambert Law may be stated as:

$$A = \epsilon cl$$

where A = Absorbance
 ϵ = molar absorption coefficient ($\text{m}^2\text{mol}^{-1}$)
c = concentration (molm^{-3})
l = path length (m)

For a given substance and flame ϵ and l are constant.

AA spectroscopy was used to monitor the concentration of platinum in the reaction solution. A Perkin Elmer 2280 AA a spectrophotometer was used under the following conditions:

Light source	:	Platinum hollow cathode lamp
Flame type	:	Air-acetylene oxidising
Wavelength	:	265.9 nm
Slit setting	:	0.7 nm

For the standard conditions described above the sensitivity is about $2 \mu\text{gml}^{-1}$ Pt for 1% absorbance. A standard solution containing $50 \mu\text{gml}^{-1}$ of Pt should typically give an absorbance reading of about 0.11 absorbance units.

It was found that the working range for Pt was linear up to concentrations of about $175 \mu\text{gml}^{-1}$ in aqueous solution. Thus prior to AA analysis it was necessary to carry out large dilutions of the reacting mixture, in which the initial concentration of K_2PtCl_6 was 83mgml^{-1} .

Ultraviolet Spectroscopy

Ultraviolet (UV) spectroscopy was carried out using a Perkin Elmer Lambda 1 UV/Vis spectrophotometer to measure the concentration of ligand remaining in the reaction mixture. Measurements were carried out at a fixed wavelength corresponding to the maximum absorbance of the particular ligand under investigation.

Using ultraviolet spectroscopy, provided the Beer - Lambert law applies and provided a region of the UV spectrum is chosen where the absorbance is due to a single component in the reaction mixture, then the reaction can be followed spectrophotometrically by the measurement of the absorbance due to the ligand at the wavelength as a function of time.

Again it was found that the sensitivity of the UV spectrophotometer required that large dilutions of the reaction mixture needed to be carried out in order to bring the absorbance value of the ligand into scale.

Preliminary investigations into the use of both AA and UV spectroscopy indicated that both techniques provided a suitable and comparatively straightforward method of monitoring the kinetics in solution of reactions of the type K_2PtCl_6 + ligand, since both methods were sufficiently sensitive to determine the concentrations of Pt or ligand at the dilutions required to freeze the reaction.

3.3 Development of Experimental Technique

Work was carried out on following the kinetics of formation in solution of reactions of the type K_2PtCl_6 + ligand by monitoring the decreases in platinum concentration and decrease in ligand concentration by Atomic Absorption and Ultraviolet spectroscopy respectively. A valid and reproducible methodology behind both types of analysis needed to be established to enable the kinetics of platinum - ligand interaction in solution to be monitored. The development of the technique depended on the facts that the reactants and any intermediates are soluble in aqueous solution and that the product precipitates out of solution.

3.3.1 Development of Atomic Absorption Method

Before any developmental AA spectroscopy could be carried out a certain amount of preliminary work was required. This included deciding on what concentration of reactants was to be used and finding a suitable reaction vessel for the experimental analysis to be carried out in. It was also necessary to establish the linear range over which the absorbance of platinum was directly proportional to the concentration of K_2PtCl_6 . Finally a sampling methodology had to be devised and efforts made to establish its reproducibility.

To make the kinetic analysis easier it had already been decided that the reactants K_2PtCl_6 and ligand should be present in the stoichiometric ratio 1 : 2 respectively. In order to decide upon the actual concentration of the reactants used in the kinetic analysis two factors were taken into account - the high cost of K_2PtCl_6 , and the length of the half-life of the reaction. Consequently three reactions were carried out using different concentrations of reactants in order to assess which would be the most suitable. The results are tabulated in Table 3.1.

TABLE 3.1**Comparison of Different Initial Concentrations on Rate of Formation of Product**

Reactant Concentration	Observation
0.01M K_2PtCl_4 : 0.02M 2-aminopyridine	No product
0.1M K_2PtCl_4 : 0.2M 2-aminopyridine	Reaction too slow
0.2M K_2PtCl_4 : 0.4M 2-aminopyridine	Reaction found to proceed at a suitable rate to enable kinetic analysis

The reaction vessel had several requirements to fulfil. It was required to have a volume of 5ml, but was not required to be much than this. A vessel which was quite deep was preferred as this would allow settling of the precipitate whilst still giving considerable depth of supernatant to make sampling easy. The vessel opening was required to be of a size which would not hinder sampling which was probably going to be by a pipette or syringe of some kind. These considerations pointed towards the suitability of a narrow test tube which could be easily thermostated by immersion in a water bath. The fact that centrifugation was to be investigated at a later date led to the use of a 10 ml centrifuge tube as the reaction vessel.

It was important to determine over what concentration range the atomic absorption of platinum varied linearly with its concentration. To achieve this a calibration curve of absorbance versus the concentration of standard Spectrosol platinum solution was obtained. Several standard solutions of Spectrasol platinum were prepared, the concentration of which ranged from $200 \mu\text{gml}^{-1}$ to $25 \mu\text{gml}^{-1}$, these solutions were aspirated and the absorbance measured. The resultant plot of absorbance versus concentration (figure 3.3) indicated that the absorbance of platinum is directly proportional to concentration over the concentration range $0-175 \mu\text{gml}^{-1}$. These results gave some indication as to the dilution factors required to quench the aliquot withdrawn from the reacting solution and bring its absorbance value into the linear range.

It was also necessary to establish a range over which the concentration of the Spectrasol platinum solution is linear to absorbance so that the AA spectrophotometer could be calibrated before each experimental run. The importance of this lies in the fact that a single standard of any metal aspirated over a period of time may result in differing absorbance readings. This is due to minor changes in fuel-oxidant flow, lamp energy and flame composition, all of which can alter the sensitivity of the flame. The calibration procedure involved choosing a standard solution of Spectrasol platinum which gave a high reading in the linear range. It was decided to use the $150 \mu\text{gml}^{-1}$ solution which gave an absorbance reading of 0.3735 on the calibration plot of absorbance

versus concentration of Spectrasol platinum. A stock solution of Spectrasol platinum ($150\mu\text{g ml}^{-1}$) would then be prepared before each experiment and would be aspirated immediately prior to each sample, thus acting as an external or calibration standard. Any variation in the absorbance readings due to drift in the sensitivity of the AA spectrophotometer could then be observed and compensated for by multiplying the absorbance reading of the sample by the ratio :

Absorbance reading Spectrasol Pt on calibration curve

Absorbance reading Spectrasol Pt at time t

Consequently data obtained over a long period of time could be compared directly knowing that any changes observed were genuine and not merely due to changes in the AA conditions.

Having determined the linear range of the AA spectrophotometer, it was then necessary to find the linear range of K_2PtCl_6 . Based on the above calibration plot it was decided that a hundred fold dilution of the reacting mixture should bring the absorption into the linear range. A $2 \times 10^{-3} \text{ M}$ solution of K_2PtCl_6 (100 fold dilution of initial reacting concentration) was prepared, aspirated and the absorbance found to be 0.235. As this result fell towards the higher region of the linear range of the Spectrasol platinum solution it was decided that a dilution factor of one hundred would be sufficient to quench the reaction and bring the absorbance of the reacting K_2PtCl_6 into the linear range. To ensure that the absorbance of K_2PtCl_6 varied linearly with concentration several other standard solution of K_2PtCl_6 were prepared ranging in concentration from $2 \times 10^{-3}\text{M}$ to $2 \times 10^{-4}\text{M}$. These were aspirated, the absorbance measured and a graph of absorbance against concentration plotted (Figure 3.4).

The sampling method adopted had to fulfil the following three criteria. Firstly, because the reaction volume was so small the technique adopted had to be capable of accurately removing small microlitre aliquots of solution. As the reaction volume totalled only 5ml and was to be monitored over two half-lives it was important not to alter this volume significantly during sampling. Since an aliquot needed to be withdrawn and then diluted to quench the reaction and bring the absorbance into the linear range, it was decided to remove aliquots of 200 μl which could then be added to 20 ml of water in order to achieve the proposed 100 fold dilution. Secondly, sampling from the centre of the solution phase without disturbing the precipitate was required. Thirdly, and most importantly, the sampling method adopted was required to be reproducible to a high degree of accuracy. This would allow a large amount of certainty to be assigned to the absorbance data and so any changes in this data could be attributed to the change in experimental conditions.

Bearing the above criteria in mind it was decided to assess the reproducibility of a 200 μl Gilson pipette. This was initially done by pipetting 200 μl samples of water into a previously weighed beaker which was then reweighed along with the aliquot of water. This procedure was repeated

twenty times and the standard deviation calculated, which was found to be a 1.64×10^{-4} , thus indicating that the Gilson reproducibly pipetted the amount required. Another test was also carried out, this time 0.415g of K_2PtCl_6 was dissolved in 5 ml of water. Four 200 μ l aliquots were withdrawn using a 200 μ l Gilson pipette. These were placed in four separate test tubes and a hundred fold dilution was performed on each. The samples were aspirated and the absorbance of each solution measured, the values of which are shown in table 3.2.

TABLE 3.2

Mean and Standard Deviation from Sampling with Gilson Pipette

Solution	Absorbance	
	Mean	Std Dev
1	0.0862	5.08×10^{-4}
2	0.0866	4.99×10^{-4}
3	0.0864	5.12×10^{-4}
4	0.0862	5.09×10^{-4}
Mean for 4 solutions = 0.08635 Std dev for 4 solutions = 1.66×10^{-4}		

The standard deviation for the absorbance readings performed on the one solution reflected the reproducibility of the spectrophotometer, whereas the standard deviation of the mean readings for all four solutions reflected the reproducibility of the Gilson pipette.

The results showed that the absorbance values for each solution were all very similar to each other, indeed the standard deviation fell within the variation in absorbance of the AA spectrophotometer itself. Therefore it can be concluded that this method of sampling is as reproducible as the instrumentation allows.

On the strength of the Gilson pipette's performance it was deemed not necessary to assess the reproducibility of other sampling techniques such as an Eppendorf pipette or a G C syringe. If any increases in reproducibility was actually possible with another method, it would not have been detectable due to the limitations of the AA spectrophotometer.

3.3.1.1 Trial Experiment I

A preliminary run to establish the duration of the reaction was carried out, this also provided an opportunity to ensure that the dilution factor chosen was sufficient to quench the reaction.

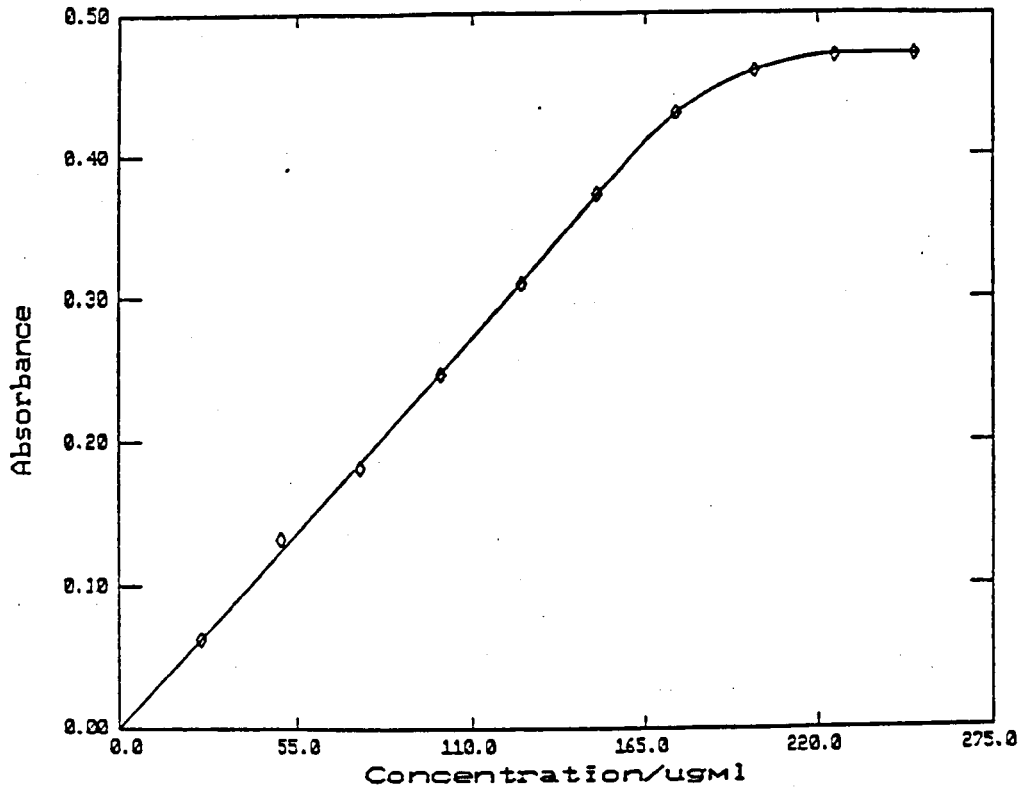


Figure 3.3 Plot of Atomic Absorbance vs Concentration of Spectrasol Platinum Solution.

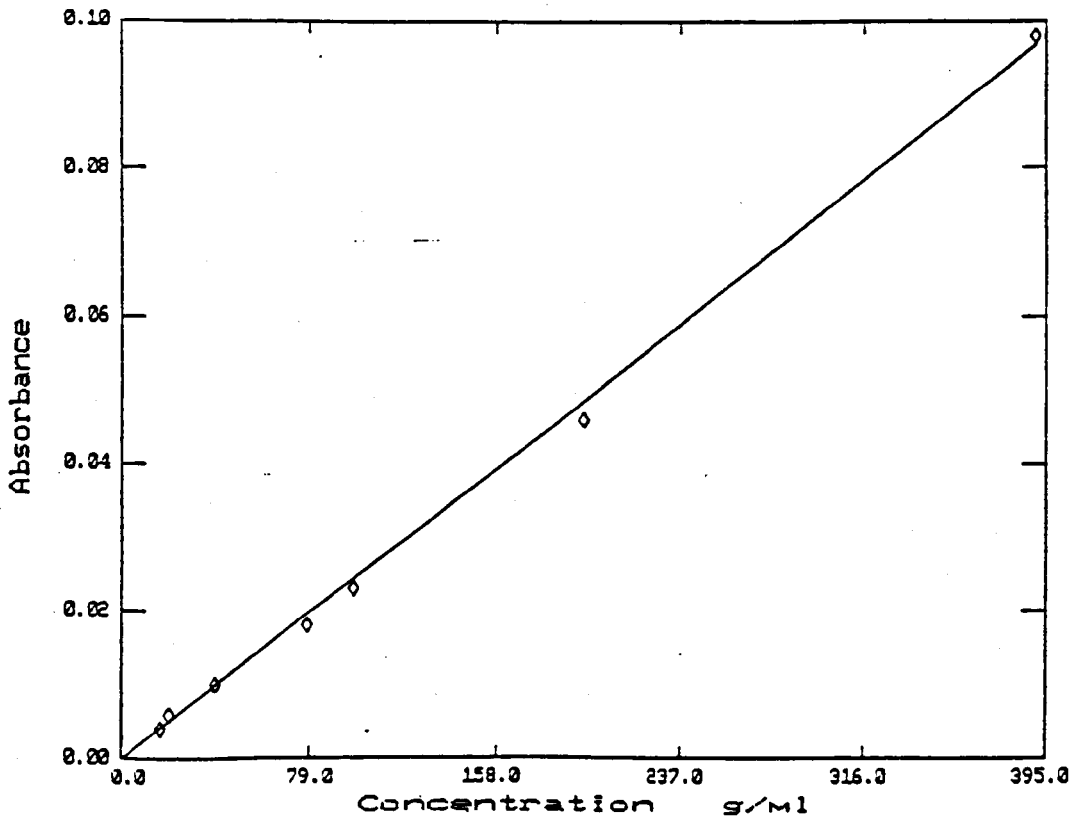


Figure 3.4 Plot of Atomic Absorbance vs Concentration of K₂PtCl₆.

In order to eliminate errors involved in preparing two solutions solid ligand was added to the K_2PtCl_4 solution. The ligand used in this and all the following trial experiments was 2-aminopyridine (2AP).

A 0.2M solution of K_2PtCl_4 (0.415g in 5 ml of water) was prepared and 0.188 g of 2AP added, and timing commenced. The reaction mixture was stirred and left to stand at room temperature and was sampled every thirty minutes over a period of three hours. The sampling procedure involved removing 200 μ l aliquots with a Gilson pipette and running this into 20 ml of water, thus resulting in a one hundred fold dilution of the original reacting mixture. Each of the samples were aspirated immediately and then put aside for aspiration again three hours later. This was done in order to establish quenching of the reaction.

Graphs of absorbance versus time were plotted (Figure 3.5).

The first point that was noted from these initial results was the small absorbance values compared to those expected. The sensitivity for Pt was approximately halved and this led to a subsequent halving of the dilution factor in all future experiments.

The plot of absorbance against time did not follow a smooth decay curve but was a scatter of points about the line. This was attributed to the Gilson pipette picking up precipitate, causing scattering of light in the flame and resulting in inconsistent absorbance readings. A reinforcing factor for this assumption was the occasional problems encountered due to the precipitate blocking the tip of the Gilson pipette. It was thought that this problem could be alleviated by carrying the reaction out in a centrifuge.

The values of absorbance for the retained samples were more or less identical to those aspirated immediately and it was concluded from this that the hundred fold dilution factor was adequate to produce a quenched system.

3.3.1.2 Trial Experiment II

A repeat of the previous experiment was carried out but several modifications were made. The dilution factor was halved to give a fifty fold dilution, achieved by running the 200 μ l aliquot into 10 ml of water. The reaction was carried out in a bench top centrifuge, spinning continuously at maximum speed. The centrifuge was switched off one minute prior to sampling and allowed to come to rest. It was hoped that this procedure would clear the supernatant and alleviate the problems caused by the precipitate. Sampling was carried out every five minutes over the initial stages of the reaction. The quenching of the system was checked in the same way as with the previous experiment and the results plotted on a graph of absorbance versus time (Figure 3.6).

It can be seen from these results that the fifty fold dilution quenched the reaction sufficiently and hence it was adopted as the dilution in all future work.

The results indicated that there appeared to be some sort of induction period of the start of the reaction, the Pt concentration in solution remaining constant for up to 45 minutes. The cause of this induction had to be identified and eliminated before the data could be used for kinetic analysis.

The factors considered as possible causes were centrifuging, supersaturation or possible aquation of K_2PtCl_4 in solution.

Centrifuging could have interfered with what was some sort of diffusion control process, or by removing the precipitate from the bulk of the reaction so quickly that no sites of nucleation were present for the formation of further precipitate, hence slowing the reaction down and introducing an essentially steady state period as indicated by the results.

Rund ⁽²⁷⁾ found that before K_2PtCl_4 undergoes substitution of chloride for ligand, the chloride is replaced by water in a solvolysis step. An incomplete, or not yet equilibrated aquation step would slow down the initial reaction and would indicate that a minimum period of aquation is required to eliminate the rate limiting step.

It was found easiest to test the effect of centrifuging by centrifuging just prior to sampling.

3.3.1.3 Effect of Centrifuging on the Induction Period

A repeat of the previous experiment was carried out but this time the reaction mixture was only centrifuged for one minute prior to sampling. The supernatant was cleared by this method but the diffusion control process, if present, would not be disturbed to any great extent.

Samples were taken at various time intervals, diluted, aspirated and a graph of absorbance versus time plotted (Figure 3.7)

The data obtained was not free from an induction period and this observation led to the conclusion that a diffusion control process was not responsible for the induction period. However it was decided to centrifuge for one minute prior to sampling in future experiments to clear the supernatant of finely divided, Pt-containing precipitate.

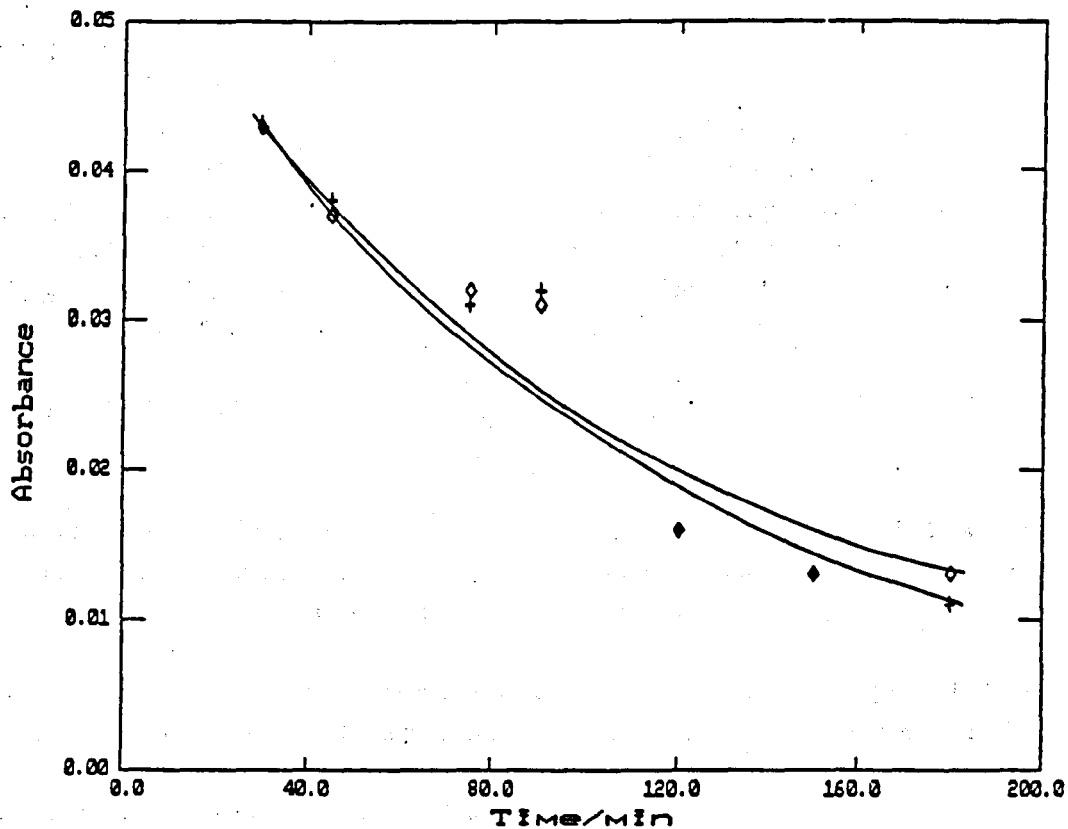


Figure 3.5 Plot of Atomic Absorbance vs Time for Trial Experiment I.

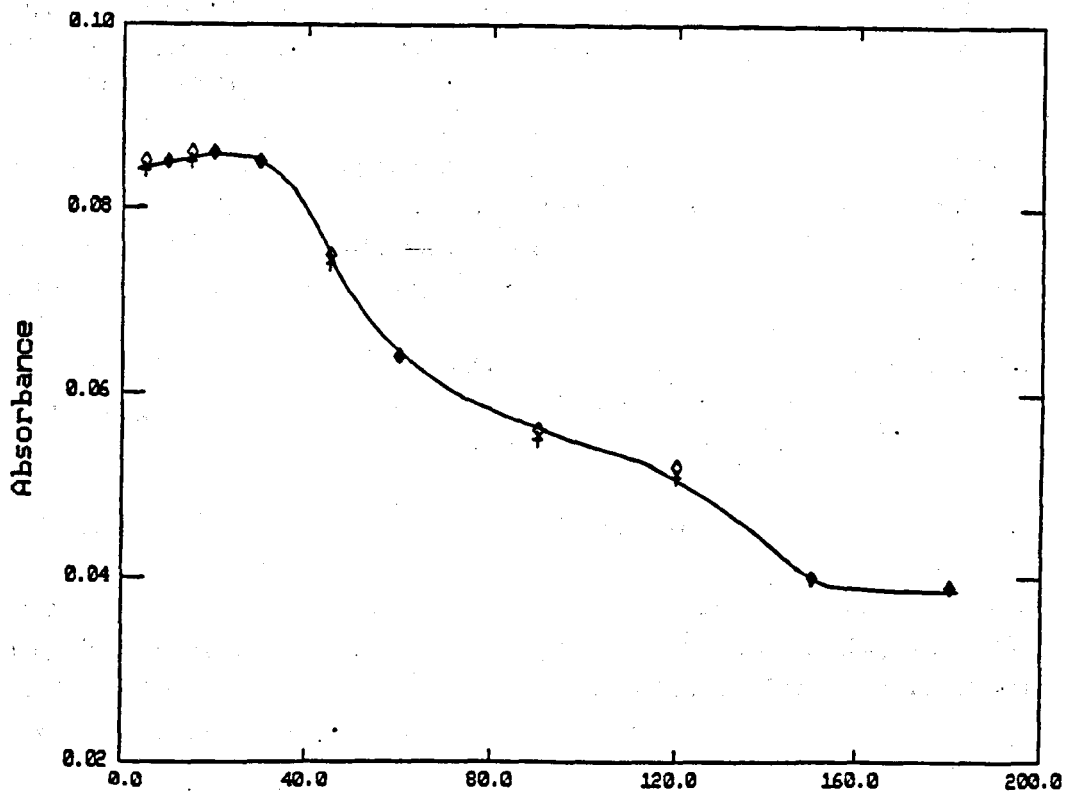


Figure 3.6 Plot of Atomic Absorbance vs Time for Trial Experiment II.

3.3.1.4 The Aquation of K_2PtCl_4

From a consideration of Rund's work it was now thought that the induction period was caused by incomplete aquation of K_2PtCl_4 . Rund found that the reaction between K_2PtCl_4 and ligand proceeds, like most substitution reactions of platinum (II), by a direct path and also by a path that involves intermediate incorporation of a molecule of solvent. Flikkema and Hammond⁽²⁰⁾ found that a chloride ligand of $PtCl_4^{2-}$ in its aqueous solution was replaced reversibly by H_2O with a reaction period of a few hours according to the reaction



They also found that the replacement of chloride by water was first order in $PtCl_4^{2-}$. This first order term arising from the solvent path to the product involving the slow attack by solvent followed by rapid displacement of solvent by substituting ligand.

The above is consistent with the observation that the reactions under investigation had an induction period. It was considered that preparation of the K_2PtCl_4 solution some time before the reaction with the hetero-cyclic base would eliminate the induction period and generate data amenable to investigation by initial rate and integral methods.

A 0.2M solution of K_2PtCl_4 was prepared and left to stand for two hours before the ligand was added, time zero was taken as the addition of ligand. The sampling and centrifuging processes, already developed, were adopted and the absorbance measured. A graph of absorbance versus time was plotted (Figure 3.7).

The data showed that an induction phase was still present but even with this short aquation time it was greatly reduced. These results looked quite promising and helped to confirm that the aquation of K_2PtCl_4 was the cause of the induction period. It was hoped that the induction period could be greatly minimised, or even lost, by increasing the time allowed for the aquation.

To measure the length of the aquation period required UV spectroscopy was used. The shift in position of λ_{max} was studied with the change of $PtCl_4^{2-} \rightarrow PtCl_3(H_2O)^-$.

3.3.1.5 Investigation of Aquation of K_2PtCl_4 by UV Spectroscopy

A dilute solution of K_2PtCl_4 was prepared and its UV spectrum measured at various time intervals over a period of four days. It was found that after a period of forty eight hours the position of λ_{max} changed quite significantly from 328 nm to 317 nm (Figure 3.8). Thereafter no further shifts were observed and it may be assumed that the aquation reaction:

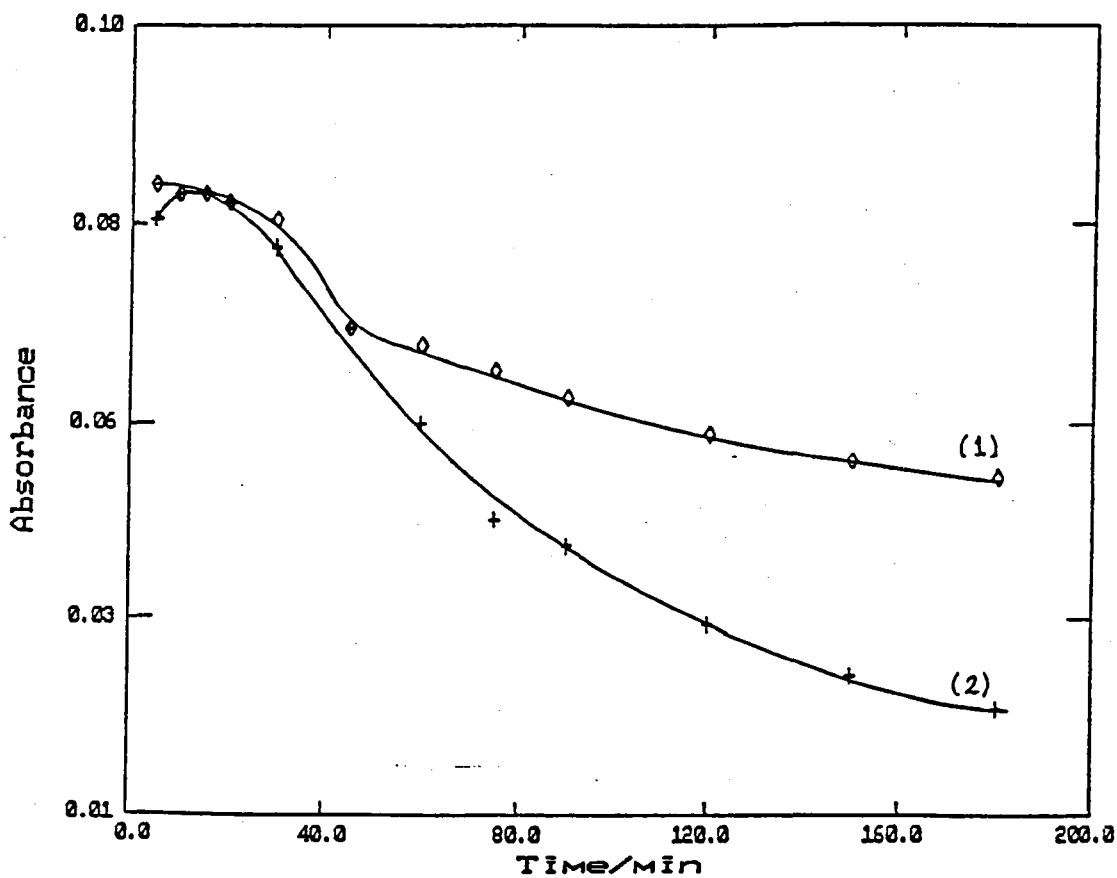


Figure 3.7 Effect of (1) Centrifugation and (2) Aqation on Plot of Atomic Absorbance vs Time.

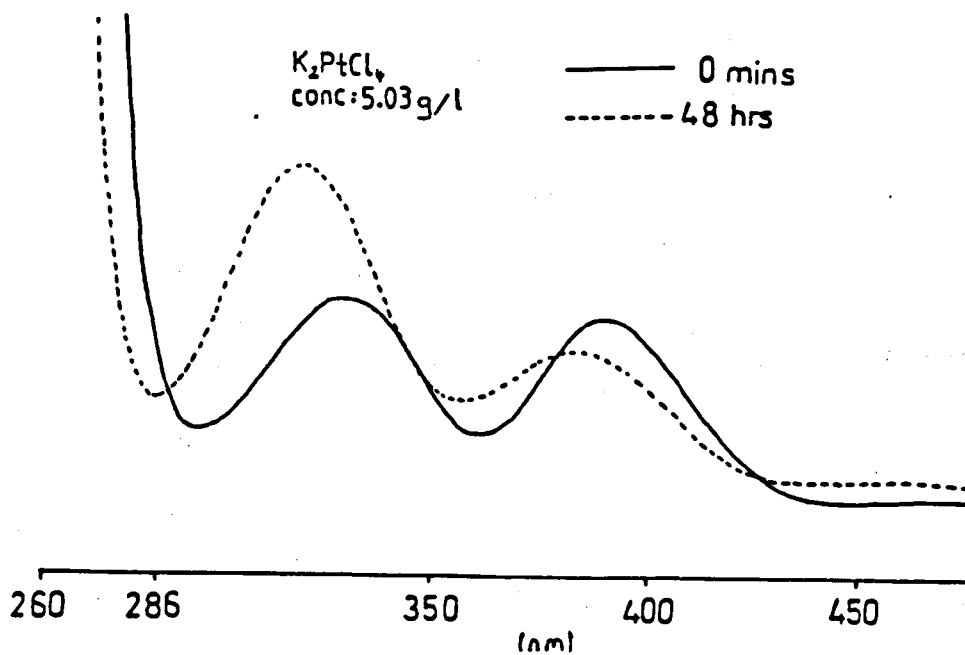


Figure 3.8 Shift in the Position of λ_{max} after 48 Hour Aquation Period.

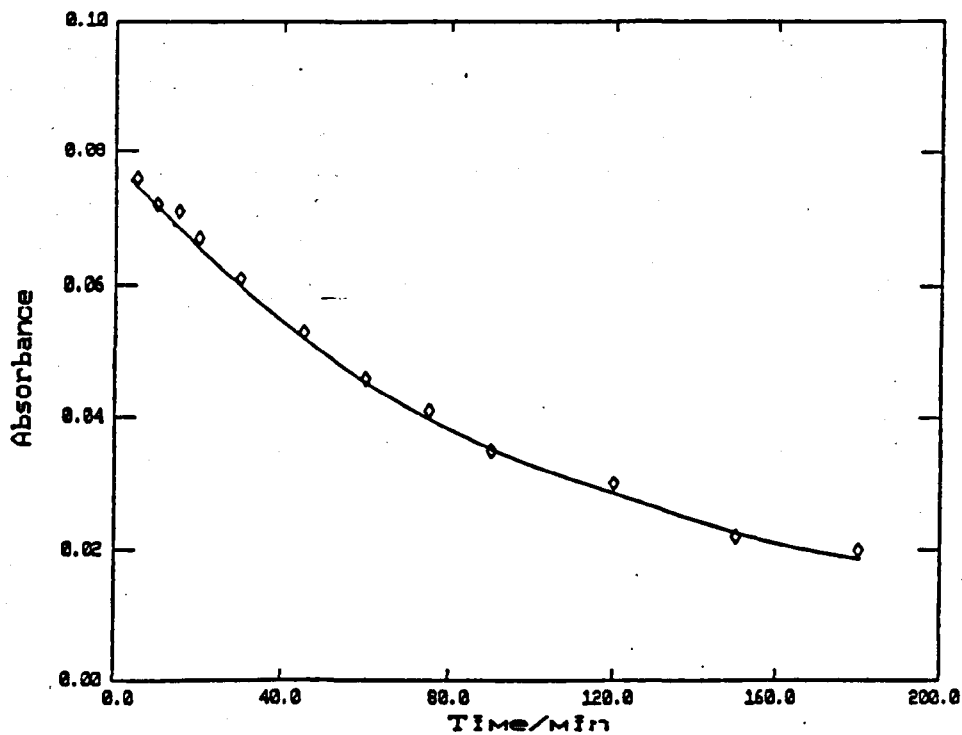
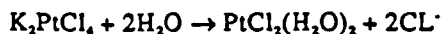


Figure 3.9 Effect of 48 Hour Aquation on Plot of Atomic Absorbance vs Time.



was completed within forty eight hours. It may also be assumed that because of the very high water concentration the above hydrolysis reaction is 100% to the right at this stage.

3.3.1.6 Effect of 48 Hour Aqueation on Induction Period

The experiment carried out in section 3.3.1.3 was repeated with the exception of the time allowed for aqueation. A 0.2M solution of K_2PtCl_4 was prepared forty eight hours in advance before the addition of the solid ligand. The results are plotted on an absorbance versus time graph (Figure 3.9).

It can be seen from the results that the induction period has effectively been removed and a normal type of decay curve was obtained.

The development of the method had now reached a stage where the results were of the standard required for kinetic analysis.

3.3.1.7 Summary of Development Method

A 0.2M solution of K_2PtCl_4 was prepared forty eight hours in advance. The K_2PtCl_4 solution and ligand were then mixed, the ligand as a solid or liquid. This point corresponded to time zero. The reaction mixture was thermostated in a water bath at a constant temperature. One minute prior to sampling the reaction mixture was centrifuged. A 200 μ l aliquot was removed from the reacting mixture using a 200 μ l Gilson pipette. The aliquot was then added to 10 ml of water resulting in a fifty fold dilution. The diluted sample was aspirated, the absorbance measured, corrected with respect to standard spectrasol platinum solution and a graph of absorbance versus time plotted.

Atomic Absorption Parameters

Atomic absorption measurements were carried out on a Perkin Elmer 2280 AA spectrophotometer using the following conditions:

Wavelength	265.9 nm
Slit setting	0.7 nm
Light source	Hollow cathode lamp
Flame type	Air- acetylene oxidising (lean, blue)

3.3.2 Development of Ultraviolet Spectroscopic Method

It was envisaged that the complementary AA and UV spectroscopic methods of monitoring the kinetics of formation in solution would eventually be carried out simultaneously. Consequently much of the experimental method already developed for AA was incorporated into the UV methodology. This included the preparation of a 0.2 M solution of K_2PtCl_4 , forty eight hours in advance and centrifuging one minute prior to sampling. However it was still necessary to investigate certain factors, such as the dilution required, determination of the most suitable wavelength, and to check that the UV absorbance of the ligand varied linearly with its concentration.

As the UV technique was to involve measurement of the ligand at a fixed wavelength (λ), the first problem was to find the most suitable value of λ . A 0.4M solution of 2-aminopyridine (2AP) was prepared and subsequent dilutions carried out until a UV spectrum was obtained which was on scale. It was found that the original 0.4M solution, which corresponded to the concentration of 2AP required for the reaction $K_2PtCl_4 + 2AP$, needed to be diluted one thousand times. The UV spectrum of 2AP, is given in Figure 3.10 and it can be seen that it gives rise to two peak maxima at 286 nm and 226 nm. As UV spectroscopy was to be implemented to monitor the decrease in ligand concentration, it was necessary to ensure that there was no contribution to the absorbance value from the K_2PtCl_4 in solution. The same 1 000 fold dilution of a 0.2 M solution of K_2PtCl_4 , was carried out and its UV spectrum obtained (Figure 3.11). It can be seen that although the K_2PtCl_4 solution absorbs strongly at a wavelength less than 250 nm, at the required dilution the absorbance above 250 nm can be considered negligible. Consequently it was decided that provided the aliquot removed from the reaction mixture was diluted a thousand fold then the change in absorbance of 2AP could be monitored at the fixed wavelength of 286 nm.

UV spectra (Fig 3.12) were obtained for the other five ligands and the most suitable value of λ chosen in order to carry out fixed wavelength measurements (table 3.3).

TABLE 3.3

UV Wavelengths of Ligands

Ligand	2AP	2APm	Pm	Py	AMPm	Pu
λ /nm	286	291	245	255	286	267

The next stage was to ensure that the UV absorbance of the ligand varied linearly with its concentration. For each of the six ligands several standard solutions were prepared in the concentration range 0.4×10^{-4} - 0.4×10^2 , and the UV absorbance at each concentration measured. Graphs of UV absorbance versus concentration were plotted (Fig 3.13). The results prove that the Beer-Lambert Law is obeyed in each case and thus making it possible to monitor the kinetics by measuring the UV absorbance of the ligand.

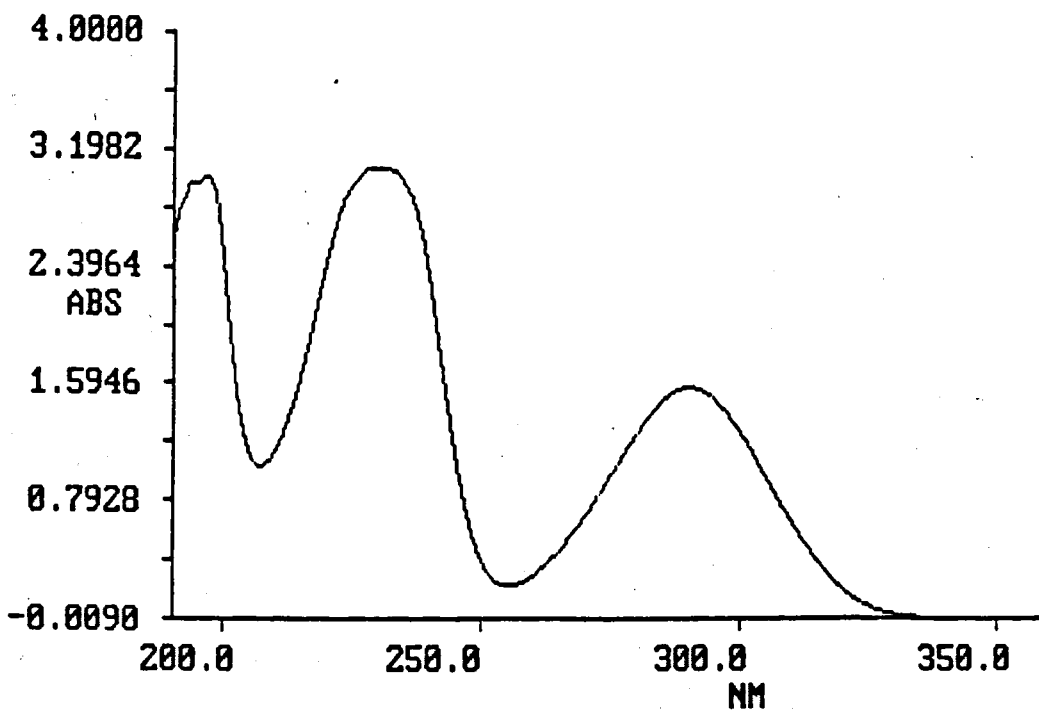


Figure 3.10 UV Spectrum of 2-aminopyridine.

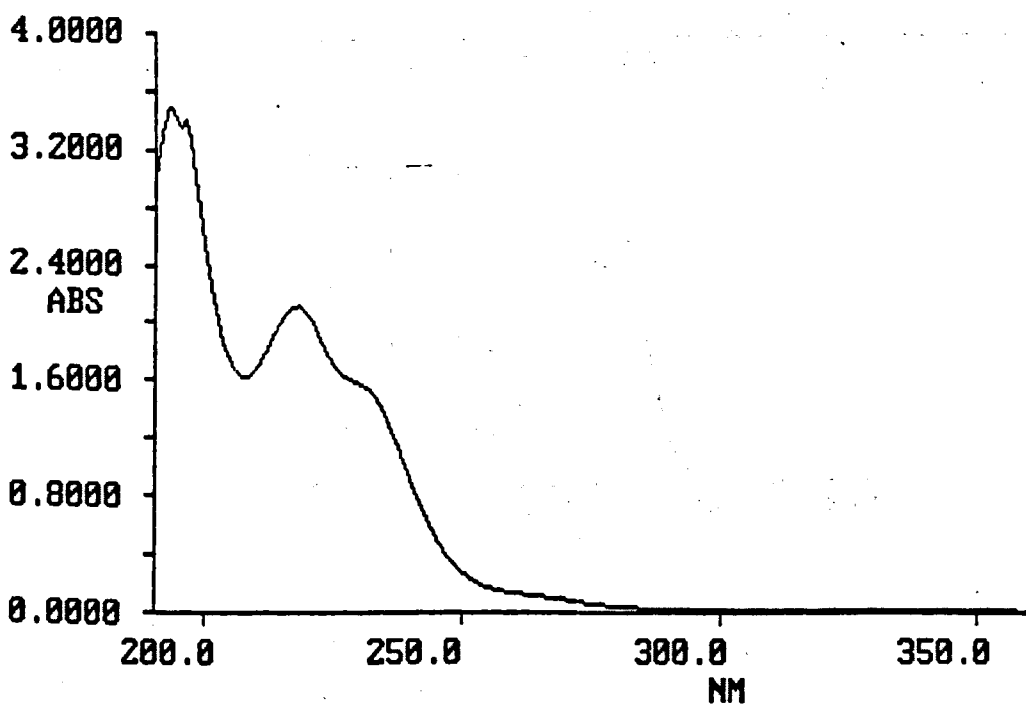


Figure 3.11 UV Spectrum of K_2PtCl_6 .

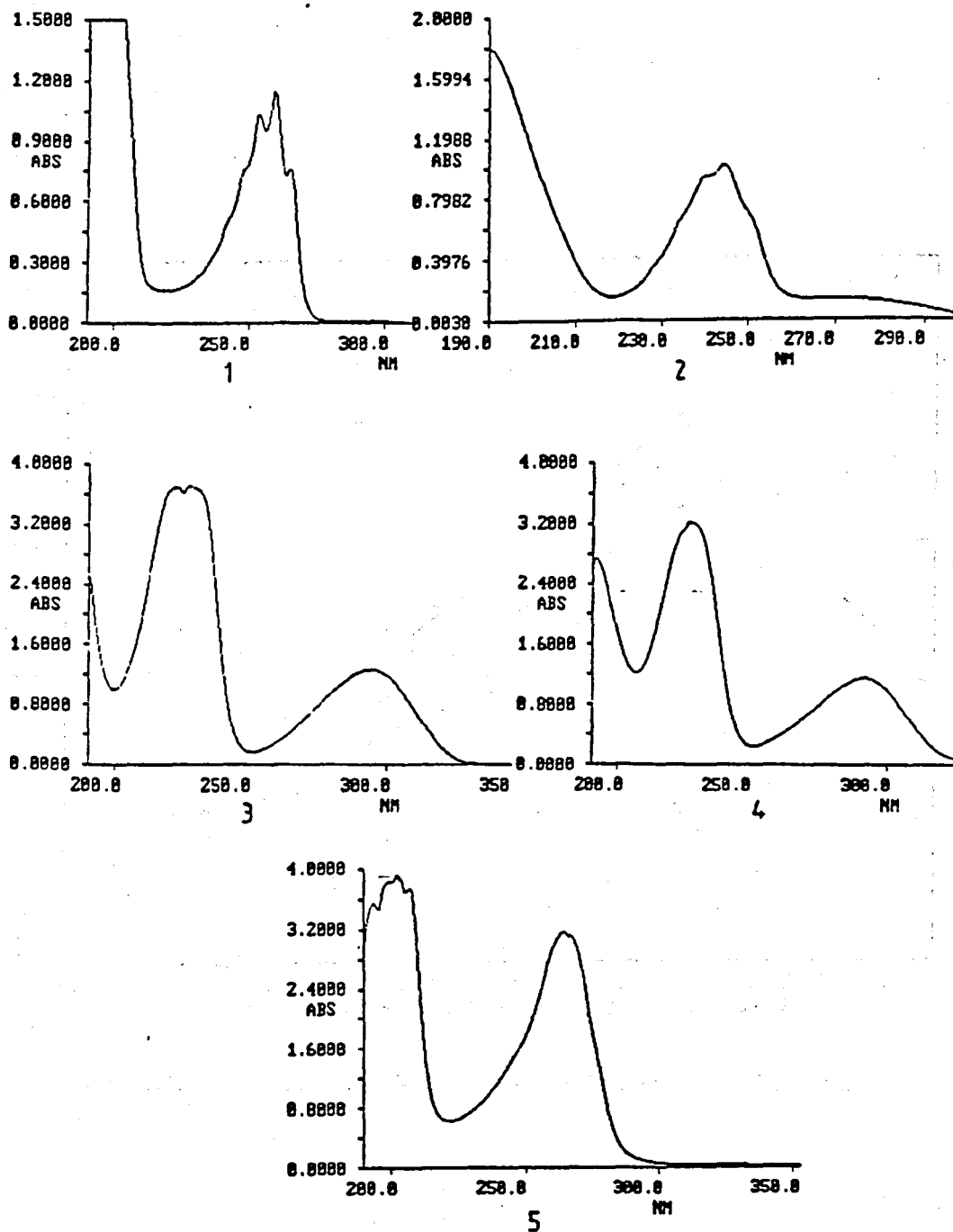


Figure 3.12 UV Spectra of (1) 2-aminopyrimidine (2) pyridine (3) pyrimidine (4) 2-amino-4-methylpyrimidine and (5) purine.

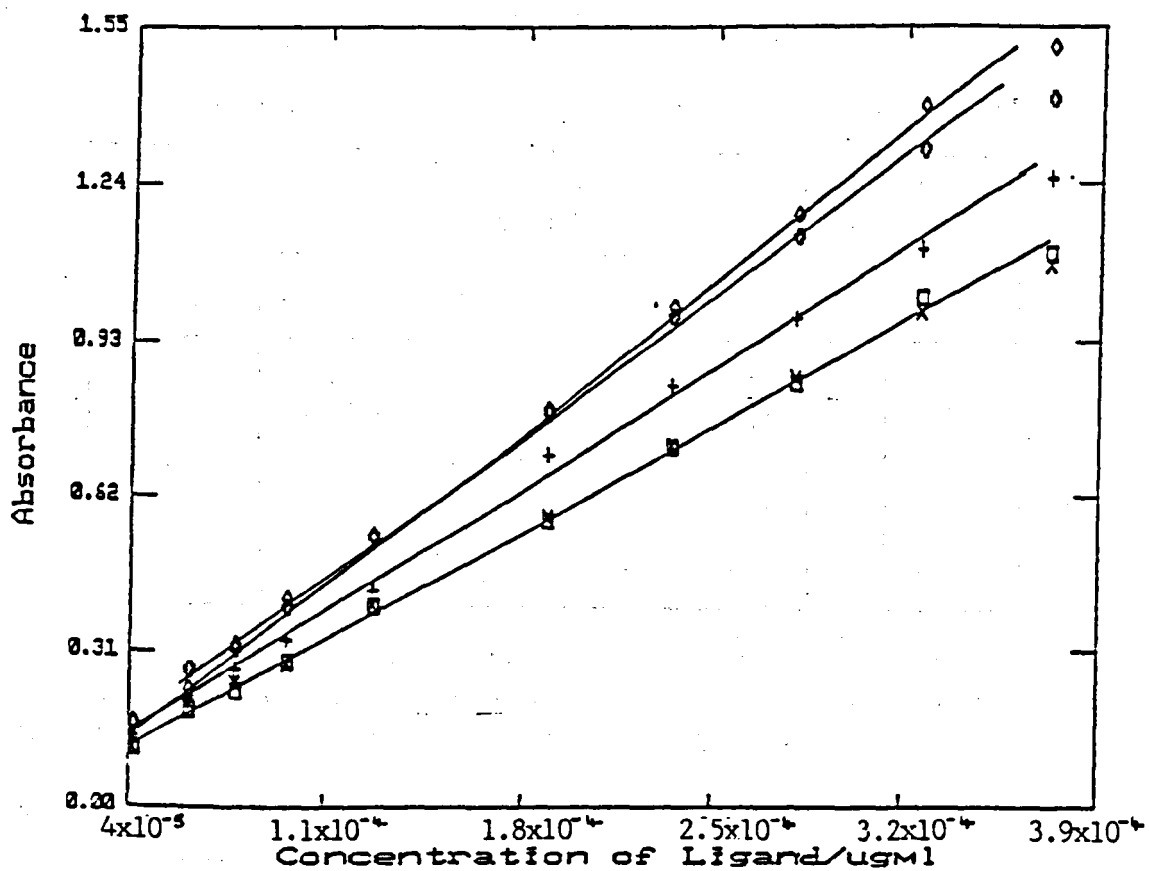


Figure 3.13 Plots of UV Absorbance vs Concentration of Ligand.

As has previously been mentioned a thousand fold dilution was required to bring the absorbance of the ligand on scale. This meant that a further modification was required to the sampling method already adopted for the AA technique. Here 200 µl aliquots were removed and added to 10 ml of water (50 fold dilution), it was decided that, to obtain the necessary 1 000 fold dilution to remove a 1 ml aliquot from the already quenched solution and add this to 20 ml of water. As two successive dilutions were now required it was thought necessary to test the reproducibility of such a method. A 0.4M solution of each ligand was prepared and the above dilute procedure carried out. The UV absorbance of each dilute solution was measured four times and the absorbance values averages. This was repeated four times for each ligand and the standard deviation calculated (Table 3.4).

TABLE 3.4

Standard Deviations Calculated from UV Absorbance of Diluted Solutions of each Ligand.

Ligand	Std. Dev. of each solution x 10 ⁴				Std. Dev. of four solutions x 10 ⁴
	1	2	3	4	
2AP	6.16	6.38	6.25	6.50	1.54
2APm	6.08	5.99	5.82	6.11	1.32
Py	6.08	6.10	6.09	6.12	1.68
Pm	6.13	6.24	6.19	6.23	1.47
AMPm	6.41	6.32	6.38	6.37	1.90
Pu	6.11	6.19	6.09	6.13	1.92

The standard deviation for the absorbance readings performed on the one solution reflected the reproducibility of the spectrophotometer, whereas the standard deviation of the mean readings for all four solutions reflected the reproducibility of the sampling technique.

On the basis of the above results it was concluded that although the UV sampling method required an additional dilution step the results obtained were still reproducible.

One final check was carried out and that was to ensure that the absorbance of the ligand in solution did not vary with time. 0.4M solutions of each ligand were prepared and the UV absorbance measured, after dilution, over a period of three hours. The results confirmed that the absorbance of ligand in solution did not vary with time.

A trial experiment to establish that UV spectroscopy was a valid method for monitoring kinetic parameters was carried out on the reaction between K_2PtCl_4 and 2AP. To an aged solution of K_2PtCl_4 (0.2M, 48 hours) 0.188 g of 2AP were added. At various time intervals 200 μ l aliquots were withdrawn and added to 10 ml water, a 1 ml aliquot was then removed from this solution and added to 20 ml of water. This latter solutions was magnetically stirred for a couple of minutes, the UV absorbance measured and a graph of absorbance versus time plotted (Fig 3.14). The data obtained gave rise to a similar decay curve to that obtained from the AA spectroscopic method.

3.4 Method of Simultaneous AA and UV Measurement

The reaction between K_2PtCl_4 and ligand was initiated by adding ligand to a thermostated aged solution of K_2PtCl_4 , so that the molar ratio was 2 : 1 respectively.

Time zero was taken as the addition of the ligand. Aliquots (200 μ l) were withdrawn at various time intervals after centrifuging for one minute and pipetted into 10 ml of water resulting in a 50 fold dilution. This sample was aspirated and the absorbance of $PtCl_4^{2-}$ remaining in the reacting solution recorded. Further dilution was carried out by pipetting 1 ml into 20 ml of water, and the absorbance of the ligand remaining in the reacting solution was measured by at a fixed UV wavelength.

The order of reaction was determined by monitoring a number of experiments, each time varying the initial concentration of the two reactants. All experiments were carried out at a fixed temperature of 313K. Initial rate studies were carried out using the following variation in initial reactant concentration.

- | | | |
|---------------------|---|-------------|
| 1) 0.2M K_2PtCl_4 | : | 0.4M Ligand |
| 2) 0.2M K_2PtCl_4 | : | 0.3M Ligand |
| 3) 0.2M K_2PtCl_4 | : | 0.8M Ligand |
| 4) 0.4M K_2PtCl_4 | : | 0.4M Ligand |

The reactions were followed for approximately thirty minutes and both the AA and UV absorbances measured. Graphs of absorbance versus time were plotted and the tangent to the initial slopes drawn. The gradient of this tangent corresponds to the rate constant for the initial stage of the reaction for that particular concentration. The log of this rate constant was then plotted against the log of the initial concentration of the ligand and the rate constant and order determined from the intercept and slope respectively.

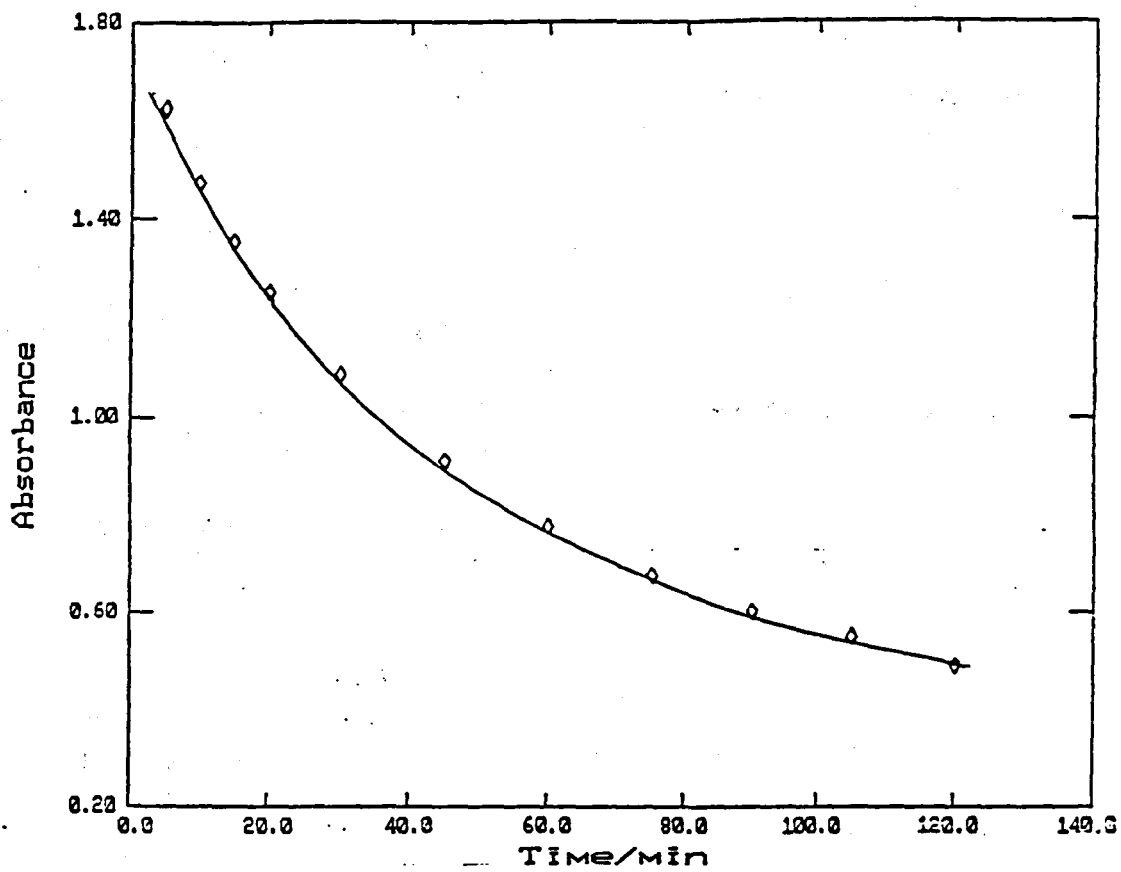


Figure 3.14 Plot of UV Absorbance vs Time for Reaction between K_2PtCl_6 and 2-aminopyridine.

Having established the overall order of reaction, the rate constants were determined using integrated rate equations. In these cases the reaction was monitored by UV and AA spectroscopy over at least two half-lives and a plot of absorbance versus time plotted. The experimental variation of concentration versus times was then compared to the first and second order rate equations by plotting $\ln(\text{Abs})$ versus time and $1/\text{Abs}$ versus time respectively as necessary.

The slopes of these graphs yield the rate of reaction (k).

Experiments were carried out at several different but constant temperatures and the rate constant calculated for each temperature. The activation energy could then be calculated by applying the Arrhenius equation

$$\ln(k) = E/RT + \text{Constant} \quad (i)$$

For each ligand investigated a graph of $\ln(k)$ versus $1/\text{Temp}$ was plotted and the activation energy determined from the slope $E_{\text{act}} = \text{slope} \times R$.

The entropy of activation, ΔS , was determined from the intercept of the Arrhenius plot, since the constant in equation (i) is represented by

$$\text{Constant} = \text{Intercept} = \ln \left(\frac{kT}{h} \right) + \frac{\Delta S}{R} \quad (h)$$

where k = Boltzmann Constant
 T = Room temperature
 h = Planck's Constant
 R = Universal Gas Constant

Thus $\ln(kT/h)$ can be regarded as virtually constant and ΔS can therefore be determined from the equation:

$$\Delta S = R (\text{Intercept} - \ln \frac{kT}{h})$$

3.5 Results

For the reactions between K_2PtCl_6 and each ligand the initial rate results and the integrated rate equation results are reported graphically. The rate constants have been calculated and Arrhenius plots drawn in order to determine the activation energy and entropy values for each reaction. The raw data for each experiment are appended.

3.5.1 Initial Rate Results

The initial rate studies were carried out using the following variation in initial reactant concentration:

- (i) 0.2 m K_2PtCl_4 : 0.4 m Ligand
- (ii) 0.2 m K_2PtCl_4 : 0.8 m Ligand
- (iii) 0.2 m K_2PtCl_4 : 0.3 m Ligand
- (iv) 0.4 m K_2PtCl_4 : 0.4 m Ligand

The reactions were monitored using both AA and UV spectroscopy. The plots of absorbance against time are shown in Figures 3.15 to 3.23.

Tables 3.5 and 3.6 lists the gradients of the tangents to the initial slopes from the various initial reactant concentrations obtained from AA and UV spectroscopic methods respectively.

TABLE 3.5

Initial Rate Results from AA Spectroscopy.

Ratio	Initial rate ($10^3/\text{min}^{-1}$) for each ligand				
K_2PtCl_4 : Ligand	2AP	2APm	Py	AMPm	Pu
1 : 2	1.54	2.43	11.45	2.47	5.86
1 : 3	1.10	1.89	8.57	1.86	4.44
1 : 4	3.30	4.77	22.75	4.79	11.60
2 : 2	3.35	4.95	22.21	4.77	11.60

TABLE 3.6

Initial Rate Results from UV Spectroscopy

Ratio	Initial rate ($10^3/\text{min}^{-1}$) for each ligand			
K_2PtCl_4 : Ligand	2APm	Py	AMPm	Pu
1 : 2	15.88	26.72	14.32	37.35
1 : 3	11.79	20.09	10.75	27.94
1 : 4	30.25	56.64	28.13	72.17
2 : 2	30.32	56.45	28.10	75.57

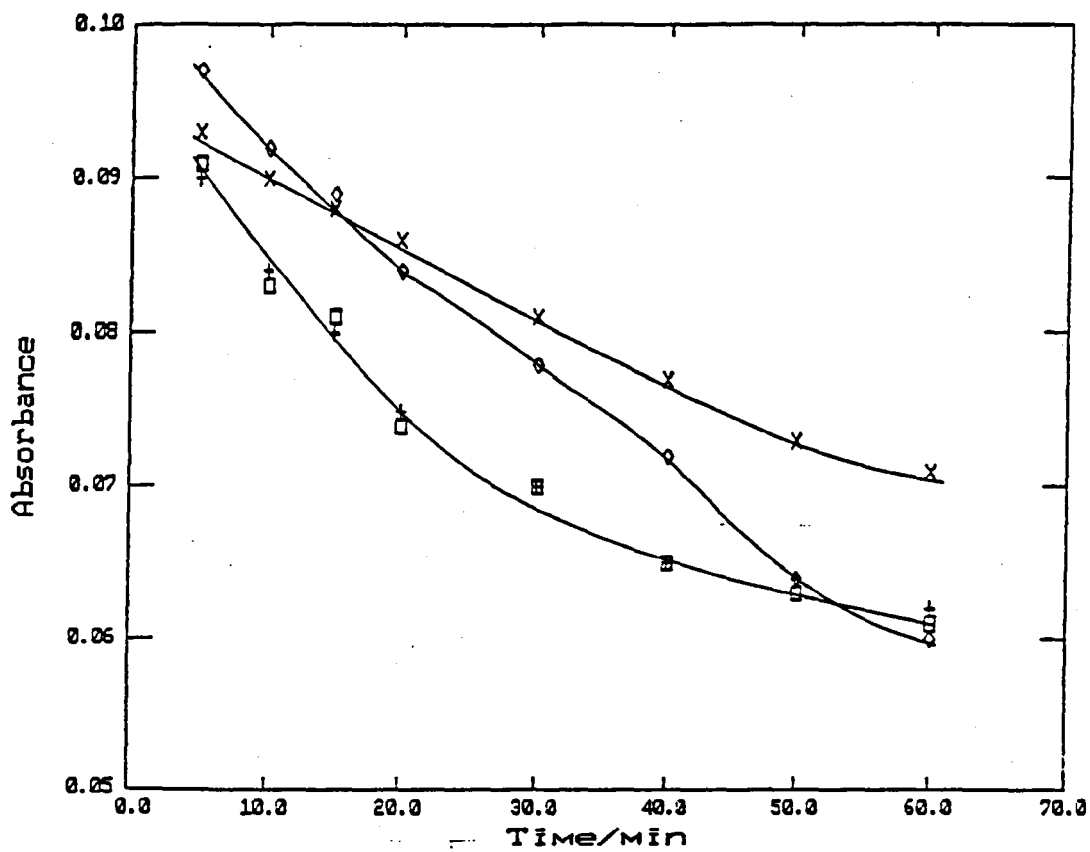


Figure 3.15 Plots of Atomic Absorbance vs Time for Reactions between K_2PtCl_6 and 2-aminopyridine with Different Initial Concentrations.

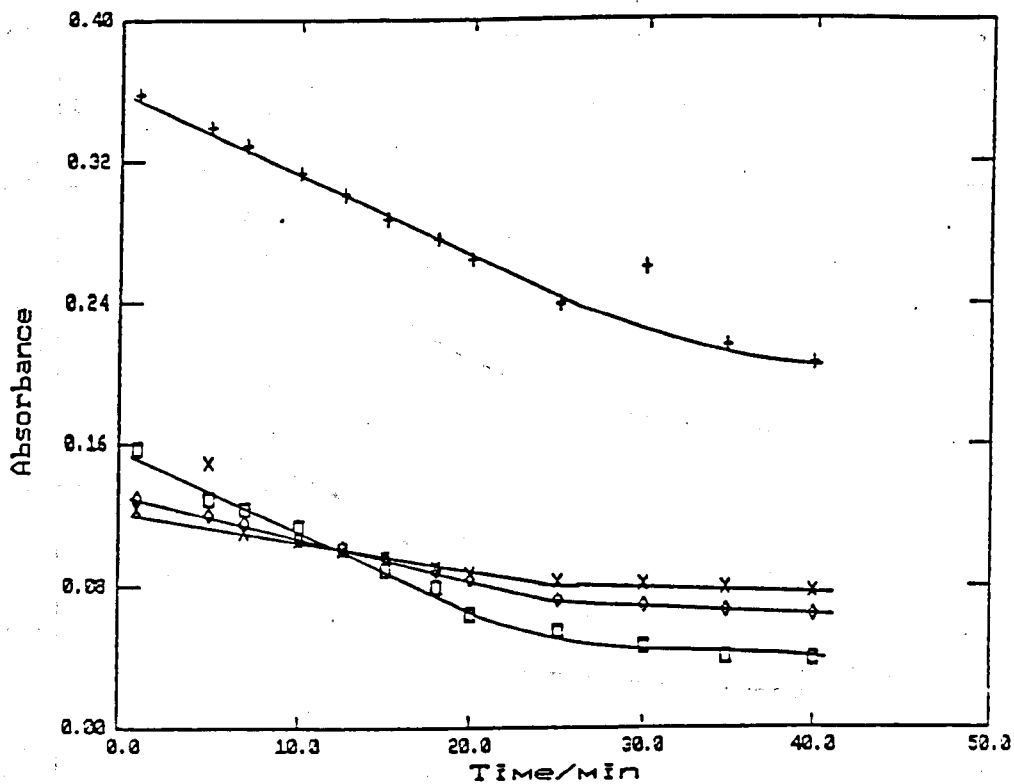


Figure 3.16 Plots of Atomic Absorbance vs Time for Reactions between K_2PtCl_6 and 2-aminopyrimidine with Different Initial Concentrations.

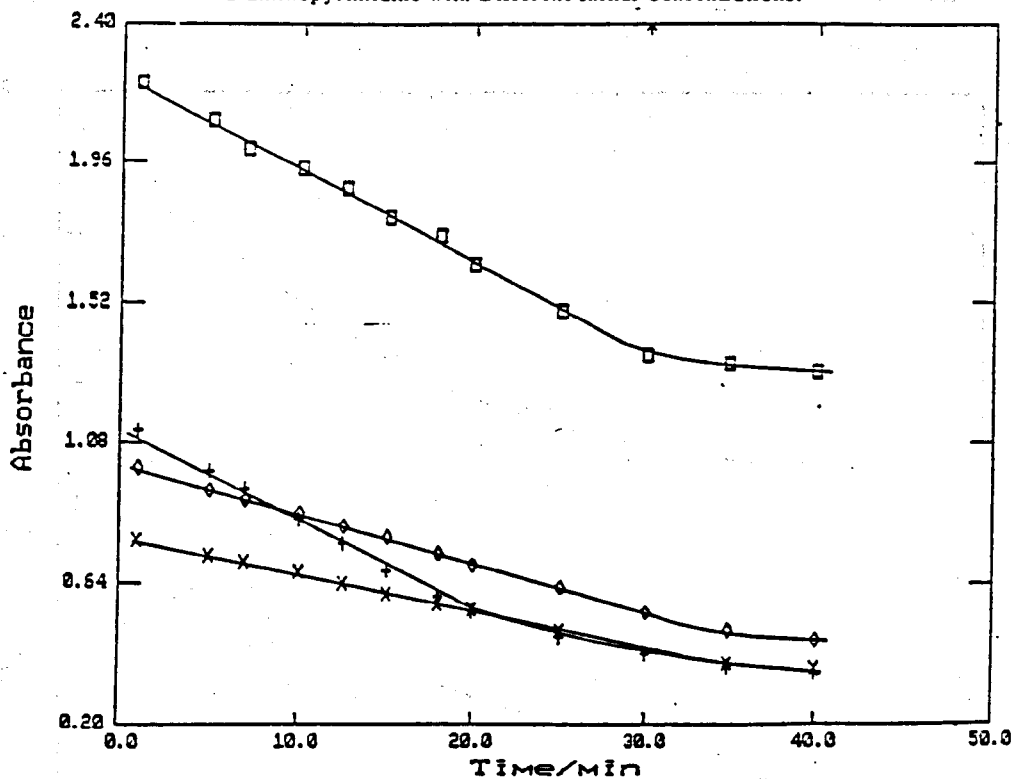


Figure 3.17 Plots of UV Absorbance vs Time for Reactions between K_2PtCl_6 and 2-aminopyrimidine with Different Initial Concentrations.

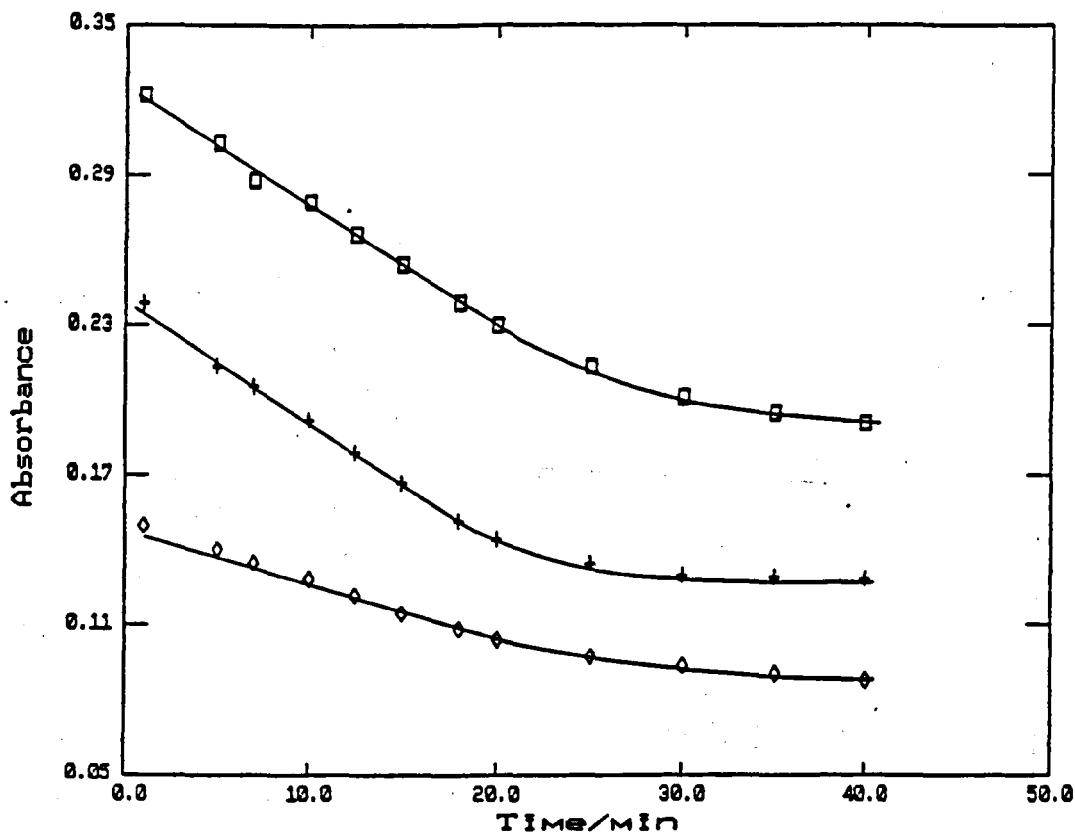


Figure 3.18 Plots of Atomic Absorbance vs Time for Reactions between K_2PtCl_6 and Pyridine with Different Initial Concentrations.

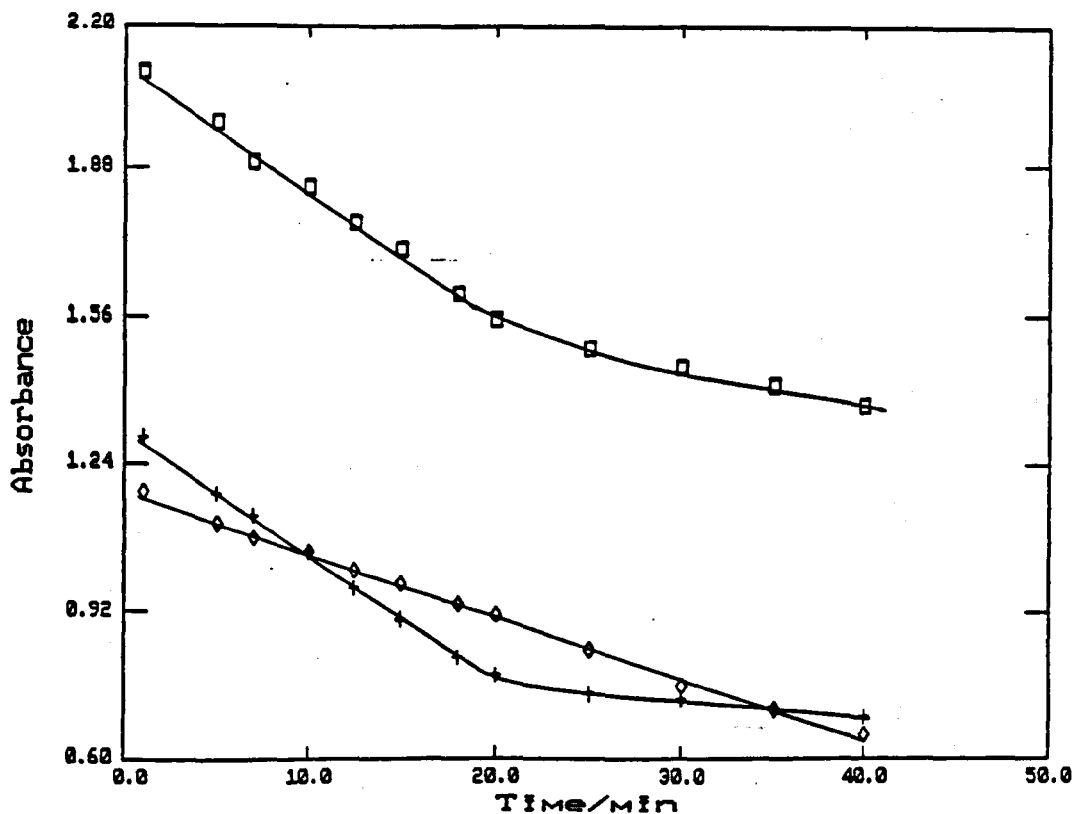


Figure 3.19 Plot of UV Absorbance vs Time for Reactions between K_2PtCl_6 and pyridine with Different Initial Concentrations.

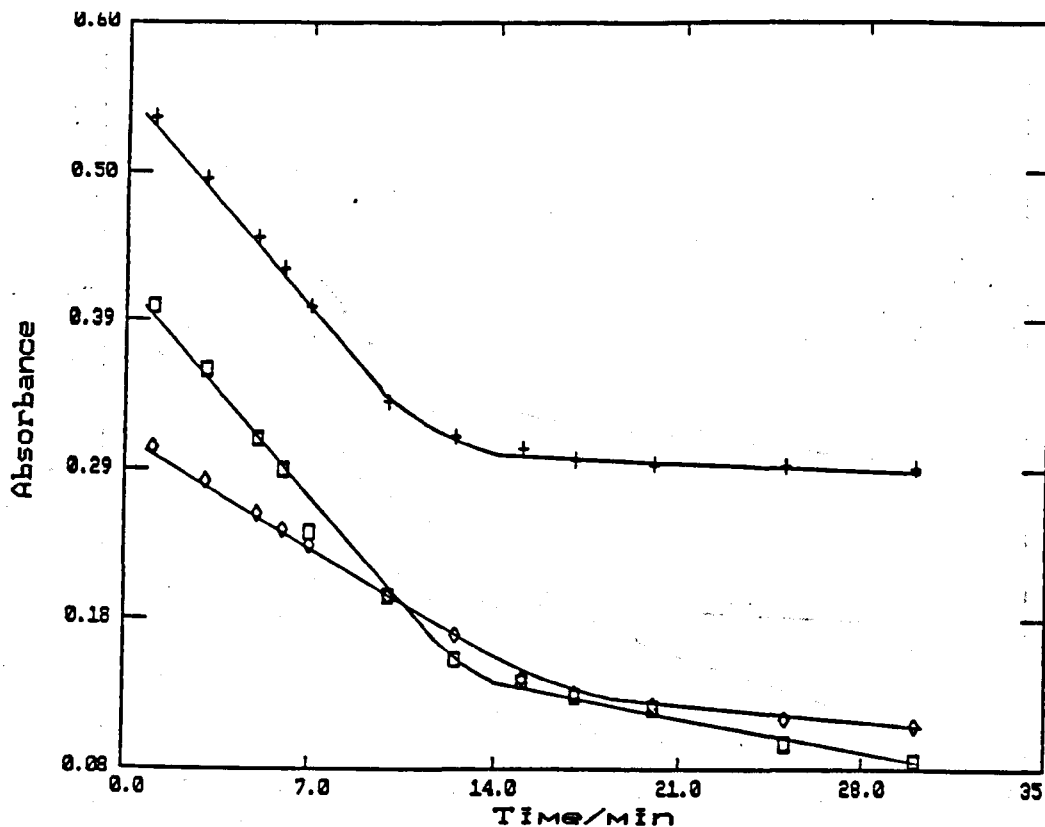


Figure 3.20 Plots of Atomic Absorbance vs Time for Reactions between K_2PtCl_6 and 2-amino-4-methylpyrimidine with Different Initial Concentrations.

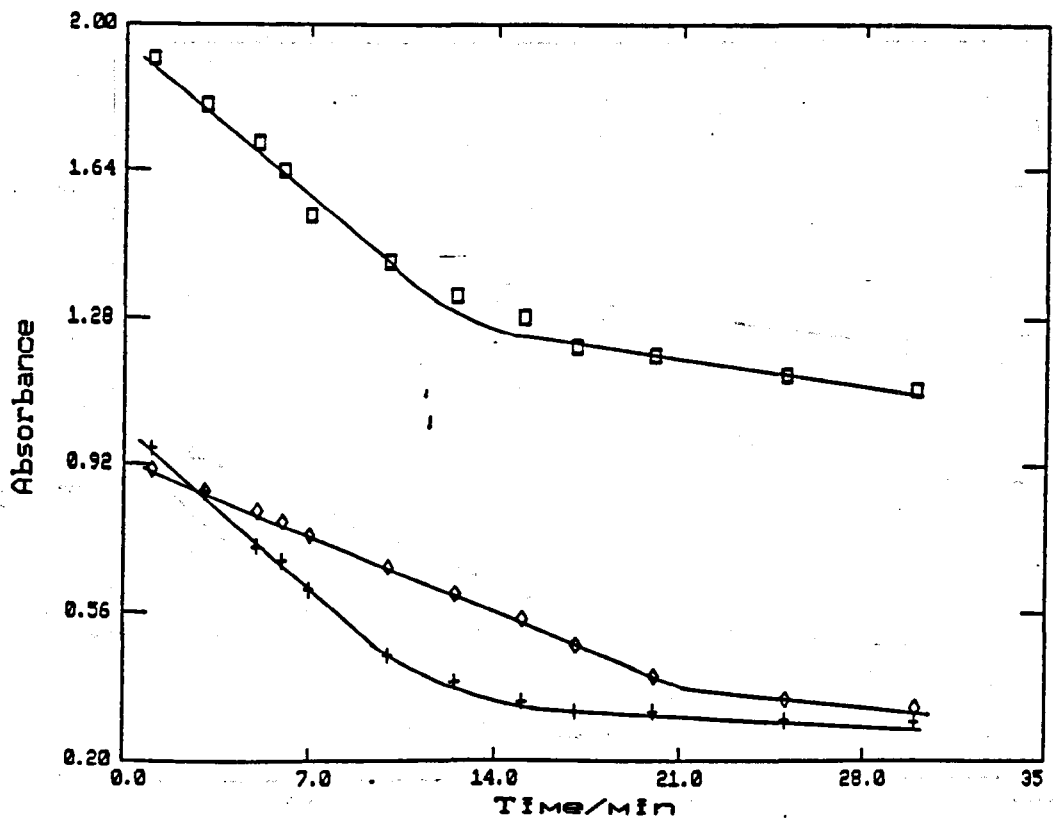


Figure 3.21 Plots of UV Absorbance vs Time for Reactions between K_2PtCl_6 and 2-amino-4-methylpyrimidine with Different Initial Concentrations.

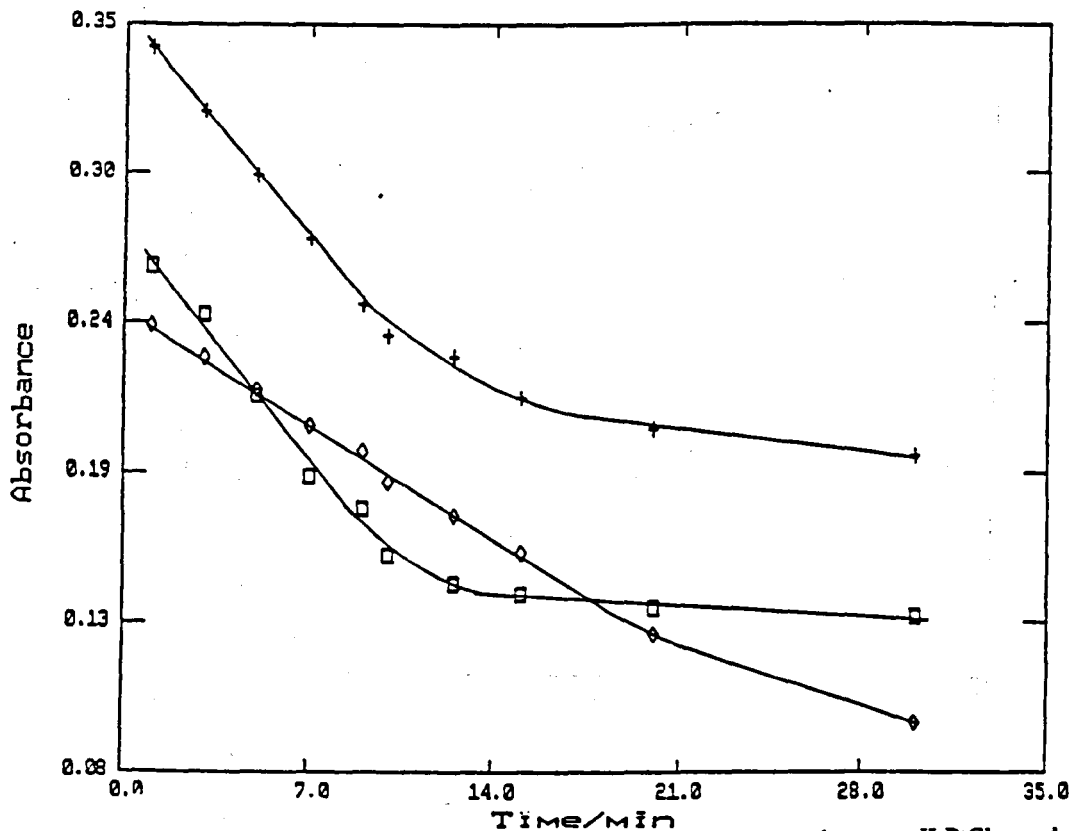


Figure 3.22 Plots of Atomic Absorbance vs Time for Reactions between K_2PtCl_6 and Purine with Different Initial Concentrations.

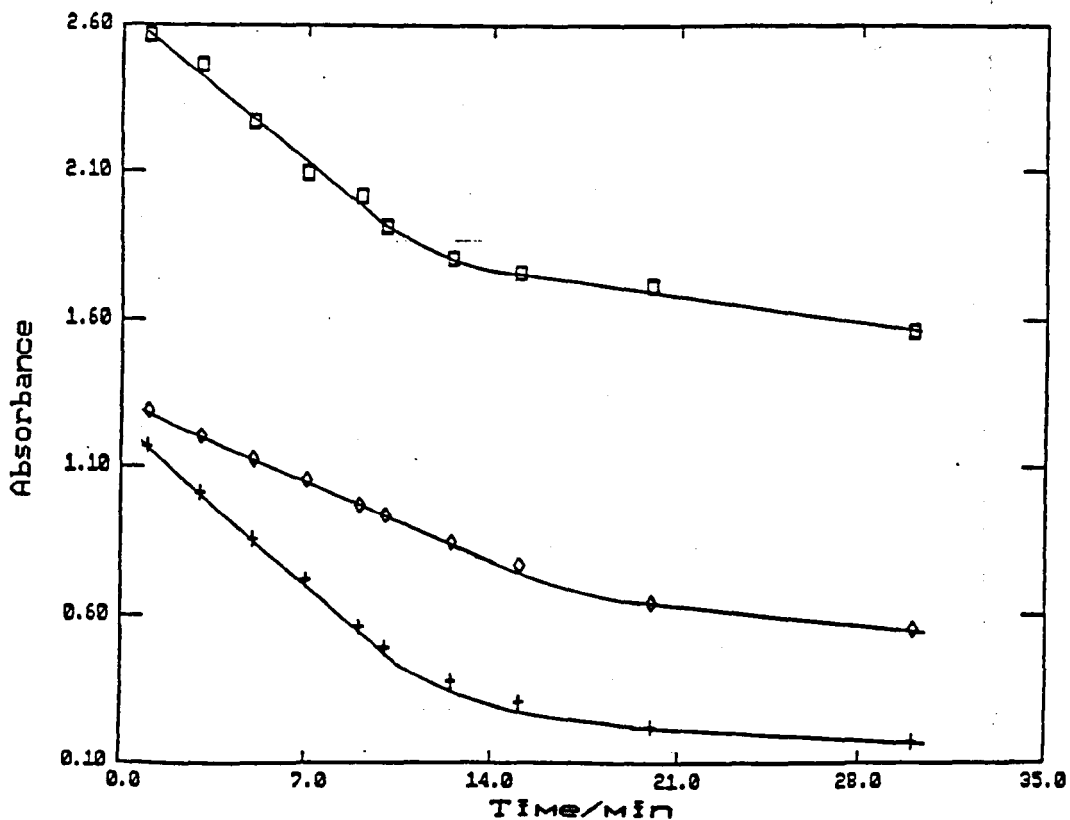


Figure 3.23 Plots of UV Absorbance vs Time for Reactions between K_2PtCl_6 and purine with Different Initial Concentrations.

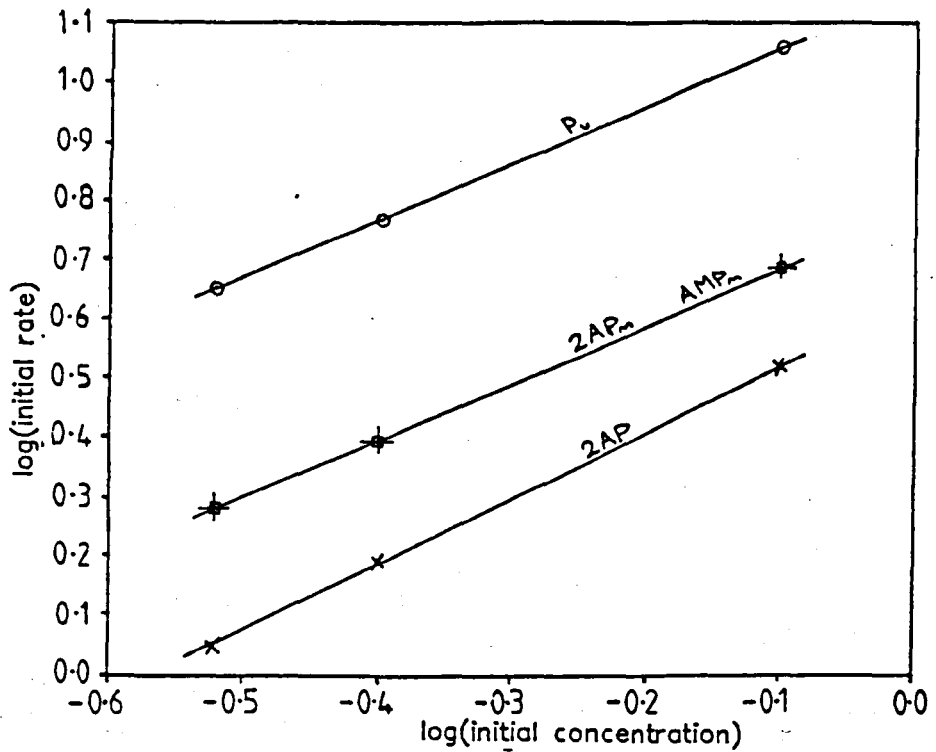


Figure 3.24 Typical Plots of $\log(\text{Initial Rate})$ vs $\log(\text{Initial Concentration})$ obtained from AA Studies.

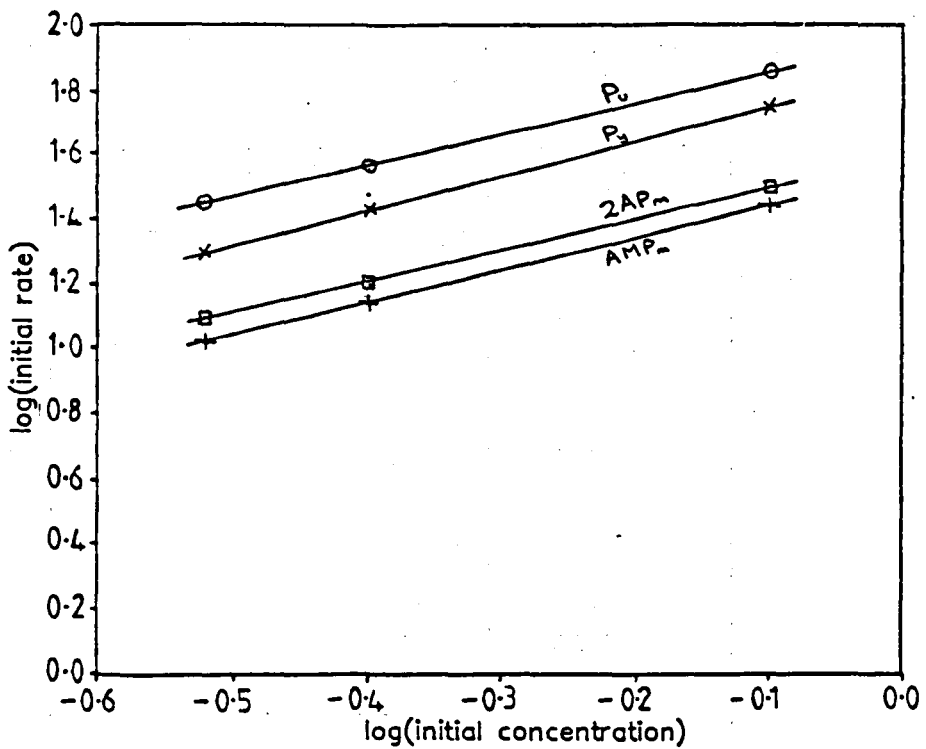


Figure 3.25 Typical Plots of $\log(\text{Initial Rate})$ vs $\log(\text{Initial Concentration})$ obtained from UV studies.

Graphs of log (initial rate) versus log (initial concentration of ligand) were plotted (Typical plots are shown in Figures 3.24 and 3.25) and in each case the slope was found to be 1 ± 0.09 .

It can also be seen from the above results that when the initial concentration of K_2PtCl_4 was doubled the initial rate of reaction also doubled.

These observations indicate that the reaction is first order with respect to the ligand and is also first order with respect to K_2PtCl_4 . Thus the form of the rate equation is:

$$\text{Rate} = k [K_2PtCl_4] [\text{Ligand}]$$

3.5.2 Integrated Rate Equation Results

Since the overall order had been established from initial rates, second order rate constants were therefore obtained from plots of $1/\text{absorbance}$ versus time (Figures 3.26 to 3.36). Rate constants obtained at various temperatures allowed use of the Arrhenius equation to calculate the activation energy and entropy. Tables 3.7 - 3.12 show the variation in second order rate constants with temperature for each reaction investigated.

TABLE 3.7

Second Order Rate Constants Obtained from the Reaction
between K_2PtCl_4 + 2-aminopyridine

Temperature/k	Rate Constant/min ⁻¹	
	AA	UV
303	0.0330	0.0122
	0.0310	0.0122
306	0.0392	0.0154
	0.0387	0.0150
308	0.0454	0.0176
	0.0453	0.0173
313	0.0677	0.0257
	0.0691	0.0263

TABLE 3.8

**Second Order Rate Constants obtained from the Reaction between
K₂PtCl₆ + 2-aminopyrimidine**

Temperature/k	Rate	Constant/min ⁻¹
	AA	UV
296	-	0.0129
298	-	0.0142
303	0.0872	0.0203
308	0.1303	0.0287
311	0.1430	0.0329
313	0.1708	0.0392
316	0.1995	0.0449
318	0.2110	0.0532

TABLE 3.9

**Second Order Rate Constants obtained from the
Reaction between K₂PtCl₆ + Pyridine**

Temperature/k	Rate	Constant/min ⁻¹
	AA	UV
294.5	0.0356	0.0158
	0.0356	0.0158
297.5	0.0744	0.0184
298	0.0458	0.0223
301.5	0.0620	-
	0.0021	0.0248
306	0.0803	0.0427
	0.0803	0.0427
308.5	0.1023	0.0525
	0.1020	0.0524
312.5	0.1728	0.0844
313	0.0000	
316	0.1784	0.0971

TABLE 3.10

**Second Order Rate Constants obtained from the Reaction
between K_2PtCl_4 + 2-amino-4-methylpyrimidine**

Temperature/k	Rate	Constant/min ⁻¹
	AA	UV
303	0.0230	0.0072
305.5	0.0297	0.0088
308	0.0410	0.0126
310	0.0517	0.0164
313	0.0716	0.0227
315	0.1057	0.0305
318	0.1287	0.0395

TABLE 3.11

**Second Order Rate Constants Obtained from the Reaction
between K_2PtCl_4 + purine**

Temperature/k	Rate	Constant/min ⁻¹
	AA	UV
299	0.1533	0.0119
302	0.1690	0.0141
304	0.2101	0.0151
306	0.2224	0.0174
310	0.2735	0.0277
313	0.3318	0.0256

TABLE 3.12

**Second Order Rate Constants Obtained from the Reaction
between K_2PtCl_4 + pyrimidine.**

Temperature/k	Rate Constant/min ⁻¹
283	0.0106
294	0.0303
298	0.0458
308	0.1365

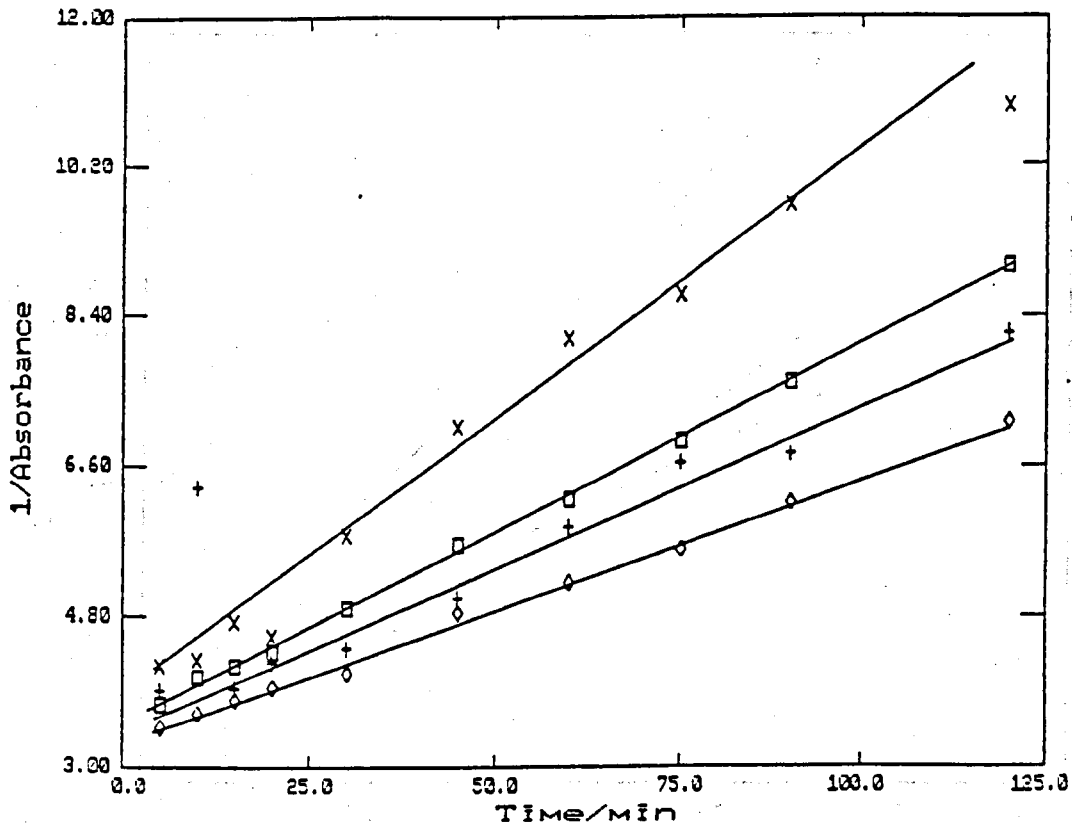


Figure 3.26 Second Order Plots obtained for the Reaction between K_2PtCl_6 and 2-aminopyridine, monitored by AAS.

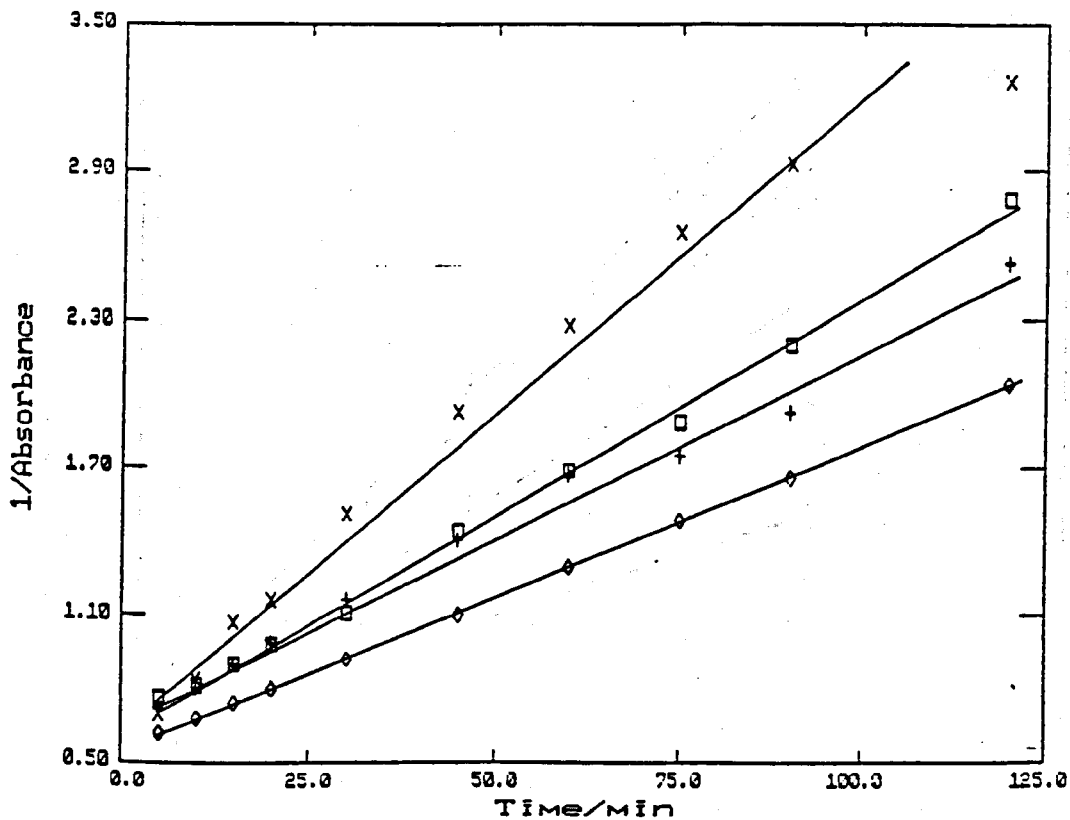


Figure 3.27 Second Order Plots obtained for the Reaction between K_2PtCl_6 and 2-aminopyridine, monitored by UV.

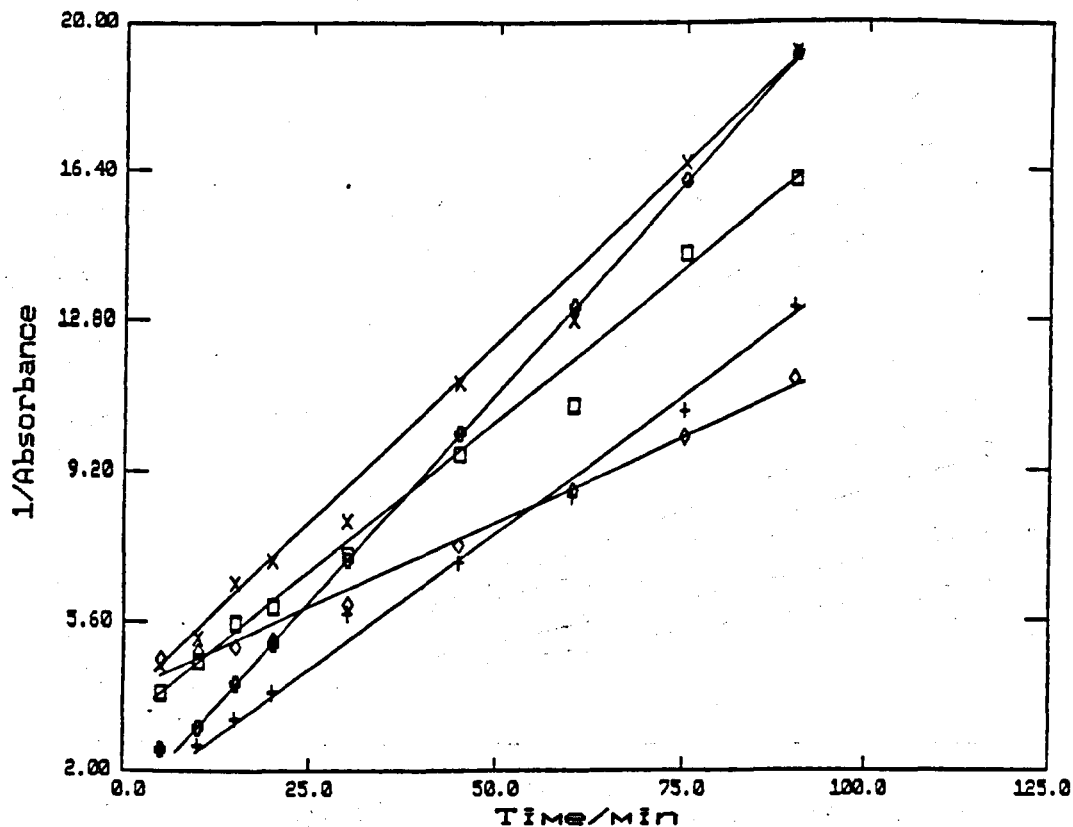


Figure 3.28 Second Order Plots obtained for the Reaction between K_2PtCl_6 and 2-aminopyrimidine, monitored by AAS.

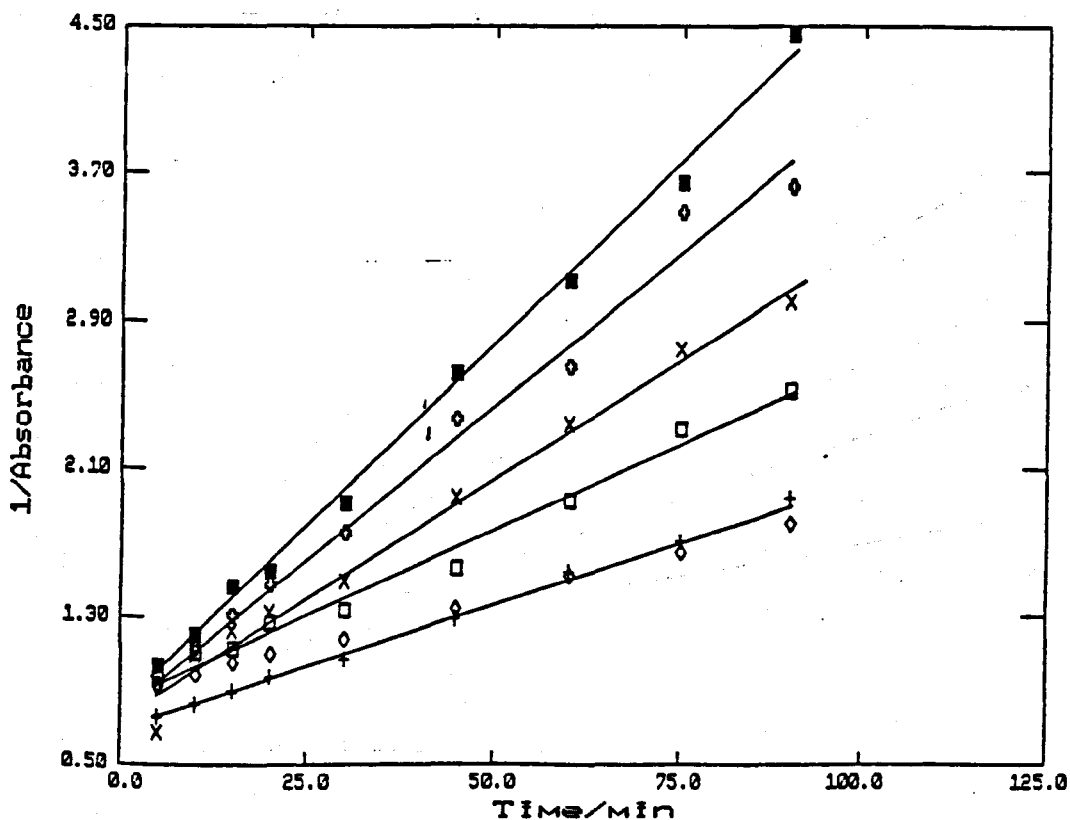


Figure 3.29 Second Order Plots obtained for the Reaction between K_2PtCl_6 and 2-aminopyrimidine, monitored by UV.

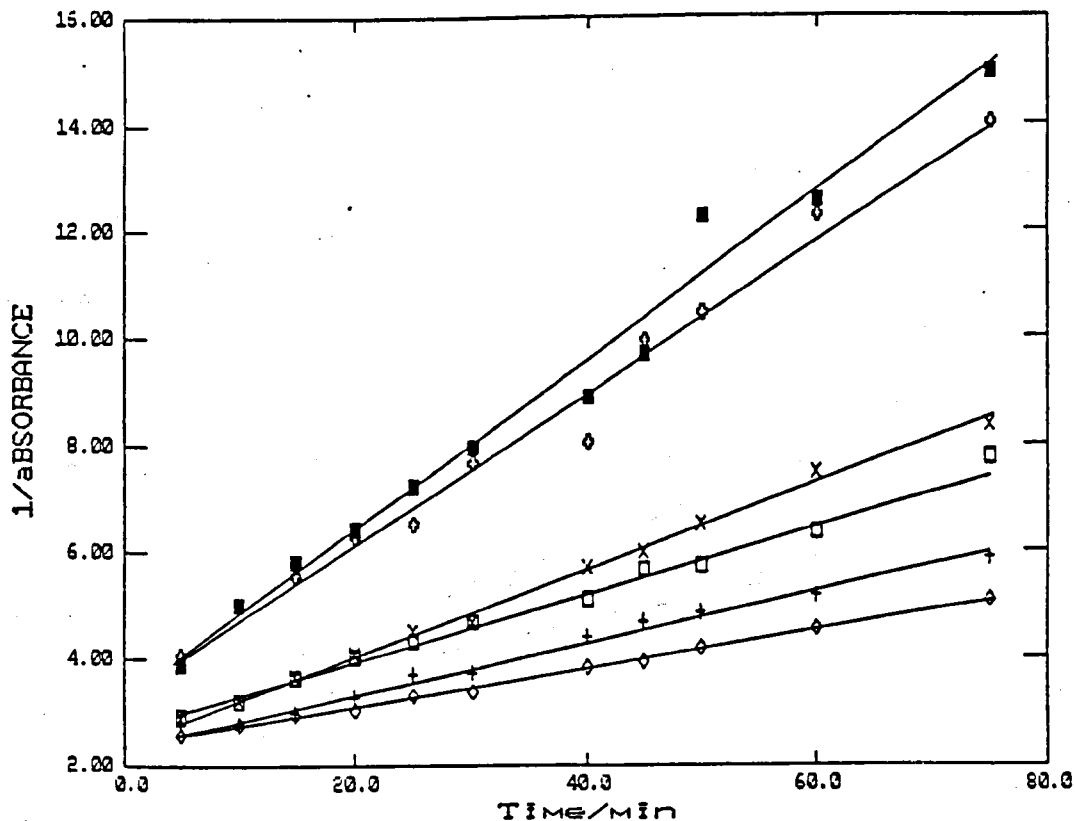


Figure 3.30 Second Order Plots obtained for the Reaction between K_2PtCl_6 and pyridine, monitored by AAS.

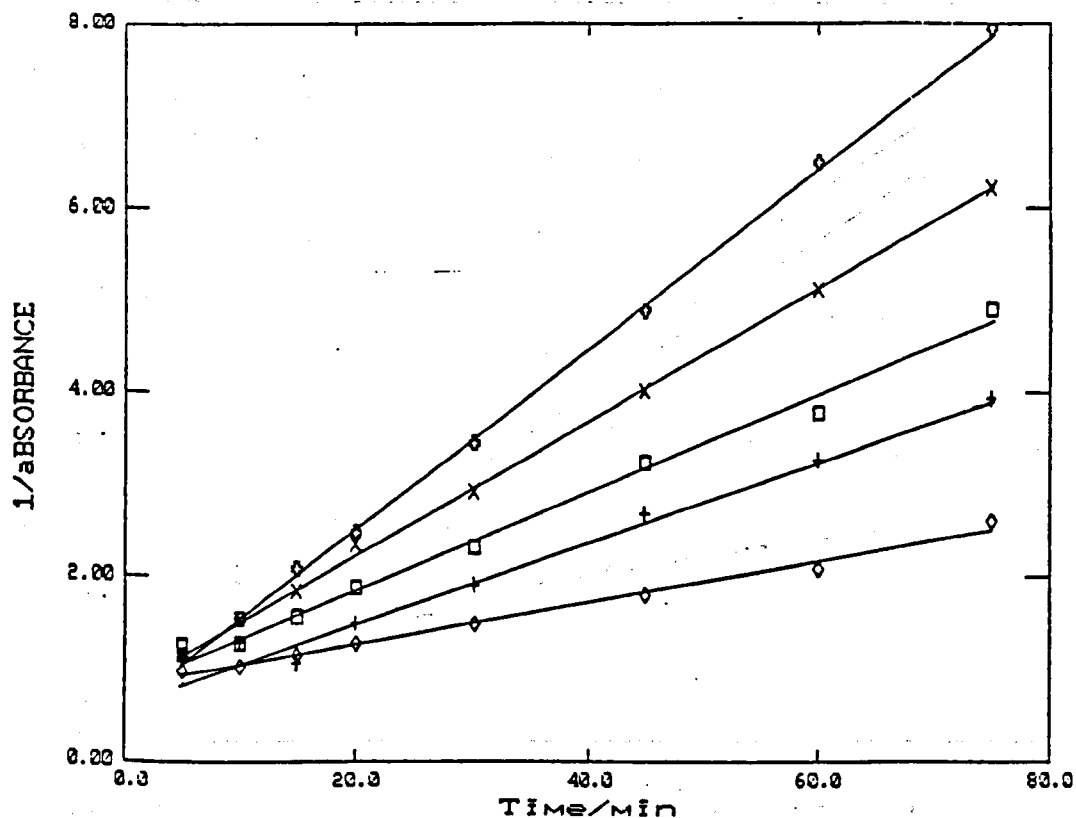


Figure 3.31 Second Order Plots obtained for the Reaction between K_2PtCl_6 and pyridine, monitored by UV.

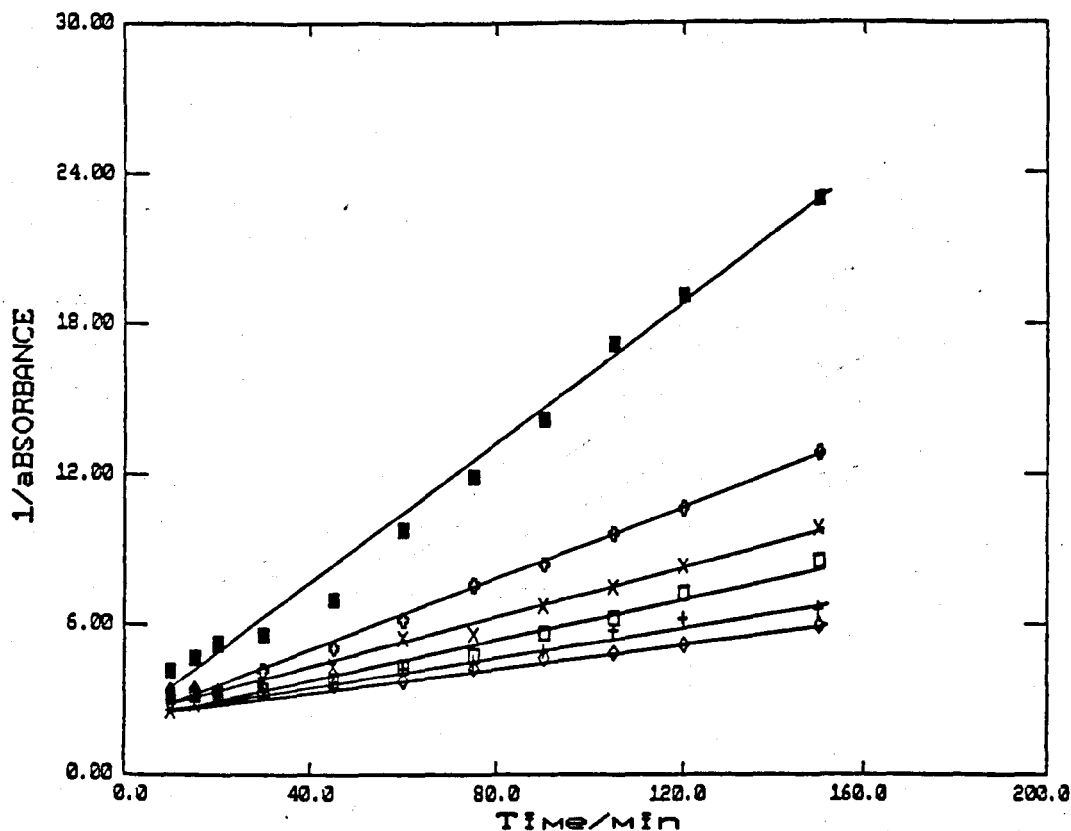


Figure 3.32 Second Order Plots obtained for the Reaction between K_2PtCl_6 and 2-amino-4-methylpyrimidine, monitored by AAS.

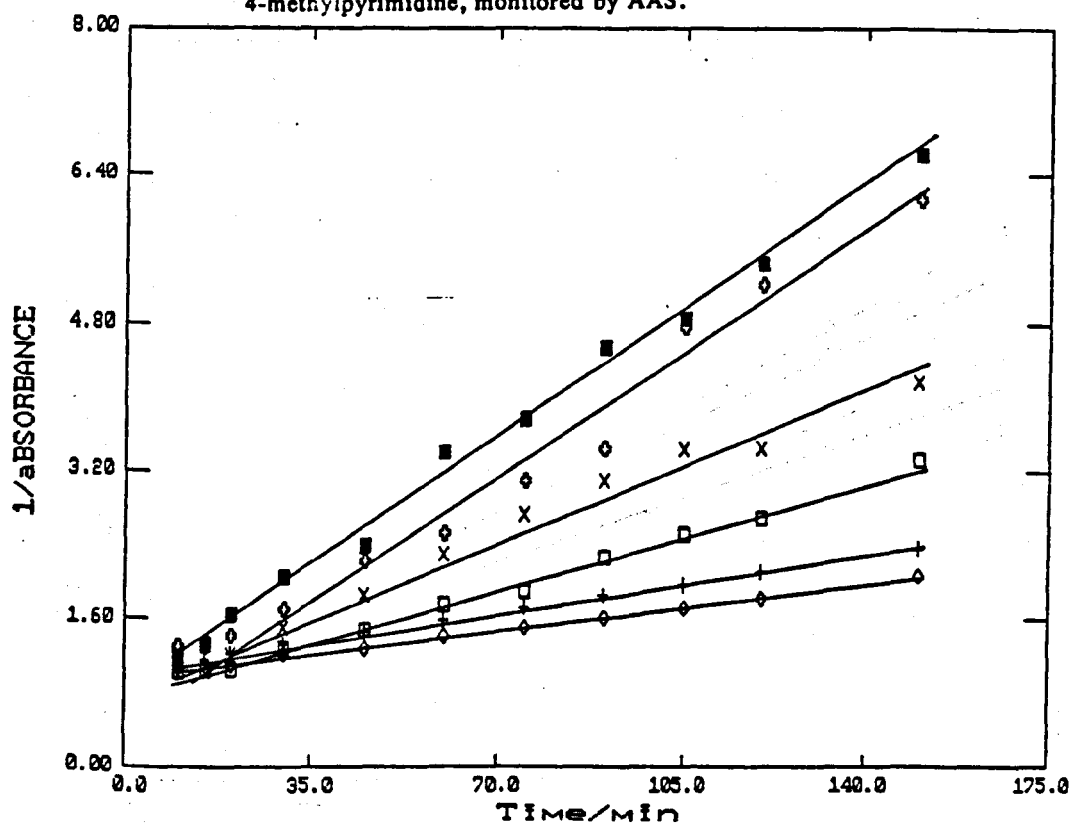


Figure 3.33 Second Order Plot obtained for the Reaction between K_2PtCl_6 and 2-amino-4-methylpyrimidine, monitored by UV.

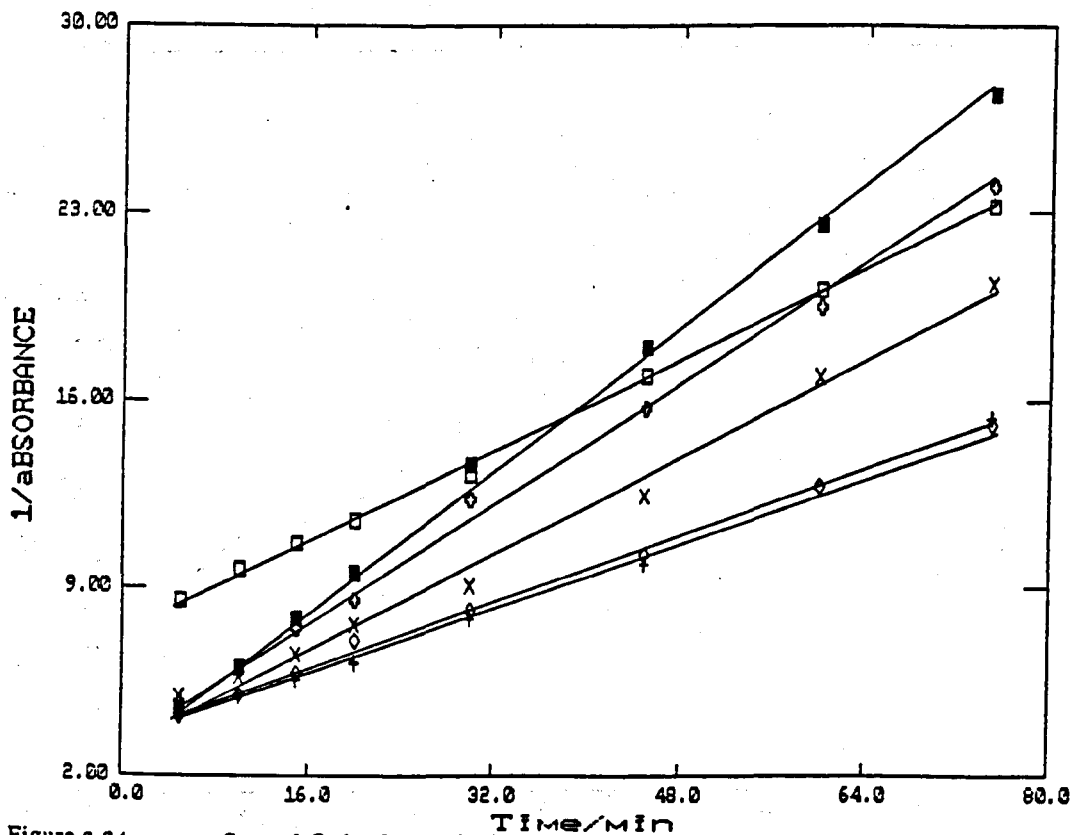


Figure 3.34 Second Order Plots obtained for the Reaction between K_2PtCl_6 and purine, monitored by AAS.

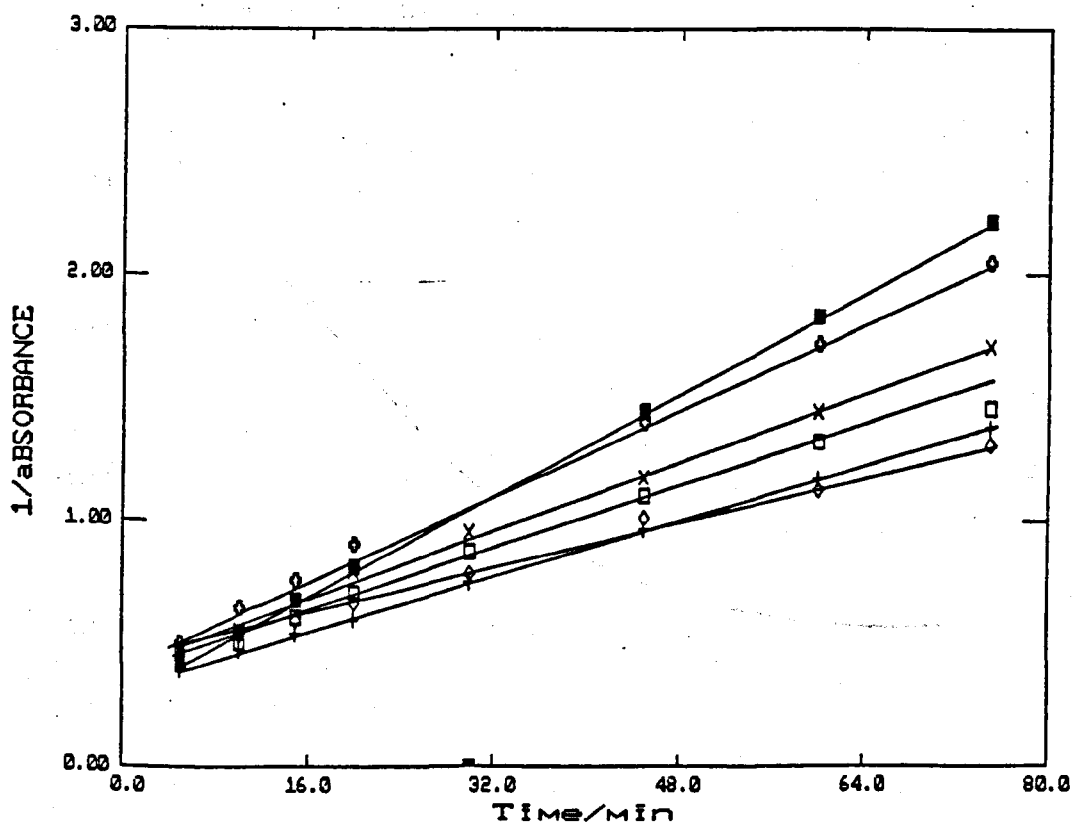


Figure 3.35 Second Order Plots obtained for the Reaction between K_2PtCl_6 and Purine, monitored by UV.

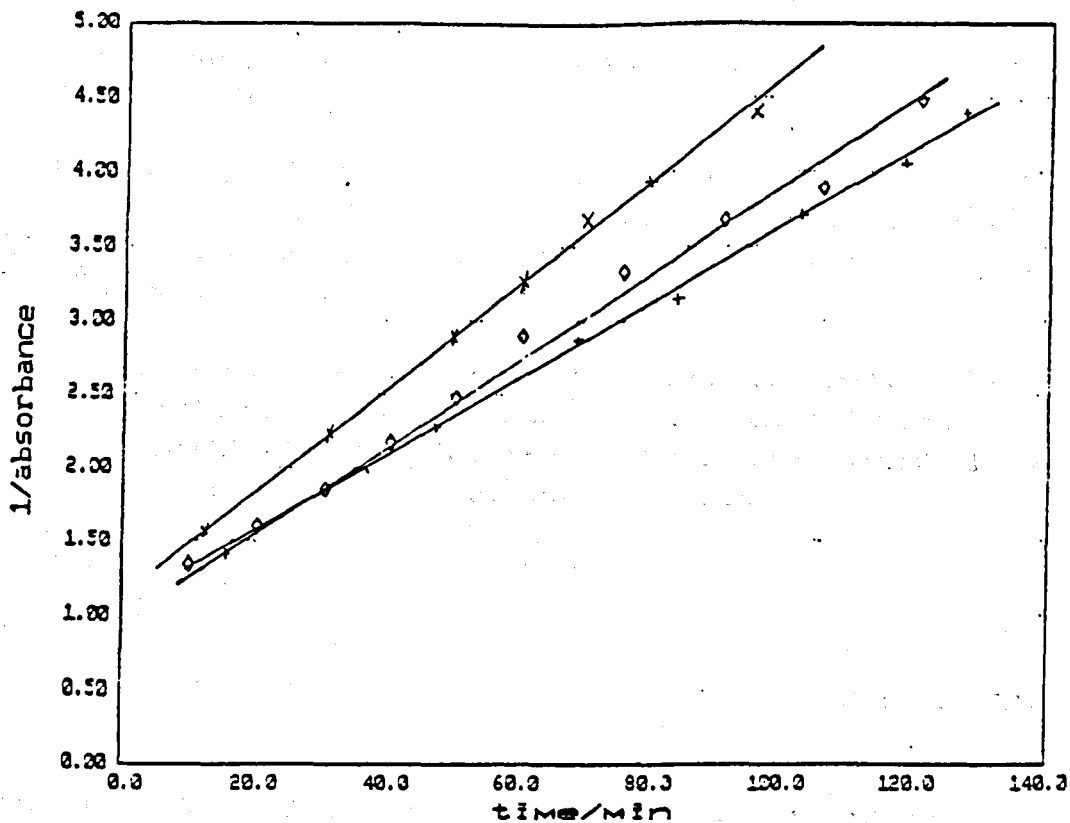


Figure 3.36 Second Order Plots obtained for the Reaction between K_2PtCl_6 and Pyrimidine, monitored by UV.

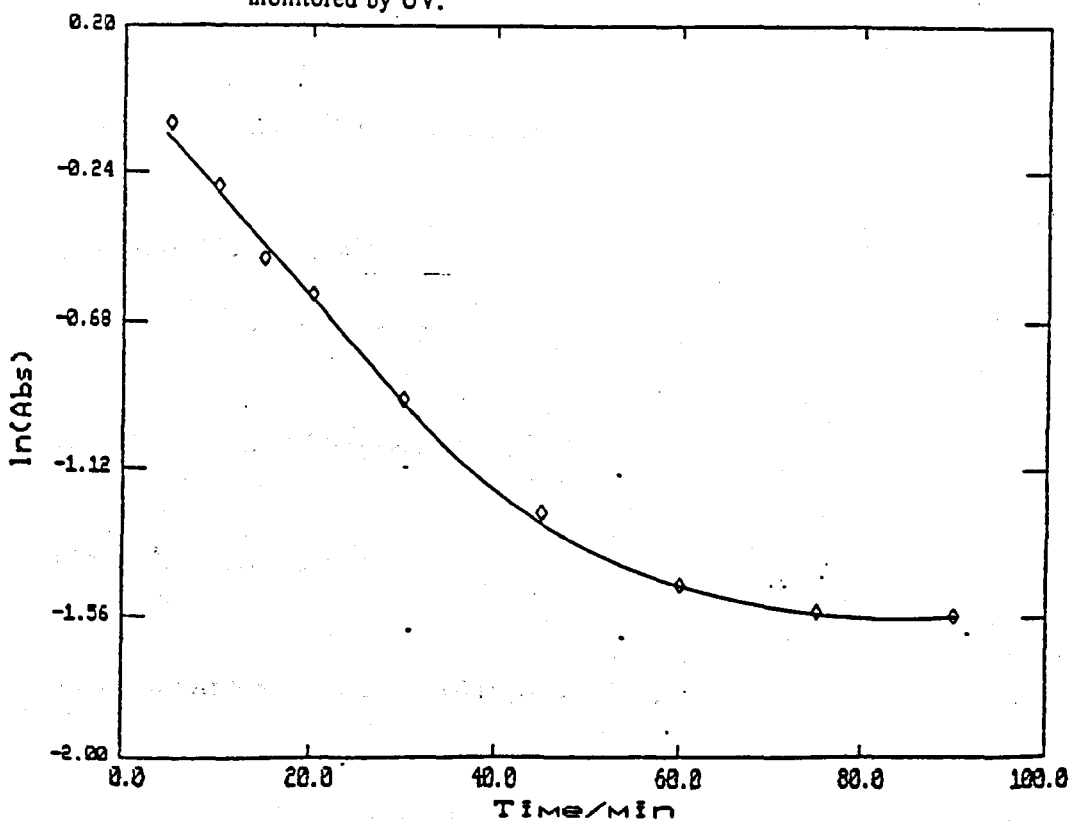


Figure 3.37 Typical First Order Plot - Reaction between K_2PtCl_6 and 2-aminopyrimidine.

The reaction between K_2PtCl_6 and 2-aminopyridine and that between K_2PtCl_6 and pyridine were monitored at the same temperature more than once to check the validity of the data obtained and to ensure the method was reproducible.

Figure 3.37 shows a typical first order plot for the reaction between K_2PtCl_6 and ligand, here \ln (Absorbance) has been plotted against time. This plot is not linear whereas the second order plots are (Figures 3.26-3.36), thus the integrated rate equation results confirm that the reaction is second order overall.

The Arrhenius equation was applied to the results obtained for each reaction by plotting the natural logarithm of the second order rate constant against the reciprocal of the absolute temperature (Figures 3.38 - 3.43). The activation energy and entropy were then calculated from the slope and intercept of the Arrhenius plot respectively (table 3.13).

$$\ln k_2 = \frac{-E}{RT} + \ln(A)$$

$$\text{where } \ln(A) = \ln \left(\frac{kT}{h} \right) + \Delta S$$

(See Section 3.1)

Thus from a plot of $\ln k$ vs $1/T$ the activation energy, E , can be determined from the slope

$$\text{since slope} = \frac{-E}{R}$$

$$E = -R(\text{slope}) \text{ J mol}^{-1}$$

The intercept is given by the equation

$$\text{Intercept} = \ln \left(\frac{kT}{h} \right) + \frac{\Delta S}{R}$$

$$\therefore \Delta S = R \left[(\text{Intercept}) - \ln \left(\frac{kT}{h} \right) \right]$$

$$\text{where } \ln \left(\frac{kT}{h} \right) \text{ is a constant}$$

The intercept on the Arrhenius plot at $1/T = 0$ is given by $\ln k_2$.

To refer ΔS to a standard state of 1 mol dm^{-3} , k_2 needs to be in the units $\text{dm}^3 \text{ mol}^{-1} \text{ s}^{-1}$. The values of k_2 obtained in this experimental work are in the units $\text{Abs}^{-1} \text{ min}^{-1}$, since $1/\text{Abs}$ instead of $1/\text{concentration}$ has been plotted against time. To convert the units of k_2 from $\text{Abs}^{-1} \text{ min}^{-1}$ to $\text{dm}^3 \text{ mol}^{-1} \text{ s}^{-1}$ the absorbance value at time equal to zero needed to be found. Since this corresponded to the initial concentration of the reagents, which was known, the absorbance value at time equal to zero needed to be found. This was best obtained by extrapolating the second order plot of $1/\text{Abs}$ against time and the conversion of units was then achieved by:

$$k_2 = (x) \text{ Abs}^{-1} \text{ min}^{-1}$$

$$= \frac{(x) \times \text{Absorbance at time} = 0}{\text{Initial concentration} \times 60} = (y) \text{ dm}^3 \text{ mol}^{-1} \text{ s}^{-1}$$

$$\therefore \Delta S = R \left(y - \ln \frac{kT}{h} \right) \text{ JK}^{-1} \text{ mol}^{-1}$$

3.5.3 Summary of Kinetics of Formation Results

TABLE 3.13

Activation Energies and Entropies, determined by Atomic Absorption (AA) and Ultraviolet (UV) spectroscopy, for each Reaction.

Reaction	Activation Energy/ kJ mol^{-1}		Activation Entropy/ $\text{JK}^{-1} \text{ mol}^{-1}$	
	AA	UV	AA	UV
$\text{K}_2\text{PtCl}_6 + 2\text{AP}$	58 ± 1	56 ± 2	-114 ± 8	-120 ± 6
	57 ± 2	56 ± 3		
$\text{K}_2\text{PtCl}_6 + 2\text{AP}_m$	47 ± 3	50 ± 0.8	-140 ± 9	-137 ± 10
$\text{K}_2\text{PtCl}_6 + \text{Py}$	60 ± 2	64 ± 1	-98 ± 11	-86 ± 6
	62 ± 6	69 ± 6		
$\text{K}_2\text{PtCl}_6 + \text{Pm}$	-	74 ± 1	-	-69 ± 9
$\text{K}_2\text{PtCl}_6 + \text{AMPm}$	94 ± 1	94 ± 2	$+6 \pm 10$	$+1 \pm 10$
$\text{K}_2\text{PtCl}_6 + \text{Pu}$	44 ± 3	44 ± 2	-144 ± 12	-152 ± 8

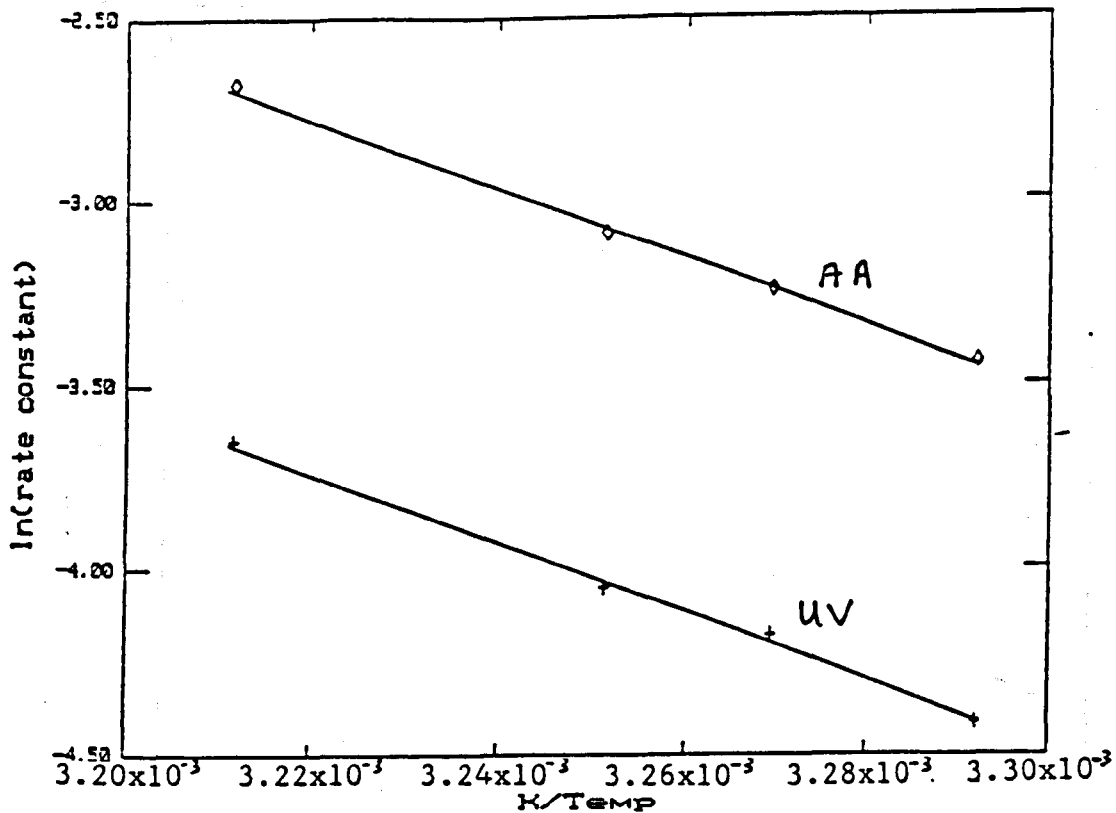


Figure 3.38 Arrhenius Plots for the Reaction between K_2PtCl_6 and 2-aminopyrimidine.

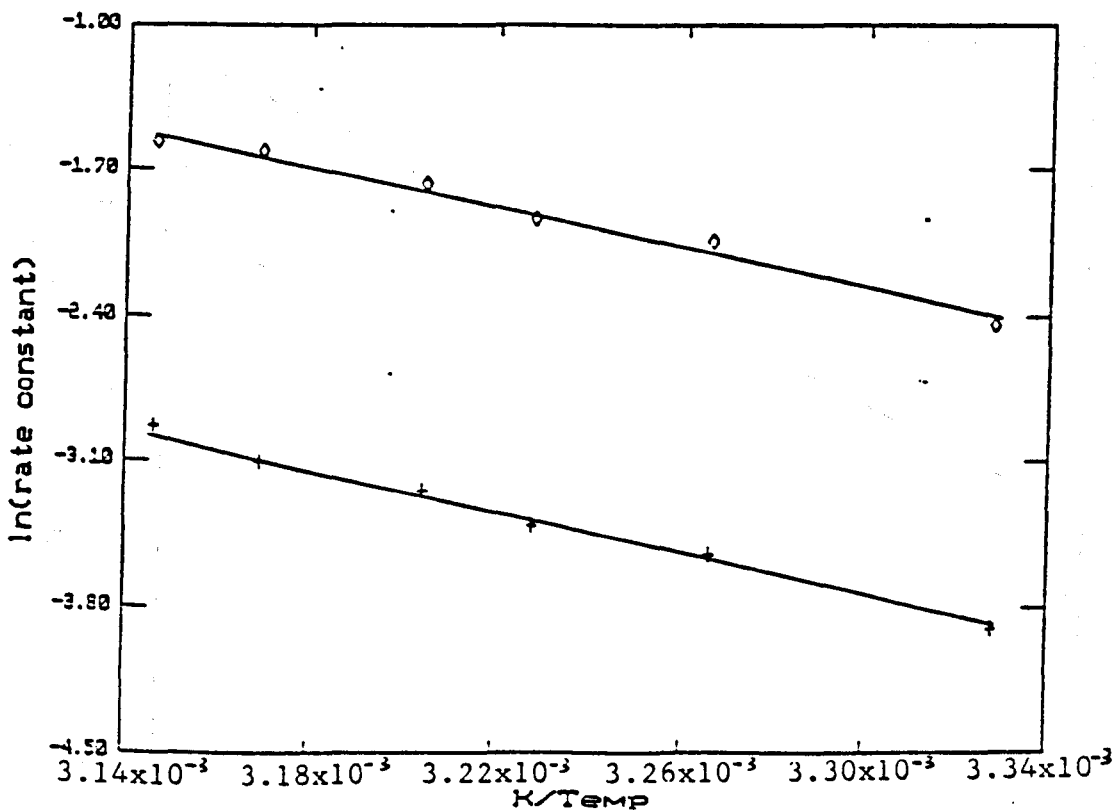


Figure 3.39 Arrhenius Plots for the Reaction between K_2PtCl_4 and 2-aminopyrimidine.

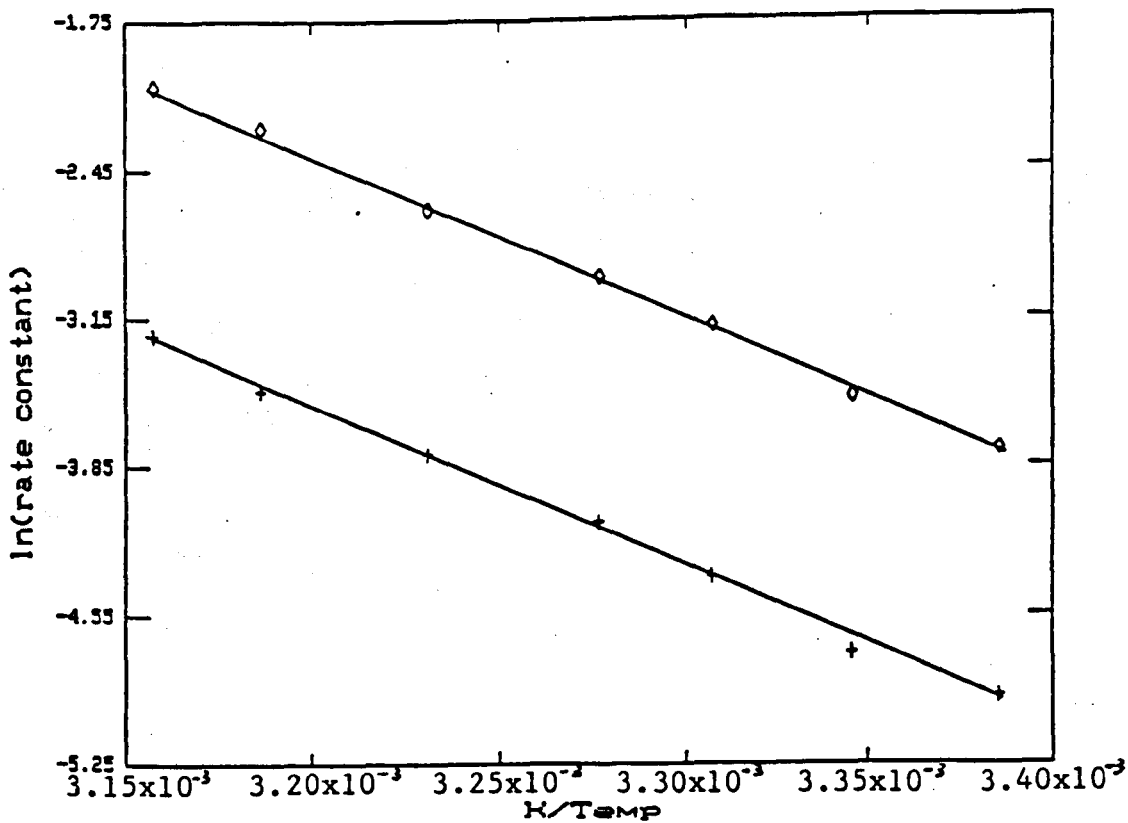


Figure 3.40 Arrhenius Plots for the Reaction between K_2PtCl_6 and Pyridine.

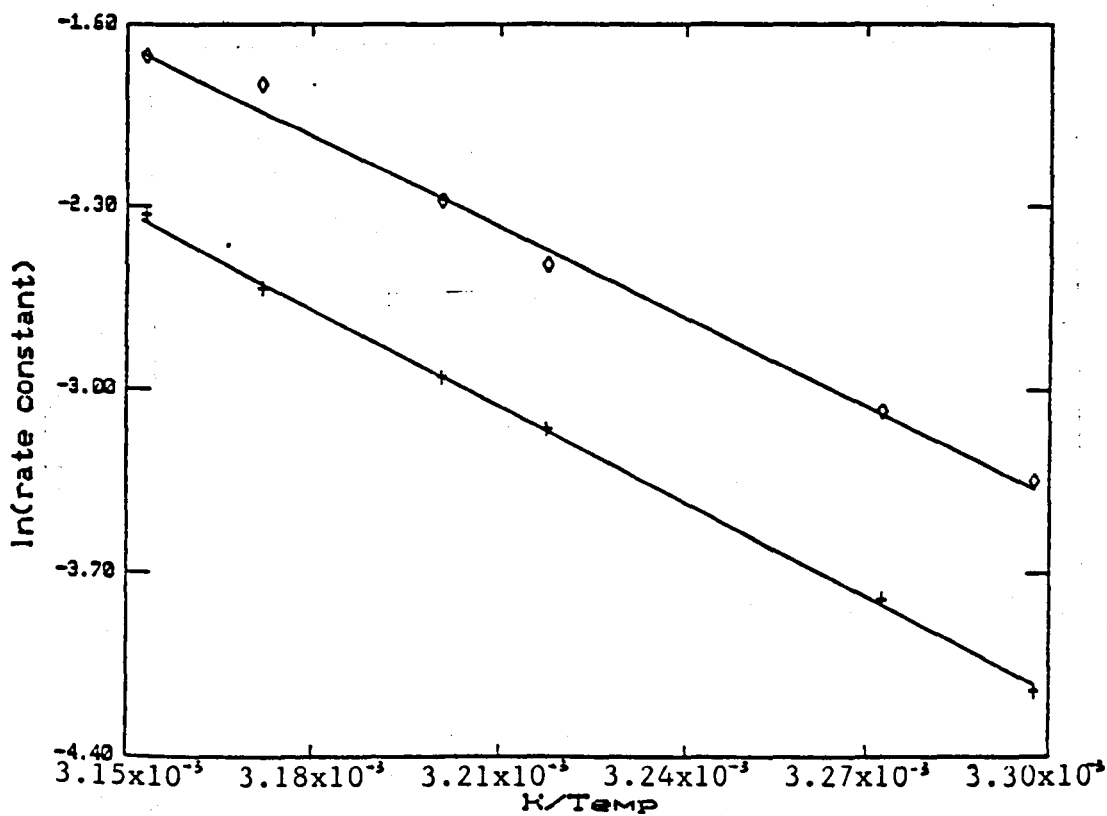


Figure 3.41 Arrhenius Plots for the Reaction between K_2PtCl_6 and 2-amino-4-methylpyrimidine.

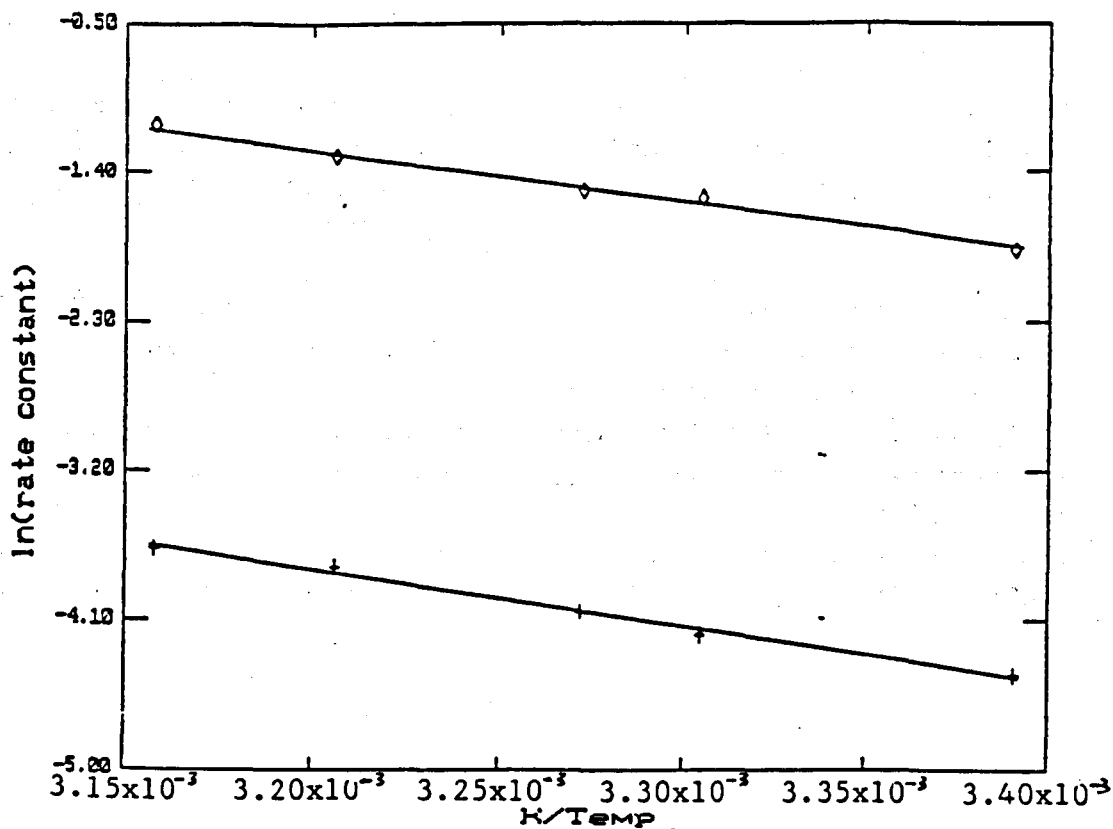


Figure 3.42 Arrhenius Plots for the Reaction between K_2PtCl_6 and Purine.

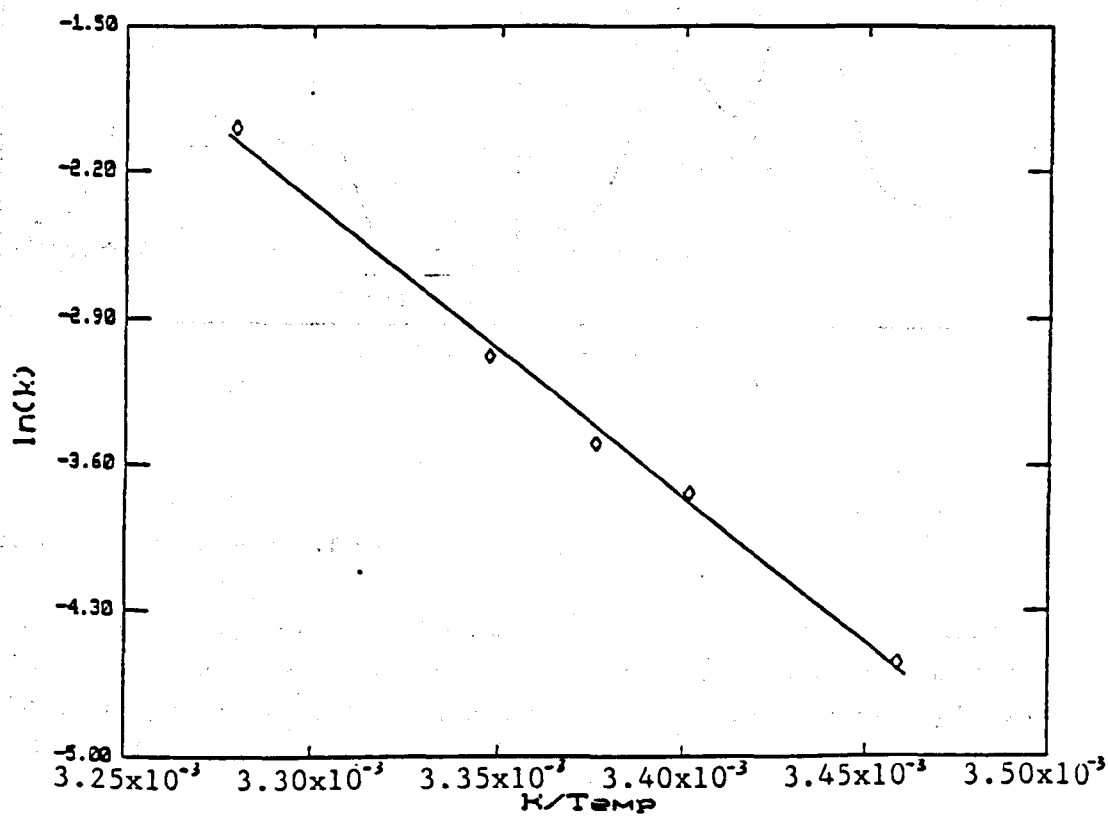


Figure 3.43 Arrhenius Plots for the Reaction between K_2PtCl_6 and Pyrimidine.

3.6 Discussion

The kinetic data obtained from the reactions between an aged solution of K_2PtCl_4 and each ligand indicated that the overall rate of reaction was second order, first order with respect to $PtCl_2(H_2O)_2$ and first order with respect to the entering ligand. This observation is consistent with typical substitution reactions of square planar platinum (II) complexes ^[28].

In theory it would appear that square planar substitution should involve a bimolecular displacement mechanism. For both steric and electronic reasons substitution reactions in these systems would seem to proceed most rapidly by an expansion of co-ordination number to include the entering ligand. The platinum metal is exposed for attack both above and below the plane. Furthermore these low spin d^8 systems have vacant p_z orbitals of relatively low energy which can help accommodate the pair of electrons donated by the entering ligand. Evidence ^[30] suggest that the transition state for Pt (II) substitution reactions involves a five co-ordinated species which acts as an active intermediate and thus the energy reaction profile may be represented by Figure 3.44.

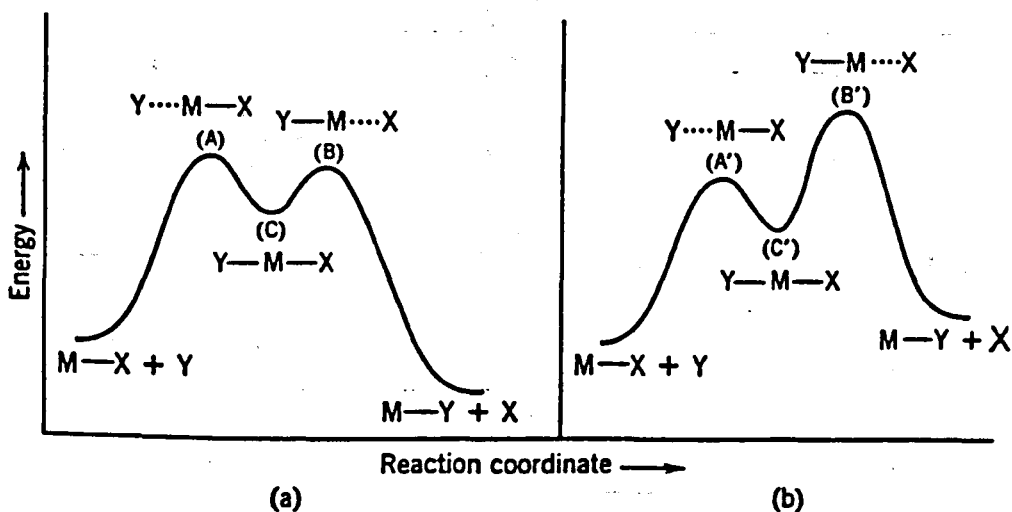


Figure 3.44 Reaction Profiles for a Displacement Mechanism

In the situation represented by Fig 3.44a the rate determining step is the addition of the nucleophile accompanied by structural rearrangement. However, the bond to the leaving group is still intact, the mechanism is in the SN_2 (lim) category. For a reaction represented by Fig 3.44b the addition of the nucleophile is reversible and the rate determining step is the

loss of the leaving group, accompanied by rearrangement. The mechanism is SN2 since both bond making and bond breaking occur. In either case the rates would show the characteristic behaviour of displacement mechanisms in that the nature and concentration of the entering group would exert a major effect on the rate of reaction.

M N Hughes^[11] suggested that such reactions proceed by an associative mechanism, reaction rate being dependent on the nature and concentration of the entering ligand. The kinetics being of the form

$$\text{rate} = k_1[\text{MA}_2\text{X}] + k_2[\text{MA}_2\text{X}][\text{Y}]$$

where MA₂X represents the platinum complex and Y the entering ligand, k₁ and k₂ are the first order and second order rate constants respectively.

This two-term rate law requires a two path reaction mechanism as shown in Figure 3.45.

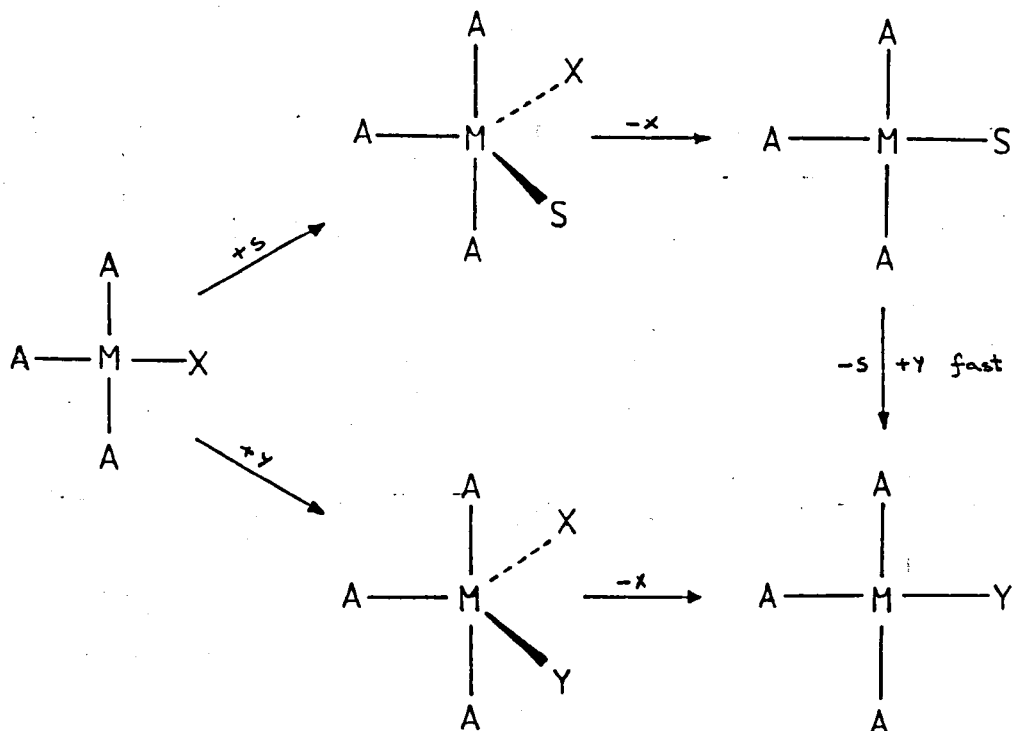


Figure 3.45 Two Path Mechanism for the Reaction of a Square Planar Complex, MA₂X with Y

The rate constant k₁ is due to the slow displacement of X by the solvent, which is then rapidly replaced by Y. A direct nucleophilic replacement of X and Y is responsible for k₂.

For a rate law with first and second order terms, the first order term will make the larger proportionate contribution to the rate when the ligand concentration is small. The good second order graphs for the data and the invariance of the second order rate constants with changes in the reactant concentrations point to a first order path that is either absent or abnormally ineffective in generating the product. In the reactions studied this first order path was essentially eliminated by allowing the K_2PtCl_4 solution to age for forty eight hours before adding the ligand. Thus the rate equation for the reactions was then considered to be

$$\text{rate} = k[PtCl_2(H_2O)_2][\text{ligand}]$$

Square planar substitution reactions of Pt (II) complexes is often considered in terms of the *trans* effect. Basalo and Pearson^[30] defined the *trans* effect as the effect of a co-ordinated group upon the rate of substitution reactions of ligands opposite to it in a metal complex. The *trans* effect can be illustrated by considering the methods of synthesis of *cis*- and *trans*- $Pt(NH_3)_2Cl_2$ (Figure 3.46).

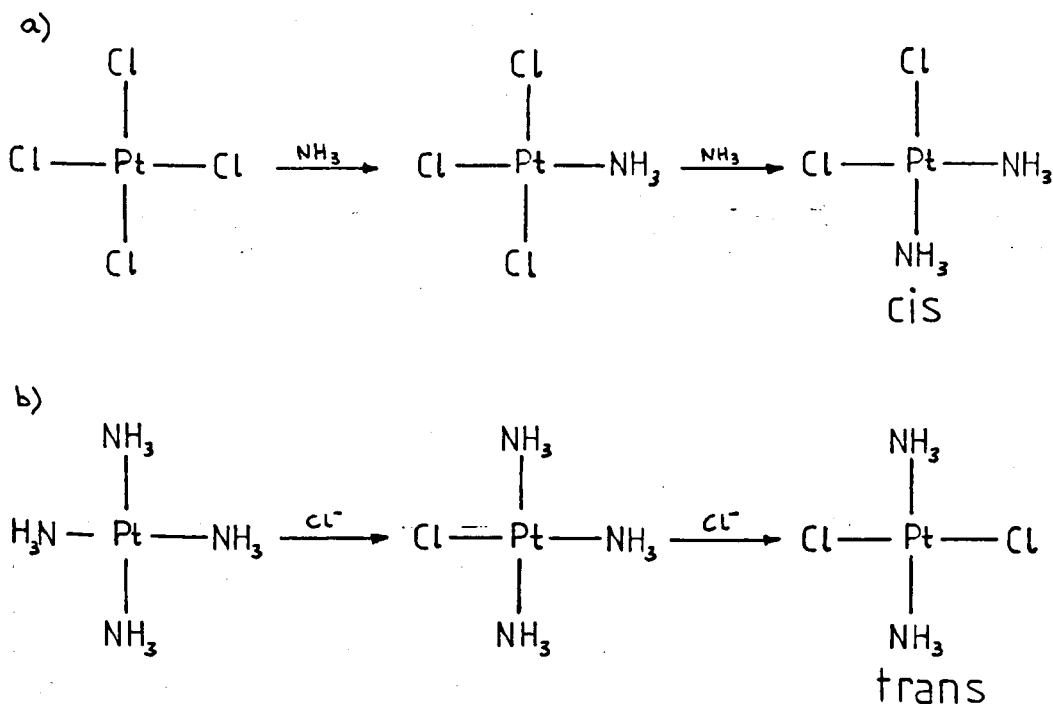


Figure 3.46 Synthesis of *cis*- and *trans*- $Pt(NH_3)_2Cl_2$

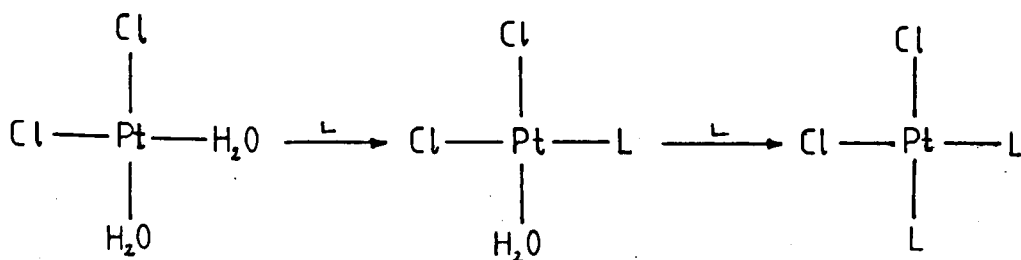
The second stage in each of the above reactions is the one of interest because a preferential replacement of groups *trans* to Cl is indicated. Thus in reaction (a) the second ammonia enters a *cis* position because the *trans*-directing influence of chloride ion is greater than that of ammonia,

which means that the least reactive chloro group in $\text{Pt}(\text{NH}_3)\text{Cl}^+$ is the one opposite ammonia. In reaction (b) the chloride ion replaces the most labile ammonia in $\text{Pt}(\text{NH}_3)_2\text{Cl}^+$ which is the one opposite the chloro group, thus resulting in the formation of *trans*- $\text{Pt}(\text{NH}_3)_2\text{Cl}_2$. The success of these reactions depends upon the greater *trans* effect of the ligand Cl^- compared to NH_3 , and the fact that the Pt-N bond strength is greater than the Pt-Cl bond strength.

The chemistry of Pt (II) complexes has many examples of the role of the *trans* effect in the synthesis of its compounds and in their chemical reactions. Extensive observations have provided qualitative information on the *trans* directing influence of various ligands, and the approximate order of decreasing *trans* effect is

$\text{CO}, \text{CN}^-, \text{C}_2\text{H}_4 > \text{PR}_3, \text{H}^- > \text{CH}_3^-; \text{SC}(\text{NH}_2)_2 > \text{C}_6\text{H}_5^-; \text{NO}_2^-, \text{I}^-, \text{SCN}^- > \text{Br}^-, \text{Cl}^- > \text{Py}, \text{H}_2\text{O}, \text{OH}^-, \text{NH}_3$.

In the reactions studied the intermediate obtained after aquation of K_2PtCl_4 is *cis*- $\text{PtCl}_2(\text{H}_2\text{O})_2$, and it is envisaged that the reaction with the ligand will then proceed as follows



The first replacement of H_2O by L takes place in accordance with the *trans* effect since H_2O is more labile than Cl^- . Although the *trans* effect is still relevant for the second substitution step it is proposed that the differences in activation energy obtained for the series of ligands investigated are due to the *cis* effect. An exhaustive investigation⁽²²⁾ has been made on rates of hydrolysis of a series of complexes from PtCl_4^{2-} through to $\text{Pt}(\text{NH}_3)_2\text{Cl}^+$. The results suggest that in these systems, for which the ligands are weakly *trans* directive, the *cis* neighbour has a somewhat greater influence on the kinetics than the *trans* neighbour to the leaving group. Since the complexes studied in this present work involve Cl^- and derivatives of pyridine and pyrimidine ligands, all of which exhibit a weak *trans* directing effect, it is considered that the *cis* effect will then play a major role in the kinetics.

Since in this work it is the second stage of the above reaction which was measured by the formation of the solid product *cis*-PtCl₂L₂, then the Cl⁻ in the *trans* position to the entering ligand is constant throughout the series of reactions investigated as is the nature of the leaving group, H₂O. This it is essentially the effect of the nature of the entering nucleophile on *cis* substitution that has been measured and could account for the variation in rate constant and hence activation energies observed for the six different ligands.

According to the transition state theory of reaction rates a good estimate of the speed with which a chemical reaction occurs can be made by a knowledge of the properties of the activated complex which consists of the aggregate of several reactant molecules in the configuration of highest potential energy. The less energy required to form the activated complex, the faster the reaction to form the activated complex, the faster the reaction will proceed, though special non-energy factors can sometimes slow down a reaction. The entropy between the activated complex and the reactants, is such a factor. The entropy of activation is defined by the equation.

$$k = \frac{kT}{h} e^{-\Delta H/RT} e^{\Delta S/R}$$

E_a is the Arrhenius activation energy, while ΔH, the enthalpy of activation in solution, is given by ΔH = E_a - RT. The entropy of activation is interpreted as being the difference in entropy between the transition state and the ground state of the reactants. It is determined largely by the loss of translation and rotational freedom as several particles come together in the activated complex. Important changes in vibrational freedom may also occur if the activated complex is more or less tightly organized than the reactants.

In solutions where charged particles are involved, solvation effects often dominate the entropy of activation^[32]. If ions are formed from neutral molecules, for example, solvent molecules are strongly orientated or 'frozen' around the ions and their entropy is lost. Hence, ΔS, becomes more negative, the effect being greater the larger the charge. If ions come together in the transition state with a neutralization of charge, then solvation molecules are released and the entropy of activation becomes more positive. From both theory and experiment, these solvation effects on the entropy are larger for non-polar solvents than for water.

The values obtained in these studies for the activation energies for the ligand substitution reactions with various heterocyclic ligands are all of the same order of magnitude and similar to those reported for similar reactions of four co-ordinated square planar platinum complexes. The strongly negative entropy (ΔS) values (table 3.13) obtained for all the reactions except that involving 2-amino-4-methylpyrimidine, support an associative mechanism, the more negative the value the more ordering implied. This again is in accordance with values reported in the literature^[33, 34].

An associative mechanism is one in which the rate determining step involves interaction of the reactants to form the activated complex in the transition state, in such cases ΔS has a negative value. If the rate determining step involves bond breaking then the value of ΔS is positive and the reaction proceeds by a dissociative mechanism. Thus it is not the numerical value but the sign of ΔS which is significant.

Nucleophilic substitution reactions may be classified according to Table 3.14.

TABLE 3.14

Classification of Nucleophilic Substitution Reactions

	$S_N1(\text{lim})$	S_N1	S_N2	$S_N2(\text{lim})$
Degree of Bond Breaking in Rate Step	Large	Large	Appreciable	None
Degree of Bond Making in Rate Step	None	None - Small	Appreciable	Large
Evidence for Intermediate of Reduced Coordination Number	Definite	Indefinite	None	None
Evidence for Intermediate of Expanded Co-ordination Number	None	None	Indefinite	Definite

Thus, consideration of the experimental results obtained in these studies and the above table indicates that the reactions studied proceed by an S_N2 associative mechanism. This correlates with evidence^[35] which suggests that the transition state of platinum (II) substitution reactions involve a five co-ordinate species and that such reactions proceed by an S_N2 mechanism.

The reaction between K_2PtCl_4 and 2-amino-4-methylpyrimidine was the only one studied which took place by a dissociative mechanism, $\Delta S = +6$ (AA analysis), $\Delta S = +1$ (UV analysis). This at first seemed to be very unusual since entropies of activation for platinum (II) substitution reactions are usually negative, however, fairly recently positive ΔS values have been observed^[35, 36].

Steric reasons may be responsible for this change in mechanism. Kukushkin and Ukrainstev^[20] found that methyl derivatives of pyridine reacted much slower than pyridine itself and assumed the chief reason for this decrease in rate was due to steric hindrance. In these studies the value of the activation energy for the reaction between K_2PtCl_4 and 2-amino-4-methylpyrimidine was nearly double that found for the reaction between K_2PtCl_4 and 2-aminopyrimidine. Since, as will be shown later, the activation energy varies directly with entropy (Figure 3.47) then it is conceivable that the positive value of ΔS may be due to steric effects. One other difference observed in this reaction compared to the others was that the 2-amino-4-methylpyrimidine (AMP_m) ligand did not totally dissolve, in which case it may be necessary to consider the enthalpy of solution (ΔH_{sol}) and entropy of solution (ΔS_{sol}).

For a reactant for example X, which is only partially soluble the concentration in the saturated solution at a given temperature will be fixed. Thus the second order rate law

$$\text{Rate} = k[\text{PtCl}_4^{2-}][\text{X}]$$

becomes

$$\text{Rate} = k'[\text{PtCl}_4^{2-}]$$

where k' is a pseudo-first order rate constant. In this case the reaction will obey first order kinetics so long as the solution remains saturated with X. In practice this may be virtually the whole period of the reaction provided the rate of dissolution of X is maintained equal to the rate of reaction, for example by stirring.

The way k increases with temperature depends not only on the activation parameters but also on the way the concentration of X varies with temperature. The effect of temperature on solubility is given by^[37]

$$\frac{d \ln C}{dT} = \frac{L_s}{RT^2} \quad (i)$$

where L_s is the so-called 'final heat of solution', that is hypothetically the enthalpy change when one mole of solute dissolves in a saturated solution. In practice L_s is often found to vary with temperature but over small temperature ranges (such as used on the experiments reported here) may be regarded as constant.

When L_s is positive (increasing the temperature increases solubility) the reaction rate in a pseudo-first order process of the type we are considering here will increase with increasing temperature at a greater rate than if the reaction were conducted with an unsaturated solution. Since equation (i) has the same form as the Arrhenius equation it is clear that:

$$E_{\text{apparent}} = E_{\text{true}} - L_s$$

where E_{apparent} is the measured activation energy. If second order kinetics are observed then the concentration of X is declining in the normal fashion during reaction. This could be due to either:

- (a) Although only partially soluble, X is very largely in solution at the start of the reaction and only a small fraction of undissolved X remains to enter solution as the reaction proceeds.
- (b) The residual solid X remains undissolved in the solid state throughout the reaction - possibly prevented from dissolving by the formation of a layer of product (which is highly insoluble) on the surface of the particles of X. In this case incomplete reaction of the PtCl_4^{2-} would be observed. In addition as the temperature increases the less this effect will be since the higher the temperature the more X will dissolve.

In case (a) the effect of temperature on solubility might be neglected since the reaction becomes unsaturated soon after the start of the reaction.

In case (b) however, the variation of solubility may not be neglected as the initial concentration of X will vary.

In the reaction between K_2PtCl_6 and 2-amino-4-methylpyrimidine the reaction did not go to completion and this points to case (b) being correct. It was observed that the higher the temperature the further the reaction progressed, for example see table 3.15, this fact also points to case (b).

TABLE 3.15

Comparison of atomic absorption values, 90 minutes after start of reaction between K_2PtCl_6 and 2-amino-4-methylpyrimidine, at different temperatures.

Temperature/k	303	305.5	308	310	313	316	318
Absorbance	0.2149	0.2035	0.1772	0.1486	0.1190	0.0912	0.0704

In this type of situation the validity of using second order rate equations in the form that applies to stoichiometric reaction mixtures may be questioned. However, this latter point can be answered by pointing to the good linearity of the plots of 1/absorbance versus time (figures 3.32 and 3.33).

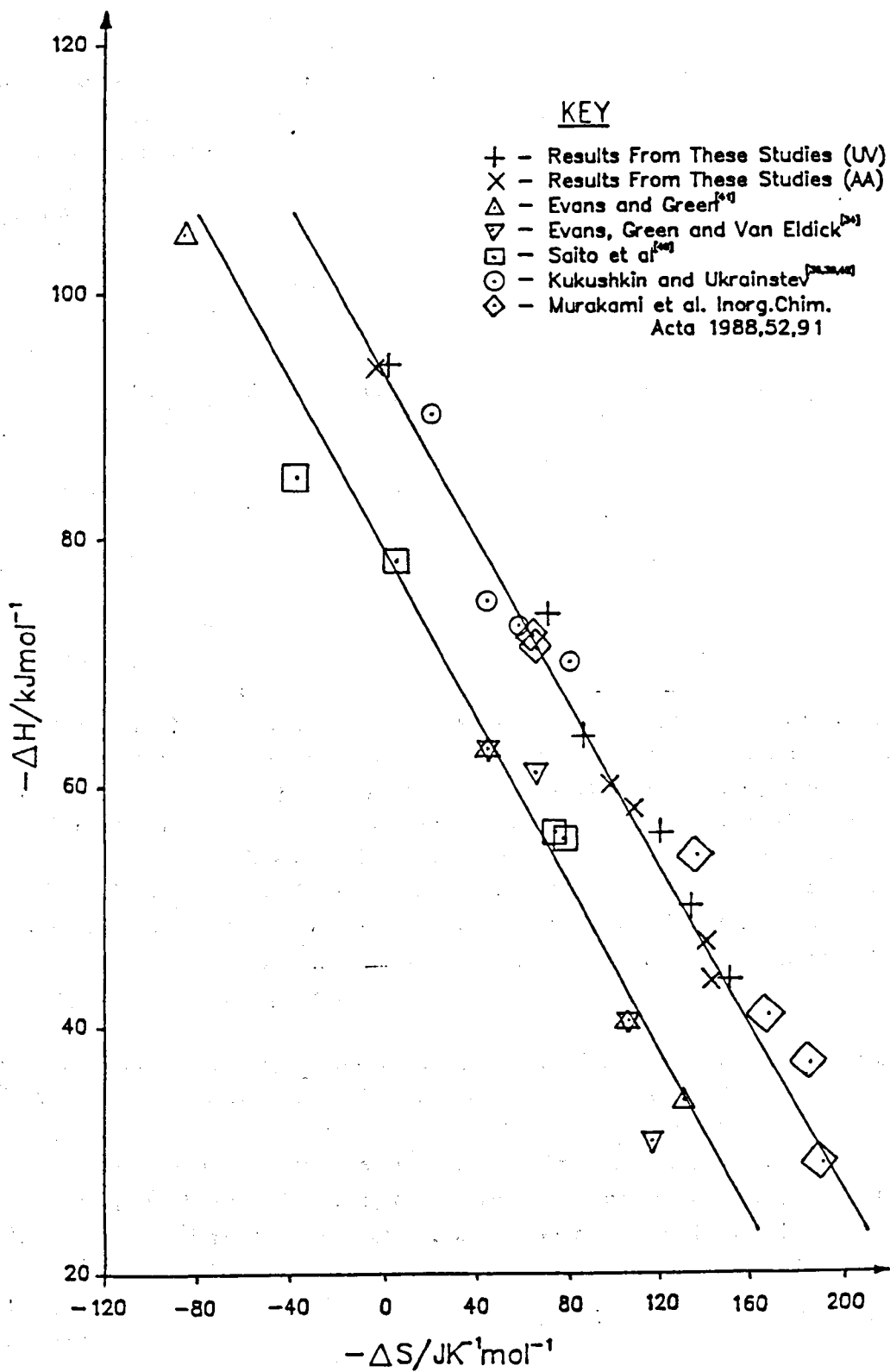


Figure 3.47 Relationship between the Activation Parameters of Reactions between Platinum Complex Ions and Nitrogen Heterocycles.

It was found that a plot of activation energy versus entropy was approximately linear with a slope of 230 K (Figure 3.47). This correlation was also observed in the published data of others^(20,24,38,39,40,41). Such a correlation requires explanation. We have investigated the mathematics of the transition state theory equation, from which both the activated energies and entropies were calculated. This investigation indicated that there should be a linear relationship between these two activation parameters.

The equation

$$k = \frac{kT}{h} e^{-\Delta H/RT} e^{\Delta S/R} \quad (1)$$

is derived from the equation $\Delta G = \Delta H - T\Delta S$ which suggests that ΔH varies linearly with ΔS , the slope of which would be equal to T .

This can be explained by considering equation (1)

$$\ln k = \ln \frac{kT}{h} - \frac{\Delta H}{RT} + \frac{\Delta S}{R}$$

$$\therefore RT \ln \frac{kT}{h} = -\Delta H + T\Delta S$$

The term on the left hand side can be regarded as virtually independent of temperature provided a small range of temperature is used in the kinetic investigations. Although the rate constant, k , is not constant when considering a variety of reactions it does not vary significantly from reaction to reaction to provide any considerable difference to the magnitude of the left hand side. For example at $T = 300\text{K}$ and $k = 1$ and 100 this term equates to 8438 Jmol^{-1} and -8791 Jmol^{-1} respectively. Thus there is a $\pm 9 \text{ kJmol}^{-1}$ variation in the intercept (when $\Delta S = 0$) in about 100 kJmol^{-1} i.e. there is an approximate 10% variation in the term on the left hand side. Thus a plot of ΔH vs ΔS will be linear for a wide variety of reactions, the slope of the line being about the experimental temperature range used.

Consequently whatever factor governs the rate of reaction, be it steric effects, electronic effects or both, should correlate with either ΔH and ΔS since these correlate with each other.

The results obtained in this study were compared with similar kinetic studies carried out on amines and in particular on lutidines and picolines. The activation energy and entropy values for various aliphatic and secondary heterocyclic amines were obtained from Kukushkin and Ukrainstev⁽⁴²⁾. This data was converted into standard units and plotted on Figure 3.47 and found to be in agreement with the correlation between the activation energy and entropy already established.

Comparison of the data on the kinetics of the reaction of K_2PtCl_4 with aliphatic amines containing additional NH_2 groups showed that with an increase in the number of amino groups the reaction rate increases. This agrees with an earlier suggestion that an increase in the number of nucleophilic groups in the aliphatic amine leads to an increase in reaction rate. It was also seen that steric hindrance due to methyl groups leads to a marked decrease in reaction rate.

These observations also apply to the reactions under investigation in these studies since the reaction involving 2-aminopyridine and 2-aminopyrimidine have much lower activation energies than pyridine or pyrimidine. The reaction between K_2PtCl_4 and 2-amino-4-methylpyrimidine has the highest value for the activation energy possibly because it is the only ligand studied which contains methyl groups. The values of the activation energy and entropy for 2,3-, 2,4- and 3,5-lutidine were calculated using rate constants from published data, unfortunately there was insufficient data to calculate these kinetic parameters for the picolines.

Kukushkin and Ukrainstev ^[20] found that the rate of reaction of K_2PtCl_4 with 3- and 4-picoline were approximately equal and were considerably greater than the rate of reaction of K_2PtCl_4 and 2-picoline. The rates of reaction of K_2PtCl_4 and the lutidines were almost equal and much less than the rate of reaction involving the picolines.

Kukushkin and Ukrainstev concluded that steric hindrance created by the methyl groups was responsible for the observed results.

The value of the activation energy and entropy calculated from published data for the reaction between K_2PtCl_4 and lutidine were similar to that obtained for the reaction between K_2PtCl_4 and 2-amino-4-methylpyrimidine. However, the value of ΔS for the former reaction was calculated as -30 kJmol^{-1} and therefore the reaction proceeded by an associative mechanism. This evidence suggests that steric hindrance is not the reason for the positive value of ΔS obtained for the reaction between K_2PtCl_4 and 2-amino-4-methylpyrimidine, but that the insolubility of this ligand caused the reaction to change from being associative to dissociative in character.

Thus it can be concluded at this stage that in reactions of tetrachloroplatinate (II) with N heterocyclic base derivatives allowance must be made for steric hindrance created by side chain substituents. However, this is clearly not the only factor involved and it may be necessary to consider the change in electron density at the nitrogen atom for each different ligand.

CHAPTER 4

Solid State Studies

Another method of studying the platinum-base bonding is by thermal analysis, in which the energetics of the complex undergoing solid state reactions are being dealt with. The aim being to determine the activation energy for the thermal decomposition processes in which the Pt-N bond is broken. This may be related to bond strength. The activation energy can be determined using either isothermal or non-isothermal techniques.

4.1 Background Theory of Isothermal Analysis

Isothermal analysis involves looking at the variation of amount of reactant and/or product with time. In order to do this several experiments need to be carried out at different but constant temperatures. The rate coefficient can then be derived by applying an appropriate rate equation and from the temperature dependence of the rate coefficient the Arrhenius parameters can be estimated.

As a measure of the reactant amount at a particular time and temperature it is convenient to use the dimensionless extent of reaction, α , where α is equal to zero at the start of the reaction of interest and is equal to one at the end. In isothermal studies of a decomposition reaction of the type



kinetic analysis then involves the identification of the function of α , such that:

$$f_n(\alpha) = k(T)t$$

where $k(T)$ = the conventional rate constant for the decomposition reaction and is a function of temperature.

There is no theoretical restriction on the form of the function of α although it is sometimes based on the concept of a simple order of reaction. Decompositions of solids are also often satisfactorily described by a limited number of expressions based on nucleation of product phase and the rate and geometry of advance of the reactant/solid product interface so called topochemical processes. Some of these expressions are listed in Table 4.1.

TABLE 4.1

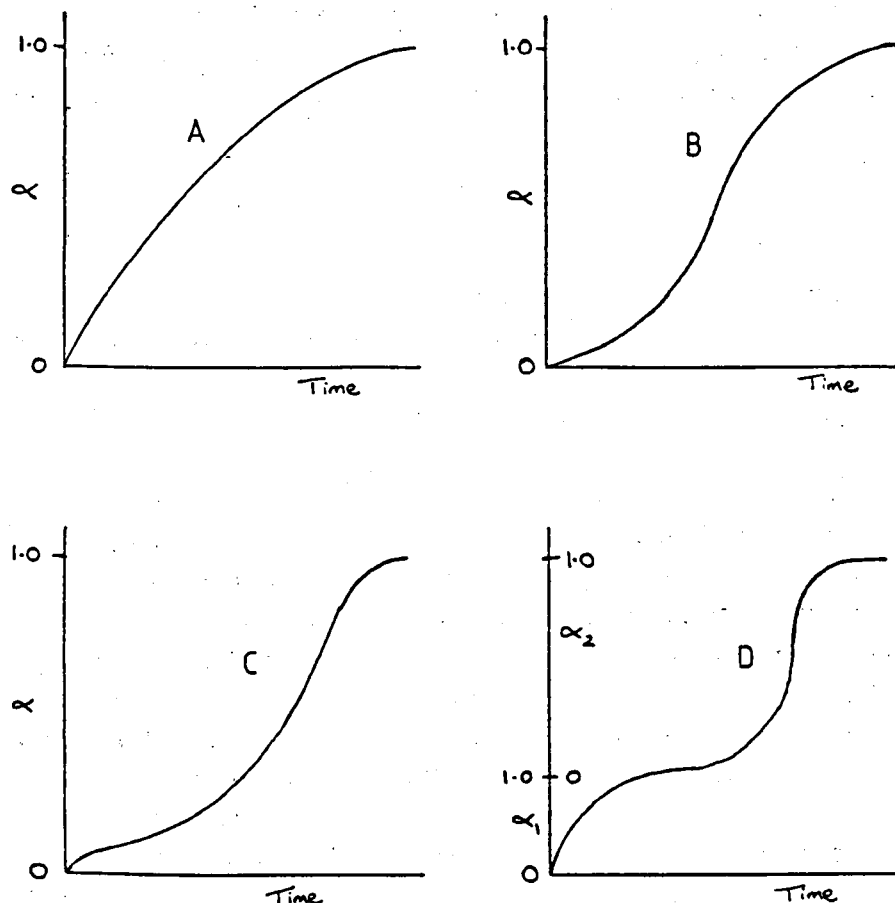
Summary of Solid State Kinetic Parameters

Mechanism	$*g(\alpha) = k(T) t$
Nucleation Controlled	
1. Power Law	$\alpha = kt^n$
Growth Controlled	
2. Contracting Sphere	$[1-(1-\alpha)^{1/3}] = kt$
3. Exponent law	$\alpha = ke^{kt}$
4. First order decay law	$1 - \alpha = e^{-kt}$
5. Two dimensional growth	$[1-(1-\alpha)^{1/2}] = kt$
6. Prout and Tompkins law	$\log \frac{\alpha}{1-\alpha} = kt$
	$\log \frac{\alpha}{1-\alpha} = k \log t$
Nucleation-Growth Controlled	
7. Avrami-Erofeev law	$1-\alpha = \exp(-kt)^n$
Diffusion Controlled	
8. One dimensional (parabolic)	$\alpha^2 = \frac{k}{x^2} t$
9. Two dimensional	$\alpha + (1-\alpha) \ln(1-\alpha) = kt$
10. Three dimensional	$[1-(1-\alpha)^{1/3}]^2 = kt$

* $g(\alpha)$ is the algebraic function of the physical model according to which the solid reaction is assumed to occur.

$k(T)$ is the rate constant for the process at a temperature, T .

Figure 4.1 shows typical α versus time plots for isothermal reactions.



- Notes: A = deceleratory throughout, ie the rate progressively decreases as reaction is carried out.
- B = short initial nucleation period during which the reaction rate increases and thereafter the reaction rate is decelerating
- C = shows a more pronounced induction period followed by a deceleratory period.
- D = more complex reaction which consists of two stages the first being of type A.

In topochemical processes, which give rise to these types of α versus time plots, the reaction takes place at a reactant/product interface, the shape and size of which governs the rate of reaction at a constant temperature. The exact form of the α versus time plot, then, is determined by the changing geometry of the decomposing system, especially the geometry of the reaction interface. In most homogeneous reactions the whole range of the process fits one kinetic expression. But in heterogeneous reactions one expression may hold for the critical few percent of the decomposition, to be followed by a second in the acceleratory stage of the reaction and a third or even fourth expression may be found to describe the reaction in the deceleratory stage of decomposition.

The following mechanistic stages will generally be present.

The reactant/product interface is usually established at a limited number of points (nuclei) on the surface of the reactant crystal by the formation of micro crystals of product. The reaction thereafter proceeds within the strained contact area of reaction/product interface. The strains result from the difference between reactant and product molar volumes.

The reaction initially takes place at those points where there is a favourable energy change, generally this occurs at surface defects such as the corners of the reactant crystal which because of an imbalance of forces will preferentially form product. This results in the formation of germ nuclei which are intrinsically unstable. At this point, after the evolution of gaseous product, the solid product is present with the same structure as the reactant and can either reabsorb the gaseous product and change back to reactant or can crystallise into product by rearrangement of the lattice. Which of these occur preferentially depends on the energetics of the system. Involved with this is strain energy which has been introduced into the lattice as the product is formed. As a result of strain a small amount of product may shatter and a common feature of topochemical reactions is to find that as the reaction proceeds the surface area of the product is much greater than that of the starting material. Once the germ nuclei have started to grow and passed the critical stage the reaction passes into an acceleratory period. Growth of the nucleus is the movement of the reactant/product interface in a direction normal to its surface due to the thermal decomposition reaction occurring in a very highly strained region of contact between the adjoining phases. The basic assumption made here is that the rate of progress of the interface linearly through the reactant material is constant at constant temperature.

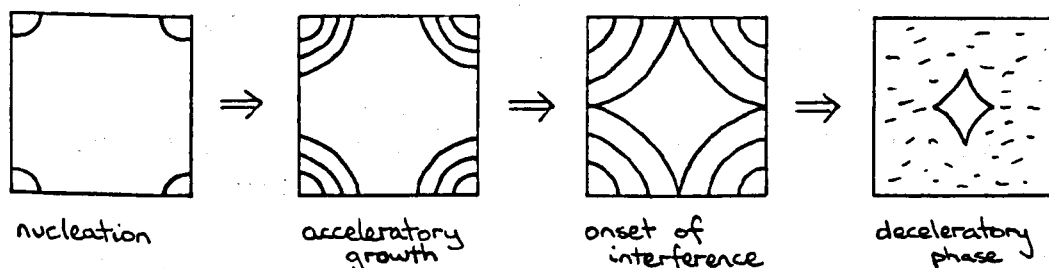


Figure 4.2 Schematic Diagram of Nuclei Growth.

Eventually the interfaces arising from the growth of two or more nuclei will start to overlap and while they will still be moving the point has been reached where the total size of the interface will decrease with time due to the overlapping of the growing nuclei (figure 4.2). Further reaction results in a progressive decrease in the area of reactant/product interface, so that the reaction is now deceleratory.

The α versus time curve thus has three major parts. The number of rate laws covering all of the sigmoid versus time curve is enormous and each part of the curve is usually treated separately to find the individual rate laws. These may be divided into three groups which depend on the location of the maximum rate of decomposition (d/dt).

- | | | | |
|-----|-----------------------------------|---|---|
| (a) | before $(d\alpha/dt)_{max}$ | - | relationship between α and time concerned with nuclei growth |
| (b) | each side of $(d\alpha/dt)_{max}$ | - | laws concerned with both growth and interference |
| (c) | After $(d\alpha/dt)_{max}$ | - | laws concerned with nuclei interference and decrease of reaction interfacial surface area |

All of the above are dependent on the nucleation law.

There are a large number of rate laws for the nucleation process and these include instantaneous nucleation and first order nucleation. In this latter case the rate of formation of growth nuclei is proportional to the number of potential nuclei forming sites remaining which is fixed at the start of the reaction.

$$\text{Rate of nucleation } dN/dt = k(N_1 - N)$$

where N_1 = number of possible sites at which nuclei may form
 N = nuclei present at time t

The above equation may be rewritten as:

$$dN/dt = k N_1 e^{-kt}$$

From this it may be seen that for reaction in solids where k is small, the rate of nucleus formation is approximately constant during the initial period of reaction, ie

$$dN/dt = k N_1$$

For systems where k is large, all possible nuclei are formed rapidly at the beginning of the reaction and so further nucleation does not occur, ie instantaneous nucleation.

Nucleation can also be dealt with by power laws. Here the number of nuclei at a given time depends on t^n , where the integer n depends on the mechanism of nucleation. This arises because the number of potential nuclei forming sites is not constant or fixed at the start of the reaction. New potential sites are created by strain in the lattice, where the crystals are under strain due to volume changes thus creating new high energy regions where nuclei can form.

In the acceleratory region of the curve the rate increases as the area of reactant/product interface increases and again there are a multitude of possible rate laws. Here the rate law is determined by the nucleation pattern and most importantly by the geometry of the reacting system. Potential nucleus forming sites may be engulfed by the advancing reaction interface, adding further to the complexities.

In the decay region other rate laws apply and again the geometry is important, but the previous pattern of events will also affect the rate law. It has been shown⁽⁴⁹⁾ that particle size distribution can have a considerable influence on the reaction kinetics. Most isothermal rate laws have been derived assuming uniform particle size.

4.1.1 Isothermal Analysis

In these studies the isothermal analysis, then, involved studying the variation of amount of reactant with time at a constant temperature. The platinum complexes with heterocyclic bases were found to be thermally unstable and in each case an early stage of the thermal decomposition resulted in the loss of one ligand molecule. The determination of the kinetic data involved a series of thermogravimetric runs in which the platinum-ligand complexes were decomposed under isothermal conditions. Several experiments were carried out on each platinum-ligand product over a range of different but constant temperatures. In order to obtain the necessary precision to enable calculation of the activation energy five isothermal runs were required. For each isothermal run the rate constant, for the appropriate step involving the loss of one ligand of the decomposition process, was derived by applying the appropriate topochemical kinetic equation.

This was achieved by first fixing the $\alpha = 0$ to $\alpha = 1$ scale, in which $\alpha = 0$ at the start of the decomposition stage of interest and $\alpha = 1$ was the point at which the isothermal thermogravimetric curve began to flatten out. The initial and final weights at $\alpha = 0$ and $\alpha = 1$ respectively were entered into the spreadsheet and the most suitable isothermal expression found by plotting, on screen, the various functions of α versus time graphs. Hence the most suitable isothermal rate law for the decomposition could be determined. The Arrhenius equation was then applied and the activation energy calculated, for each platinum-ligand product, from the slope of the resulting $\ln(k)$ versus $1/\text{Temperature}$ plot.

4.2 Background Theory of Non-isothermal Analysis

The use of isothermal methods is probably the most sound in determining kinetic parameters but it is very tedious and time consuming. However, there has been considerable interest in the use of non-isothermal methods. The advantage of this is that all the information can be obtained from one single continuous experiment and so is economical with respect to both time and sample. Also there is no uncertainty at the start, such as is found in isothermal analysis when processes can take place during the period of heating to reaction temperature.

A non-isothermal technique generally utilises a linearly varying temperature with time at a constant heating rate. In thermogravimetric analysis records of the loss of mass from the sample during heating as a function of temperature are obtained. In most non-isothermal analysis it is assumed that the reaction is taking place at conditions far removed from equilibrium so that any influence of reverse reaction can be ignored.

With isothermal methods a mechanism is assumed and by substitution of experimental data into the various rate equations the best fitting mechanism can be determined. However, this type of procedure is more complicated when the method of rising temperature is used.

The theoretical treatment of the kinetics of decomposition under rising temperature conditions rests largely on the combination of the following three equations.

- (a) the differential form of the isothermal rate law

$$d\alpha/dt = k \text{ fn}(\alpha) \quad (1)$$

- (b) The laws describing the temperature coefficient of the rate, usually described by the Arrhenius equation

$$k = Ae^{-E/RT} \quad (2)$$

where k = the specific rate constant
 A = the pre-exponential factor
 E = the activation energy
 T = the temperature
 R = the gas constant

- (c) The equation describing the imposed temperature against time which can be represented by:

$$T = T_0 + \beta t \quad (3)$$

where T_0 = the initial temperature and a linear heating rate has been assumed with a heating rate of β

Thus the temperature programmed reaction profile is:

$$d\alpha/dt = f_n(\alpha) A e^{-E/R(T_0 + \beta T)} \quad (4)$$

The $d\alpha/dt$ versus temperature curve contains information which should yield $f_n(\alpha)$, the activation energy and the pre-exponential factor.

The combination of these three equations will enable the kinetic parameters to be established, however, this combination does carry certain implications. The Arrhenius equation is almost invariably assumed to hold over the entire temperature range. This assumption may not hold and the most common deviation is the occurrence of two or more linear plots when plotting $\ln(k)$ against $1/\text{temperature}$. Another matter which is essential to the calculation is the correct choice of the specific reaction rate incorporated in the Arrhenius expression. It has been found that the activation energy and pre-exponential values for solid state decompositions are environmentally dependent and that the values calculated from rising temperature experiments should not necessarily agree with those obtained from traditional isothermal methods.

A number of methods of interpreting non-isothermal data from heterogeneous reactions and many solutions to the problems of determining the activation energy, the pre-exponential factor and the function of α , have been proposed. Sestak has classified these proposals on the basis of the mathematical methods employed or the region of the α - temperature curve which is being examined as:

- (a) differential methods
- (b) integral methods
- (c) approximation methods

One example of a differential method is that proposed by Freeman and Carroll⁽⁴⁴⁾ in which it is assumed that the reaction can be described by a simple order of reaction

$$\frac{d\alpha}{dt} = k(1-\alpha)^n \quad (5)$$

when α = extent of reaction
 n = order of reaction

Substituting equation (5) into the Arrhenius equation:

$$\frac{d\alpha}{dt} = A e^{-E/RT} (1-\alpha)^n$$

$$\therefore \ln \frac{d\alpha}{dt} = \ln A - \frac{E}{RT} + n \ln(1-\alpha) \quad (6)$$

Differentiating equation (6)

$$\frac{\Delta \ln \left(\frac{d\alpha}{dt} \right)}{\Delta \ln(1-\alpha)} = \frac{-E}{R} \frac{\Delta (1/T)}{\Delta \ln(1-\alpha)} + n \quad (7)$$

Thus the slope of a plot of the left hand side of equation (7) versus $\frac{\Delta (1/T)}{\Delta \ln(1-\alpha)}$ will enable the calculation of the activation energy.

Integral methods make use of the integrated form of equation 1.

$$\int_0^\alpha \frac{d\alpha}{(1-\alpha)^n} = \int_{T \text{ at } t=0}^{T \text{ at } t} A e^{-E/k(T_0 + t)} dt \quad (8)$$

the solution of equation 8 consists of an infinite series of which, usually, the first two terms serve for all calculations of interest. These methods were used by Doyle⁽⁴⁵⁾ and also by Coats and Redfern⁽⁴⁶⁾ who proposed the following equation.

$$\ln \left[\frac{1 - (1-\alpha)^{(1-n)}}{T^2(1-n)} \right] = \ln \left(\frac{AR}{\beta E} \left[1 - \frac{2RT}{E} \right] \right) - \frac{E}{RT} \quad (9)$$

The $\ln \left\{ \frac{AR}{BE} \left[1 - \frac{2RT}{E} \right] \right\}$ term is usually regarded

as constant over the temperature range of a peak.

Hence if the left hand side is plotted against $1/T$ using various values of n (the order of reaction) until a straight line is obtained, the value of the activation energy can then be calculated from the slope.

In order to remove the uncertainty in the isothermal rate law Ingraham and Marrier⁽⁴⁷⁾ proposed an approximation method for interpreting non-isothermal data. A cylindrical pellet of the reacting solid is formed and when the reaction occurs it does so by nucleating on the circular faces and following a contracting cylinder topochemical rate law. They put forward a modified kinetic equation which takes into consideration the temperature dependence of the pre-exponential factor

$$d\alpha/dt = A T e^{-E/RT} f_n(\alpha) \quad (10)$$

Another method of removing uncertainties is that developed by Gentry, Hurst and Jones⁽⁴⁸⁾ in which non-isothermal experiments are carried out at different heating rates. The method was actually developed for temperature programmed reduction (tpr) reactions but should be equally applicable to any topochemical process.

For a reaction of the type Solid + Gas \rightarrow Products in which gas flows over the solid at a constant rate, Gentry, Hunt and Jones derived the following equation. In doing so they assumed that the variation of rate constant with temperature can be described by the Arrhenius equation and that the temperature increases linearly with time.

$$2 \ln(T_m) - \ln B + \ln(G)_m = E/RT_m + \text{constant} \quad (11)$$

where T_m = the temperature at which rate is a maximum
 B = the heating rate
 $(G)_m$ = the composition of the gas phase in tpr which in this study can be regarded as a constant.

In order to derive the activation energy values of T_m are measured at different heating rates. From a graph of the left hand side of equation (11) the activation energy can be calculated from the slope.

Doyle's Method

Doyle eliminated the necessity for assumptions about the form of the function of α by extending experiments to include an additional isothermal run. This run is then compared at equivalent α values α_1 with the non-isothermal run. Under isothermal conditions ($T = T_0$)

$$\alpha = \alpha_1 \text{ at } T = T_0 \text{ and } f\alpha_1 = Ae^{-E/RT_0}$$

At a constant heating rate ϕ :

$$\alpha = \alpha_1 \text{ at } T = T_0 \text{ and}$$

$$f\alpha_1 = \frac{\Delta E}{R\phi} p(x_1)$$

$$\text{where } x_1 = E/RT_0$$

$$\text{so that } Ae^{-E/RT_0} = \frac{\Delta E}{R\phi} p(x_1)$$

$$\text{hence } t_1 = \frac{E}{R\phi} e^{E/RT_0} p(x_1)$$

$$\text{and } \ln t_1 = \ln\left(\frac{E}{R\phi}\right) + \frac{E}{RT_0} + \ln p(x_1)$$

Evaluation of $p(x_1)$ still requires an estimate of the activation energy. This could in principle be done by trial and error but if x is sufficiently large (>20) and the temperature interval for the non-isothermal scan is restricted (<100 K) then $\log p(x_1)$ is an approximate linear function of x , i.e. of $1/T_0$

$$\log x = a + bx$$

Doyle gives values of:

$$a = -2.315$$

$$b = 0.4567$$

so that $\log p(x) \approx -2.315 - \frac{0.4567 E}{R} \left(\frac{1}{T} \right)$

and hence:

$$\ln t_i = \ln \left(\frac{E}{R\phi} \right) + \frac{E}{RT_i} - 2.315 - \frac{0.4567E}{R} \left(\frac{1}{T} \right)$$

$$\ln t_i = m(1/T_i) + \text{constant}$$

A plot of $\ln t_i$ against $(1/T_i)$ should thus be linear with a slope $m = \frac{0.4567 E}{R}$

from which a value for the activation energy can be estimated.

The advantage of not having to assume a form of the function of α has been gained at the expense of additional experimentation. Doyle's method does have the disadvantage that the evaluation of $p(x_i)$ involves approximations and that allowance has to be made in measuring t_i for the period required for the sample to reach the isothermal reaction temperature T_i .

4.3 Method

Before any accurate thermogravimetric analysis could be carried out certain experimental conditions had to be decided upon. This involved selecting the most suitable furnace atmosphere and the most appropriate weight and particle size of the sample.

The nature of the surrounding atmosphere can have a profound effect on the temperature of a decomposition stage. Normally the function of the atmosphere is to remove the gaseous product evolved during thermogravimetry in order to ensure that the nature of the surrounding gas remains as constant as possible throughout the experiment. The most common atmospheres employed in thermogravimetry are:

- (a) static air (air flows around the furnace by convection only)
- (b) dynamic air where air is passed through the furnace at a measured rate
- (c) dynamic inert often nitrogen gas which provides a non-reactive atmosphere capable of transporting product vapours away from the sample.

Preliminary experiments were carried out employing all three types of atmosphere. Using a static air atmosphere the time taken for the complex to decompose isothermally over a range of temperatures from 545 K to 570 K was well in excess of forty eight hours. This was thought to be due to the build up of product gas around the sample which inhibited the decomposition process. It was found that when a nitrogen atmosphere was used there was a tendency of the evolved ligands to condense on the sample container hang down rod, evident by a brown tarry film, which consequently resulted in inaccurate weight changes being recorded. Thus a dynamic air atmosphere was chosen to carry out the thermogravimetric analysis since it did not give rise to any of the practical problems associated with the static air and nitrogen atmospheres.

The weight and particle size of a sample also governs the thermogravimetric results. Large particle size can often create deviations from linearity in the temperature rise so consequently each sample was finely ground before any thermogravimetric experiments were carried out.

A large volume of sample in the crucible is also a disadvantage since not all of the sample will necessarily be at the same temperature. In addition a large volume can also impede the diffusion of evolved gas. Consequently different parts of the sample may be at significantly different temperatures and will have reached different stages of decomposition at any given instant. The resulting thermal and reaction gradients across the sample will lead to the production of a poorly defined thermogravimetric curve. Use of a small volume of sample will minimise these effects, although too small a sample may result in a loss of precision. In these studies it was found that samples of approximately 5 to 10 mg proved to be the optimum.

Experimental Procedure

Thermogravimetric analysis was carried out using the METTLER TA 3000 system, the instrument layout of which is shown schematically in figure 4.3.

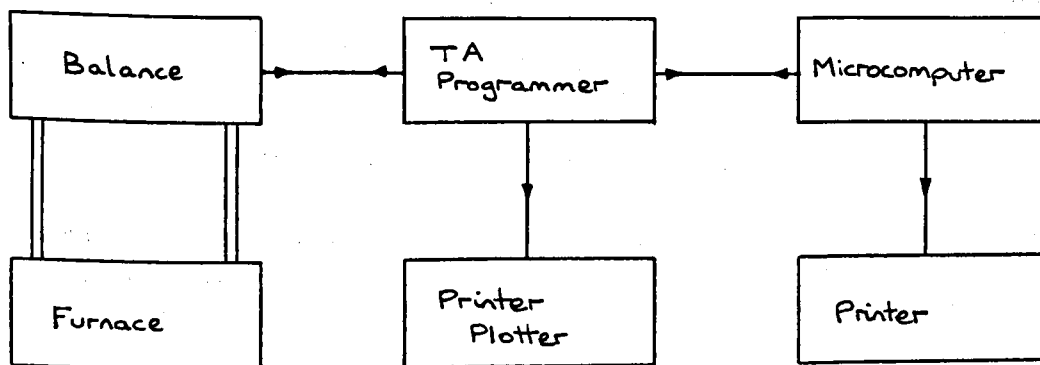


Figure 4.3 Schematic Representation of METTLER TA 3000 System

Non-isothermal thermogravimetric analysis involved accurately weighing the sample using the balance. The experimental parameters such as temperature range, heating rate and initial weight were then entered into the TA processor. The sample was transferred to the sample holder and the furnace raised while still at room temperature.

Isothermal thermogravimetric analysis involved weighing the sample and inputting the experimental parameters such as isothermal temperature, length of time of isothermal analysis and initial weight. The sample was transferred to the sample holder and the furnace preheated to the required experimental temperature before being raised. Typical input data for both isothermal and non-isothermal thermogravimetric analysis are given in the appendix.

Once the thermogravimetric analysis experiment was completed the results were temporarily stored in the TA processor. The raw data was then transferred to the Epson microcomputer for permanent storage and evaluation.

4.4 Treatment of Data

The evaluation of each isothermal experiment was carried out using a spreadsheet program. The raw data stored in the TA72 system was copied to the DOS partition on the hard disc. Changing to an alternative operating system allowed conversion of raw data to an ASCII file containing a specified number of data points. Each point had recorded values of time, temperature, weight and weight change. Typically the raw data which consists of 6 000 points would be compressed to 100 points. After loading the spreadsheet program the compressed ASCII file data could be imported, parsed and manipulated. Various spreadsheets were developed as the work progressed designed to evaluate the various isothermal kinetic expressions relative to solid state chemistry studies and allowed graphical and statistical evaluation of the validity of these in any particular experiment.

After importing and parsing, the raw data contained in cells A1 - D 14 (figure 4.4) are then manipulated by the area of the spreadsheet designed to interpret the information kinetically. This area of the spreadsheet is contained in cells A200 - N316, (figure 4.5). The time is given in cells A200 - A316. Cells B200 - B316 is denoted f which is the fraction decomposed

ie.
$$f = \frac{\text{final weight} - \text{weight at time, } t}{\text{final weight} - \text{initial weight}}$$

where initial weight and final weight are given in G8 and G9 respectively. These are variable parameters which the user can select by discretionary interpretation of the original raw data which may cover a wider weight loss range than is actually required. For example in the interpretation of data from thermal analysis of a compound where it was the second stage of decomposition which was of interest the initial weight would not be the initial experimental weight but rather the weight at the end of the first step. The values contained in column B are utilised throughout the rest of the spreadsheet.

Columns C - M correspond to the formula of various isothermal rate laws. If Row 203 (figure 4) is considered then the formulae would be as listed in table 4.2.

TABLE 4.2

Isothermal Rate Laws and Corresponding Spreadsheet Formulae

Cell	Formula	Rate Law
C203	@ ln (B203)	ln f
D203	@ ln (A203)	ln t
E203	+B203/(1-B203)	f/1-f 2nd Order Law
F203	@ ln (E203)	ln [f/(1-f)] Prout Tompkins Log Law
G203	@ ln [-ln (1-B203)]	ln [-ln(1-f)] Erofeev Equation
H203	1- (1-B203) 0.3333	1 - (1-f) ^{1/3} Contracting Sphere
I203	@ ln (1-B203) * (-1)	-ln (1-f) First Order Decay Law
J203	1/B203	1/f Reciprocal Law
K203	1/[(SLS200-1) * (1-B203) (SLS200 - 1)]	1/(n-1) (1-f) ⁿ⁻¹ where n is the 'order of reaction', a parameter which can be chosen by the user to give a best fit and is entered in L200 eg in Figure 4.5 the value is given as 3
M203	+A203/SNS200	t/t _{0.5} Reduced Time Scale where t _{0.5} is the half time of reaction chosen by the user from columns A and B and entered as a parameter in N200.

+ This variable rate law was derived from the equation:

$$\text{rate} = \frac{df}{dt} \propto (1-f)^n$$

$$\therefore \frac{df}{dt} = k(1-f)^n$$

$$\frac{df}{(1-f)^n} = k dt$$

Integration using tables of standard integrals gives

$$\frac{1}{(n-1)(1-f)^{n-1}} = kt$$

Figure 4.6 shows how the application of regression analysis was carried out on the spreadsheet. The spreadsheet incorporated a limited linear regression facility which will give the slope, intercept and correlation coefficient of any given ranges. These data were placed, by the user, in cells A307, A306 and A308 respectively. The regression analysis has been extended to include the standard deviation of the slope (useful in assessing errors in rate constants) by inserting appropriate formula in cells K307, K308, K309, H307, H308, H309 and F307.

Standard deviation is given by the equation

$$S_b = \frac{S_r^2}{S_{xx}}$$

$$\text{where } S_r^2 = \frac{S_{yy} - B^2 S_{xx}}{n-2}$$

$$S_{xx} = \sum x_i^2 - (\sum x_i)^2/n$$

$$S_{yy} = \sum y_i^2 - (\sum y_i)^2/n$$

Thus the formulae were entered into the spreadsheet as follows:

F1:Help 2:Edit 3:Macro 4:Abs Ready ! 5:Goto 6:Window 9:Calc F10:Graph
 A1: 'EXP00022.001 File

A/B/C/D/E/F/G/H/
1	EXP00022.001	File						spreadsheet for
2	31.01.89	Date						analysis of isothermal
3	17:06	Time						tg data
4	TG	Type						
5	285.00	Start temp	[Deg C]					no more than 100 points
6	285.00	End temp	[Deg C]					output in a200..a302
7	0.00	Temp rate	[K/Min]					
8	700.0	Iso time	[Min]					INIT. WT.= 9.968
9	10.394	Weight;Length	[mg;mm]					FINL. WT.= 7.3
10	1.00	Identification						
11	429	Delta time	[sec]					
12	3819	Total number of points						See A306..K309 for reg anal
13	97	Number of selected points						
14	Begin							
15	0	285	9.968	-0.00022				
16	429	285	9.82	-0.00022				
17	858	285	9.724	-0.00022				
18	1287	285	9.644	-0.00022				
19	1716	285	9.552	-0.00022				
20	2145	285	9.46	-0.00022				
	Free:80	x [329k]	Auto	[LTISO100.WKS]				12:23:11 pm

Figure 4.4

Spreadsheet Cells A1 - H20.

F1:Help 2:Edit 3:Macro 4:Abs Ready | 5:Goto 6:Window 9:Calc F10:Graph Window 9:Calc F10:Graph
 B307 (S2 W9): 0.00008723555

```

.....A/.....B/.....C/.....D/.....E/.....F/.....G/.....H/.....I/.....J/.....
303
304
305
306 Intercept 0.007853
307 Slope 8.72E-05 S.D. of slope = 6.30E-07 90090 1.22E+08
308 R^2 0.999063 8.016116 0.932245
309 Sum X^2 5.28E+08 20 0.000048
310 Sum Y^2 4.145151
311 Sum X*Y 46785.11
312
313 Type following text :in H307 @SUM(Range of x values)
314 in H308 @SUM(Range of y values)
315 in H309 @COUNT(Range of x values)
316 Regression output MUST be in A306
317
318
319
320
321
322

```

Free:80 X [329k] Auto [LTISO100.WKS] 12:20:18 pm 12:22:08 pm

Figure 4.6

Spreadsheet Cells A303 - K322.

Cell	Spreadsheet Formula	Mathematical Formula
H307	@ sum (Range of x)	Σx_i
H308	@ sum (Range of y)	Σy_i
H309	@ count (Range of x)	n
K307	+B309 - (H307 * H307/H309)	$\Sigma x_i^2 - (\Sigma x_i)^2/n = S_{xx}$
K308	+B310 - (H308 * H308/H309)	$\Sigma y_i^2 - (\Sigma y_i)^2/n = S_{yy}$
K309	+ (K308 - (B307 * B307 * K307))/(H309-2)	$S_{yy} - B^2 S_{xx}/n-2 = S_r^2$
F309	@ SQRT (K309/K307)	$S_r^2/S_{xx} = SB$

Σx_i^2 and Σy_i^2 were already incorporated in the spreadsheet and placed, by the user, in cells B309 and B310 respectively.

4.5 Results

For each of the six complexes formed by the reaction between K_2PtCl_4 and ligand the thermogravimetric analysis results are reported. In each case non-isothermal and isothermal experiments were carried out, the appropriate topochemical rate law applied and the activation energy for the decomposition calculated.

4.5.1 cis-Pt(2-aminopyrimidine)₂Cl₂

The non-isothermal thermogravimetric curve (Figure 4.7), obtained using a linear heating rate of 5 Kmin^{-1} , indicated that this complex decomposed in two distinct steps. The first of which corresponded to the loss of one molecule of 2-aminopyrimidine, that is there was a 20.8% weight loss. The theoretical percentages of 2-aminopyrimidine, platinum and chloride present in the complex were calculated.

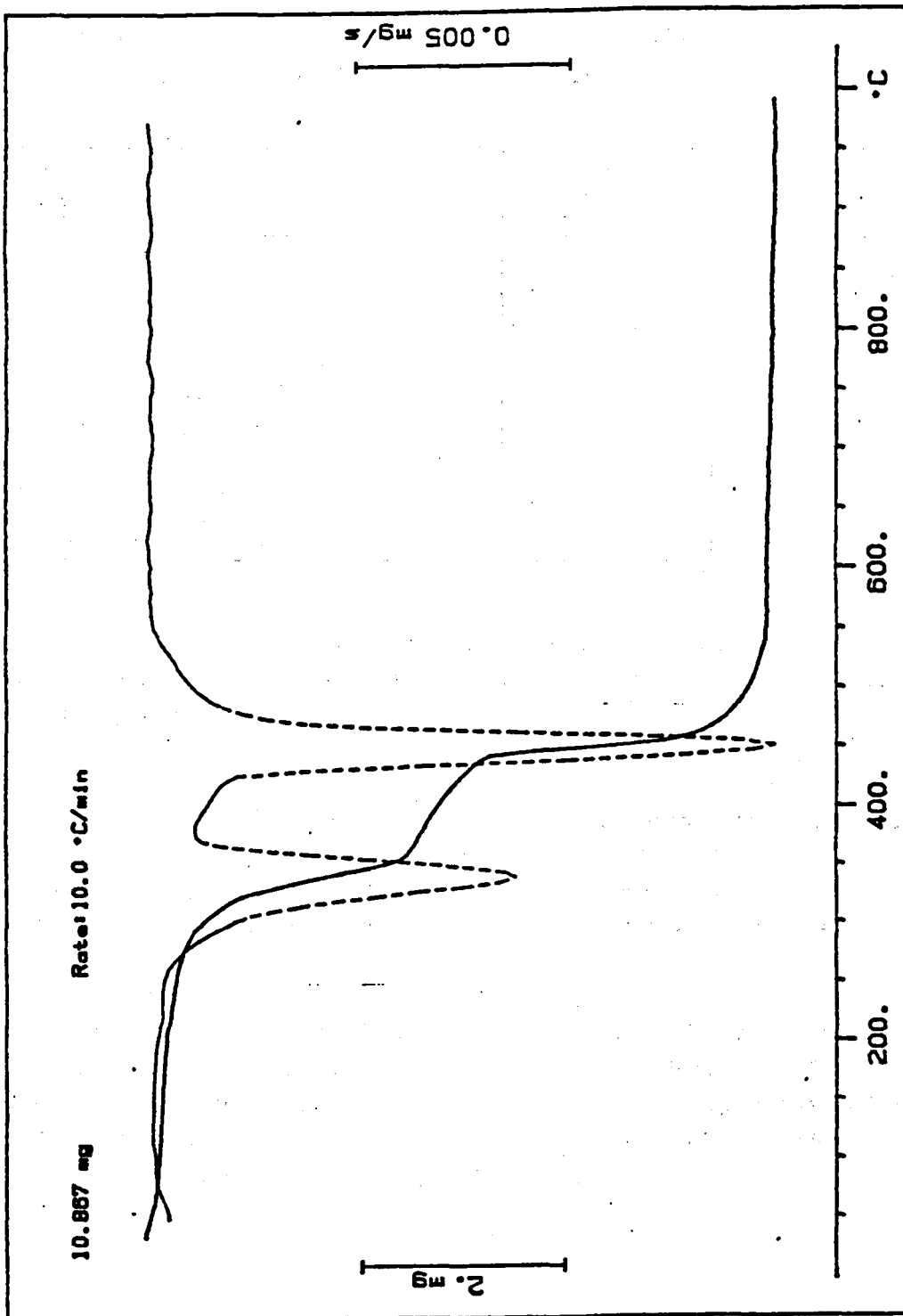


Figure 4.7

Non-isothermal Decomposition of $\text{Pt}(\text{2APm})_2\text{Cl}_2$.

TABLE 4.3

Comparison of Theoretical and Experimental weight Losses from
cis - pt (2-aminopyrimidine)₂Cl₂

Process	Percentage Weight Loss	
	Theoretical	Experimental
1. Loss of one mole of 2 aminopyrimidine	20.8	20.8 in 1st step of TG
2. Loss of two moles of Cl atoms and one mole of 2-aminopyrimidine	36.4	36.1 in 2nd step of TG
3. Loss of all ligands leaving metallic platinum	42.8	43.1 total loss at 590°C

Consequently it was decided to carry out isothermal analysis only on the first stage of decomposition reaction since this involved the loss of one ligand molecule and hence involved platinum-nitrogen bond breaking.

The differential thermogravimetric curve indicated that the temperature at which the rate law is at a maximum in this decomposition step is 545 K. Five isothermal experiments were carried out at different but constant temperatures ranging from 548 K to 568 K. Figure 4.8 shows the typical results obtained from this isothermal analysis. In each case the thermogravimetric curve flattened out at around an approximately 21% weight loss and this point was taken as $\alpha = 1$ in the subsequent evaluation.

The evaluation was carried out using the spreadsheet. For each of the five isothermal experiments a graph of α versus time was plotted and found to be of the form shown in Figure 4.9. Since these α versus time plots were linear for the whole range of the decomposition step, ie from $\alpha = 0$ to $\alpha = 1$ and since $fn(\alpha) = kt$, then the rate constant, k , for this decomposition reaction can be determined directly from the gradient of this plot (Table 4.4).

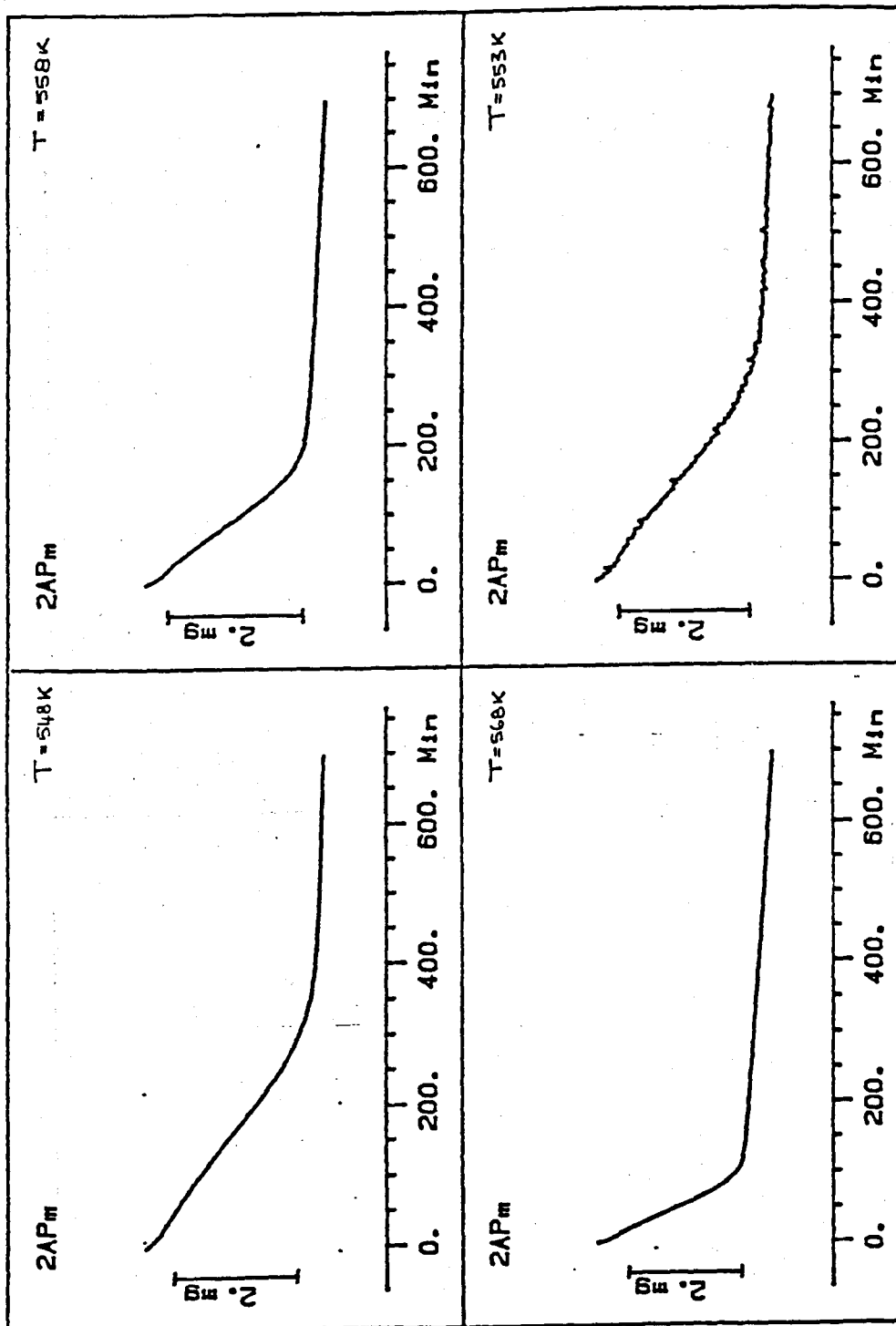


Figure 4.8 Isothermal Decomposition, involving Loss of One Molecule of 2-aminopyrimidine from Pt(2APm)₂Cl₂.

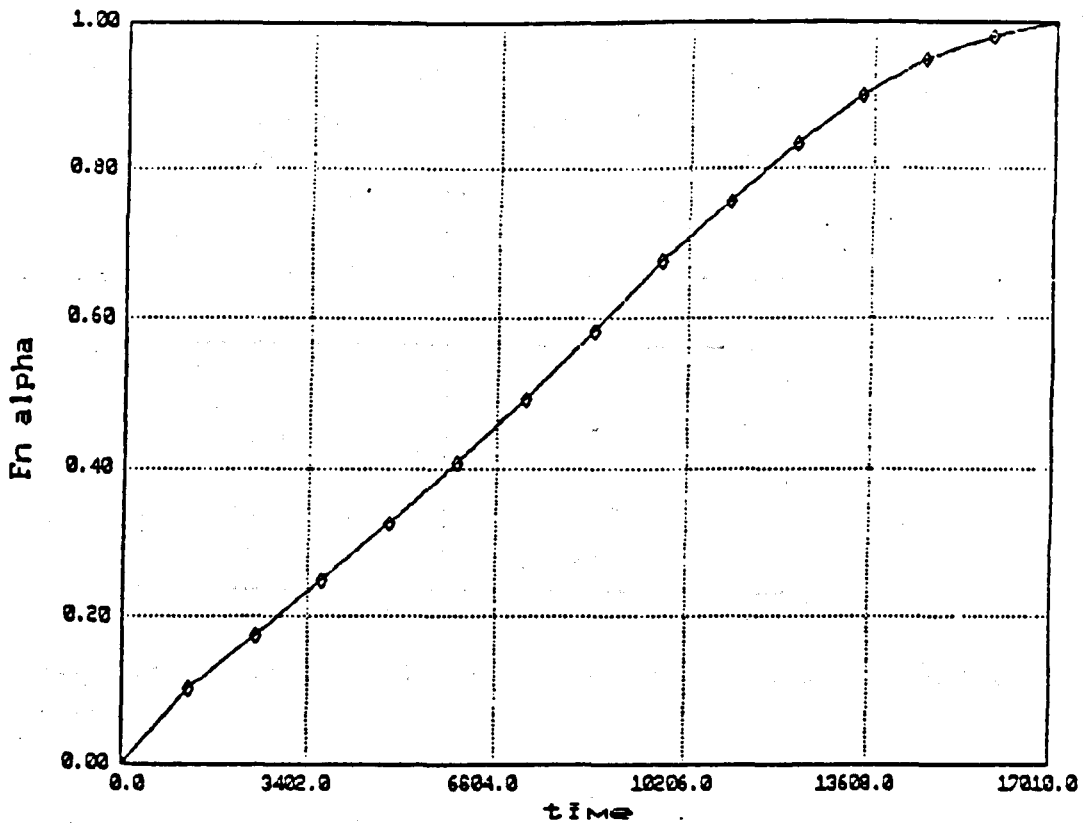


Figure 4.9 Typical Plot of α vs Time for First Stage of the Decomposition Reaction of $\text{Pt}(\text{2APm})_2\text{Cl}_2$

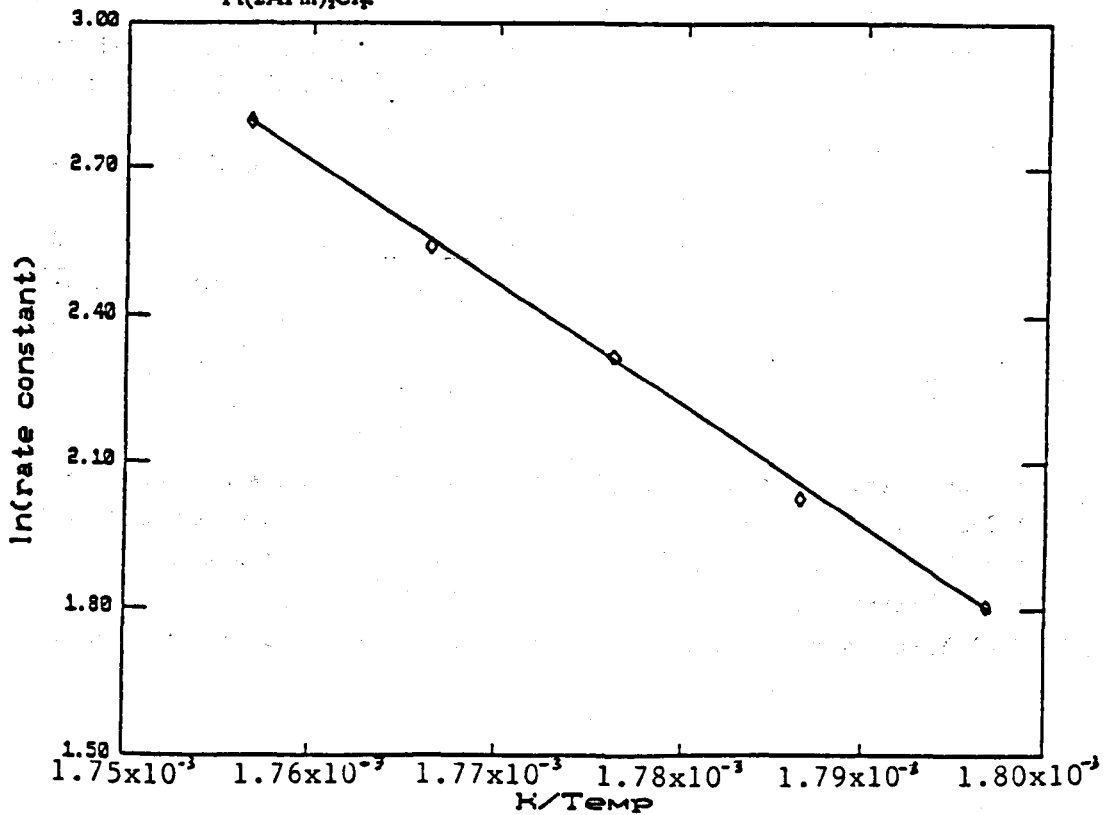


Figure 4.10 Arrhenius Plot for the First Stage of the Decomposition Reaction of $\text{Pt}(\text{2APm})_2\text{Cl}_2$

TABLE 4.4

Rate Constants Obtained at each Isothermal Temperature Corresponding to the loss of one mole of 2-aminopyrimidine

Temperature/k	Rate constant/ 10^3s^{-1}
548	6.09
553	7.60
558	11.7
563	12.7
568	16.4

A graph of $\ln(k)$ against $1/\text{temp}$ figure 4.10 was plotted and the activation energy calculated from the slope as $129 \pm 9 \text{ kJmol}^{-1}$

Doyle's Method

Doyle eliminated the necessity for assumptions about the form of the function of α by comparing experimental results from the isothermal analysis with equivalent α values obtained from a non-isothermal analysis experiment. Doyle derived the following equation:

$$\log(t_i) = m(1/T_i) + C$$

- where t_i = time corresponding to α in the isothermal run
 T_i = temperature corresponding to α in the non-isothermal run
 C = constant
 m = $0.4567E/R$

Non-isothermal analysis was carried out on the $\text{Pt}(2\text{APm})_2\text{Cl}_2$ complex at a heating rate of 1 Kmin^{-1} . this was compared with equivalent values of α from the isothermal experiments at 553 K, 558 K and 563 K. The evaluation of both isothermal and non-isothermal curves was achieved using the step evaluation function of the TA72 graphware. Table 4.5 summarises the results when the non-isothermal data was compared with the isothermal data obtained at a temperature of 553 K

TABLE 4.5

Comparison of Time (Isothermal Analysis) with Temperature (Non-Isothermal Analysis) at Equivalent and Values

α	Time (t)	log (t)	Temperature (T)/K	1/T/10 ³ K ⁻¹
0.1	19.42	1.29	574	1.74
0.2	49.55	1.70	592	1.69
0.3	75.02	1.88	599	1.67
0.5	123.94	2.09	608	1.64
0.75	181.59	2.26	619	1.62

A graph of log(t) versus 1/T_i was plotted (Figure 4.11), the activation energy was calculated from the slope and found to be 146 ±3 kJmol⁻¹.

Similar graphs of log(t) versus 1/T_i were plotted using data from the isothermal curves obtained at temperatures of 558 K and 568 K. The activation energy was calculated in each case and found to be 146 ±3 kJmol⁻¹ and 145 ±2 kJmol⁻¹ respectively. Doyles method was also applied by comparing equivalent values obtained using a non-isothermal heating rate of 2 Kmin⁻¹ and the isothermal at 253 K. Again the activation energy was found to be 147 kJmol⁻¹.

These results indicated that Doyles method is consistent within itself. As a further check of the reproducibility of Doyles method the value of the actual intercept can be compared with that calculated by the equation:

$$\text{intercept} = \log(E/R) + \frac{E}{2.303 R \cdot T_0} - 2.315$$

where T₀ = the temperature of the isothermal run.

This value should correspond to the actual intercept from the plot of log(t) versus 1/T_i.

Actual intercept = 15.30

$$\begin{aligned} \text{Calculated intercept} &= \log \frac{146 \times 10^3}{8.314} + \frac{146 \times 10^3}{2.303(8.314)533} - 2.315 \\ &= 15.72 \end{aligned}$$

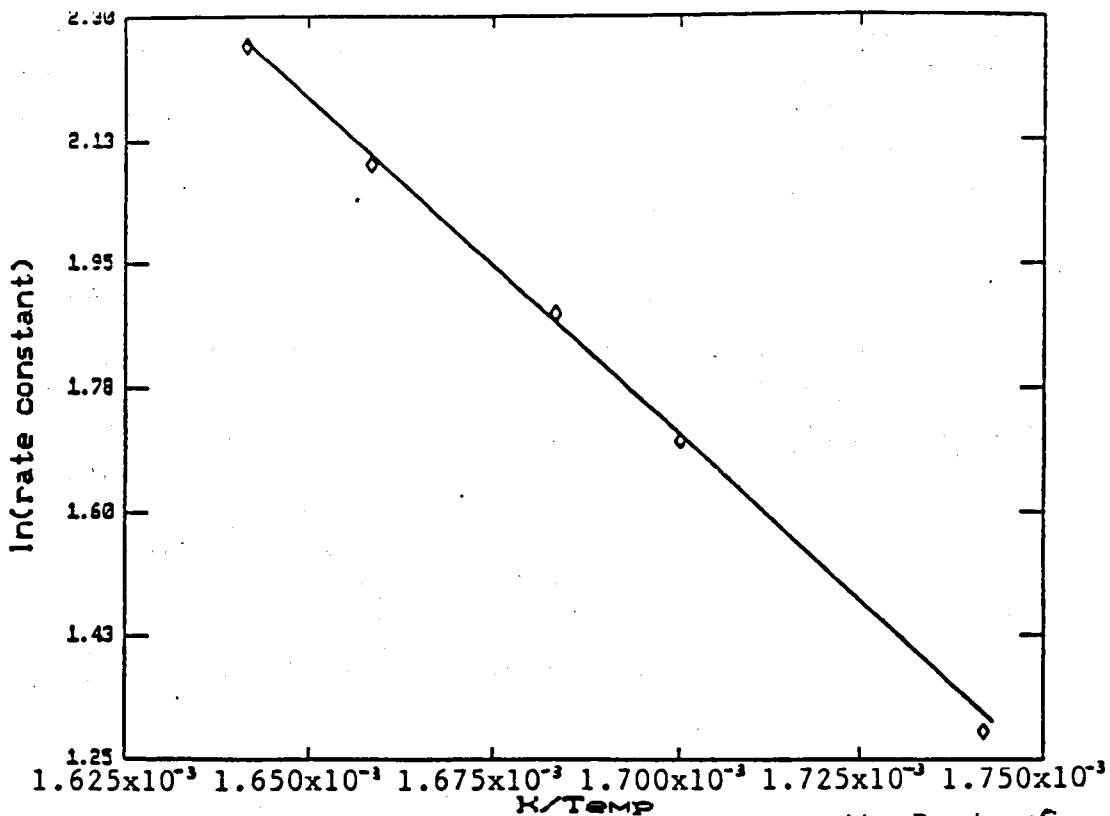


Figure 4.11 Doyle's Plot for the First Stage of the Decomposition Reaction of $Pt(2APm)_2Cl_2$.

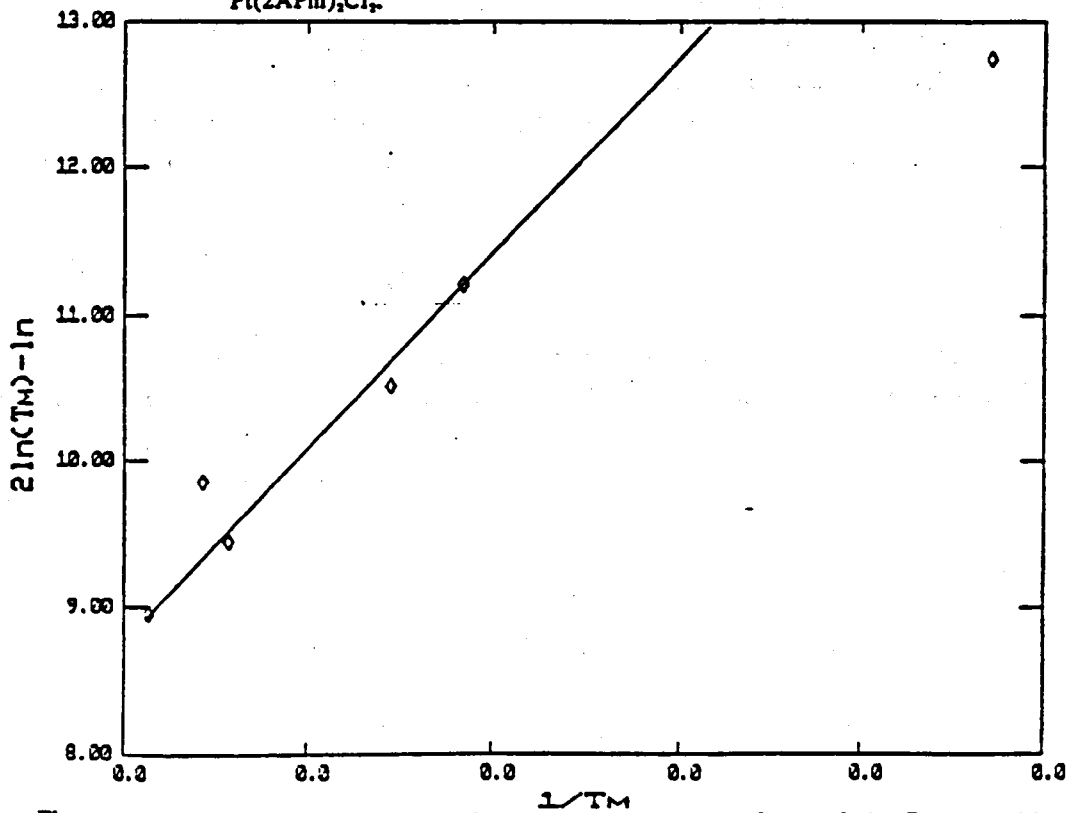


Figure 4.12 Gentry, Hurst and Jones Plot for the First Stage of the Decomposition Reaction of $Pt(2APm)_2Cl_2$.

These results appear to confirm that the theory of Doyle's method applies. However, the fact that there is an unacceptable difference in the value of the activation energy compared with that obtained isothermally (129 kJmol⁻¹) places doubt upon the validity of Doyle's method in estimating the activation energy for the decomposition of the types of complexes under investigation.

Application of Gentry, Hurst and Jones' Method

Non-isothermal analysis was carried out using heating rates of 1, 5, 10, 20 and 30 kmin⁻¹. The first step of the decomposition reaction was analysed by the method of Gentry, Hurst and Jones, which can be adapted from its original purposes in temperature programmed reduction experiments to give.

$$2\ln(T_m) - \ln\beta = E/RT_m + \text{constant}$$

where T_m = temperature at which rate law is a maximum
 β = heating rate

A graph of $[2\ln(T_m) - \ln(\beta)]$ versus $1/T_m$ was plotted (Figure 4.12), from which it can be seen that there is a wide scatter of points and the data does not give rise to a satisfactory linear plot. However, the best straight line through the data resulted in an activation energy of 413 kJmol⁻¹ compared to 129 kJmol⁻¹ obtained isothermally. These results indicated that the Gentry, Hurst and Jones method is not acceptable for calculating the activation energy of decomposition for complexes of the type under investigation.

4.5.2 *cis*-Pt(2-amino-4-methylpyrimidine)₂Cl₂

The theoretical percentages of platinum, 2-amino-4-methylpyrimidine and chloride in the complex were calculated for comparison with experimental weight losses in order to identify decomposition processes.

TABLE 4.6

**Comparison of Theoretical and Experimental Weight Losses
from cis - Pt (2-amino-4-methylpyrimidine)₂ Cl₂**

Process	Percentage Weight Loss	
	Theoretical	Experimental
1. Loss of one mole of 2-amino-4-methylpyrimidine	22.5	22.5 in 1st step of TG
2. Loss of two moles of Cl atoms and one mole of 2-amino-4-methylpyrimidine	37.1	36.9 in 2nd step of TG
3. Loss of all ligands leaving metallic platinum	40.4	40.6 total loss at 500°C

The non-isothermal thermogravimetric curve (Figure 4.13) obtained for the decomposition of this complex again gave rise to two distinct steps, the first of which corresponded to a 22% loss in weight which is equivalent to the theoretical percentage of one molecule of 2-amino-4-methylpyrimidine. Consequently isothermal analysis was carried out on this first step of the decomposition over a range of temperatures between 548 K and 568 K. Figure 4.14 shows the typical isothermal curves obtained.

Using the spreadsheet it was found from reduced time plots that for all five isothermal experiments the α versus time curves were of the same type as shown in Figure 4.15. On investigation it can be seen that the plot of α versus time is linear for approximately the first eighty percent of this first decomposition step. Thus the rate can be determined directly from the slope of this line. The results from each of the five isothermal experiments are summarised in Table 4.7.

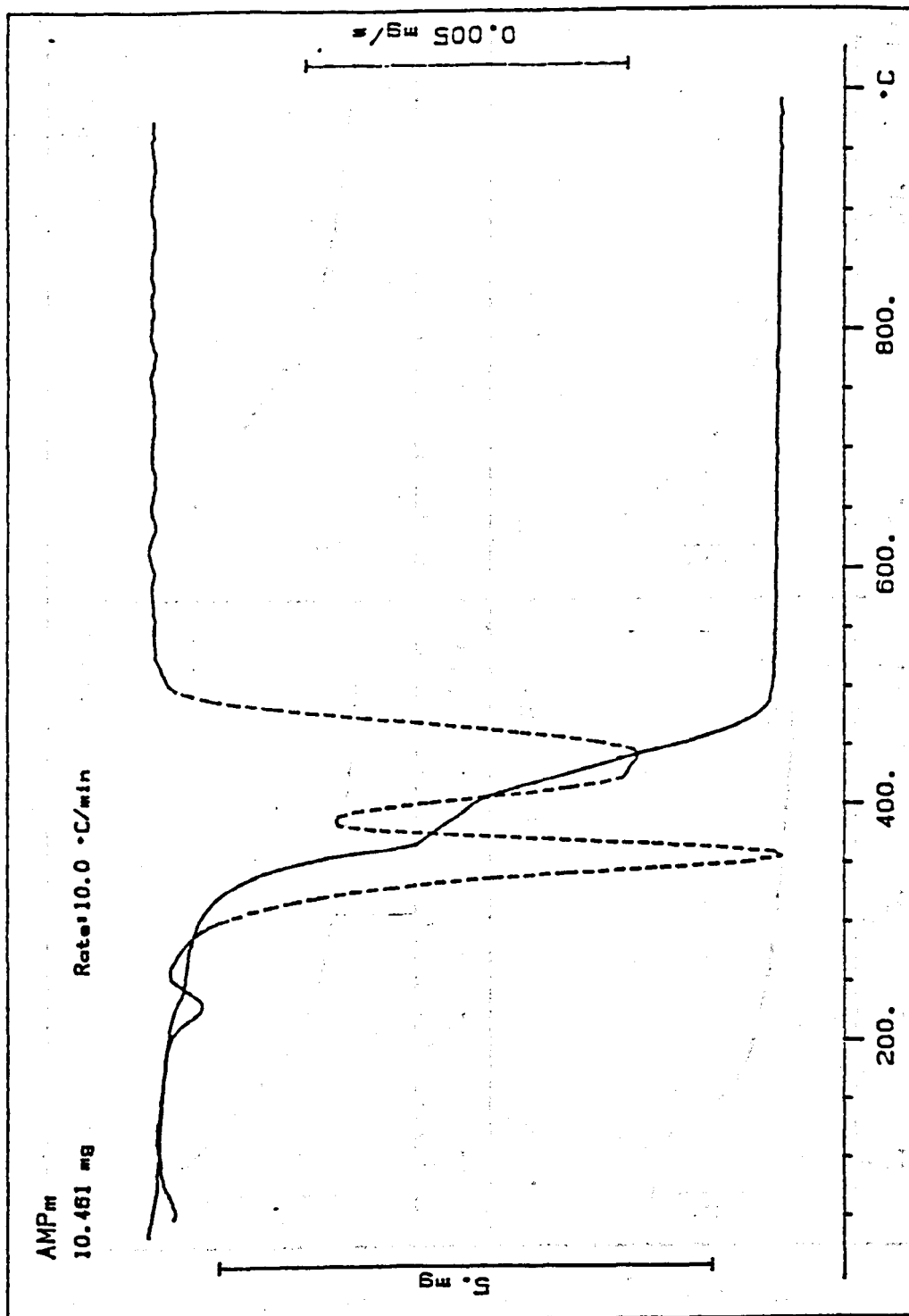


Figure 4.13

Non-isothermal Decomposition of $\text{Pt}(\text{AMPm})_2\text{Cl}_2$.

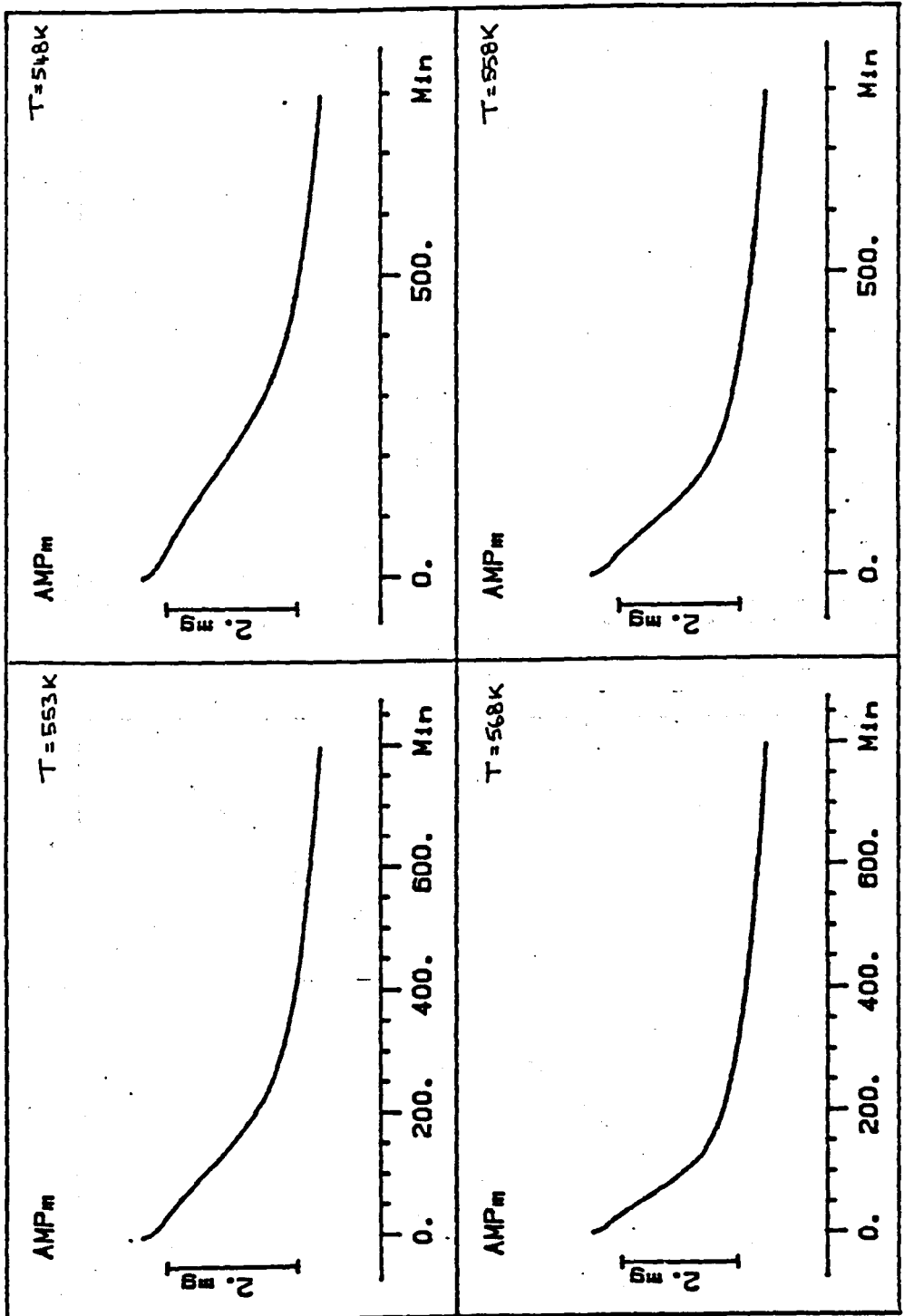


Figure 4.14 Isothermal Decomposition, Involving the Loss of One Molecule of 2-amino-4-methylpyrimidine from Pt(AMPm)₂Cl₂.

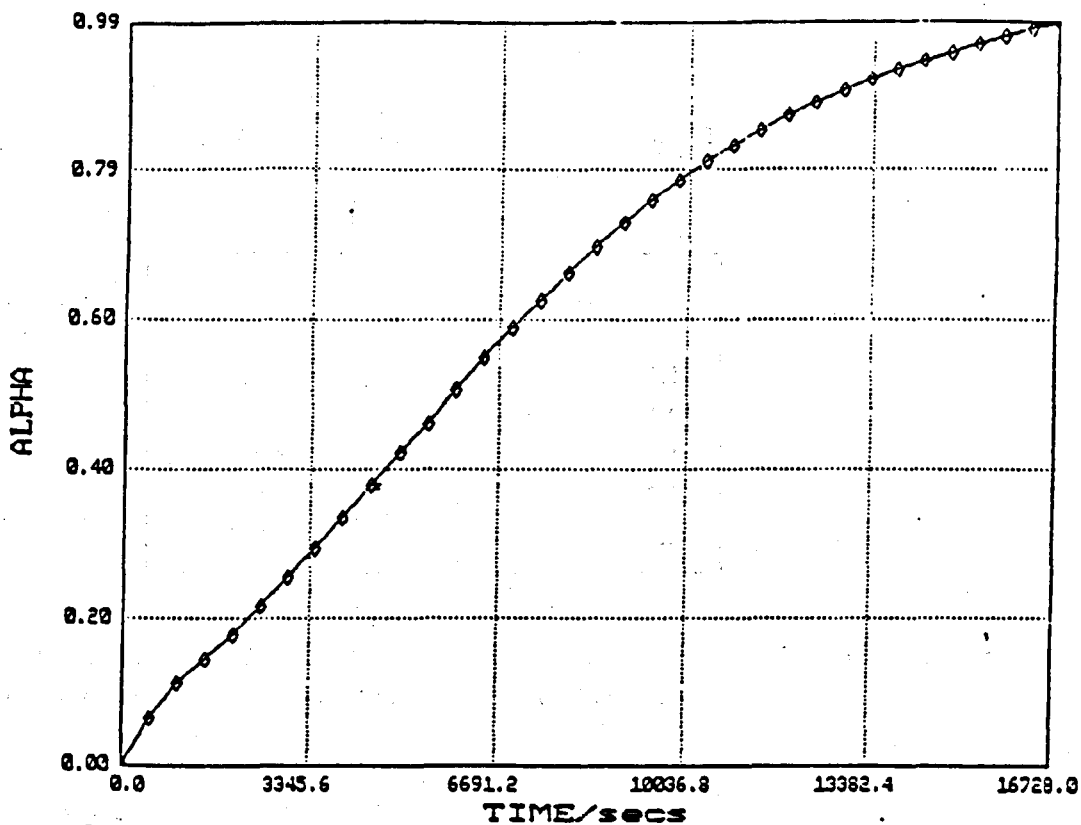


Figure 4.15 Typical Plot of α vs Time for the First Stage of the Decomposition Reaction of $\text{Pt}(\text{AMPm})_2\text{Cl}_2$.

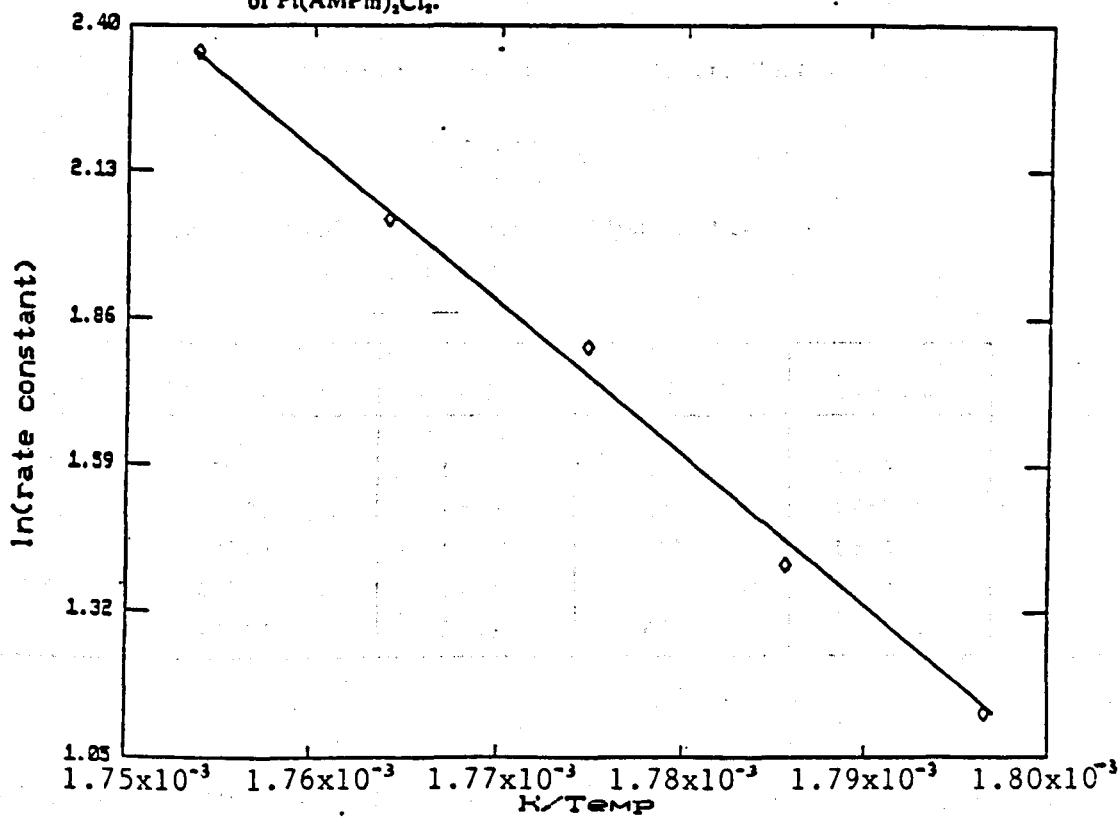


Figure 4.16 Arrhenius Plot for the First Stage of the Decomposition Reaction of $\text{Pt}(\text{AMPm})_2\text{Cl}_2$.

TABLE 4.7

**Rate Constants obtained at each Isothermal Temperature
Corresponding to the Loss of one Mole of
2-amino-4-methylpyrimidine**

Temperature/K	Rate/ 10^5s^{-1}
548	3.1
553	4.08
558	6.1
563	7.7
568	10.5

The activation energy for this decomposition process was calculated from the slope of the Arrhenius plot (Figure 4.16) and found to be $161 \pm 8 \text{ kJmol}^{-1}$.

Doyles' Method

Doyles' method was applied using data from a non-isothermal at a heating rate of 1 Kmin^{-1} and comparing it with equivalent α values from the isothermal run at 558 K (Table 4.8).

TABLE 4.8

**Comparison of Time (Isothermal analysis) and Temperature
(Non-Isothermal analysis) at Equivalent α Values**

α	Time (t_i)	$\log(t_i)$	Temp (T_i)/K	$1/T_i/10^3\text{K}^{-1}$
0.1	16.06	1.206	586	1.707
0.2	45.87	1.662	603	1.659
0.3	73.07	1.864	612	1.633
0.5	123.96	2.093	624	1.602
0.75	198.04	2.297	633	1.581

A graph of $\log(t_i)$ versus $1/T_i$ was plotted (Figure 4.17) and from the slope the activation energy was calculated as 147 kJmol^{-1} .

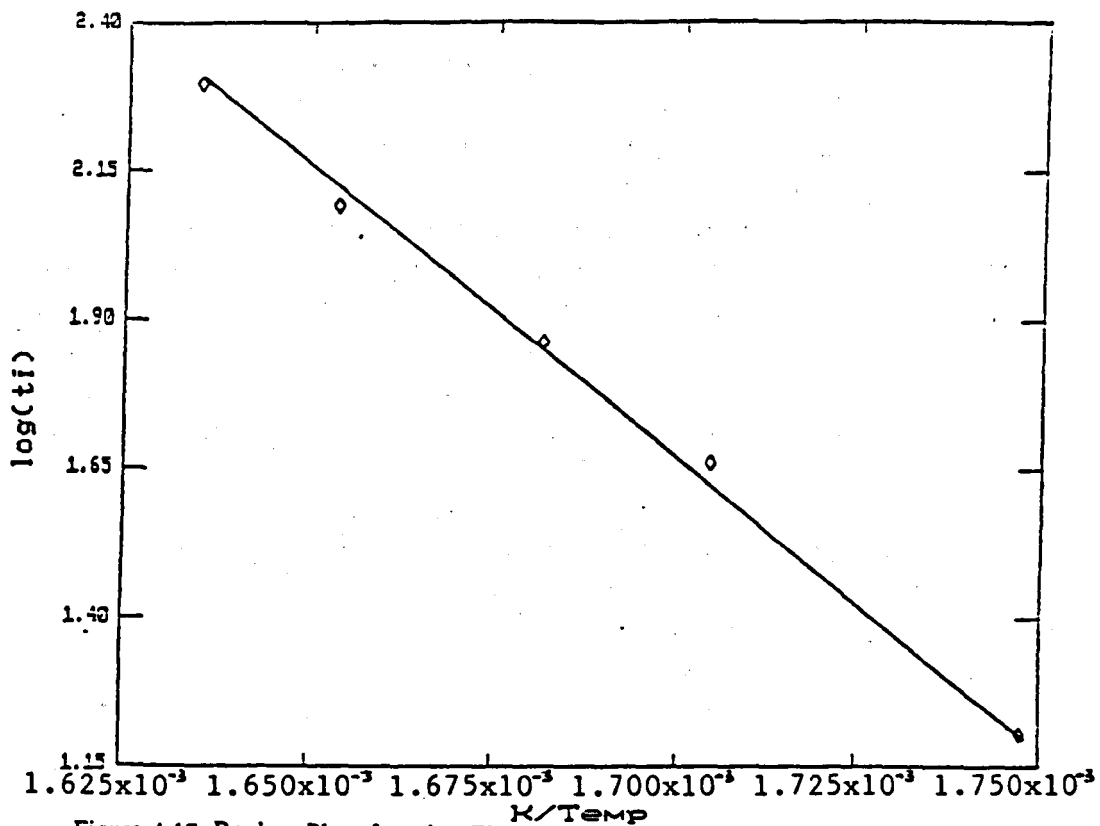


Figure 4.17 Doyle's Plot for the First Stage of the Decomposition Reaction of Pt(AMPm)₂Cl₂.

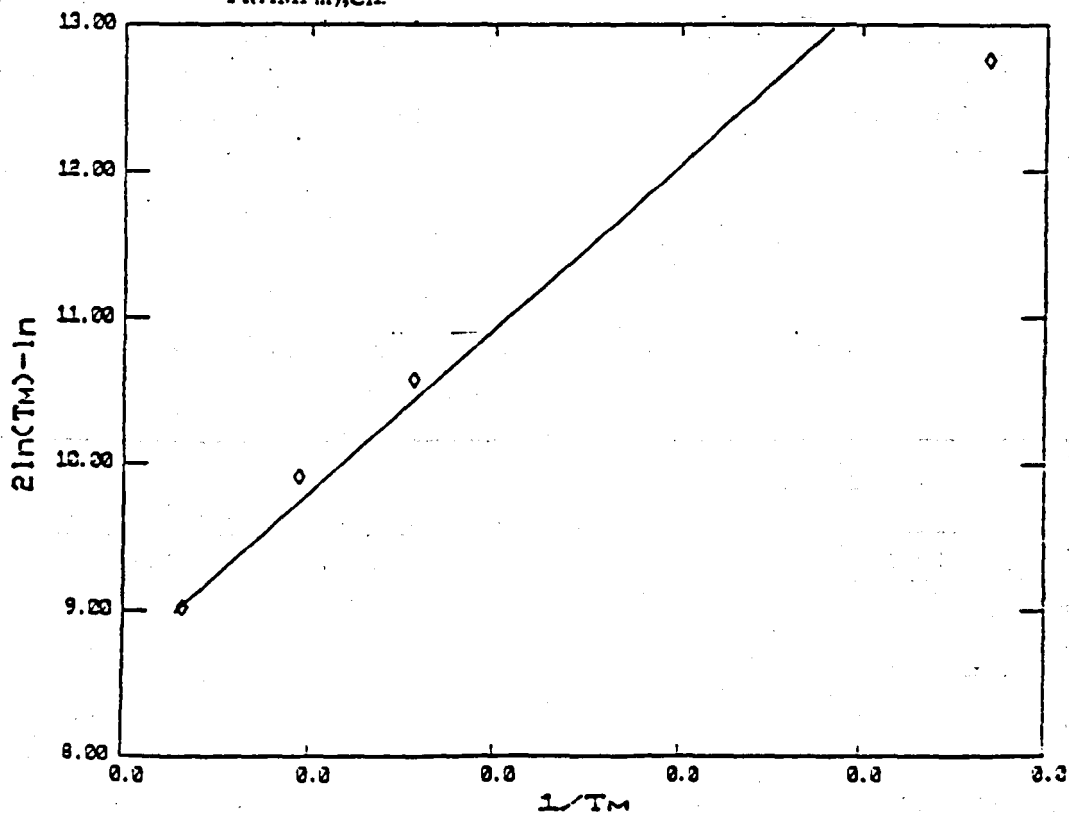


Figure 4.18 Gentry, Hurst and Jones Plot for the First Stage of the Decomposition Reaction of Pt(AMPm)₂Cl₂.

Application of Gentry, Hurst and Jones' Method

Non-isothermal analysis was carried out at heating rates of 1, 10, 20 and 50 Kmin⁻¹. Gentry, Hurst and Hones method for interpreting non-isothermal results was applied to the data and a graph of $[21n(T_m) - \ln]$ vs $1/T_m$ was plotted (Figure 4.18). Again there was a wide scatter of points and a satisfactory linear plot was not obtained. The activation energy, calculated by the best straight line through the points, was found to be 358 kJmol⁻¹ which is not compatible with that obtained isothermally (161 kJmol⁻¹).

It was thus decided to reject the Gentry, Hurst and Jones method as a means of interpreting non-isothermal data since it produced unacceptable results for both complexes so far investigated. This was not too surprising since the method was developed specifically for temperature programmed reduction reactions using hydrogen which is an extremely highly diffusive gas. In these studies it is evolution of the ligand which is occurring and so consequently the diffusion rate for the larger molecule will be much slower and could result in the onset of a diffusion control process when the chemical rate is high. This is particularly true at higher heating rates.

4.5.3 *cis*-Pt(pyridine)₂Cl₂

The differential thermogravimetric curve (Figure 4.19) from the non-isothermal experiment carried out using a linear heating rate of 2 Kmin⁻¹ indicated that there were four stages of decomposition. The weight loss for steps one and two were found to be 4.1% and 17.9% respectively. It was thought that the first step in the decomposition process may be due to the loss of a molecule of water. Consequently in the calculation of the theoretical weight percentages the formula of the complex was taken to be Pt(Py)₂Cl₂ · H₂O.

TABLE 4.9

Comparison of Theoretical and Experimental Weight Losses
from *cis* - Pt (pyridine)₂ Cl₂

Process	Percentage Weight Loss	
	Theoretical	Experimental
1. Loss of one mole of water	4.1	4.1 in 1st step of TG curve
2. Loss of one mole of pyridine	17.9	17.9 in 2nd step of TG curve
3. Loss of two moles of Cl atoms and one mole of pyridine	33.9	33.2 in 3rd step of TG Curve
4. Loss of all ligands leaving metallic platinum	44.1	44.8 total loss at 500°C

Thus from these theoretical values it was predicted that the first step did correspond to the loss of a water molecule and that the second corresponded to the loss of a pyridine molecule.

In order to verify that water was involved in the initial decomposition Mass Spectrometry was utilised. This technique involved the setting up of a small reaction tube and programable heater on the spectrometer sample inlet system. A small quantity (100 mg) of the complex was heated in the reaction tube and the change in the m/e 18 peak intensity was monitored during the course of heating.

On heating the sample at a temperature of approximately 423 K a small peak at $m/e = 18$ was detected, the intensity of which did increase. However, the appearance of this peak was not convincing confirmatory evidence for the presence of bound water in the complex for the following reasons:

- the peak was smaller than expected.
- the origin of the peak may have been absorbed water on the tube surface, desorbing on heating.
- the glassware above the furnace would have been at a lower temperature and therefore any water vapour present may have condensed or absorbed onto the glass walls.

As a result of the inherent practical problems it was decided that it was not worthwhile pursuing this technique, but rather to concentrate on experiments designed to study the second decomposition step which is unequivocally loss of one molecule of pyridine.

Isothermal decompositions were carried out on the second step of the decomposition reaction since this involved the loss of a ligand molecule. The procedure adopted involved rapidly raising the temperature from a starting temperature of 308 K to the required isothermal temperature (which ranged from 491 K to 508 K) using a linear heating rate of 100 Kmin^{-2} in order to remove any traces of water present over this heating period.

This was preferred to the normal procedure of plunging the sample into a preheated furnace which would probably result in simultaneous reactions involving both first and second steps of decomposition.

The isothermal analysis of the second stage of the decomposition then proceeded as normal. Typical isothermal curves obtained for the second step of the decomposition are shown in Figure 4.20.

It was found that for each of the seven isothermal experiments the α versus time plots (Figure 4.21) yielded a straight line for approximately the first 85% of the decomposition reaction. The rate constants were calculated directly from the slope and the results are tabulated below

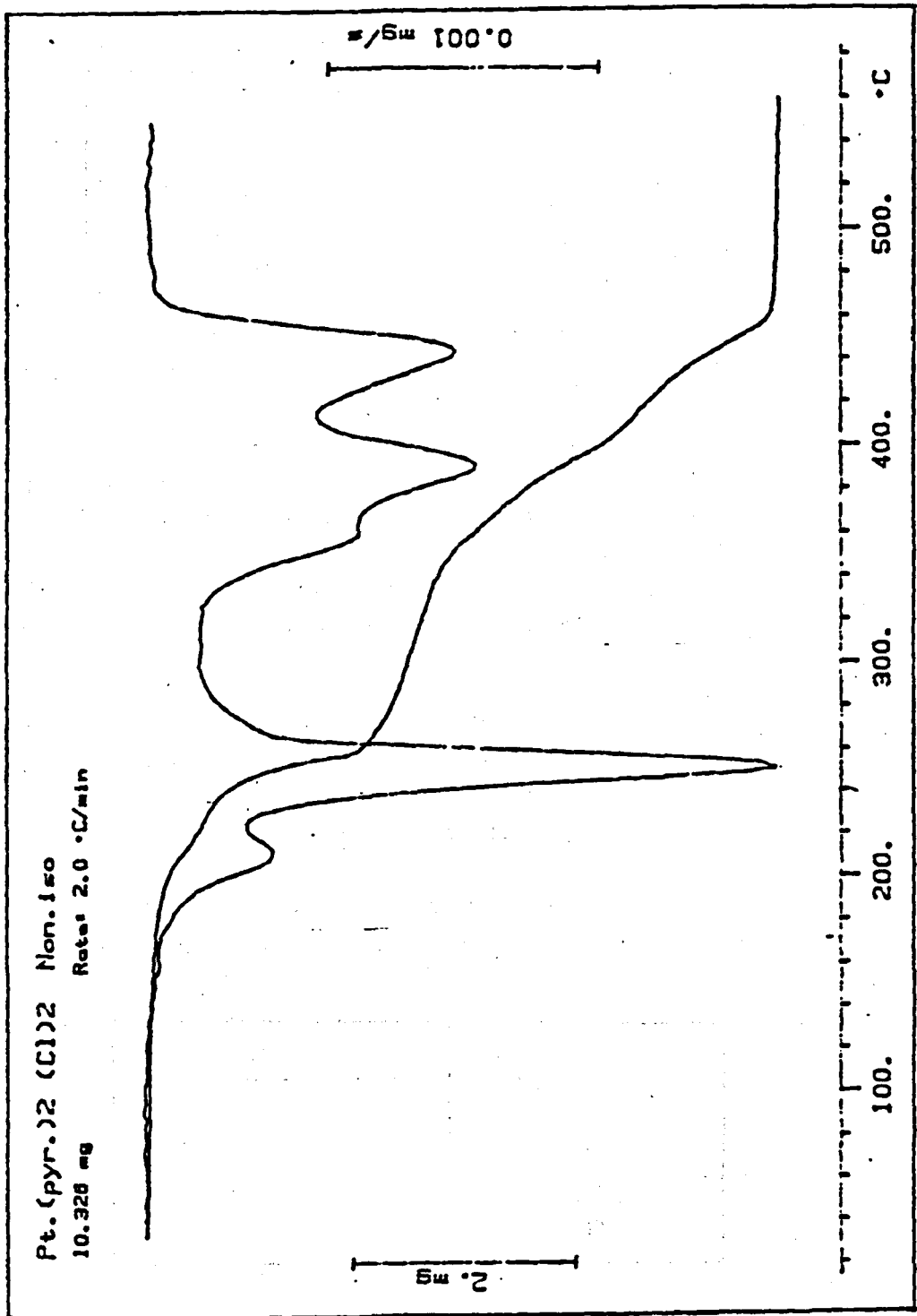


Figure 4.19 Non-isothermal Decomposition of $\text{Pt(Py)}_2\text{Cl}_2$.

TABLE 4.10

Rate Constants obtained at each Isothermal Temperature corresponding to the loss of One mole of Pyridine

Temperature/K	Rate constant/ 10^5s^{-1}
487	5.85
491	4.84
493	9.14
498	10.1
503	14.5
505	26.9
508	37.1

An Arrhenius plot was plotted (Figure 4.22) and the activation energy calculated as $173 \pm 9 \text{ kJmol}^{-1}$.

The kinetics of the decay portion of the isothermal curve was also investigated. However the decay portion of the curve is not well defined in the higher temperature range, and the runs at 498 K, 503 K, 505 K and 508 K were omitted from decay region analysis.

From the shape of the isothermal curves it was thought that the decay region might obey the first order decay law, in which case $-\ln(1 - \alpha) = kt$ in which α the fraction reacted is a fraction of the decay region.

The first order decay law was found to be obeyed and the rate constants were determined from the slope of the plot of $-\ln(1 - \alpha)$ vs time (Figure 4.23). The results are summarised in Table 4.11.

TABLE 4.11

Rate Constants obtained at each Isothermal Temperature corresponding to the Decay Portion of the α vs time plot

Temperature/K	Rate constant/ 10^5s^{-1}
487	2.89
489	3.36
491	3.98
493	5.11

An Arrhenius graph was plotted (Figure 4.24) and the activation energy found to be 194 kJmol^{-1}

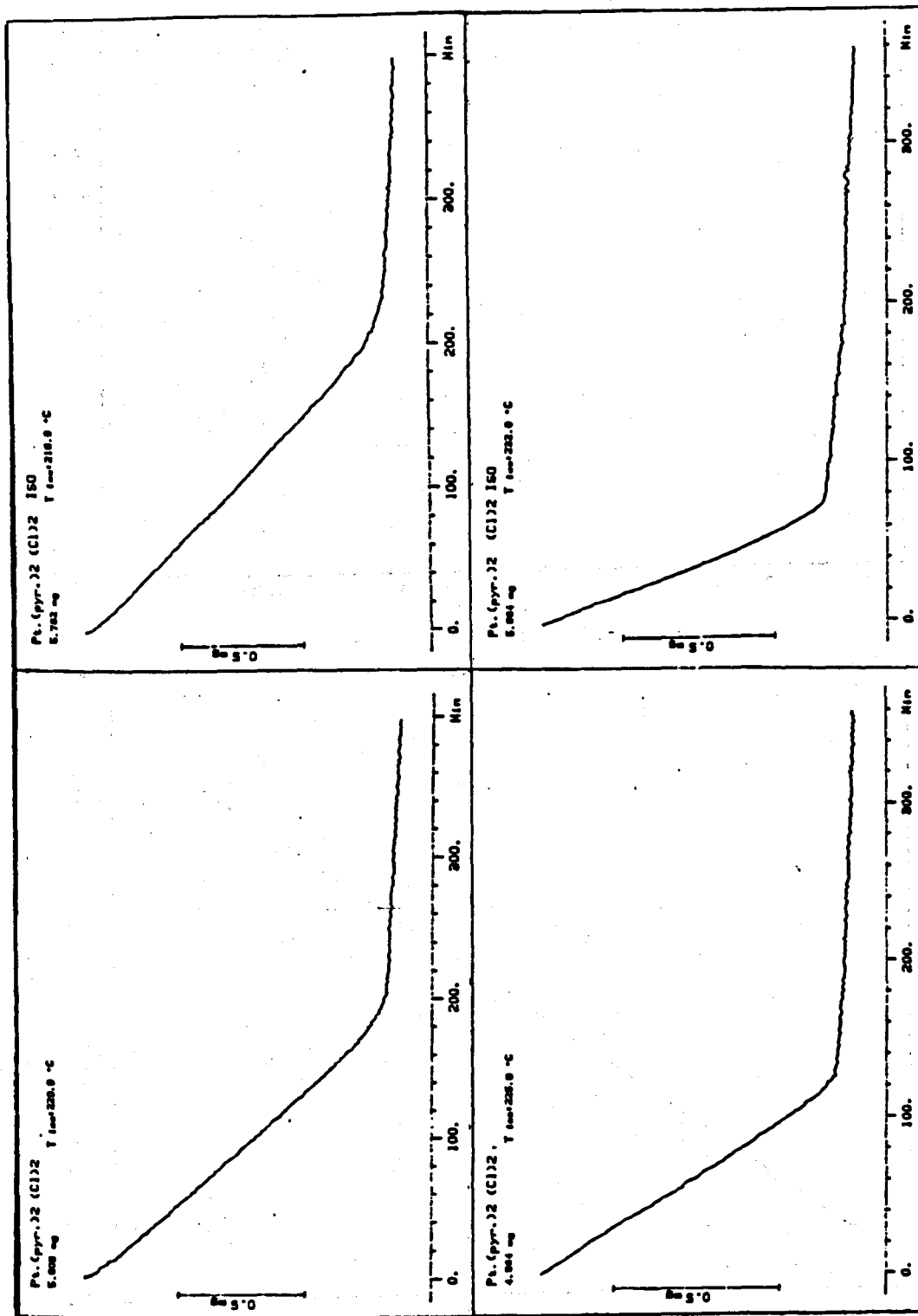


Figure 4.20

Isothermal Decomposition, Involving Loss of One Molecule of Pyridine from $\text{Pt}(\text{Py})_2\text{Cl}_2$.

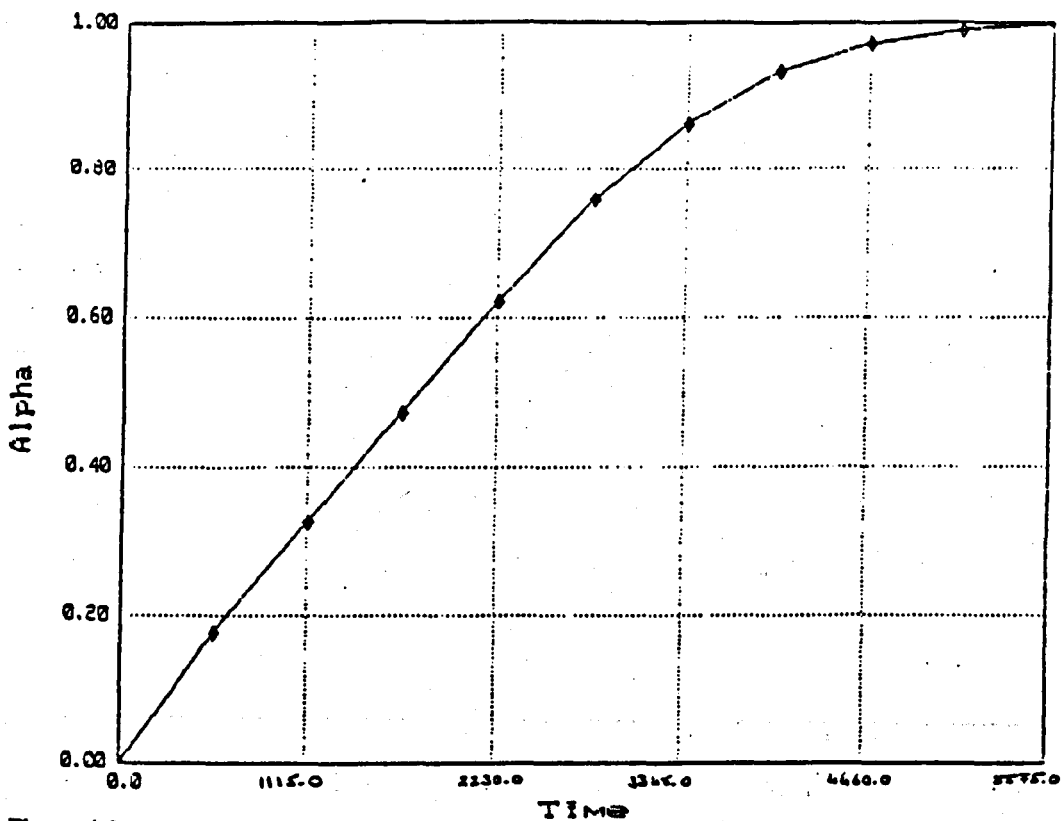


Figure 4.21 Typical Plot of α vs Time for the Loss of One Molecule of Pyridine.

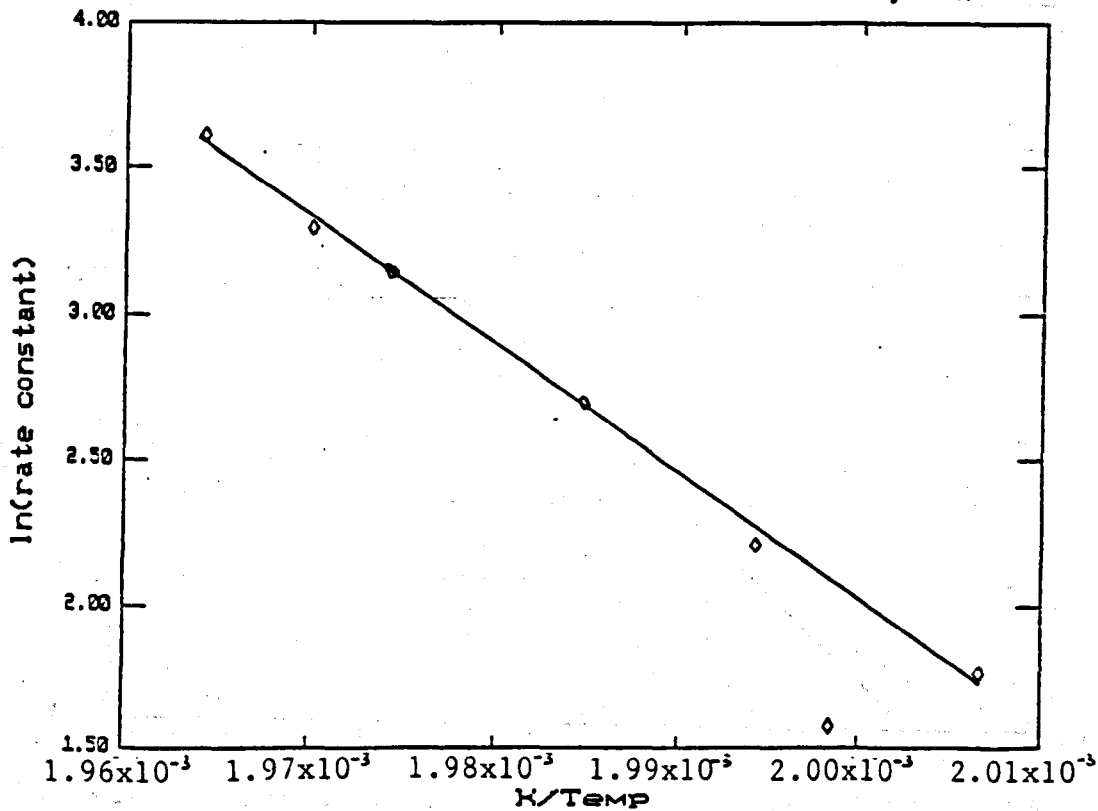


Figure 4.22 Arrhenius Plot for the Decomposition Reaction Involving the Loss of One Molecule of Pyridine.

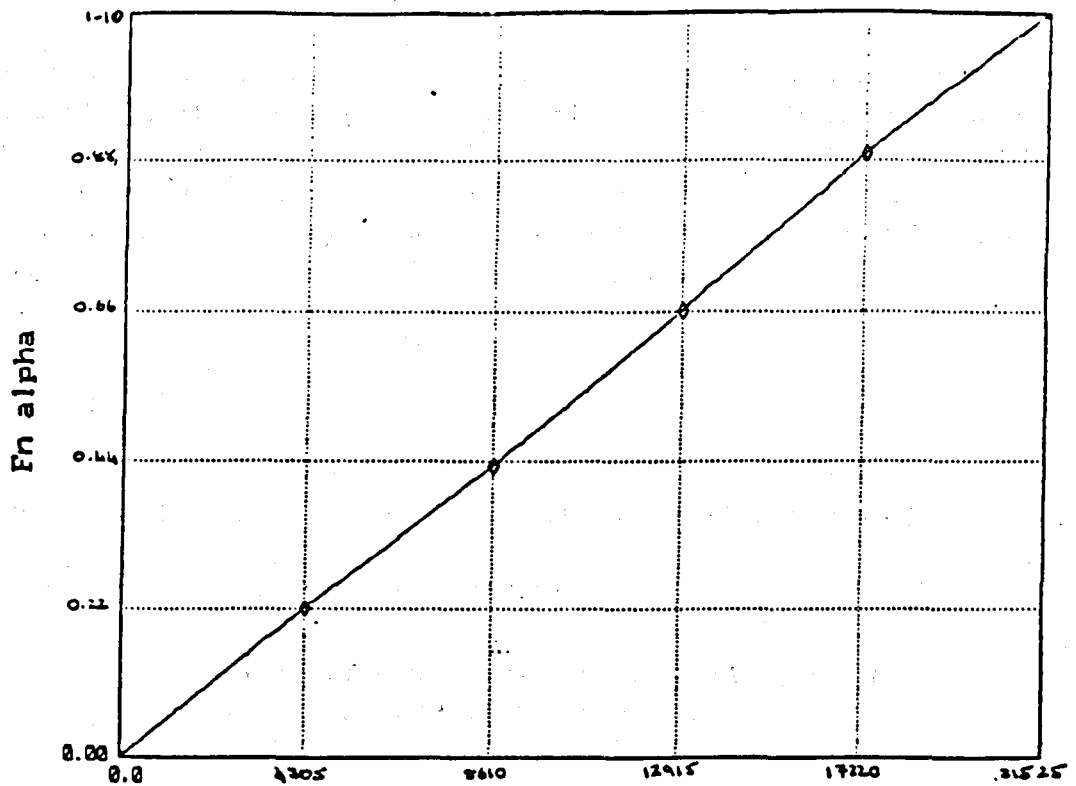


Figure 4.23 Typical Plot of $-\ln(1 - \alpha)$ vs Time for the Decay Region of the Decomposition Step Involving the Loss of One Molecule of Pyridine.

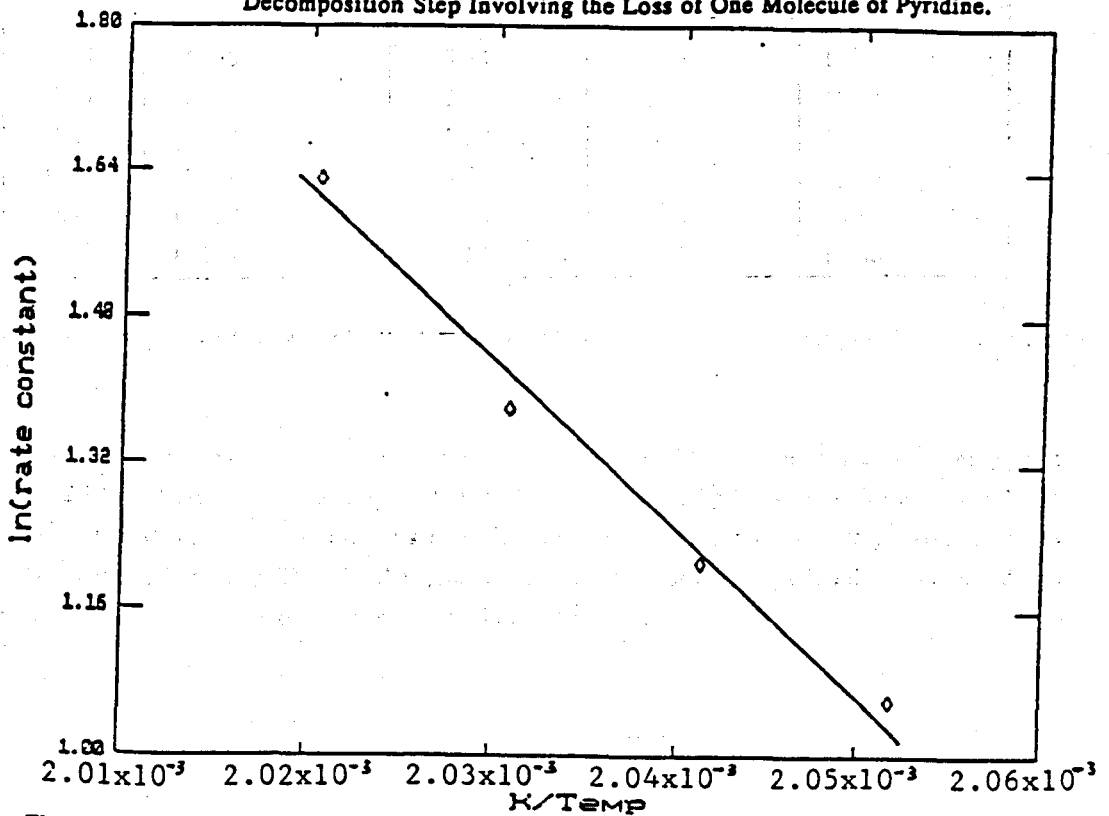


Figure 4.24 Arrhenius Plot for the Decay Region of the Decomposition Step Involving the Loss of One Molecule of Pyridine.

The difference in activation energy between the linear and decay portions of the isothermal curve, 173 and 194 KJmol⁻¹ respectively, indicate a change in the mechanism of decomposition once the reaction has undergone 85% of decomposition. It is interesting to note that the first order rate law is only obeyed at lower temperatures, the isothermal runs at higher temperatures gave non-reproducible results. This may point to a temperature dependence of the first order decay law being obeyed.

Doyles Method

Doyles method was applied using non-isothermal data obtained at a linear heating rate of 2 Kmin⁻¹ and isothermal data taken from the experiment at temperature 478 K (Table 4.12).

TABLE 4.12

Comparison of Time (Isothermal Analysis) and Temperature (Non-Isothermal Analysis) at Equivalent α Values

α	Time (t_1)	log (t_1)	Temp (T_1)/K	1/ T_1 /10 ³ K ⁻¹
0.37	5495	3.74	519	19.27
0.41	6273	3.80	521	19.21
0.50	7749	3.89	525	19.06
0.60	9594	3.98	528	18.94
0.70	11439	4.06	530	18.88
0.80	13284	4.12	532	18.80

A graph of log(t_1) vs 1/ T_1 was plotted (figure 4.25) and the activation energy calculated as 146 kJmol⁻¹.

For each of the three complexes studied so far Doyles method has given an activation energy of 146 ± 2 kJmol⁻¹ thus making it impossible to distinguish binding between different ligands. In addition the value of the activations energies do not correlate with the respective energies determined isothermally. Thus for the type of complexes under investigation Doyles method was rejected as a valid means of calculating the kinetic parameters.

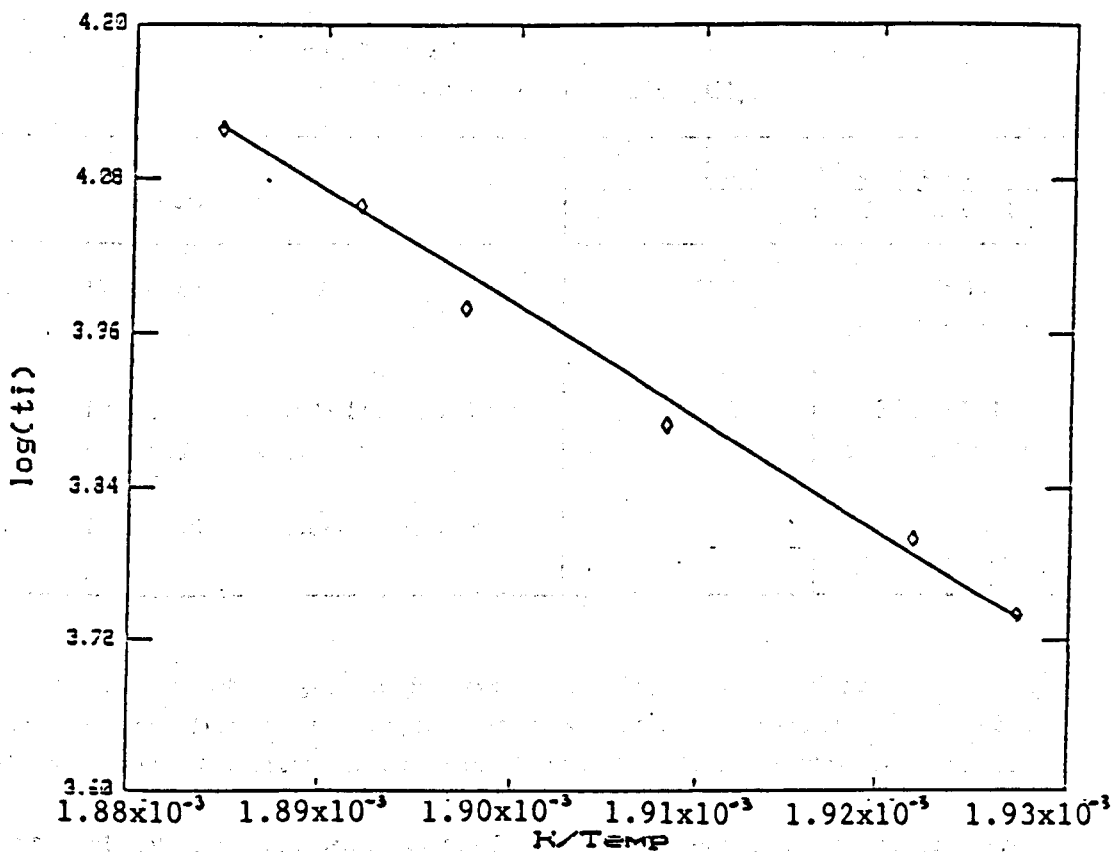


Figure 4.25 Doyles plot for the Decomposition Reaction Involving the Loss of One Molecule of Pyridine.

4.5.4 *cis*-Pt(2-aminopyridine)₂Cl₂

The theoretical percentages of platinum, 2-aminopyridine and chloride present in the complex were calculated for comparison with experimental weight losses in order to identify decomposition processes.

TABLE 4.13

Comparison of Theoretical and Experimental Weight Losses
from *cis* - Pt (2-aminopyridine)₂ Cl₂

Process	Percentage Weight Loss	
	Theoretical	Experimental
1. Loss of one mole of 2-aminopyridine	20.7	20.6 in 1st step of TG curve
2. Loss of two moles of Cl atoms and one mole of 2-aminopyridine	36.3	36.3 in 2nd step of TG curve
3. Loss of all ligands leaving metallic platinum	42.95	43.1 total loss at 500°C

The non-isothermal thermogravimetric curve (Figure 4.26) obtained for this complex indicated that it decomposed in two distinct steps, the first of which corresponded to a weight loss of 20.6% which is equivalent to the calculated theoretical percentage of one molecule of 2-aminopyridine.

Isothermal analysis were carried out on this first stage of the decomposition reaction at a range of constant but different temperatures between 531 K and 543 K. Figure 4.27 shows the typical isothermal thermogravimetric curves obtained.

Plots of α versus time (figure 4.28) were not linear and indicated that most of the decomposition reaction took place between $\alpha = 0.6$ to $\alpha = 1.0$. Various topochemical rate laws were applied to the raw data and it was found that the most appropriate was the Prout-Tompkins plots in which $\ln[\alpha/(1 - \alpha)] = kt$ (Figure 4.29).

The Prout-Tompkins plots were linear only over the range $\alpha = 0.5$ to $\alpha = 0.95$. Using regression analysis the rate constants were calculated from the slope of the linear portion of the Prout-Tompkins plot obtained for each of the five isothermal experiments. The results are summarised in Table 4.14.

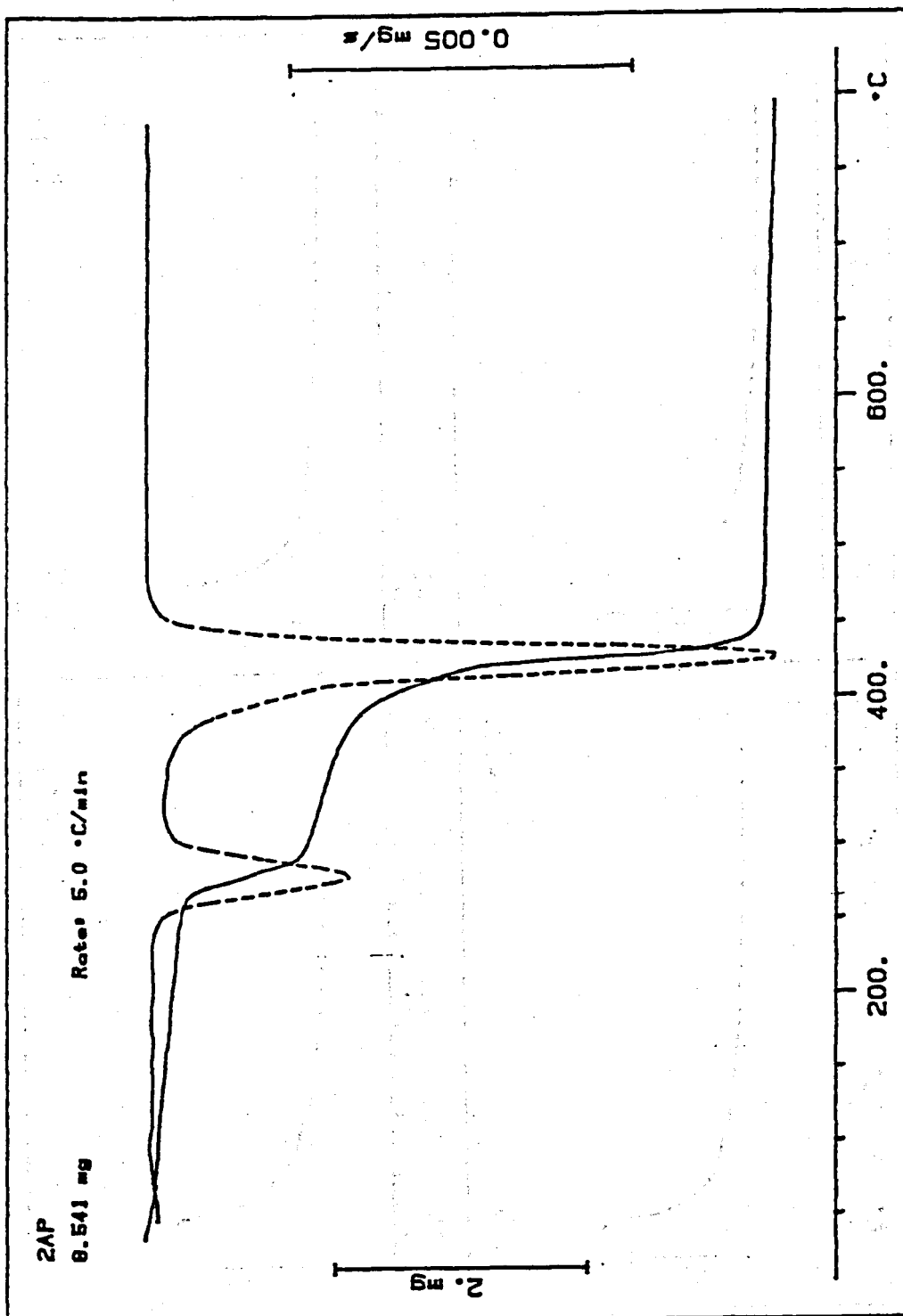


Figure 4.26 Non-isothermal Decomposition of $\text{Pt}(\text{2AP})_2\text{Cl}_2$

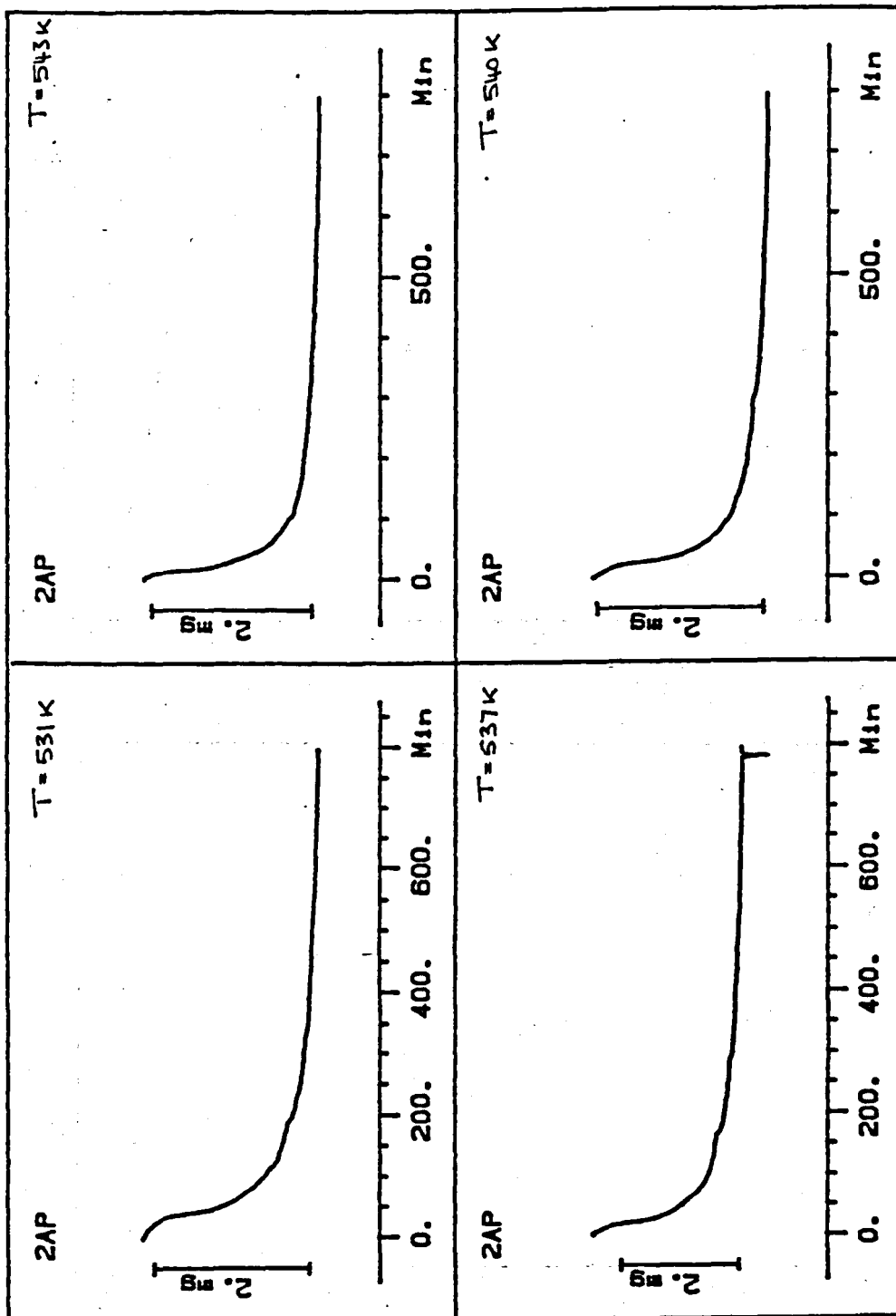


Figure 4.27

Isothermal Decomposition, Involving the Loss of One Molecule of 2-aminopyridine from Pt(2AP)₂Cl₂.

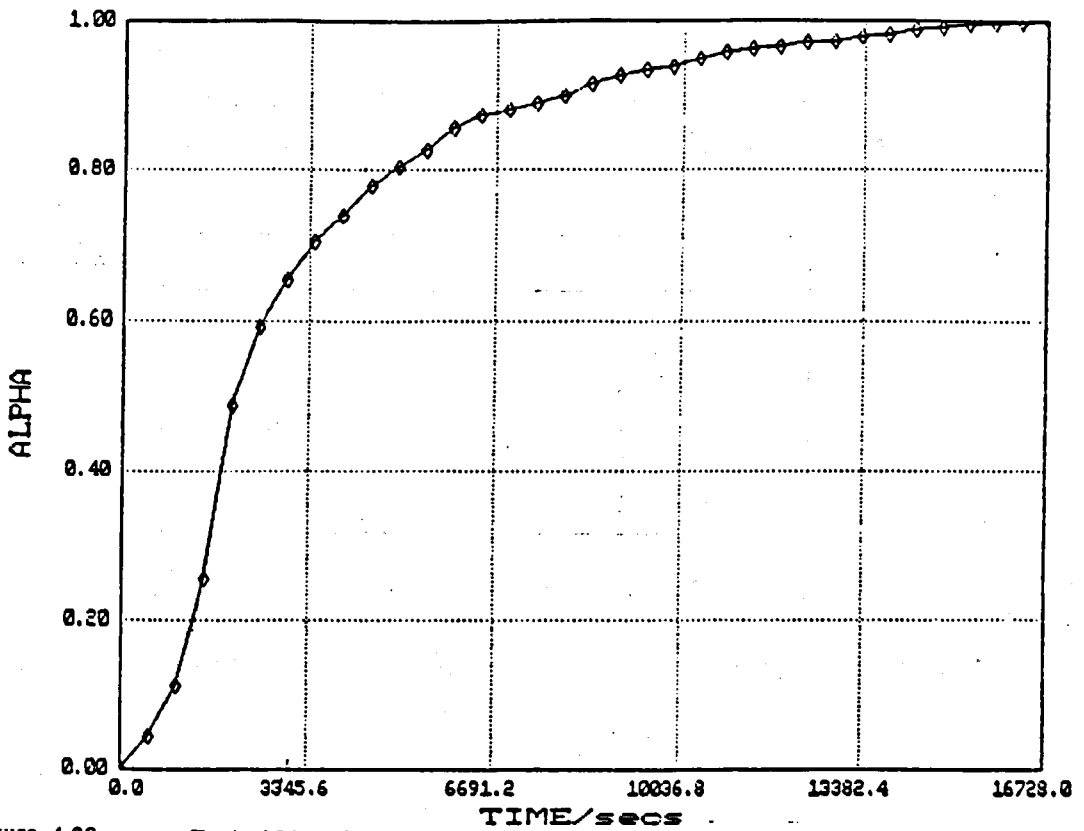


Figure 4.28 Typical Plot of α vs Time for the First Stage of the Decomposition Reaction of $\text{Pt}(\text{2AP})_2\text{Cl}_2$.

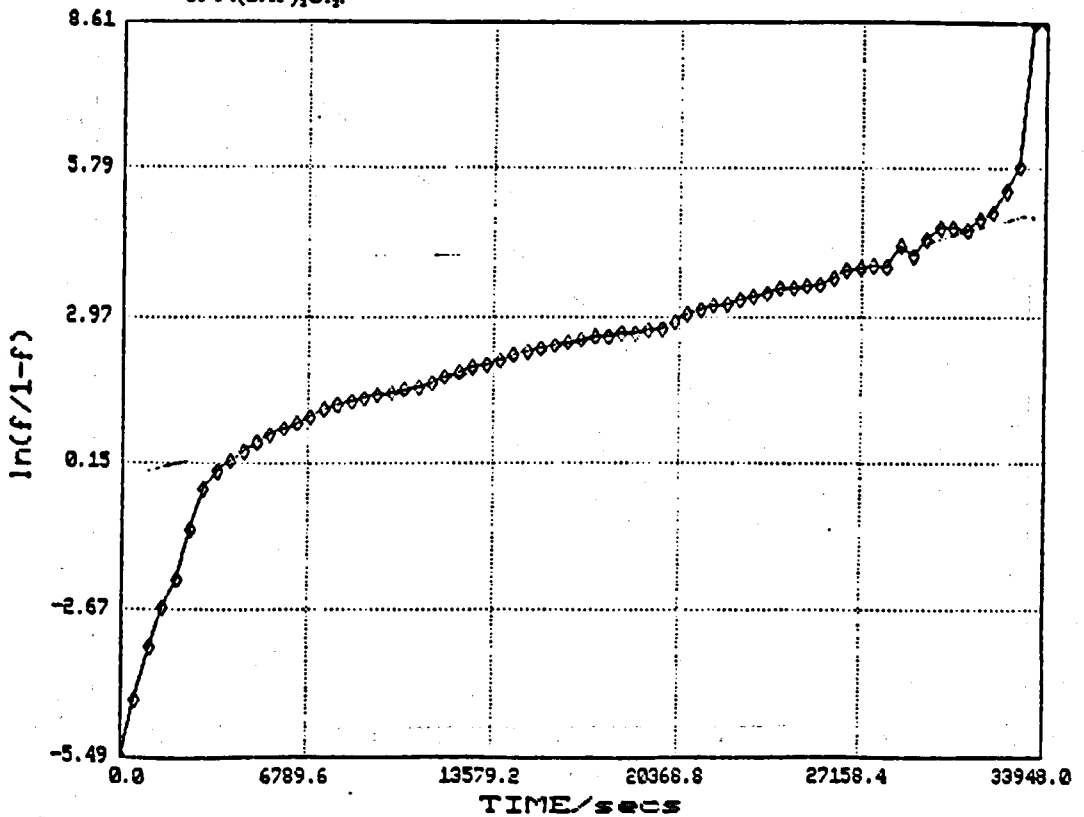


Figure 4.29 Prout-Tompkins Plot for the First Stage of the Decomposition Reaction of $\text{Pt}(\text{2AP})_2\text{Cl}_2$.

TABLE 4.14

Rate Constants obtained at each Isothermal Temperature
Corresponding to the Loss of one Mole of 2-aminopyridine

Temperature/K	Rate constant/ 10^3s^{-1}
531	2.03
534	2.49
537	2.86
540	3.35
543	3.98

This complex appears to be a material which does not obey any of the common solid state reaction rate laws over a wide range of α values. However, a linear Arrhenius plot was obtained (Figure 4.30) using the Prout Tompkins rate constants and the activation energy calculated as 137 ± 10 kJmol^{-1} .

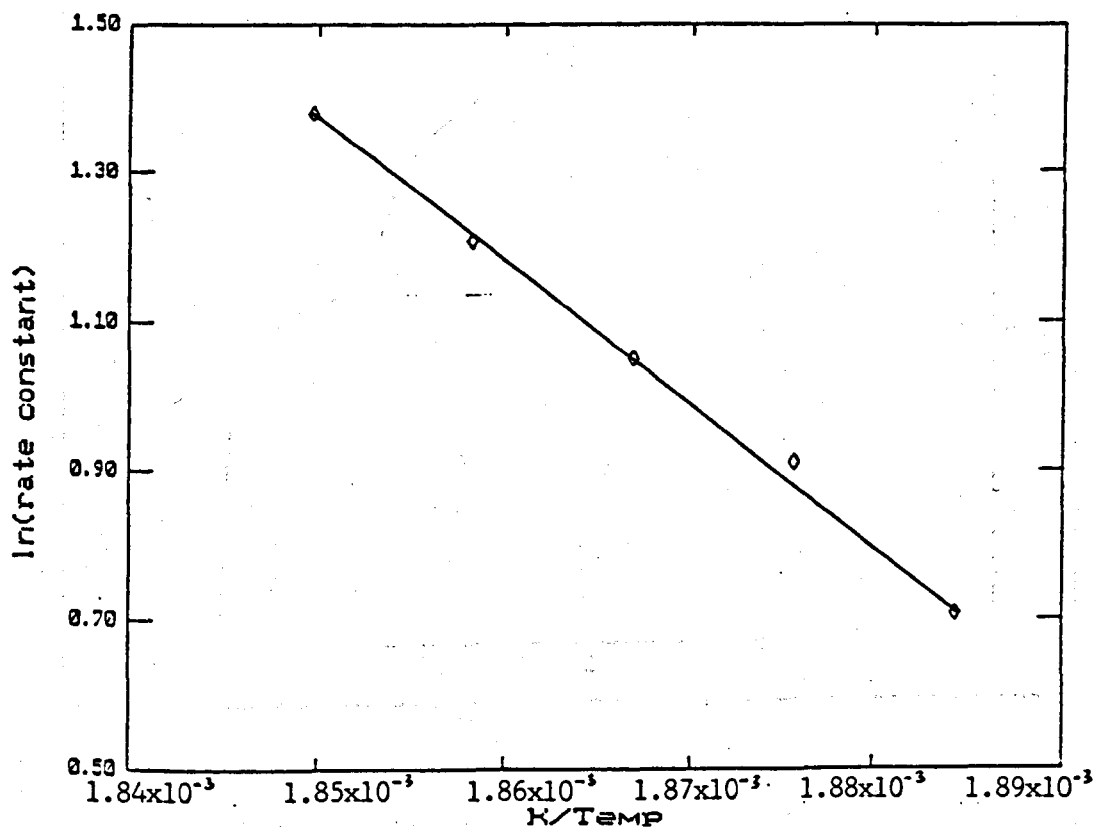


Figure 4.30 Arrhenius Plot from Isothermal Studies of the First Stage of Decomposition of $\text{Pt}(\text{2AP})_2\text{Cl}_2$

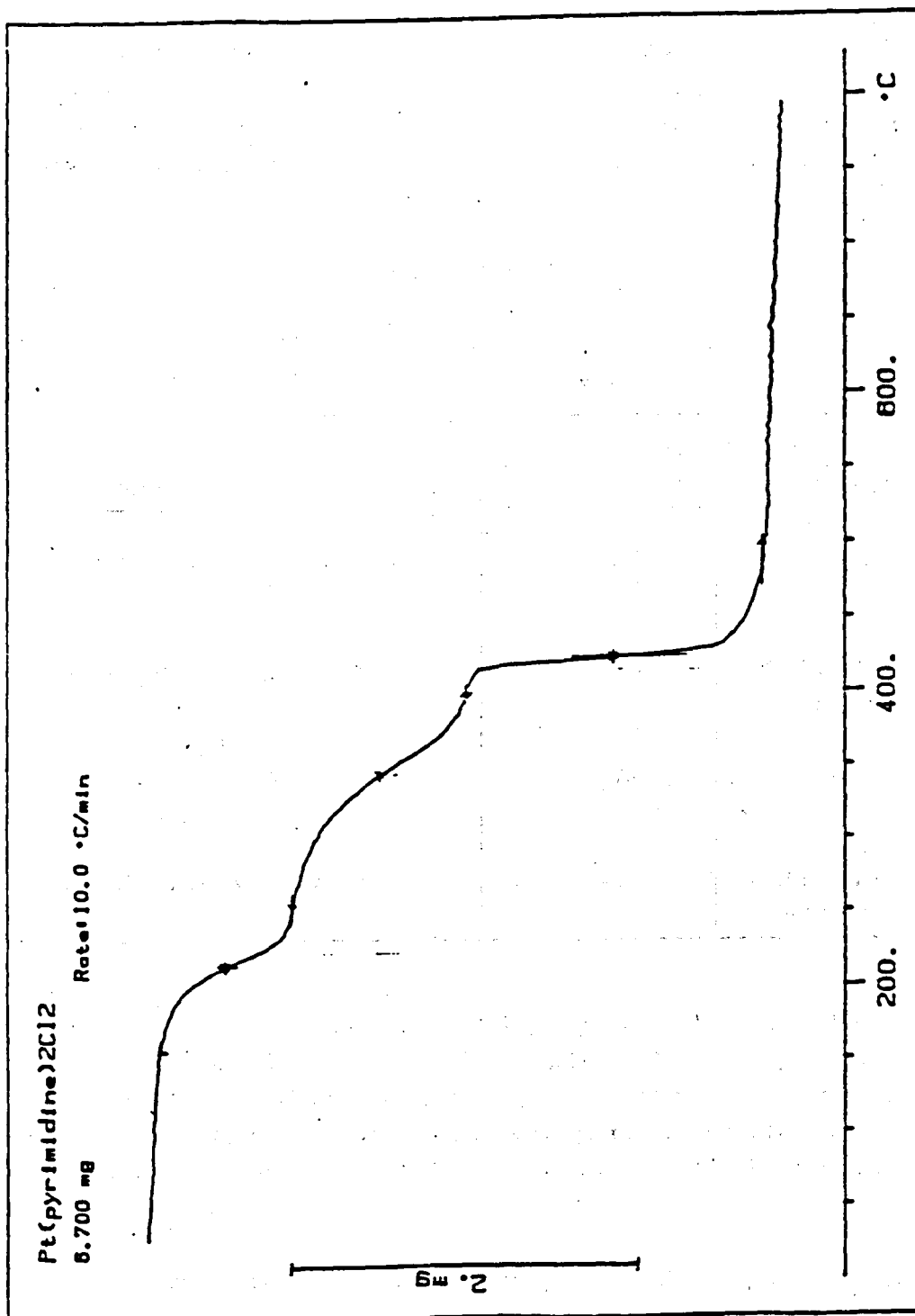


Figure 4.31

Non-isothermal Decomposition of Pt(PM)₂Cl₂.

4.5.5 *cis*-Pt(pyrimidine)₂Cl₂

The differential curve obtained from the non-isothermal analysis, carried out a heating rate of 2 Kmin⁻¹, indicated three distinct stages of decomposition (figure 4.31). The percentage weight losses for steps one and two were found to be 8.9% and 18.1% respectively. Comparison with the calculated theoretical percentages of pyrimidine and chloride in the complex suggested that the first step was due to the loss of chloride and the second stage due to the loss of a molecule of pyrimidine.

TABLE 4.15

Comparison of Theoretical and Experimental Weight Losses
from *cis* - Pt (Pyrimidine)₂ Cl₂

Process	Percentage Weight Loss	
	Theoretical	Experimental
1. Loss of one mole of Cl atoms	8.3	8.9 in 1st step of TG curve
2. Loss of one mole of pyrimidine	18.7	18.1 in 2nd step of TG curve
3. Loss of one mole of chlorine and one mole of pyrimidine	27.0	26.9 in 3rd step of TG curve
4. Loss of all ligands leaving metallic platinum	45.8	46.1 total loss at 500°C

In order to verify the assumption that the first step did correspond to the loss of chloride a simple experiment was carried out. A test tube containing the solid *cis*-Pt(Pm)₂Cl₂ complex was heated to approximately 503 K. Moist blue litmus paper was placed at the top of the tube and a change in colour of the litmus paper to red was observed as the complex decomposed. This was taken to indicate that HCl gas had evolved and not Cl₂ gas, as in the latter case the litmus would have bleached.

It was concluded from these experiments that the decomposition of this complex involved, first the loss of HCl followed immediately by the loss of a molecule of pyrimidine. Consequently the energetics of the second step of the decomposition reaction was of interest since the breaking of the platinum-nitrogen bond is involved.

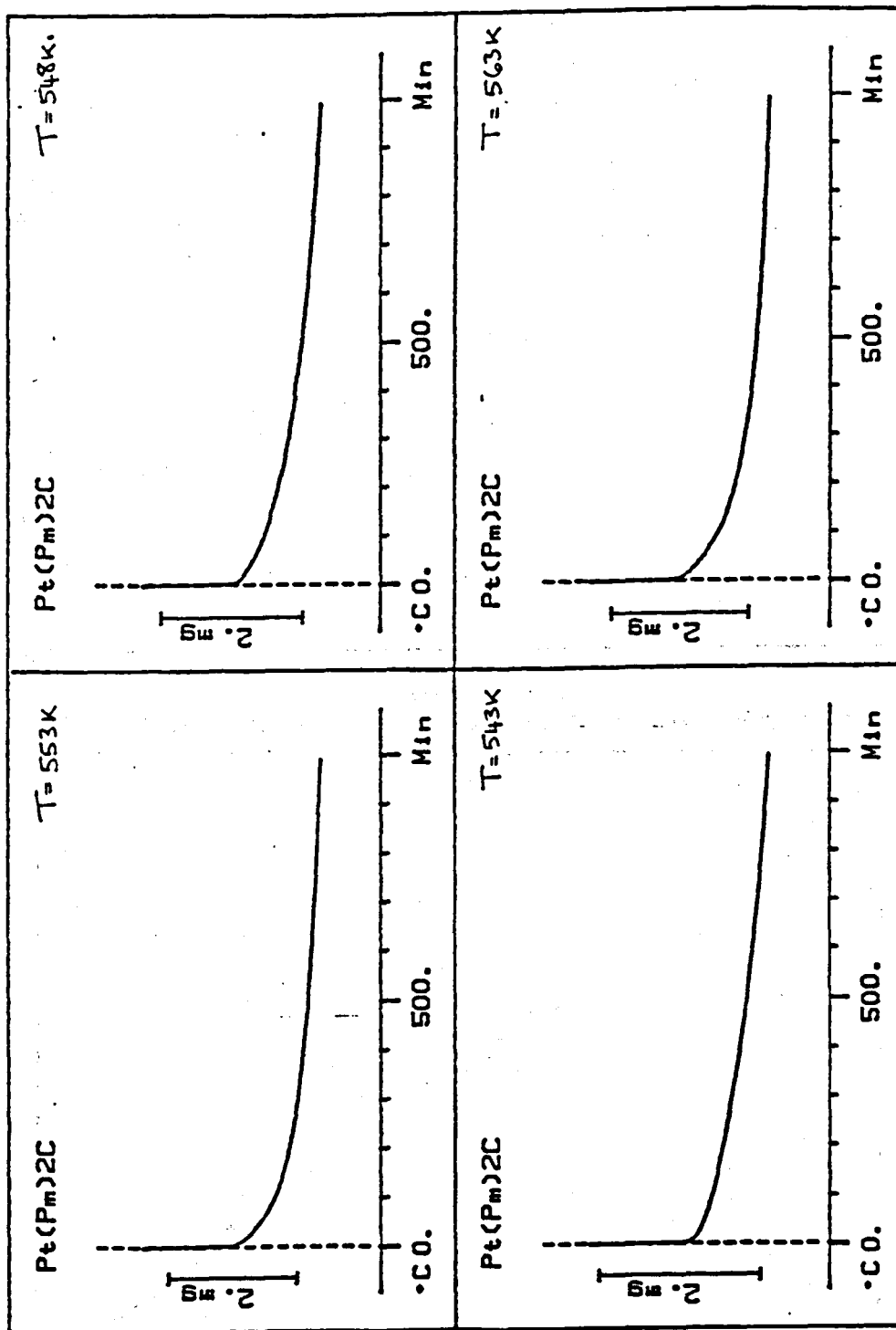


Figure 4.32

Isothermal Decomposition, Involving the Loss of One Molecule of Pyrimidine from $\text{Pt(Pm)}_2\text{Cl}_2$.

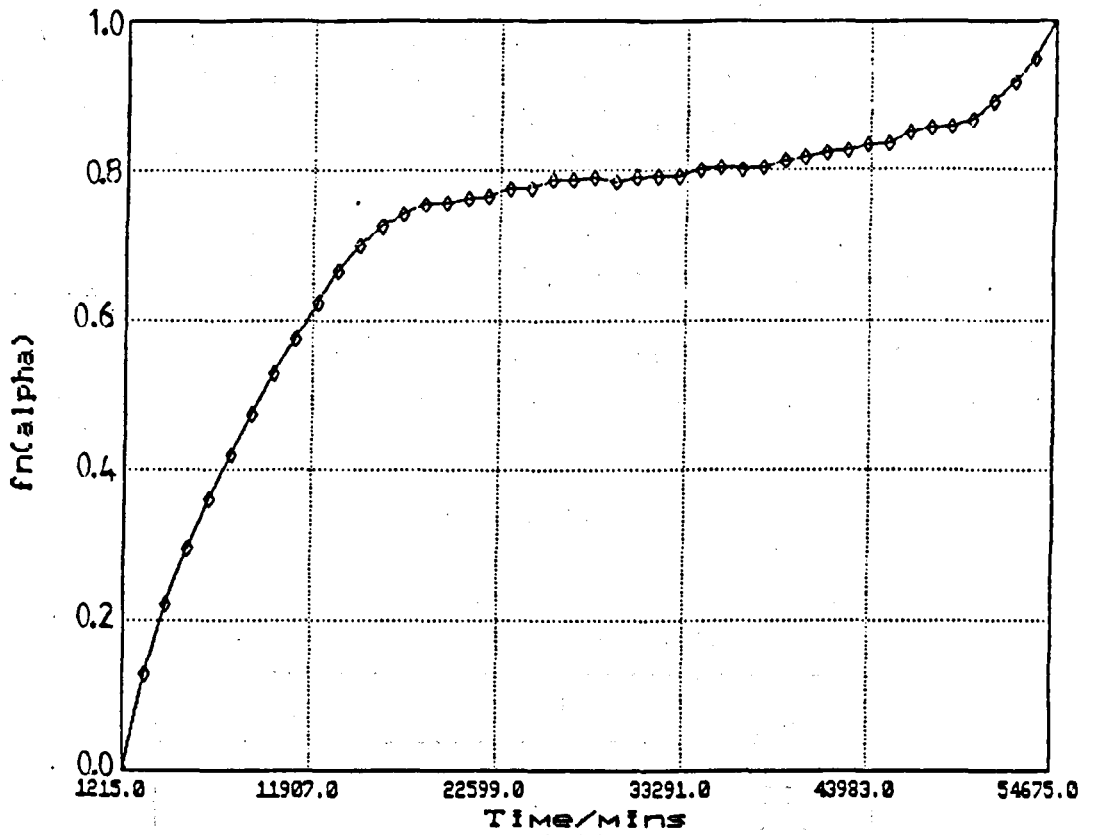


Figure 4.33 Typical Plot of α vs Time for the Loss of One Molecule of Pyrimidine.

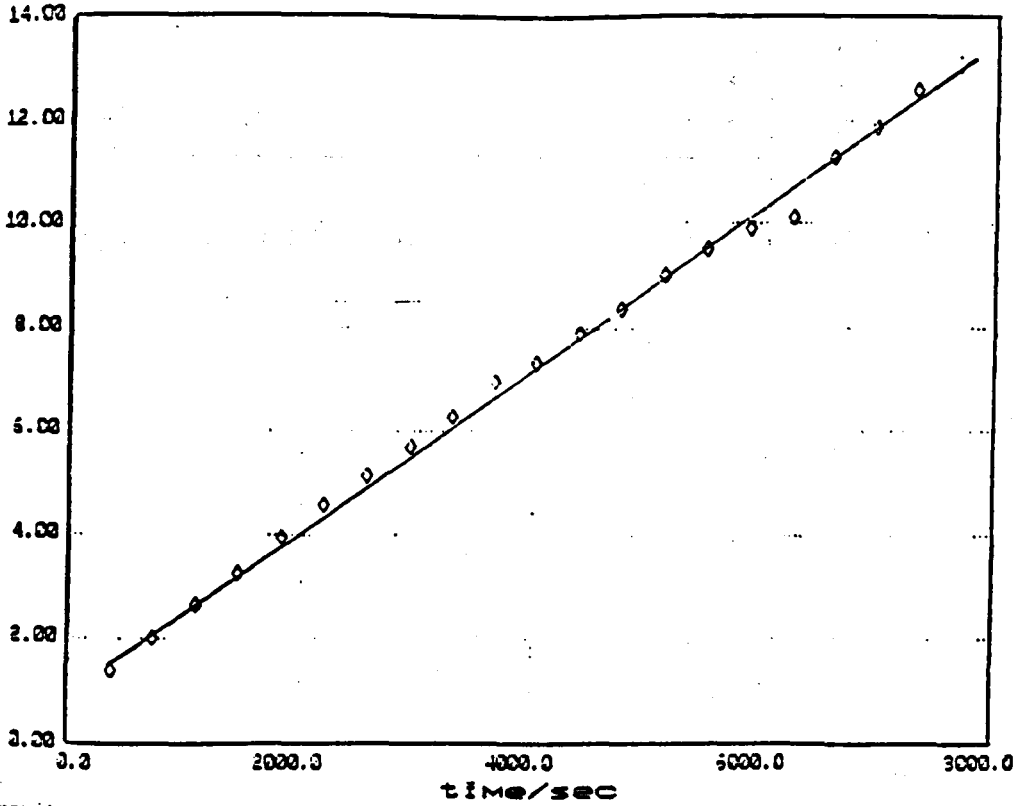


Figure 4.34 Typical Plot of $1/(1 - \alpha)$ vs Time for the Loss of One Molecule of Pyrimidine.

Based on the fact that the first stage of the decomposition was the loss of HCl the procedure adopted for the isothermal analysis involved rapidly raising the temperature from 308 K to the required isothermal temperature (which ranged from 538 K to 553 K) using a linear heating rate of 100 Kmin⁻¹. Isothermal analysis of the second step then followed, and typical plots are shown in Figure 4.32.

Plots of α versus time were not linear (figure 4.33), various topochemical rate laws were applied and it was found that a second order rate law gave rise to a plot which was linear over the whole range of $\alpha = 0$ to $\alpha = 1$. The rate law obeyed in this case is $1/(1-\alpha) = kt$, and from a plot of $1/(1 - \alpha)$ versus time (Figure 4.34) the rate constant was calculated, the results are summarised in Table 4.16.

TABLE 4.16

**Rate Constants obtained at each Isothermal Temperature
Corresponding to the loss of one mole of pyrimidine**

Temperature (K)	Rate (10 ³ /s)
538	2.22
543	2.87
548	3.63
553	4.15
558	5.27
563	6.02

An Arrhenius graph was plotted (Figure 4.35) and the activation energy found to be 102 kJmol⁻¹.

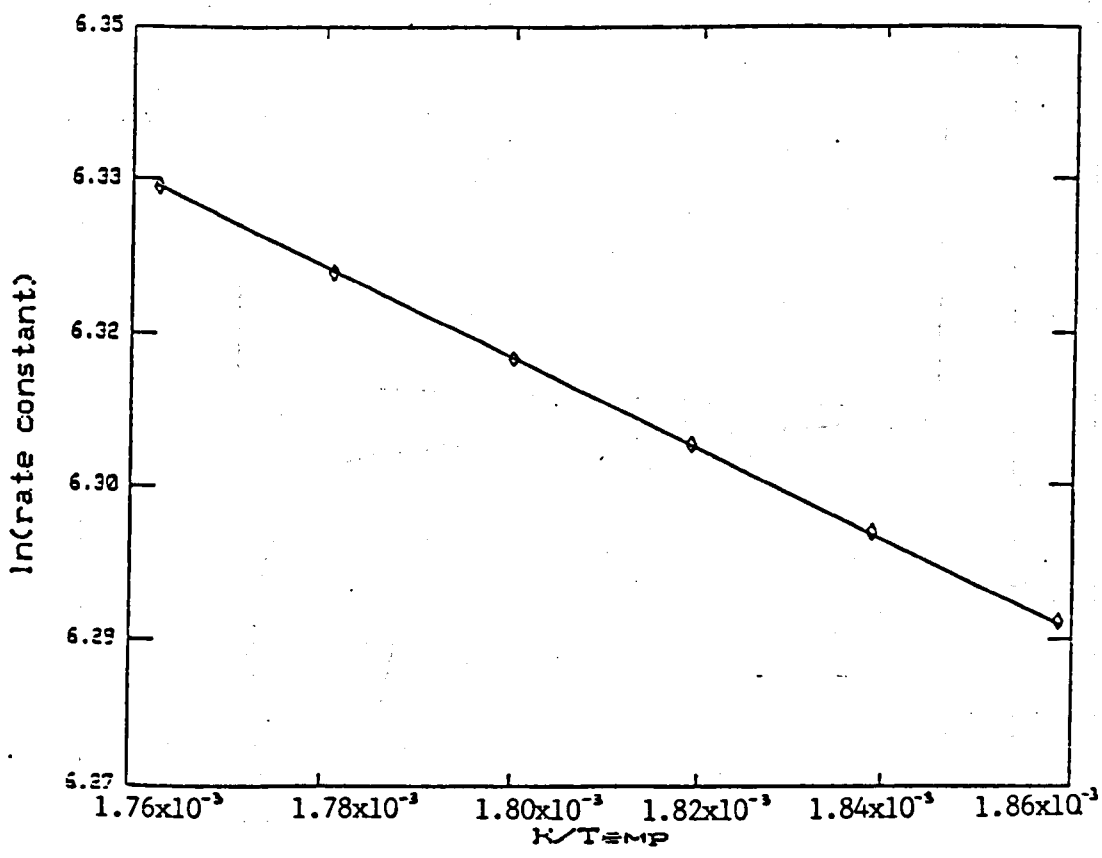


Figure 4.35 Arrhenius Plot for the Decomposition Reaction Involving the Loss of one Molecule of Pyrimidine.

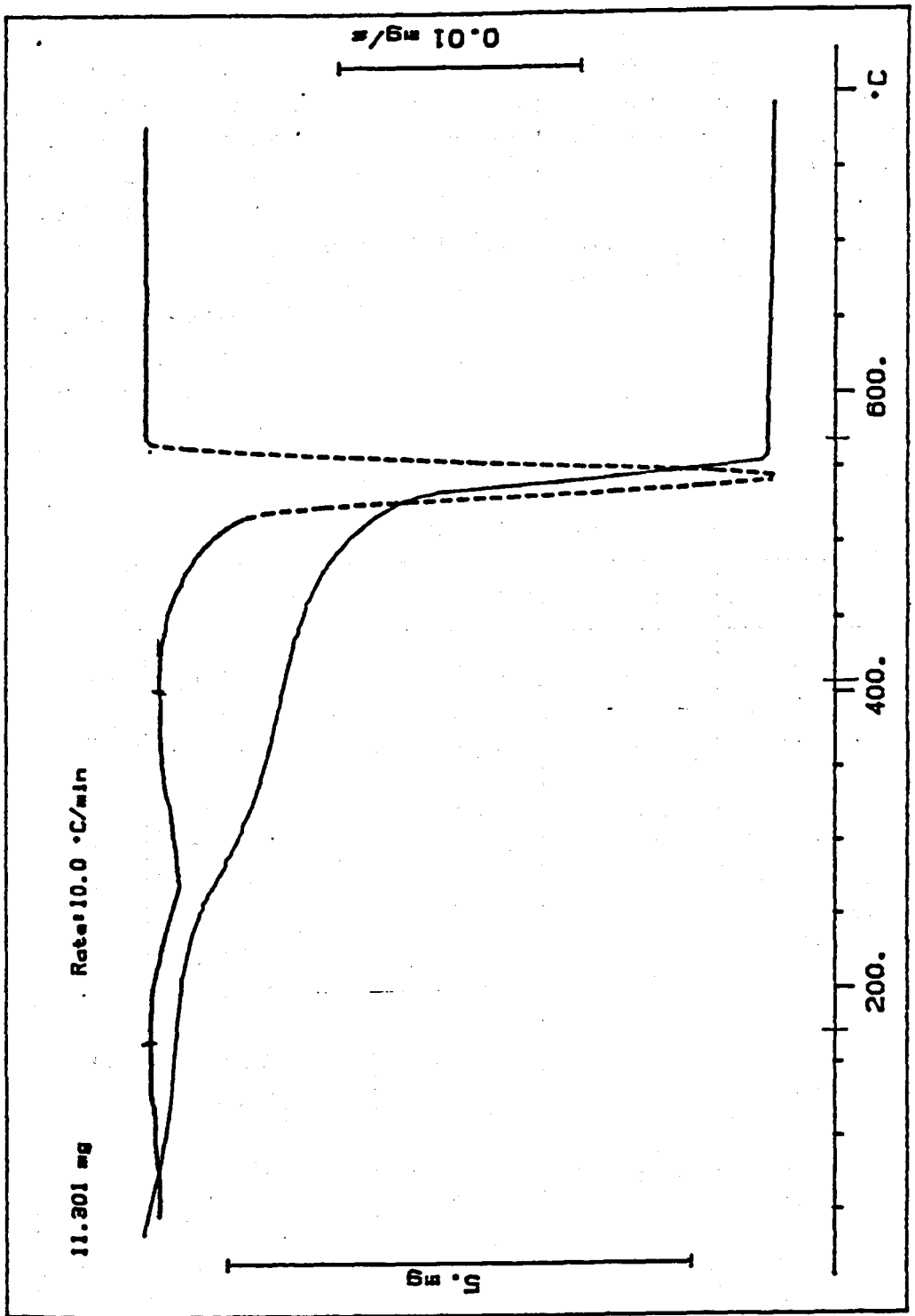


Figure 4.36

Non-isothermal Decomposition of $\text{Pt (Pu)}_2\text{Cl}_2$.

4.5.6 $\text{cis-Pt(purine)}_2\text{Cl}_2$

The non-isothermal thermogravimetric curve (figure 4.36) for this complex was difficult to interpret since $\text{Pt(Pu)}_2\text{Cl}_2$ did not decompose in a distinct stepwise manner. However, the first stage at a temperature of 554 K corresponded approximately to the loss of one chloride ligand. The main weight loss step which follows corresponded to the loss of two molecules of purine and one of chloride leaving a residual weight of 39.9% which is equivalent to the theoretical percentage of platinum present in the complex $\text{Pt(Pu)}_2\text{Cl}_2$. However, it was impossible to assign any part of this decomposition step purely to the loss of a purine molecule and consequently isothermal analysis was not attempted.

4.5.7 Summary of Results

TABLE 4.17

Summary of Typical TG Data

X=	Step Nr	Step Range/°C	Process	Obs %wt loss	Thcor %wt loss
py	1	170-225	-H ₂ O	4.1	4.1
	2	225-300	-py	17.9	17.9
	3	335-500	-(py)Cl ₂	33.2	33.9
pm	1	150-260	-Cl	8.9	8.3
	2	260-400	-pm	18.1	18.7
	3	400-500	-(pm)Cl	26.9	27.0
apy	1	250-340	-apy	20.6	20.7
	2	340-500	-(apy)Cl ₂	36.3	36.3
apm	1	250-380	-apm	20.8	20.8
	2	380-590	-(apm)Cl ₂	36.1	36.4
ampm	1	250-390	-ampm	22.5	22.5
	2	390-500	-(ampm)Cl ₂	36.9	37.1
pu	1	170-405	-Cl	7.7	7.0
	2	405-570	-(pu) ₂ Cl	52.4	54.4

TABLE 4.18

Activation Energy Data from Isothermal TG

X=	TG step Nr	Rate Law	Valid α range	$E_a/kJ mol^{-1}$
py	2	$\alpha = kt$	0-0.85	173 ± 9
pm	2	$1/(1-\alpha) = kt$	0-1.0	102 ± 6
apy	1	$\ln(\alpha/(1-\alpha)) = kt$	0.6-1.0	137 ± 10
apm	1	$\alpha = kt$	0-0.75	129 ± 9
ampm	1	$\alpha = kt$	0-0.8	161 ± 8

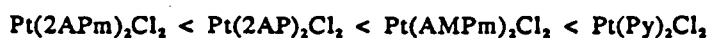
4.6 Discussion

The use of non-isothermal analysis to establish the kinetic parameters for the solid state decomposition of the complexes under investigation proved to be unsuccessful. The use of both Doyle's method and that of Gentry, Hurst and Jones for interpreting non-isothermal data resulted in unacceptable differences in the values of the activation energies from those obtained isothermally. It thus appeared that the decomposition reactions of these types of complexes were not amenable to non-isothermal analysis and it was decided to reject these methods as a way of determining the kinetic parameters of interest.

The use of isothermal thermogravimetric analysis, however, proved to be more successful in that linear Arrhenius plots were readily obtained and an activation energy for the decomposition process involving the loss of one ligand molecule was obtained for each of the complexes studied except $Pt(Pu)_2Cl_2$. Significant differences between the values of the activation energies were observed making it possible to distinguish binding between the platinum and the different ligands. In order to calculate the activation energy of decomposition it was found that different topochemical rate laws applied to different complexes. However, these rate laws are determined by topochemical factors which are not particularly relevant to this study as it is the differences in activation energy which is of interest.

It was found that for the $Pt(Pm)_2Cl_2$ complex the pyrimidine ligand was bound so tightly that a molecule of HCl was lost preferentially. This loss appeared to destabilise the remaining weight complex and the decomposition step involving the loss of a pyrimidine molecule took place with the lowest activation energy. The loss of a water molecule, (presumably not complexed) as in the case of the $Pt(Py)_2Cl_2$ complex, did not have the same effect on the decomposition step of interest, i.e. the loss of a molecule of pyridine, took place with the highest energy.

Leaving the $\text{Pt(Pm)}_2\text{Cl}_2$ complex aside because of its peculiar decomposition behaviour the ranking order in terms of increasing activation energy for the remaining complexes is as follows:



Steric hindrance does not appear to have much effect on the decomposition since the least bulky ligand, pyridine, gives rise to the highest activation energy and the most bulky ligand, 2-amino-4-methylpyrimidine the second highest energy.

If the effect of the electron withdrawing properties of nitrogen is considered then the above increase in activation energy can be explained. The presence of additional nitrogen atoms, other than that involved in bonding, will result in electron density being withdrawn away from the nitrogen atom involved in bonding, weakening the platinum-nitrogen interaction and resulting in a lower energy being required to break the bond. The 2-aminopyrimidine ligand has two such additional nitrogen atoms and consequently has the lowest activation energy. On this simple basis it would be expected that the $\text{Pt(AMPm)}_2\text{Cl}_2$ complex would have a similar activation energy to the $\text{Pt(2APm)}_2\text{Cl}_2$ complex since it too has two additional nitrogen atoms. However, the methyl group gives rise to an electron donating effect which counteracts the electron withdrawing properties of the nitrogen atoms resulting in this complex requiring a higher energy for decomposition than either the $\text{Pt(2APm)}_2\text{Cl}_2$ or $\text{Pt(2AP)}_2\text{Cl}_2$ complexes. Because pyridine has no additional nitrogen atoms then it will form the strongest bond with platinum and consequently the $\text{Pt(Py)}_2\text{Cl}_2$ requires the greatest energy for decomposition.

Leading on from this simple explanation the $\text{Pt(Pm)}_2\text{Cl}_2$ complex would be expected to have an activation energy around the middle of the above sequence, but because HCl is lost preferentially the pyrimidine must be more tightly bound than any of the other ligands and would therefore have the highest activation energy. This observation seems to confound the simple theory that the strength of the platinum-nitrogen bond depends on the presence of electron withdrawing or donating groups. The decomposition behaviour of the $\text{Pt(Pu)}_2\text{Cl}_2$ does not fit the above theory either. However, there is a similarity between the pyrimidine and purine ligands in that they both have additional ring nitrogen atoms which are equally available for co-ordination with the platinum metal. This along with the absence of steric hindrance makes it possible for the platinum to co-ordinate to another nitrogen atom during the course of the solid state decomposition. Thus it can be envisaged that for the pyrimidine and purine complexes it is easier to lose chloride and link or polymerise rather than break the platinum-nitrogen bond preferentially, this is shown schematically in Figure 4.37.

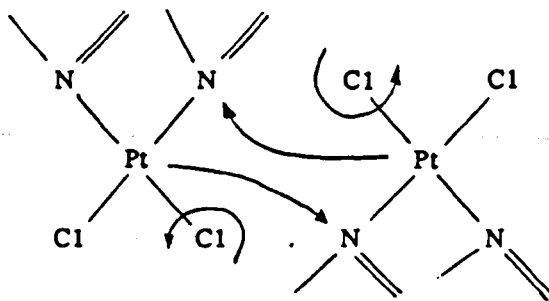


Figure 4.37 Schematic Representation of loss of Cl and possible formation of a Pt - N Bond

This is only a very tenuous suggestion and in order to find out more about the decomposition of these two complexes a detailed study of the structures of the reaction intermediates and of the kinetics of the solid state reaction, in particular the loss of HCl in first step, would need to be carried out.

4.7 Differential Scanning Calorimetry

Differential Scanning Calorimetry (DSC) measures the differential energy required to keep both the sample and a reference material at the same temperature. Thus, when an endothermic transition occurs, the energy absorbed by the sample is compensated by an increased energy input to the sample in order to maintain a zero temperature difference. Because the energy input is precisely equivalent in magnitude to the energy absorbed in the transition direct calorimetric measurement of the energy of the transition is obtained from this balancing energy. The DSC curve is recorded with the chart abscissa indicating the transition temperature and peak area measures the total energy transfer to or from the sample.

To obtain reliable results from DSC certain requirements in terms of sample and heating rate need to be considered. The sample should be in powder form and the smaller the size of the sample the better, although care must be taken as if too small a sample is used this can result in unacceptable losses of sensitivity. For comparison purposes it is important that the sample and the reference material should have similar thermal conductivities. The most widely used reference material is alumina which must be analytical reagent quality.

In order to maximise the rate of heat in/output during the course of the chemical/physical process optimum heating rates are required. A low heating rate will result in ill defined broad peaks whereas a high heating rate will produce much better defined sharp peaks.

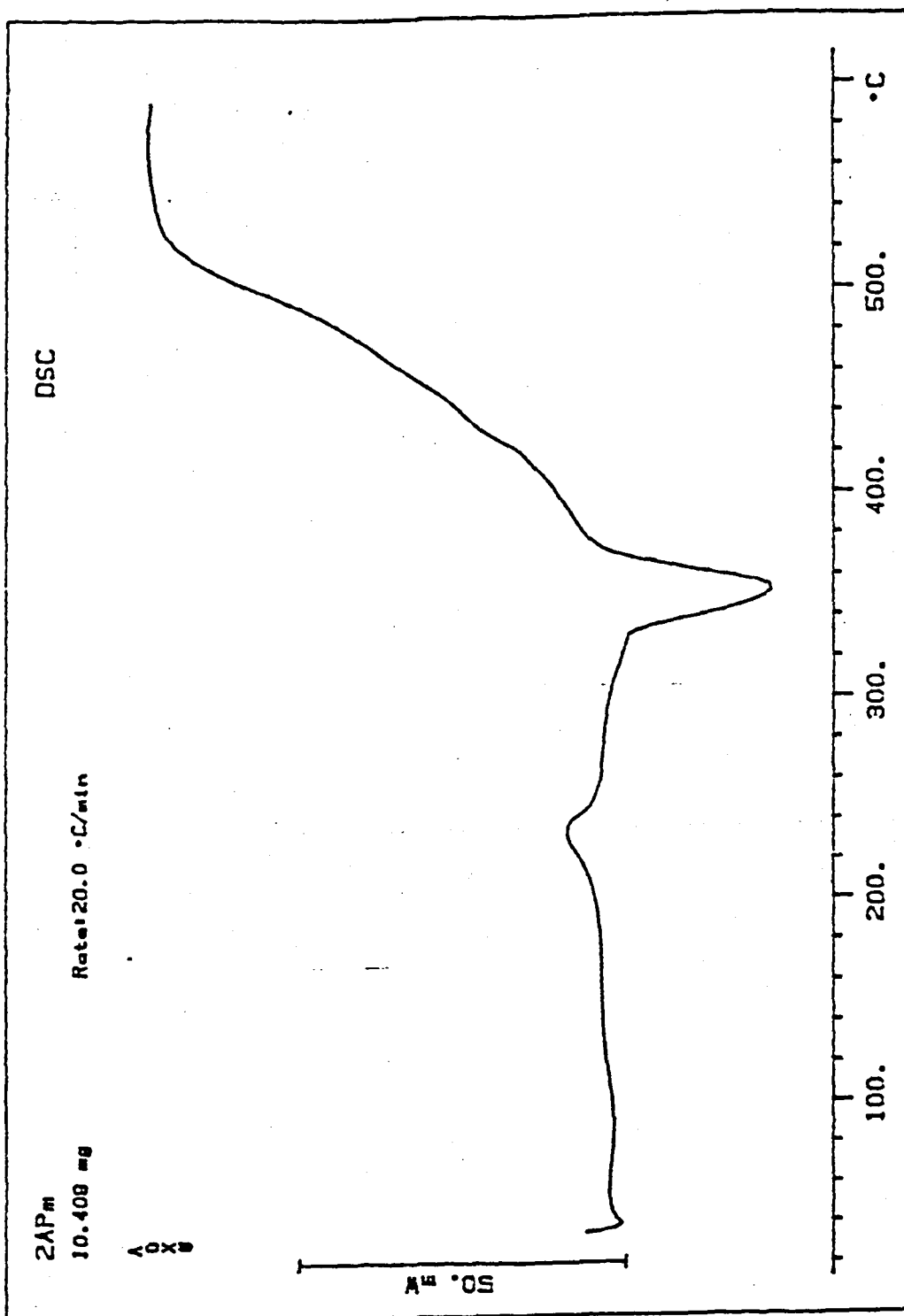


Figure 4.38

DSC Curve for Decomposition of $\text{Pt}(\text{2APm})_2\text{Cl}_2$.

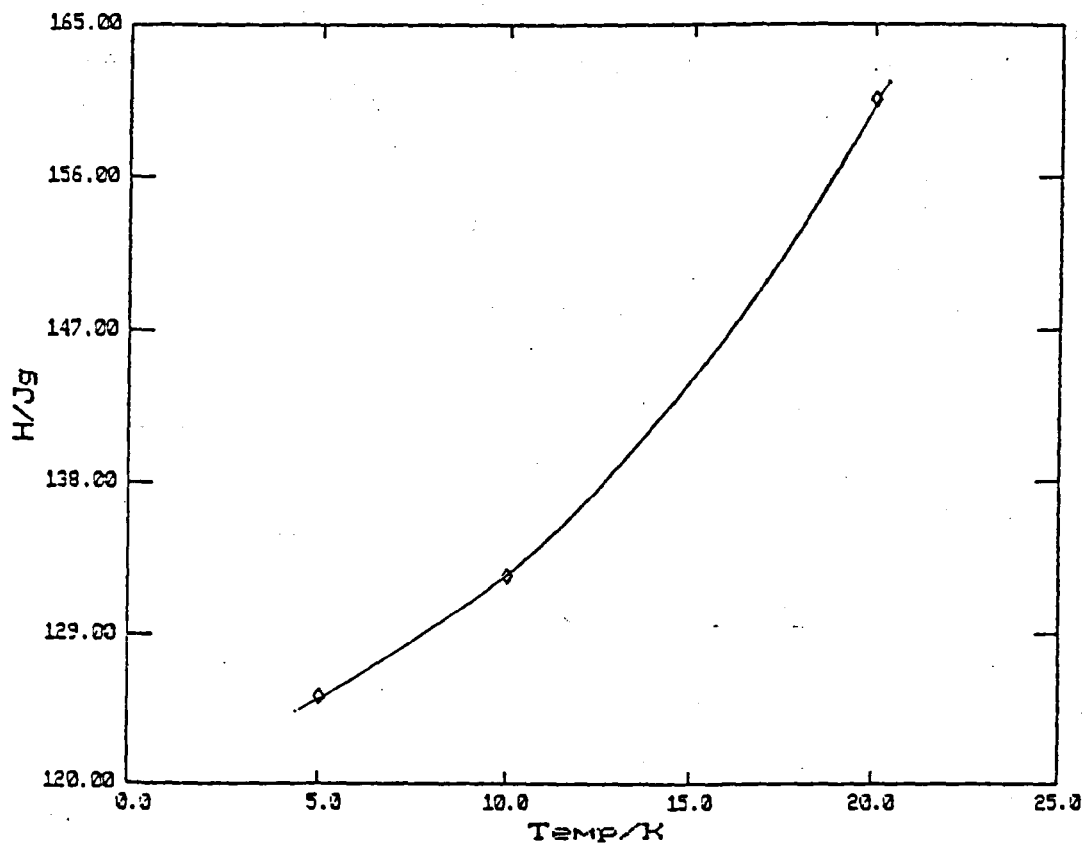


Figure 4.39 Plot of Enthalpy Change vs Heating Rate.

Results

DSC was carried out on the $\text{Pt}(\text{2APm})_2\text{Cl}_2$ complex at linear heating rates of 5, 10 and 20 Kmin^{-1} (Figure 4.38). In each case an endothermic peak was observed at around 612 K to 623 K which corresponded to the temperature of the first stage of the decomposition reaction on the equivalent non-isothermal differential thermogravimetric curve. ΔH was evaluated from the peak area, which is proportional to the amount of heat absorbed, using the TA72 processor and a graph of ΔH versus heating rate was plotted (Figure 4.39).

TABLE 4.19

Comparison of Temperatures for the First Stage of Decomposition from DSC and DTG at the value of ΔH at these Temperatures

Heating rate/ Kmin^{-1}	Temperature/K	$\Delta H/\text{Jg}^{-1}$	DTG Temperature/K
5	613.7	125.3	607.26
10	617.8	132.5	610.13
20	625.9	160.6	617.76

From these results it can be seen that the change in enthalpy is highly dependent on the heating rate, as the latter increases so does the value of ΔH .

The plot of ΔH versus heating rate was not linear and so it was impossible to extrapolate in order to determine the absolute enthalpy change for this decomposition process, that is the loss of one molecule of 2-aminopyrimidine.

Problems were also encountered instrumentally, in that the evolved vapours caused gumming of the sample cell rendering its dismantling and cleaning impossible.

In other cases severe baseline drift was observed making precise area measurements impossible and therefore this study was abandoned.

CHAPTER 5

Theoretical Studies

5.1 Introduction

Chemical systems can be subject to calculations of a sufficiently sophisticated nature to have introduced into the range of methods available to the experimentalist a new tool, namely 'computational chemistry'. It is now possible to compute some properties of many molecules with an accuracy that rivals or even exceeds experimental methods. These properties include molecular structure, heat of formation, ionization potential, charge densities and nature of bonding. The reducing real costs of computers and the ready availability of software has resulted in an upsurge of interest in computational methods as complimenting experimental studies.

The methods used in computational chemistry include Molecular Graphics, Molecular Mechanics and Molecular Orbital Theory. Molecular graphics allows the rapid building and manipulation of structures and the creation of geometry data in a form which permits easy input to molecular mechanics and quantum mechanics packages. Molecular mechanics is a technique in which a molecule is modelled as a set of atoms held together by 'springs' known as the force field. The various components of the force field are represented by mathematical equations showing the relationship between potential energy and some geometry parameter such as bond length, angle, etc. The minimisation of potential energy with respect to the various geometric parameters creates stable conformers of the given molecule. This is a purely empirical method which is dependent on the introduction of the appropriate geometry and force field parameters.

The various molecular orbital theories are based on quantum mechanics. The starting point is the electronic Schrodinger equation which on solution yields the electronic wave functions and eigen values (electronic energy levels) for the system. Knowledge of the wave function (eigenfunction) of a system allows computation of virtually any property of the system. The Born-Oppenheimer approximation is generally used in molecular calculations so that total energies are obtained from the minimisation of the electronic energy and the internuclear repulsion energy, which have a fixed value for a given molecular geometry.

Molecular orbital calculations performed at differing geometries can yield optimum molecular geometries. The methodology generally adopted consists of:

- (1) Use molecular graphics to construct the molecule of interest.
- (2) Optimise the geometry by a molecular mechanics method.
- (3) Carry out molecular orbital calculation at the optimum geometry.

- (4) Sometimes the geometry may be reoptimised by further molecular orbital calculations.

The exact details of a particular calculation are very dependent on the nature and size of the molecule. Large molecules containing very heavy atoms do not lend themselves to the most sophisticated molecular orbital calculation methods, and in these cases one may be limited to carrying out only molecular mechanics calculations on the whole molecule and a more restricted molecular orbital calculation on some smaller part of the molecule.

5.2 Introduction to Molecular Mechanics

Molecular mechanics, or force field calculations are based on a simple classical-mechanical model of molecular structure. Molecular mechanics treats the molecule as an array of atoms governed by a set of classical-mechanical potential functions. This principle is best illustrated by considering the bond-stretching term in a molecule. The potential at any given interatomic distance, r , is described by the Morse curve (Figure 5.1).

The energy minimum occurs at the equilibrium bond length r . The expression for a Morse curve is, however, complicated and would require too much computer time. This is not a critical problem, as the vast majority of molecules have bond lengths within a limited range, symbolized by the shaded portion of figure 5.1. Within this part of the curve one of the simplest types of potential function, Hookes law, gives a good fit to the more realistic energy profile as shown by the dashed curve in figure 5.1.

The Hookes expression
$$V = k(r - r_0)^2/2$$

where V is the potential energy, r is the interatomic distance, r_0 is the equilibrium bond length and k is a constant, is particularly simple to calculate and gives very fast execution of energy minimization computer programs.

The second type of function is the angle-bending potential. This is in principle exactly the same as the bond-stretching function. The potential energy arises as a given bond angle is deformed away from the optimum value.

Once again, a simple potential function proportional to $(\Theta - \Theta_0)^2$ is often used, although higher order terms may also be used.

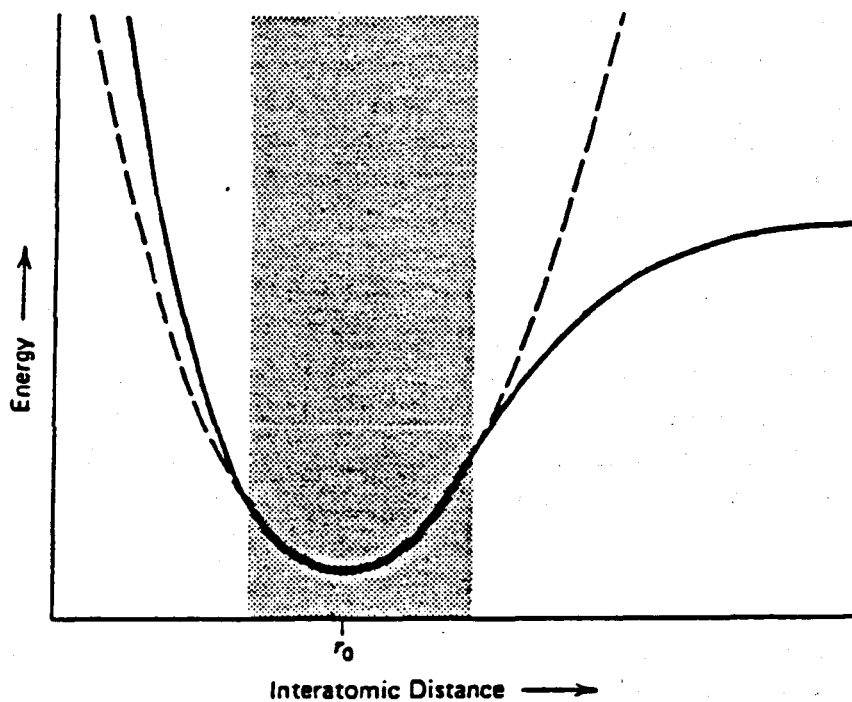


Figure 5.1 The Potential-Energy Curve for Stretching a Chemical Bond

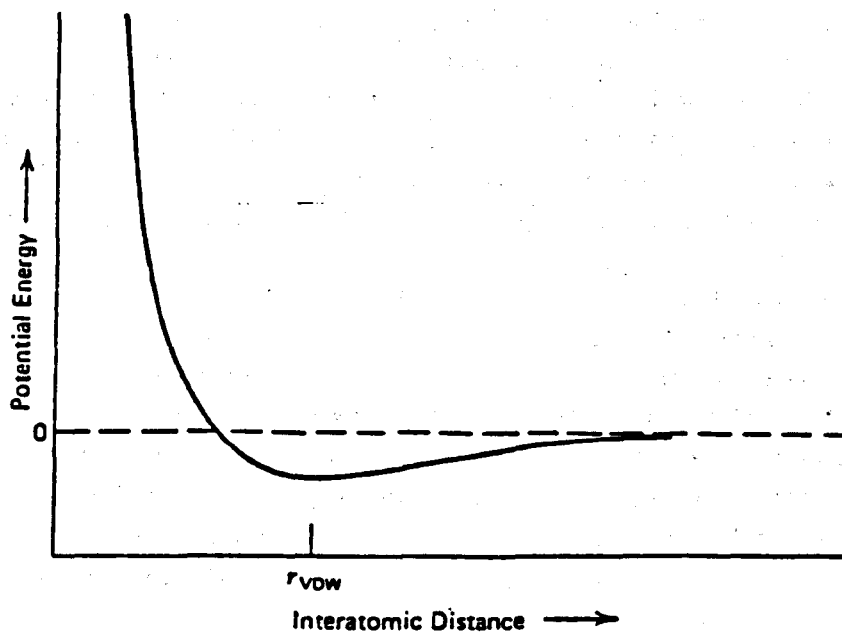


Figure 5.2 The Potential-Energy curve for the Van der Waals Interaction between Two Atoms.

Modern force fields contain many more types of potential function designed to give a good fit to experimental data. The most important of these additional functions are the torsional parameters. The rotation barrier of ethane, for example, cannot be represented by a reasonable force field that does not include an inherent three fold potential function for the C-C bond. Steric interactions alone do not give good results. The combination of bond-stretching, angle-bending and torsional potential functions is often known as valence force field because it accounts for the properties normally attributed to chemical bonds.

Valence force fields are, however, still not adequate for high-quality quantitative calculations. Force fields intended for such applications include the so-called Van der Waals functions used to account for steric interactions. Van der Waals potentials often take the form of either a Leonard-Jones 6/12 function; or uses the computationally more efficient Buckingham type of expression which uses a sixth power and an exponential term. The form of such function is shown in Figure 5.2.

Note there is a shallow minimum at an ideal interatomic distance. The inclusion of steric interactions in molecular mechanics force fields is, however, not without problems. Steric repulsions can never be completely separated from other interactions, and are therefore difficult to define and strongly dependent on the other potential functions used in the force field.

Other types of interaction may have to be considered for molecules with polar groups. The charge that builds up on these groups and the dipole moment associated with them interact with each other to affect the energy of the molecule. It is therefore not uncommon to use electrostatic terms and dipole-dipole interactions in the force fields. The charges on a given type of group are relatively constant, so simple electrostatic calculations can be used for the charge-charge interaction. The total dipole moment of a molecule may also be represented as the vector sum of the dipole attributed to each bond. Generally the conformation or isomer in which the total dipole is the lowest is the most stable. The bond dipoles are included in many force fields to make possible calculation of the dipole-dipole terms. This has the useful side effect that a dipole moment for the entire molecule is easy to calculate once the geometry has been optimised.

The force field defines the mechanical model used to represent the molecule. The purpose of the molecular mechanics program is to determine the optimum structure and energy based on this mechanical model. The input to the program must therefore define a starting structure for the molecule. This involves giving Cartesian (x,y,z) coordinates for the individual atoms and defining the bonds joining them. The model nature of molecular mechanics calculations requires that bonds be defined in the input. The model corresponds strictly to the classical valence bond picture of chemical bonding. Carbon atoms, for instance, may be either sp^3 , sp^2 or sp and there are three completely different force fields for the three different types.

The first step in the molecular mechanics calculation is determination of the interatomic distances, bond angles and torsional angles in the starting geometry. The values obtained are then used in the different potential function expressions to calculate an initial steric energy, which is simply the sum of the various potential energies, non-bonded pairs of atoms and so forth in the molecule. It is important to note that the steric energy is specific to the force field. It does not correspond to any classical definition of strain energy, although it is related to the heat of formation by a simple expression. Because all other factors remain constant throughout the optimization of a structure it is sufficient to find a minimum with respect to the steric energy.

Optimization is generally by a Newton-Raphson method, which uses analytically evaluated second derivatives of the molecular energy with respect to the geometrical parameters. The relatively simple form of the potential functions used in the force field makes them particularly suitable for this type of treatment, since they differentiate to give expressions that are equally simple, and therefore also easily evaluated. The second derivatives, or force constants, indicate the curvature of the potential energy curve, and can therefore be used to estimate the position of the minimum.

Once the optimization has converged (ie once the energy and structure remain constant from iteration to iteration and the first derivatives are all close to zero) the program prints out the final steric energy and the optimised geometry. This geometry may then be used to calculate such parameters as the moment of inertia and dipole moment (from the vector sum of the bond moments).

However, in this study the purpose of carrying out molecular mechanics calculations was to establish a set of molecular geometries for the ligand molecules all based on the same model. Quantum mechanical studies could then be carried out with the fixed molecular geometries determined in a standardized way. This is necessary because it is known that results of quantum mechanics calculations are geometry dependent.

5.2.1 Form of the Energy Expression used in the CHEMMOD Minimiser

In these studies the geometry of the ligands under investigation was carried out using the CHEMMOD molecular graphics system which incorporates a molecular mechanics program. The following describes the form of the potential energy function used in the evaluation of the overall steric potential energy.

The overall energy is given by

$$E_{\text{steric}} = V(b) + V(a) + V(t) + V(nb) + V(opb) + V(q)$$

where the V terms are defined as follows:

V(b) bond stretching potential energy

This is the sum of all the individual bond energies. The individual bond stretching energies, for bond n, are given by the equation

$$V(b)(n) = SK(n) * [L - Lo(n)] **2$$

where SK is the harmonic stretching constant, L is the observed bond length and Lo is the equilibrium bond length.

V(a) angle bending potential energy

This is the sum of all the bond angle potential energies. The individual angle bending energies, for angle n, are given by

$$V(a)(n) = BK1(n) * [DELTH **2 - BK2(n) * (DELTH ** 3)]$$

where Bk1(n) and BK9(n) are the harmonic and harmonic bending constants respectively, and DELTH is the observed minus the strain free (equilibrium) bond angles.

(V)t torsional potential energy

The torsional or dihedral potential energy is the sum of the individual energies given by the expression of the form, for each torsional angle n

$$V(t)(n) = VO * \{1 + SIGN(FD) * (COS (FD : *W))\}$$

The various terms in the above expression are defined as follows: Vo is the portion of the barrier height to free rotation assigned to the particular torsional angle about a given bond; FD determines the periodicity and the form of the cosine function, thus for H-C-C-H, FD = +3 and an expression of the form $1 + \cos(3w)$ is used; w is the observed torsional angle.

V(nb) non-bonded potential energy

The individual non-bonded (van der Waals) energies are calculated by an expression of the form

$$V(nb)(n) = EPS * \{-2 * (r12/rstar12)** -6 + EXP[12 * (1 - r12/rstar12)]\}$$

where EPS is the non-bonded force constant, rstar12 is the sum of the van der Waals radii of the two atoms and r12 is the observed contact distance

V(opb) out of plane bending potential energy

This is the total of the energies derived from the non-planarity at trigonal atoms such as =C etc. These are obtained used the expression

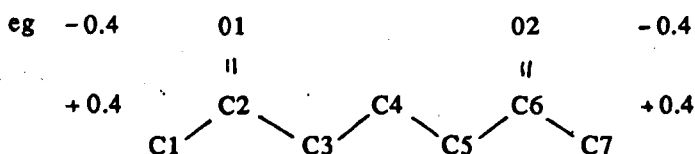
$$V(\text{opb})(n) = \text{OPBK} * (\text{pi-chi})^{**2}$$

where chi is the improper torsional angle describing the non-planarity of the system and OPBK is the force constant for the out of plane bending.

$V(q)$ coulombic potential energy

This is the energy due to charged interactions. Information regarding charged atoms and their charges must be present and a realistic minimisation of energy is required. This should be entered in the following format sign (group number) partial charge.

The charge atom should be arranged in groups which are usually neutral overall



This allows the program to differentiate between intra and inter group interactions (the former are ignored). The expression is of the form

$$V(q) = q_i + q_j / D * R_{ij}$$

where q_i and q_j are the partial charges on i and j , D is the dielectric constant and R_{ij} is the distance between i and j .

Note that the construction used for charge only allows for partial charges, that is fully charged ions of charge >1 cannot be dealt with.

5.3 Introduction to Molecular Orbital Theory

Molecular orbital have their origin in quantum mechanics and one of its central equations, the Schrodinger Wave equation, which may be expressed as:

$$a \Psi = A \Psi \quad \text{equation 5.3.1}$$

where a is an observable property of a system, A is the corresponding operator and Ψ is the wave function of the system.

For the chemist the usual form of equation 5.3.1 is

$$E \Psi = H \Psi \quad \text{equation 5.3.2}$$

where the observable is the energy E and its corresponding operator H is the Hamiltonian. The Hamiltonian operator for a molecular system is a sum of kinetic and potential energy terms relating to the motions and relative positions of all the electrons and nuclei in the molecule. For simplicity the nuclei are generally considered fixed so that the nuclear repulsions can be represented by a constant. The modified Hamiltonian, which includes terms relating only to the nuclei-electron and electron-electron potential interactions and the electronic kinetic energies, yields a form of the equation 5.3.2 which is referred to as the 'molecular electronic Schrodinger equation'. This is a differential equation which is incapable of exact solution for all but the very simplest molecular system (ie H_2^+). Further approximations (in addition to Born-Oppenheimer) must be introduced. Typically the form of the molecular wave function, Ψ , is assumed to be that of a linear combination of atomic orbitals (LCAO), X equation 5.3.3.

$$\Psi = \sum C_i X_i \quad \text{equation 5.3.3}$$

The coefficients, C_i , are determined by an iterative energy minimisation procedure so that $dE/dC_i = 0$ where E is the molecular electronic energy. The procedure is known as the Self Consistent Field (SCF) method and is terminated when the energy has been minimised within a given criterion.

The atomic wave functions, X_i , (or basis sets) are chosen to suit the degree of accuracy required and can be very approximate (minimal basis set) or very accurate (extended basis set).

In arriving at a solution of the electronic Schrodinger equation a variety of integral types must be evaluated. Some integral (one electron integral) are easily evaluated by analytical methods but those involving repulsion operators (two electron integral) may require the use of time consuming numerical methods. The number of such integral arising in a calculation is roughly proportional to n^4 where n is the size of the basis set.

Methods in which all integrals are evaluated are said to be *ab initio*. *Ab initio* methods are often subject to approximation by using Gaussian functions for the atomic basis set which although less accurate, mathematically than the normal, exponential, Slater type orbital (STO's) lend themselves to analytical evaluation.

Another approach to the integral problem is to adopt semi-empirical methods. In these some integrals, known to have negligibly small values are not evaluated and others which may be transferable from molecule to molecule are represented by fixed parameters. These parameters are chosen to yield the correct molecular properties for known systems. Semi-empirical molecular orbital calculations are very varied depending on the nature of the approximations made.

Typical methods include AM1 used in this study. In AM1 only valence electrons are included in the Hamiltonian and many integrals are either neglected or parameterised.

Solution of the molecular electronic wave equation yields a set of energies (roots or eigen values) and a corresponding set of wave functions (eigenfunctions or molecular orbitals). The number of molecular orbitals is determined by the size of the basis set (one molecular orbital for each atomic orbital included in the basis). Electrons doubly occupy the lowest available molecular orbital giving a set of occupied orbitals and a set of unoccupied (virtual) orbitals. The highest occupied molecular orbital (HOMO) and lowest unoccupied molecular orbital (LUMO) are often of most significance in chemistry since these are often the source and sink for electrons in molecular interactions involving charge transfer.

Secondary information readily available from the fundamental solutions to the wave equation include the shapes of the molecular orbital and the electron density distribution. These likewise are often important allowing speculation on the possible sites for electrophilic or nucleophilic attack.

Most molecular orbital calculation programs, such as the AMPAC suite used in these studies, include properties packages in which secondary molecular information is calculated and output in response to keywords used in the input data.

5.4 Method

The geometry was optimised by the molecular mechanics method for the four ligands pyridine, pyrimidine, 2-aminopyridine and 2-aminopyrimidine.

Pyridine and Pyrimidine

The structures of these two ligands were already present in the CHEMMOD library and energy minimisation calculations were carried out using these structures (Figure 5.3).

2-aminopyridine

The structure of this ligand was built from the pyridine structure already present in the CHEMMOD library (Figure 5.3). First all the hydrogen atoms were removed and an sp^3 nitrogen atom jointed to carbon atom 2. The bond length from carbon atom 2 to the nitrogen atom 7 was entered as 1.4Å, the bond angle between atoms 1, 2 and 7 entered as 120 and the torsional angle between atoms 6, 1, 2 and 7 as 180, (Figure 5.4). The hydrogen atoms were then added.

Before any geometry optimisation calculations could be carried out it was important to ensure that the out of plane hydrogen atoms of the amino group were in the conformation with the minimum global energy. This was done by considering the torsional angle between atoms 13, 7, 2 and 1. A torsion angle potential energy plot was then obtained for this angle (Figure 5.5) from which it can be seen that the potential energy is at a global minimum when the torsion angle 13, 7, 2, 1 is at 60. Subsequently energy minimisation calculations were carried out with the hydrogen atoms of the amino group in this particular conformation.

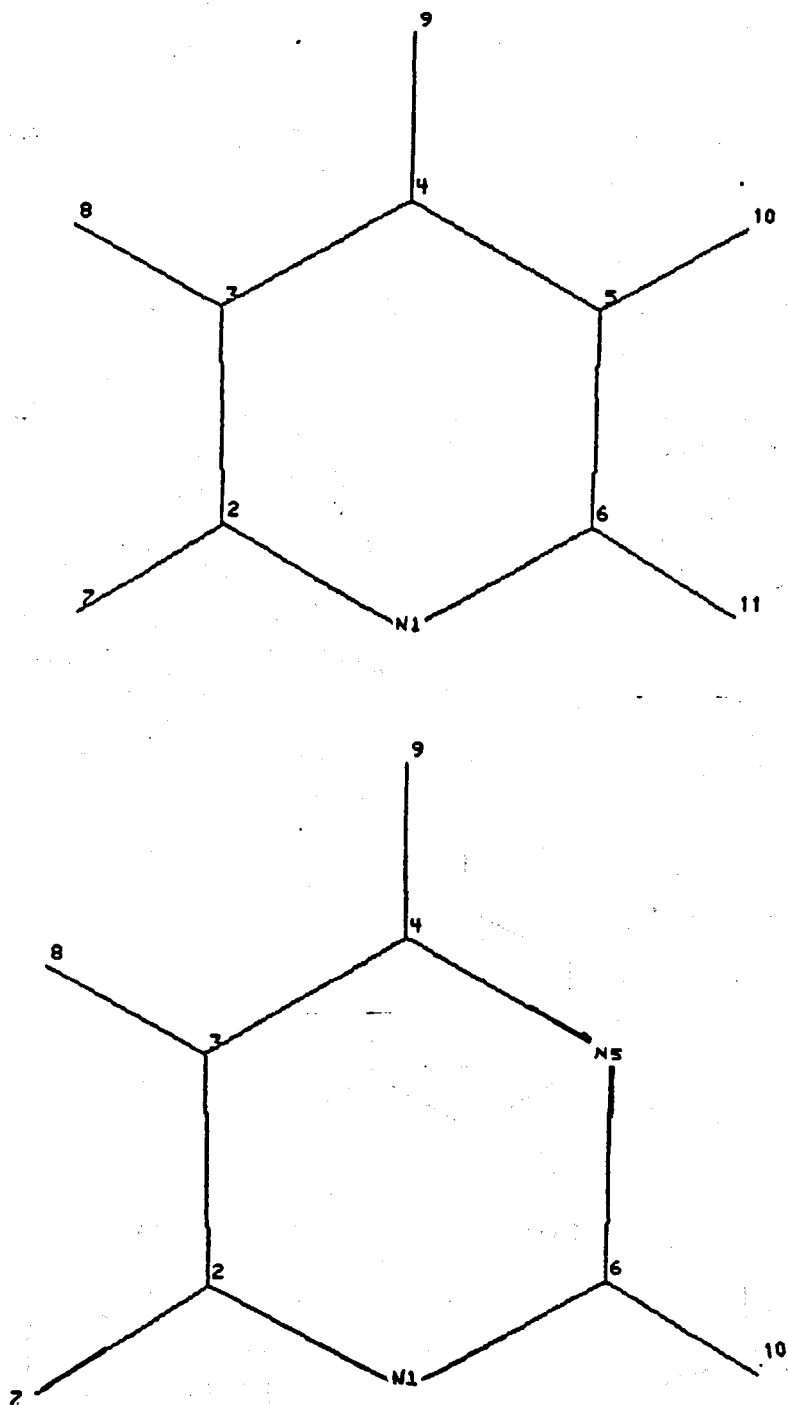


Figure 5.3 CHEMMOD Structures of Pyridine and Pyrimidine

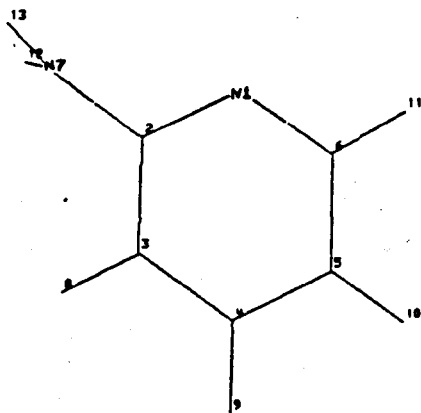


Figure 5.4 CHEMMOD Structure of 2-aminopyridine

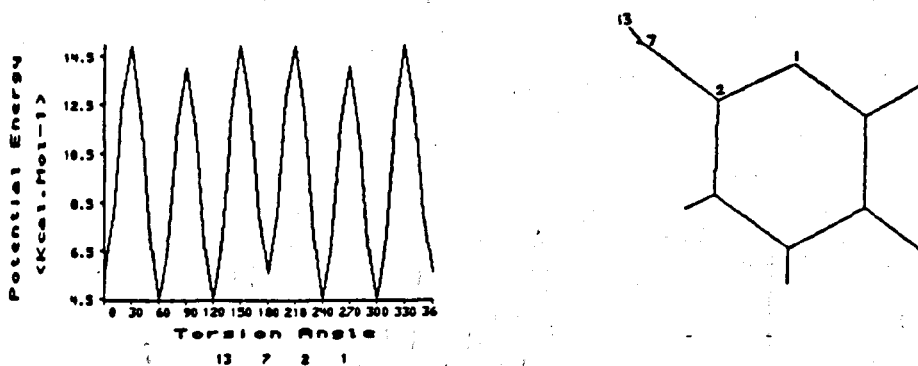


Figure 5.5 Potential Energy Plot of Rotation about the Torsion angle 13, 7, 2, 1 of 2-aminopyridine

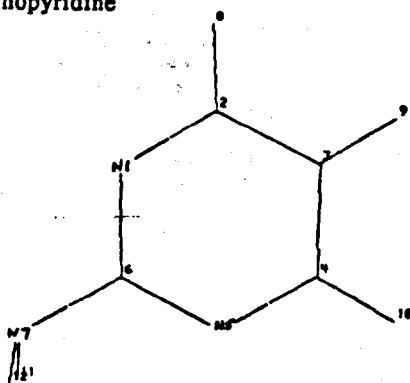


Figure 5.6 CHEMMOD Structure of 2-aminopyrimidine

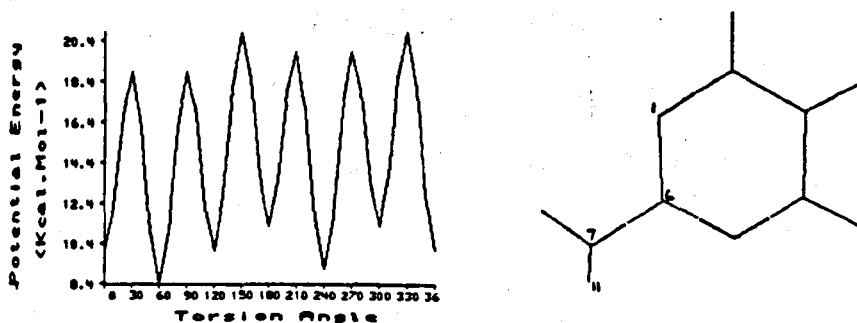


Figure 5.7 Potential Energy Plot of Rotation about the Torsion Angle 11, 7, 6, 1 of 2-aminopyrimidine.

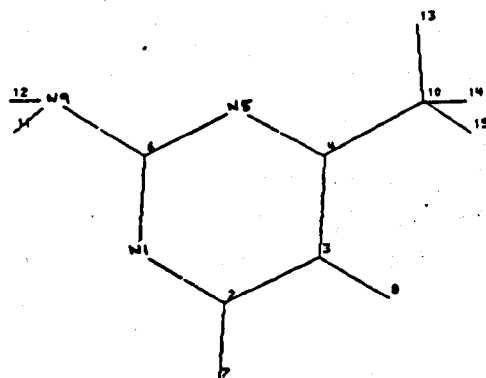


Figure 5.8 CHEMMOD Structure of 2-amino-4-methylpyrimidine.

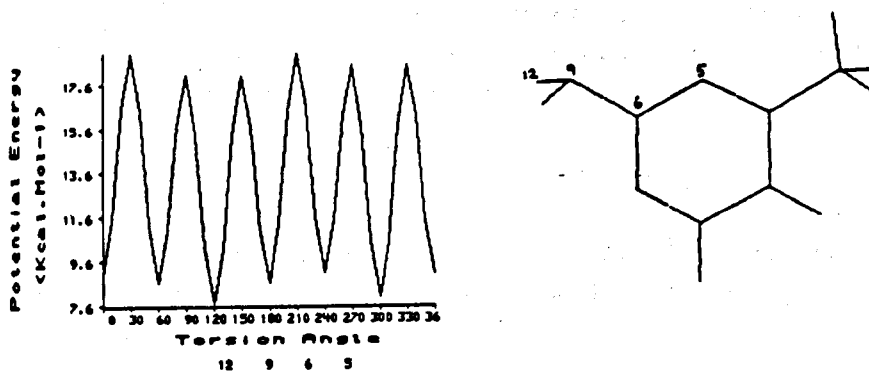


Figure 5.9 Potential Energy Plot of Rotation about the Torsion Angle 12, 9, 6, 5 of 2-amino-4-methylpyrimidine.

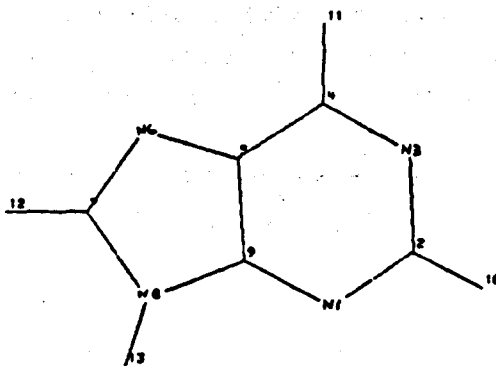


Figure 5.10 CHEMMOD Structure of Purine

2-aminopyrimidine

The structure of this ligand was built in a similar way to that of 2-aminopyridine, only in this case the basic building block was the pyrimidine structure already present in the CHEMMOD library (figure 5.6).

Again it was important to ensure that the out of plane hydrogen atoms of the amino group were in the conformation which exhibited the minimum global energy. This time the torsion angle 11, 7, 6, 1 was considered and from the potential energy plot (Figure 5.7) it can be seen that the global minimum was obtained when this torsion angle (11, 7, 6, 1) was 60.

2-amino-4-methylpyrimidine

To the 2-aminopyrimidine structure a methyl group was joined to carbon atom 4, (Figure 5.8). Again to ensure that the out of plane hydrogen atoms of the amino group were in the minimum global energy conformation the torsion angle 12, 9, 6, 5 was considered. From the potential energy plot (Figure 5.9) it can be seen that the global minimum energy was obtained when this torsion angle was 120°. Subsequently energy minimisation calculations were performed with the hydrogen atoms of the amino group in this particular conformation.

Purine

The structure of this ligand was built from the indole ring structure already present in the CHEMMOD library. The aromatic carbon atoms at ring positions 1, 3 and 6 were replaced with aromatic nitrogen atoms (Figure 5.10).

Once the energy minimisation calculations had been carried out on the above four ligand structures it was possible to obtain from the output a list of all the bond lengths, bond angles and torsional angles for each structure. This information could then be transformed into a Z-matrix and used as input for the AMPAC semi-empirical program.

A Z-matrix is simply a compact means of defining the position of the atoms in terms of atomic numbers, bond lengths, bond angles and dihedral angles. Information from the Z-matrix is used to calculate the Cartesian coordinates of the atoms and in conjunction with the charge, atomic number and multiplicity to work out the total number of electrons and the orbital occupancies.

The Z-matrices for each of the four ligand structures were built up in the following way, using one line per atom. The Z-matrix of pyridine is given below.

Atom	Bond Length		Bond Angle		Torsion Angle		Connected Atoms		
N									
C	1.363	0							
C	1.409	0	120.45	0					
C	1.408	0	119.04	0	0	0	3	2	1
C	1.408	0	119.60	0	0	0	4	3	2
C	1.409	0	119.05	0	0	0	5	4	3
H	1.090	0	118.86	0	180	0	2	1	6
H	1.091	0	120.44	0	180	0	3	2	1
H	1.091	0	120.20	0	0	0	4	3	8
H	1.091	0	120.52	0	0	0	5	4	9
H	1.090	0	120.69	0	0	0	6	5	10

The 0 after each bond length, bond angle and torsion angle indicates that no further optimisation of the geometry is required in the calculation. If the 0 is replaced by a 1 then AMPAC will carry out a geometry optimisation calculation on the parameter.

The first atom is placed at the origin of the coordinate system and therefore only the atomic code needs to be given.

Because the second atom is always placed on a predetermined axis only its distance from atom 1 needs to be defined.

The third atom is defined using the distance from the second atom and the angle between atoms, 1, 2 and 3.

The fourth atom is defined exactly as the third except that an additional parameter is needed to specify its position uniquely. The exact position is defined using the torsional angle between atoms 1, 2, 3 and 4.

Further atoms are defined in the same way, their unique position being specified by the connected atom numbers given in the final three columns of the Z-matrix.

5.5 Quantum Chemical Calculation Results

5.5.1 The Program

The computer program was used in this study (AMPAC, QCPE 506) has a large number of features built in and which are invoked by the use of keywords in the input data file. If no keywords are specified the program will perform an RHF calculation with geometry optimisation but without symmetry constraints on the ground state of the molecule.

The keywords used in this study included:

AM1: in which the AM1 (Austin Model 1) Hamiltonian method is to be used.

Charge: when the system beign studied is anion the charge, n, on the ion can be supplied by Charge = n. For cations n can be 1, 2, 3 etc, and for anions, -1, -2, -3 etc.

Density: at the end of the calculation the density matrix is printed.

Mulliken: a full Mulliken population analysis is to be done on the final wave function yielding an electron density distribution over all the orbitals in the molecule.

Vectors: the eigenvectors are to be printed.

A typical input file for pyridine is shown in Figure 5.11. The keywords are seen in the first line of the input data. The Z matrix then follws and the presence of Os indicate that the geometry is fixed.

For pyridine three different input data files were used. One contained the geometry information from the CHEMMOD molecular mechanics program, one contained published geometry data^[47] and the third utilizes the geometry optimization facility of the AMPAC program.

Table 5.1 summarises some of the output data obtained using the three different starting input geometries.

TABLE 5.1
Comparison of Output Data

	CHEMMOD Geometry	AMPAC Geometry	Published Geometry
Atomic Charge N1	-0.13	-0.14	-0.13
Atomic Charge C2	-0.08	-0.07	-0.08
Atomic Charge C3	-0.18	-0.18	-0.18
Atomic Charge C4	-0.09	-0.09	-0.09
Atomic Charge C5	-0.18	-0.18	-0.18
Atomic Charge C6	-0.08	-0.07	-0.08
Atomic Charge H7	+0.15	+0.16	+0.15
Atomic Charge H8	+0.14	+0.14	+0.14
Atomic Charge H9	+0.14	+0.14	+0.14
Atomic Charge H10	+0.14	+0.14	+0.14
Atomic Charge H11	+0.15	+0.16	+0.15
Ionisation Potential	-10.13	-9.90	-10.13
LUMO Energy	0.13	0.12	0.16
Dipole Moment	2.03	1.97	2.03

There were no differences in output such as electron density distribution, wave function and eigen values, using the different starting geometries, which at this level of theory, could be regarded as significant. Hence it was concluded that any consistent geometry data would be suitable. To save computing time it was decided to use the molecular mechanics (CHEMMOD) equilibrium geometry throughout the study, except for the work on the quaternized bases when AMPAC optimization of the extra hydrogen bond length and bond angle was required.

5.5.2 Results for Neutral Bases

It was considered that the activation energy parameters for reactions in solution and in solid state might correlate with one or more of the following calculated parameters; dipole moment, charge distribution, HOMO and LUMO energies or energy difference and wave function. Thus all this data were calculated and are summarised in Table 5.2.

However, no correlations were found. This could be accepted and understood for reactions in solution where the species undergoing reaction are probably solvated and quite dissimilar to the isolated gas phase species of the calculations. However, the situation in the solid state is different, here the complex is a molecular solid and the situation is not complicated by solvent presence.

Absorption of radiation in the ultraviolet region of the spectrum results from electronic transitions between molecular orbitals. The UV wavelength at which the ligand absorbs results from the transition from HOMO to LUMO, and the energy difference between these orbitals can be used to calculate the wavelength as follows:

$$E = \frac{hc}{\lambda}$$

where E is the energy difference (J)
 h is Plancks constant (6.63×10^{-34} Js)
 c is the speed of light (2.998×10^8 ms⁻¹)
 λ is the wavelength (m)

Since 1ev = 1.602×10^{-19} J

$$\text{then } \lambda = \frac{1.986 \times 10^{-25}}{E \times (1.602 \times 10^{-19})} \quad \text{cm}$$

The wavelengths calculated in this way were compared with those found spectrophotometrically for each ligand. It was found that they did not correspond and this possibly reflects the limitations of the AMPAC program, but is more likely to be due to the fact that calculations on isolated gas phase molecules may be of limited value quantitatively when dealing with reactions in aqueous solution.

TABLE 5.2
Summary of Results for Neutral Bases

Compound	Activation Energy		Ionisation Potential	Energy LUMO	Dipole Moment	Charge on Ring N's	Energy Change HOMO → LUMO	
	Solution	Solid state					λ	UV λ
P _y	64	173	10.13	-0.16	2.03	N1 -0.125	120	258
P _m	74	102	10.30	-0.19	1.97	N1 -0.204 N5 -0.203	118	259
2AP	56	137	9.87	-0.18	2.35	N1 -0.140	123	286
2AP _m	50	129	10.04	-0.27	2.57	N1 -0.172 N5 -0.254	120	291
AMP _m	94	161	9.93	-0.19	2.48	N1 -0.252 N5 -0.181	122	286
P _u	44	-	9.60	-0.63	3.19	N1 -0.202 N3 -0.214 N6 -0.140 N8 -0.235	121	267

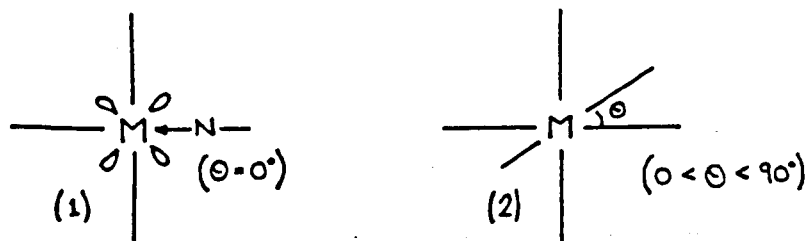
AM1 CHARGE = 1 VECTORS PYRIDINE QUATERNISED										
ATOM NUMBER (I)	CHEMICAL SYMBOL	BOND LENGTH (ANGSTROMS) NA: I	BOND ANGLE (DEGREES)		TWIST ANGLE (DEGREES)			NA	NB	NC
			NB: NA: I	NC: NB: NA: I	NA	NB	NC			
1	N									
2	C	1.35500					1			
3	C	1.37800	129.07000				2	1		
4	C	1.39700	118.38000		.00000		3	2	1	
5	C	1.39700	118.33000		.00000		4	3	2	
6	C	1.37800	118.38000		.00000		5	4	3	
7	H	1.09200	114.30000		180.00000		2	1	6	
8	H	1.08000	120.50000		.00000		3	2	7	
9	H	1.08000	120.83000		.00000		4	3	8	
10	H	1.08000	121.12000		.00000		5	4	9	
11	H	1.09200	120.63000		.00000		6	5	10	
12	H	1.09000 *	120.00000 *		180.00000		1	2	3	

Figure 5.11

AMPAC Input Data File

5.5.3 Results for Quaternized Bases

During the course of this work the studies by Clack and Gillard were considered^[50]. The analogy between quaternization and coordination of unsaturated tertiary nitrogen atoms has been examined^[51]. It was pointed out, using arguments based on qualitative molecular orbital theory, that N-heterocycles are not only σ donors but may also be π acceptors. However, one problem in assessing relative contributions to charge density on a particular atom in N-heterocycles is that there are no known cases where the plane of the heterocyclic ring lies parallel to the axis of the molecular framework (!). In general the actual structure of the ligand-metal moieties in complexed compounds are shown in (2) with the plane of the heterocyclic ring tilted at some angle to the plane containing the metal^[52]. This probable propeller shape of the complexes results in steric hindrance and affects the ability for π back donation from the metal to the ligand.



Clack and Gillard^[53] carried out INDO calculations on quaternized pyridine, a number of cationic pyridine complexes of Fe(II) and Fe(III) and the free pyridine molecule. The obtained values for electron densities in both σ and π orbitals of the heterocyclic ring. These results showed that for free pyridine the C2 and C4 positions are deficient in π electrons which is in keeping with the resonance structure. It was also found that these atoms are deficient in σ electrons resulting in an overall positive charge on them. On coordination to a metal ion there is a net flow of electrons from the ring to the metal, thus the heterocyclic ring becomes more positive on coordination. Most of the electron loss from the ring occurs through the σ framework with very little change overall to the π electrons of the ring. The π electron distribution within the pyridine ring is modified upon both coordination and quaternization as a result of changing electronic repulsions between σ and π electrons as σ electrons are pulled out of the ring. The heterocyclic ring is very similar electronically in both its σ and π distributions when quaternized and when it is coordinated to a metal ion. It is thus noteworthy that quaternized bases might be used to model complexed ligands.

Consequently a new series of calculations were carried out, obtaining equivalent data to that found earlier but with the addition of a hydrogen atom at the supposed coordination position (ring nitrogens only) and with the keyword Charge=1 used. The results now did show correlation with the solid state decomposition information and this correlation is discussed in Chapter 6.

Tables 5.3 to 5.11 show the most important quantum chemical information obtained from the calculations.

TABLE 5.3

Quantum Chemical Information Obtained for
Quartenized Pyridine

Structure																																																																		
Charge on Quaternary Nitrogen	-0.0678																																																																	
Ionisation Potential	15.621																																																																	
LUMO Energy	-5.892																																																																	
LUMO Wave Function	<table border="1"> <thead> <tr> <th></th> <th>s</th> <th>P_x</th> <th>P_y</th> <th>P_z</th> </tr> </thead> <tbody> <tr> <td>N 1</td> <td>0.00000</td> <td>0.00000</td> <td>0.00000</td> <td>-0.47571</td> </tr> <tr> <td>C 2</td> <td>0.00000</td> <td>0.00000</td> <td>0.00000</td> <td>0.44258</td> </tr> <tr> <td>C 3</td> <td>0.00000</td> <td>0.00000</td> <td>0.00000</td> <td>0.14651</td> </tr> <tr> <td>C 4</td> <td>0.00000</td> <td>0.00000</td> <td>0.00000</td> <td>-0.58233</td> </tr> <tr> <td>C 5</td> <td>-0.00000</td> <td>0.00000</td> <td>0.00000</td> <td>0.18479</td> </tr> <tr> <td>C 6</td> <td>0.00000</td> <td>0.00000</td> <td>0.00000</td> <td>0.44163</td> </tr> <tr> <td>H 7</td> <td>0.00000</td> <td></td> <td></td> <td></td> </tr> <tr> <td>H 8</td> <td>0.00000</td> <td></td> <td></td> <td></td> </tr> <tr> <td>H 9</td> <td>0.00000</td> <td></td> <td></td> <td></td> </tr> <tr> <td>H10</td> <td>0.00000</td> <td></td> <td></td> <td></td> </tr> <tr> <td>H11</td> <td>0.00000</td> <td></td> <td></td> <td></td> </tr> <tr> <td>H12</td> <td>0.00000</td> <td></td> <td></td> <td></td> </tr> </tbody> </table>		s	P _x	P _y	P _z	N 1	0.00000	0.00000	0.00000	-0.47571	C 2	0.00000	0.00000	0.00000	0.44258	C 3	0.00000	0.00000	0.00000	0.14651	C 4	0.00000	0.00000	0.00000	-0.58233	C 5	-0.00000	0.00000	0.00000	0.18479	C 6	0.00000	0.00000	0.00000	0.44163	H 7	0.00000				H 8	0.00000				H 9	0.00000				H10	0.00000				H11	0.00000				H12	0.00000			
	s	P _x	P _y	P _z																																																														
N 1	0.00000	0.00000	0.00000	-0.47571																																																														
C 2	0.00000	0.00000	0.00000	0.44258																																																														
C 3	0.00000	0.00000	0.00000	0.14651																																																														
C 4	0.00000	0.00000	0.00000	-0.58233																																																														
C 5	-0.00000	0.00000	0.00000	0.18479																																																														
C 6	0.00000	0.00000	0.00000	0.44163																																																														
H 7	0.00000																																																																	
H 8	0.00000																																																																	
H 9	0.00000																																																																	
H10	0.00000																																																																	
H11	0.00000																																																																	
H12	0.00000																																																																	

TABLE 5.4

Quantum Chemical Information Obtained
for Quarternized Pyrimidine

Structure				
Charge on Quaternary Nitrogen	-0.1303			
Ionisation Potential	16.165			
LUMO Energy	-6.255			
LUMO Wave Function				
	s			
	p _x			
	p _y			
	p _z			
N 1	0.00021	-0.00010	-0.00019	0.46843
C 2	-0.00005	0.00010	0.00010	-0.46364
C 3	0.00002	-0.00002	-0.00007	-0.12403
C 4	0.00002	-0.00001	0.00000	0.58511
N 5	-0.00001	0.00000	-0.00010	-0.14796
C 6	-0.00005	-0.00006	0.00008	-0.43126
H 7	-0.00002			
H 8	-0.00003			
H 9	0.00002			
H10	0.00001			
H11	-0.00027			

TABLE 5.5

Quantum Chemical Information Obtained
for Quarternized 2-aminopyridine

Structure					
Charge on Quaternary Nitrogen		-0.3139			
Ionisation Potential		14.964			
LUMO Energy		-5.929			
LUMO Wave Function		s	P _x	P _y	P _z
	N 1	-0.36234	-0.04648	-0.05843	-0.00042
	C 2	0.26400	-0.37949	-0.04046	0.00062
	C 3	-0.06619	0.05755	0.11698	0.00019
	C 4	-0.03915	0.03380	0.01154	-0.00075
	C 5	-0.02638	0.03904	0.07338	0.00011
	C 6	0.22518	0.26113	-0.36966	0.00064
	N 7	-0.12424	0.11718	-0.02869	-0.00007
	H 8	0.09082			
	H 9	-0.01114			
	H10	0.10252			
	H11	-0.14152			
	H12	0.10345			
	H13	0.10334			
	H14	0.51978			

TABLE 5.6

Quantum Chemical Information Obtained for
Quarternized 2-aminopyrimidine.

Structure				
Charge on Quaternary Nitrogen	-0.1155			
Ionisation Potential	15.827			
LUMO Energy	-6.089			
LUMO Wave Function	s	p _x	p _y	p _z
N 1	0.00000	0.00000	0.00000	0.46691
C 2	0.00000	0.00000	0.00000	-0.42599
N 3	0.00000	0.00000	0.00000	-0.16065
C 4	0.00000	0.00000	0.00000	0.58343
C 5	0.00000	0.00000	0.00000	-0.12563
C 6	0.00000	0.00000	0.00000	-0.45529
N 7	0.00000	0.00000	0.00000	0.02894
H 8	0.00000			
H 9	0.00000			
H10	0.00000			
H11	-0.07215			
H12	0.07215			
H13	0.00000			

TABLE 5.7

Quantum Chemical Information Obtained for
2-amino-4-methylpyrimidine, Quarternized at N1

Structure				
Charge on Quaternary Nitrogen	-0.1786			
Ionisation Potential	15.508			
LUMO Energy	-5.937			
LUMO Wave Function				
	s	p _x	p _y	p _z
N 1	0.00000	0.00000	0.00000	-0.45155
C 2	0.00000	0.00000	0.00001	0.43544
C 3	-0.00000	0.00001	0.00001	0.12373
C 4	-0.00003	-0.00001	-0.00004	-0.57956
N 5	0.00001	0.00001	0.00000	0.11411
C 6	-0.00001	0.00000	-0.00001	0.45585
N 7	0.00000	0.00000	0.00000	-0.02101
C 8	0.00002	0.00000	-0.00001	0.0417
H 9	0.00000			
H10	0.00000			
H11	0.07883			
H12	-0.07884			
H13	0.00002			
H14	-0.09964			
H15	0.09965			
H16	0.00000			

TABLE 5.8

Quantum Chemical Information Obtained for
2-amino-4-methylpyrimidine, quarternized at N3

Structure					
Charge on Quaternary Nitrogen		-0.1227			
Ionisation Potential		15.382			
LUMO Energy		-5.865			
LUMO Wave Function		s	p _x	p _y	p _z
	N 1	0.00000	0.00000	0.00000	-0.15003
	C 2	0.00000	0.00000	0.00000	0.57854
	C 3	0.00000	0.00001	0.00001	-0.14152
	C 4	-0.00003	-0.00001	-0.00003	-0.45654
	N 5	0.00001	0.00001	0.00000	0.46106
	C 6	-0.00001	0.00000	-0.00001	-0.42262
	N 7	-0.00000	0.00000	0.00000	0.02719
	C 8	0.00002	0.00000	-0.00001	0.02557
	H 9	0.00000			
	H10	0.00000			
	H11	0.07102			
	H12	-0.07102			
	H13	0.00001			
	H14	-0.07637			
	H15	0.07637			
	H16	0.00000			

TABLE 5.9

Quantum Chemical Information Obtained for
Purine Quarternized at N1

Structure				
Charge on Quaternary Nitrogen	-0.1276			
Ionisation Potential	14.542			
LUMO Energy	-6.089			
LUMO Wave Function	s	p _x	p _y	p _z
N 1	0.00000	0.00000	0.00000	-0.41944
C 2	0.00000	0.00000	0.00000	0.53205
N 3	0.00000	0.00000	0.00000	0.04649
C 4	0.00000	0.00000	0.00000	-0.58210
C 5	0.00000	0.00000	0.00000	0.20854
N 6	0.00000	0.00000	0.00000	0.12465
C 7	0.00000	0.00000	0.00000	-0.25812
N 8	0.00000	0.00000	0.00000	-0.01433
C 9	0.00000	0.00000	0.00000	0.27227
H10	0.00000			
H11	0.00000			
H12	0.00000			
H13	0.00000			
H14	0.00000			

TABLE 5.10

Quantum Chemical Information Obtained for
Purine Quarternized at N3

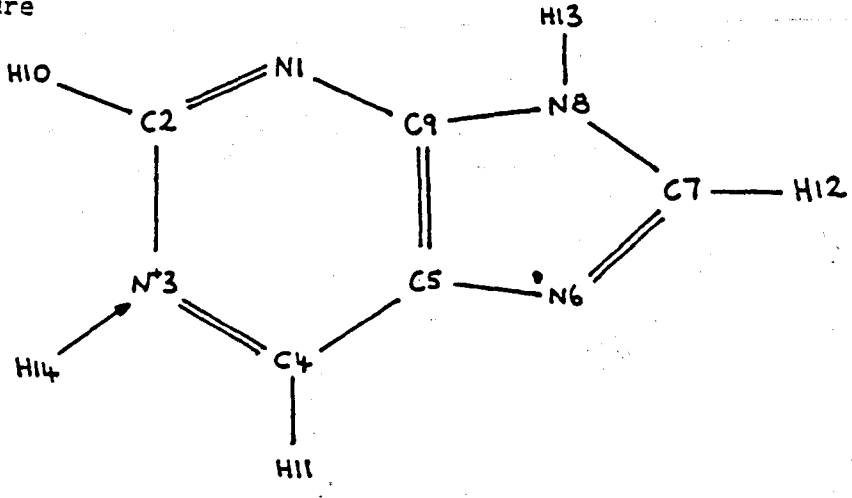
Structure					
					
Charge on Quaternary Nitrogen		-0.1366			
Ionisation Potential		14.358			
LUMO Energy		-5.821			
LUMO Wave Function		s	P _x	P _y	P _z
	N 1	0.00000	0.00000	0.00000	0.28931
	C 2	0.00000	0.00000	0.00000	0.10511
	N 3	0.00000	0.00000	0.00000	-0.40244
	C 4	0.00000	0.00000	0.00000	0.67726
	C 5	0.00000	0.00000	0.00000	-0.12738
	N 6	0.00000	0.00000	0.00000	-0.17067
	C 7	0.00000	0.00000	0.00000	0.23654
	N 8	0.00000	0.00000	0.00000	0.09331
	C 9	0.00000	0.00000	0.00000	-0.41658
	H10	0.00000			
	H11	0.00000			
	H12	0.00000			
	H13	0.00000			
	H14	0.00000			

TABLE 5.11

Quantum Chemical Information Obtained for
Purine Quarternized at N7

Structure					
Charge on Quaternary Nitrogen		-0.1155			
Ionisation Potential		15.827			
LUMO Energy		-5.893			
LUMO Wave Function		S	P _x	P _y	P _z
	N 1	0.00000	0.00000	0.00000	0.23549
	C 2	0.00000	0.00000	0.00000	-0.24238
	N 3	0.00000	0.00000	0.00000	-0.16134
	C 4	-0.00000	0.00000	0.00000	0.35359
	C 5	0.00000	0.00000	0.00000	-0.00233
	N 6	0.00000	0.00000	0.00000	-0.37570
	C 7	0.00000	0.00000	0.00000	0.68134
	N 8	0.00000			
	C 9	0.00000			
	H10	0.00000			
	H11	0.00000			
	H12	0.00000			
	H13	0.00000			
	H14	0.00000			

CHAPTER 6

Discussion and Conclusion

6.1 Discussion

Six insoluble complexes of the type *cis*-PtCl₂L₂ were successfully prepared by reacting an aqueous solution of K₂PtCl₆ with the appropriate soluble ligand, L, using the method described by Kong and Rochon⁽¹⁹⁾. The six products were characterised by thermogravimetric analysis (TGA), CHN analysis and infrared spectroscopy (IR). The TGA showed that each of the products decomposed in a stepwise manner. In each case by 873K the percentage weight loss was equivalent to the calculated theoretical percentage of two moles of chlorine plus two moles of ligand, suggesting that the molecular formula is of the form PtCl₂L₂. The three products on which CHN analysis was carried out confirmed the results obtained by TGA since the percentage weights expected for C, H and N agreed to within ±0.5% to those found experimentally. The IR spectra of the products compared to those of the corresponding ligand exhibited extra bands in the regions of 450 cm⁻¹ and 330 cm⁻¹. These bands are assigned as Pt-N and Pt-CL respectively indicating that the ligand binds to the platinum through a nitrogen atom. The fact that a single band was observed at 450 cm⁻¹ also indicated that the PtCl₂L₂ was present in the *cis* configuration. In order to monitor the kinetics of platinum-heterocyclic base interaction in solution several techniques were investigated, these included potentiometric methods, high performance liquid chromatography (HPLC) atomic absorption (AA) and ultraviolet (UV) spectroscopy. Preliminary studies into the monitoring of kinetic parameters by both potentiometric and HPLC methods were carried out. In each case a number of practical problems arose not the least of which was a lack of reproducibility. These two techniques were thus rejected as feasible methods of studying the kinetics of formation of complexation.

Initial investigations into the use of both AA and UV spectroscopy proved more successful. Subsequently a valid and reproducible methodology was developed and established for both techniques. During the developmental stage it was found that when a freshly prepared solution of K₂PtCl₆ was reacted with the ligand an induction period at the start of the reaction was evident. On further investigation it was determined that in aqueous solution PtCl₆²⁻ becomes hydrolysed to Pt(H₂O)₂Cl₄ and that this hydrolysis reaction occurs at a faster rate than the ligand substitution reaction. Consequently it was found necessary to prepare solutions of K₂PtCl₆ forty eight hours in advance, prior to reaction with the ligand, in order to take into account the aquation reaction. This has been discussed more fully in Chapter three.

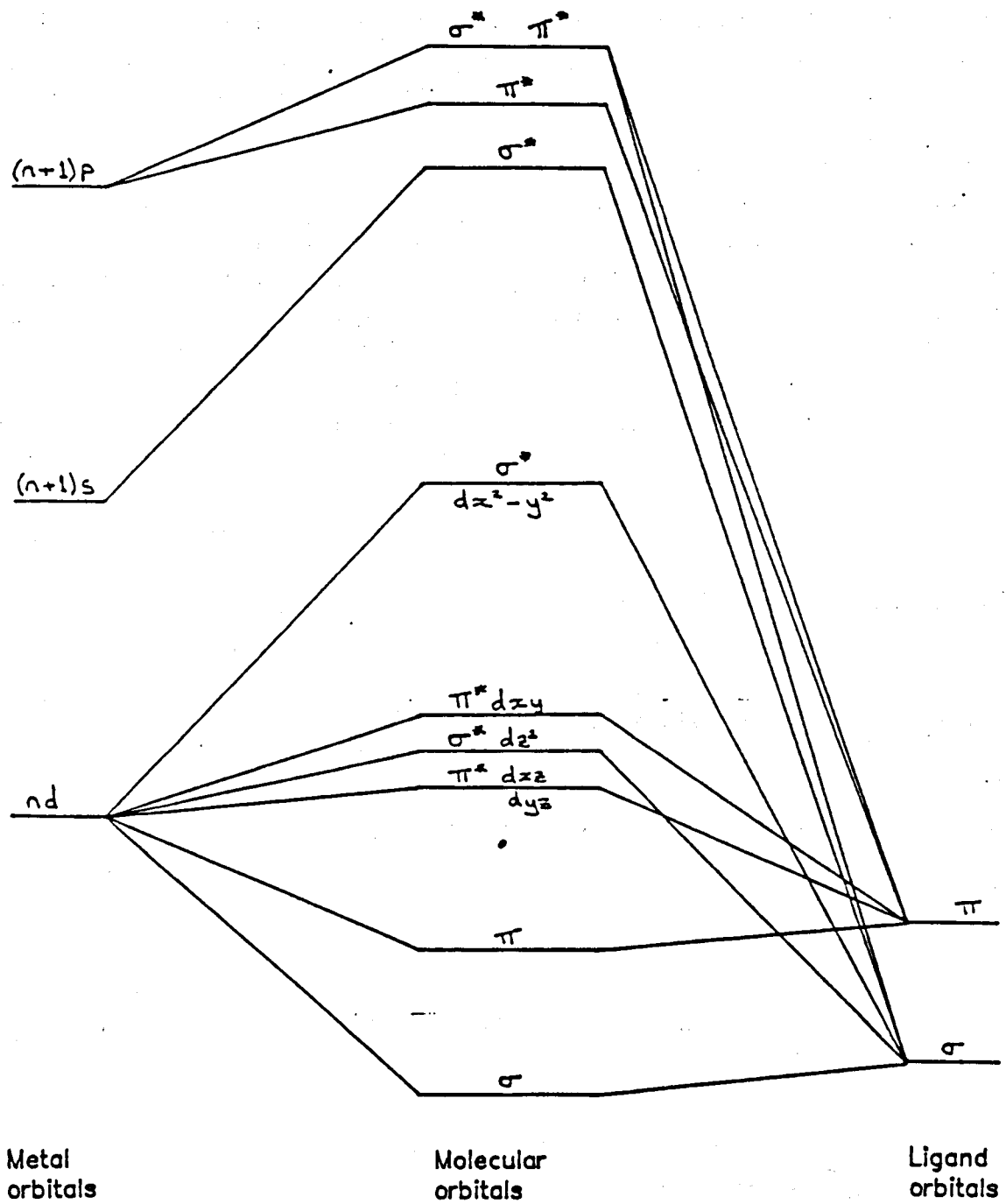
An initial rates method was used to establish the order of reaction with respect to each component. In each of the six reactions studied the results indicated an overall second order reaction, first order with respect to both the PtCl_4^{2-} and the ligand. Using the Arrhenius equation the value of the second order activation energy and entropy were obtained for each reaction studied from both AA and UV absorption data. The value of activation energy and entropy obtained for a particular reaction from UV spectroscopy and those obtained from AA spectroscopy were totally compatible with one another, both methods giving results which were within the experimental error. Thus from a reproducibility and accuracy point of view there is nothing to choose between the two methods. However, UV is the simpler of the two techniques and does not require such specialised equipment. UV spectroscopy is also less susceptible to variation from day to day such as encountered in AA spectroscopy with regards to flame conditions and the positioning of lamp and burner.

The method of monitoring the kinetics of formation of complexes of the type PtCl_2L_2 developed, so far, depends on the solubility of the ligand in aqueous solution and the fact that the solid product precipitates out of solution. However, there is in principle no reason why the method could not be extended to incorporate ligands which are insoluble in aqueous solution so long as care is taken to avoid coprecipitation or occlusion of ligand in the product. One way of approaching this problem could be to carry out the reaction using a two phase system. Osa et al.⁽²⁴⁾ synthesised *cis*-dichloroplatinum complexes of nitrogen-cyclic compounds through the reaction of K_2PtCl_4 with the corresponding ligand at an interfacial layer between water and an organic solvent.

An interesting feature of the results obtained in this study and comparison with those cited in the literature was the fact that there is a linear relationship between the activation energies and activation entropies. The reason behind this, which is basically mathematical, has been discussed in Chapter 3.6. However, an important point to note is that when looking for correlation between kinetic parameters and other properties of the system, which will be discussed later, is that either energy or entropy of activation can be used since these correlate well with each other.

The theoretical studies yielded a large amount of data related to the electronic properties of the ligands and this has been discussed in Chapter 5.

The electronic structure of the metal - ligand bonding has been considered in terms of Molecular Orbital theory. The Molecular Orbital theory starts with the premise that overlap of atomic orbitals occurs, where permitted by symmetry, to an extent determined by the spatial nature of the orbitals. All degrees of overlap, including the electrostatic situation, come within its scope. The first task when considering molecular orbital treatment for a complex is to determine which orbital overlaps are or are not possible because of the inherent symmetry requirements of the problem. In platinum square planar complexes there are nine valence shell orbitals of the metal ion to be considered, four of which have lobes lying along the metal-ligand bond directions and are suitable for σ bonding, whereas the other five are orientated as to be suitable only for π bonding.



π - π bonding orbitals
 σ - σ bonding orbitals
 \neq - anti bonding orbitals.

Figure 6.1

A Qualitative Molecular Orbital Diagram for a Square Planar Platinum complex.

Each metal orbital overlaps with its matching symmetry orbital of the ligand system to form bonding and antibonding molecular orbitals. The molecular orbitals of the same symmetry class, which are equivalent apart from their spatial orientation, have the same energy. Orbitals of different symmetry classes do not in general have the same energy since they are not equivalent. Figure 6.1 illustrates how the atomic orbitals of the metal and ligand combine.

A characteristic feature of the d group transition metals is their ability for form complexes with a wide variety of neutral molecules and molecules with delocalised π orbitals such as the N-heterocycles. In these complexes the metal atoms are in low positive, zero or negative formal oxidation state and it is a characteristic of ligands with delocalised electrons that they can stabilize low oxidation states. This property is associated with the fact that these ligands possess vacant π orbitals in addition to lone pairs. These vacant orbitals accept electron density from filled metal orbitals to form a type of π bonding that supplements the σ bonding arising from lone pair donation. High electron density on the metal, of necessity in low oxidation states, can thus be delocalised onto the ligand.

Thus for Platinum-Nitrogen bonding it is envisaged that:

- (a) there is a dative overlap from the lone pair on the nitrogen to an empty platinum σ orbital;
- (b) back donation occurs from a filled $d\pi$ or hybrid $dp\pi$ platinum orbital into an empty $p\pi$ orbital of the nitrogen.

This bonding mechanism is synergic since the effects of the σ bond formation strenghtens the π bond and vice versa.

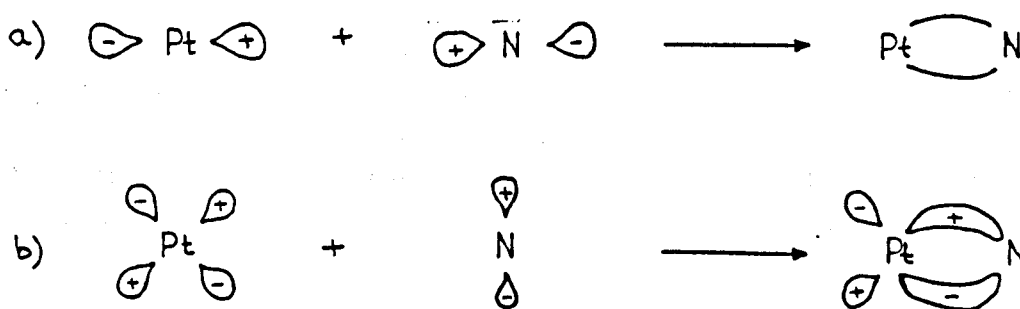


Figure 6.2 (a) The formation of the $\text{Pt} \leftarrow \text{N}$ σ bond using an unshared pair of electrons. (b) The formation of the $\text{Pt} \rightarrow \text{N}$ π bond.

Table 6.1 summarizes some of the important data obtained from solution and solid state studies along with data obtained from theoretical consideration of the quaternized bases.

Several correlations of the kinetic and energetic properties of the complexes with the electronic properties of the ligands were attempted but only one was found. This was the relationship between the solid state decomposition energy and the LUMO energy of the quaternized base (Figure 6.3). It is significant that in solid state chemistry there are no interfering solvent effects. The calculations which relate to isolated gas phase molecules are more relevant to the solid state situation than they would be in reactions in solution.

The graph of solid state decomposition energy versus LUMO energy indicates good correlation for pyridine, pyrimidine, 2-aminopyrimidine and 2-amino-4-methylpyrimidine quaternized at N1. This suggests that complexation of 2-amino-4-methylpyrimidine occurs at the N1 position and not the N3 position, which one would expect from steric hindrance considerations.

The bases showing good correlation all have a high coefficient for the $2p_x$ orbitals on the nitrogen in the LUMO eigenvector. 2-aminopyridine has only a $2s$ wavefunction LUMO and very significantly does not fit into the general trend. Because there is no contribution from the P_x orbitals back donation cannot operate and the bond between platinum and nitrogen would therefore be weaker. This is the likely reason for the significantly low activation energy, obtained from solid state studies, which is approximately 30 KJmol^{-1} less than predicted by the graph.







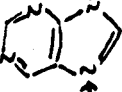
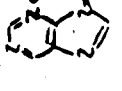
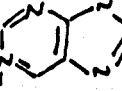
Each of the nitrogen atoms of purine, when quaternized, have a large p_x component in the LUMO wavefunction, but only when quaternized at N1 does the LUMO exhibit the very high energy (-5.82 eV) expected in order to rationalize the stability of the platinum-nitrogen bond found in the $\text{Pt(Pu)}_2\text{Cl}_2$ complex. Solid state studies indicated that the platinum-nitrogen bond in this complex was so stable that dissociation of the platinum-chloride bond took place preferentially and much higher temperatures were required before dissociation of the platinum-nitrogen bond occurred. Thus comparison of the LUMO energies for the various quaternized forms of purine suggest that complexation of purine to platinum occurs at the N1 positions.

Molecular orbital calculations were also carried out on NH_4^+ , which was found to have a LUMO energy of -4.79 eV and the nitrogen has a wavefunction which is almost entirely $2s$ in character. Although this suggests a weak bond, because of the absence of back donation, the LUMO energy is so high that this would result in a very stable platinum-nitrogen bond. Like the purine complex it is thus expected that the platinum-nitrogen bond, in complexes such as *cis*-platin ($\text{PtCl}_2(\text{NH}_4)_2$), would be more stable than the platinum-chloride bond. This is a very noteworthy observation and corresponds with the fact that *cis*-platin complexes with nucleolases by Cl^- replacement rather than substitution of the NH_4 ligands.

The results obtained from the molecular orbital studies appear to justify the view that quaternization models complexation provided solvent effects are absent, as in the case of solid state chemistry.

TABLE 6.1

Summary of Some Significant Results

	H ⁺ Position	E _a Soln	E _a Solid	IP	E LUMO	Charge at N ⁻	LUMO p _z at N ⁻	N-H Length
Py		64	173	15.62	-5.89	-0.07	0.47	1.0115
Pm		74	102	16.16	-6.26	-0.13	0.48	1.0147
2AFy		56	137	14.96	-5.93	-0.32	0.00	1.0900
2AFm		50	129	15.83	-6.09	-0.12	0.47	1.0181
AMP _m		94	161	15.38	-5.86	-0.12	0.46	1.0130
AMP _m		94	161	15.51	-5.94	-0.18	0.45	1.0093
Pu		44	-	14.75	-5.82	-0.09	0.38	1.0014
Pu		44	-	14.54	-6.08	-0.13	0.42	1.0061
Pu		44	-	14.36	-5.89	-0.14	0.40	1.0080
NH ₄ ⁺		-	-	24.80	-4.79	-0.09	0.00	1.0220

E_a - Activation Energy

IP - Ionisation Potential

6.2 Conclusion

At the outset this study was planned to look for structure activity relationships in a series of platinum complexes which could be regarded as very simple models of the interactions between platinum anticancer drugs and the nucleobases of DNA. In the course of this study it has been found that:

- (1) For soluble heterocyclic ligands, yielding insoluble products, the reaction between K_2PtCl_6 and the ligand is best monitored by pre-aquating the $PtCl_6^{2-}$ and measuring the decrease in concentration of platinum or ligand by AA or UV spectrophotometry respectively.
- (2) The activation parameters for the reactions of platinum complexes in solution are strongly correlated (both for this work and that of other authors); the higher the activation energy the greater is the tendency towards a dissociative mechanism.
- (3) There is no correlation between the experimentally measured reaction parameters for the $PtCl_6^{2-} + \text{Ligand}$ reaction in solution and the quantum mechanically calculated quantities for the ligand such as electron density, molecular orbital energies, dipole moment and wave functions. This is probably due to the possibility that in solution the ligand is solvated and quite dissimilar to the isolated gas phase used in the quantum calculations.
- (4) Solid state reactions, easily followed by thermogravimetric analysis and the stepwise thermal decomposition of complexes, often involve a step which must be directly related to the platinum-nitrogen bond breaking reaction. Isothermal studies allow calculation of the activation energies for these processes but non-isothermal methods are of little value in this respect.
- (5) No correlation between the solid state results (which involve bond breaking) and synthesis of complexes was found probably because in solution the reaction is complicated by solvent effects and the reaction profile involves two steps. The rate determining step involves the addition of the ligand which is accompanied by structural rearrangement to form a six co-ordinated intermediate. Thus steric effects and the nature of the entering group exert a major effect on the rates of reaction. Whereas in the solid state the complex is a molecular solid and hence not affected by solvent effects. Here the decomposition energies were rationalised in terms of electronic structure of the ligand and steric effects appeared to exert very little influence on the energy required to break the platinum-nitrogen bond.
- (6) Good correlation was found between the solid state activation dissociation energy and the energy of the LUMO of the ligand, when this was found to be predominantly p_z on the relevant nitrogen. The higher the energy required for dissociation of the platinum-nitrogen bond, the higher the energy of the LUMO of the quaternized base.

It is considered that studies such as these carried out here, particularly the solid state and the theoretical work could be usefully applied to larger systems which more closely model drugs and their DNA interaction products. For example thermal studies on the interaction complexes of second generation anti-cancer drugs such as CHIP and carboplatin would be worthwhile since semi-empirical molecular orbital calculations are particularly suitable for such complexes.

Authors studying kinetics of formation should perhaps look for deviations from correlation between the activation energy and activation entropy as being of some significance.

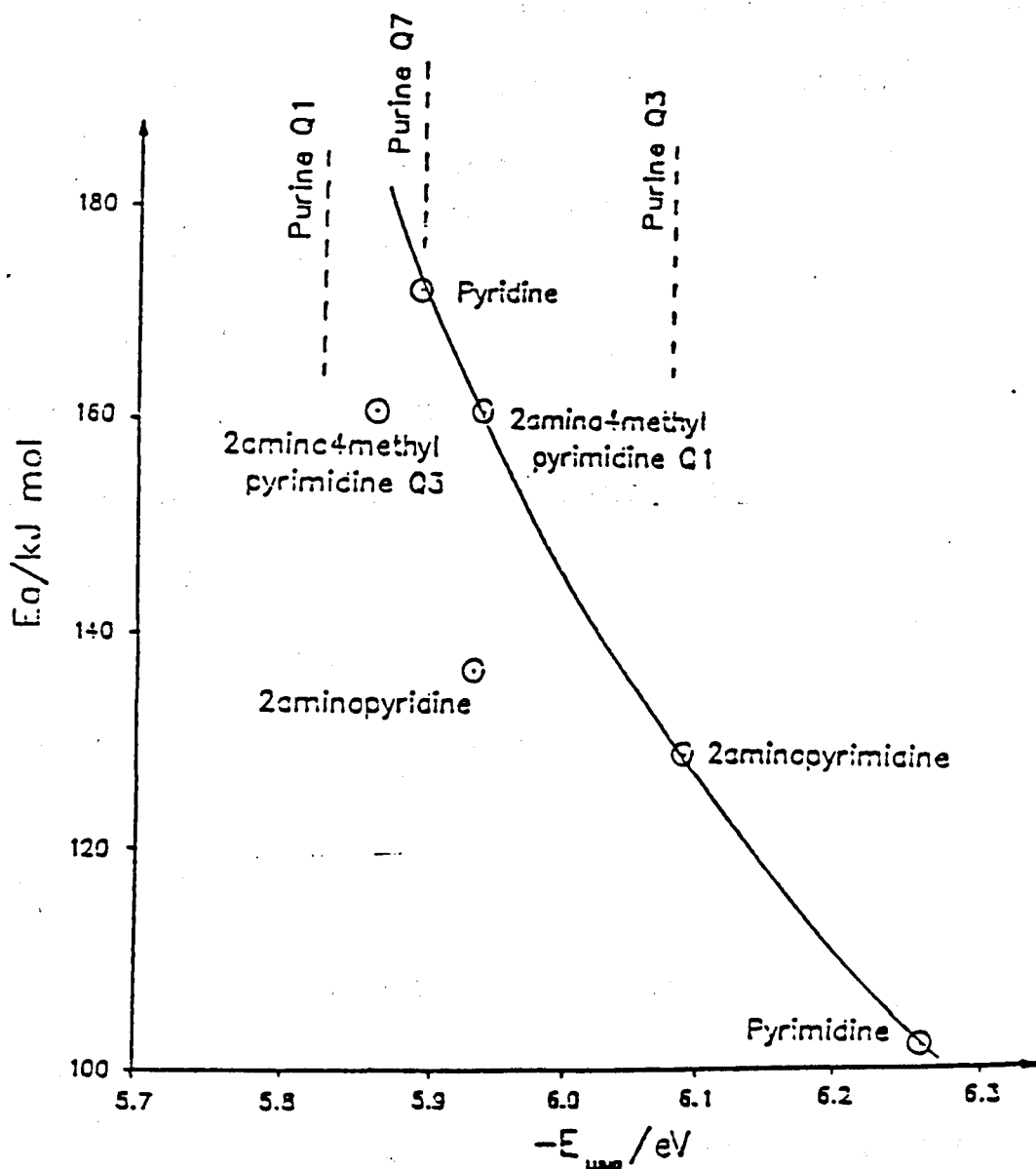


Figure 6.3 Plot of Solid State Activation Energy vs LUMO Energy of the Ligand.

REFERENCES

1. E J Ambrose and F J C Roe, Ed, 'The Biology of Cancer', Van Nostrand, London, 1966.
2. S A Stock, Chem Brit, 1970, 11.
3. P A Plattner, 'Chemotherapy of Cancer', Elsevier, Amsterdam, 1964.
4. B Rosenberg, L Van Camp, J E Trosko and V H Mansour, Nature (London), 1969, 222 385.
5. J J Roberts and A J Thomson, Progr, Nucleic Acid Res, Mol, Biol, 1979, 22 71.
6. J Reedijk et al, Struct Bonding, 1987, 67 53.
7. B Rosenberg, Plat Met Rev, 1971 15 42.
8. B Reslova, Chem, Biol Interact, 1972, 4 66.
9. S J Lippard, Science, 1982, 218 1075.
10. P J Stone, A D Kelman and F M Sinex, Nature, 1974, 251 736.
11. A T Marcelis, C Erkelens and J Reedijk, Inorg Chem Acta, 1974, 91 129.
12. S Eapen, M Green and I M Ismail, J Inorg Biochem, 1985, 24 333.
13. F W Sunderman, Bio Trace Elem, 1979 1 63.
14. B Lippert, Inorg Chem, 1981, 20 4326.
15. N C Thomas and J Cox, Polyhedron, 1988 7 731.
16. F Basalo and R G Pearson, Progr Inorg Chem, 1962 4 318.
17. F Basalo, Advan Chem Ser, 1965 49 81.
18. V Belluco, L Cattalini, F Bassalo, R G Pearson and A Turco, J Am chem Soc, 1965 87 241.
19. P C Kong and F D Rochon, Can J Chem, 1981 59 3293.
20. Y N Kukushkin and V B Ukrianstev, Russ J Inorg Chem, 1964 14 (5), 664.

21. C J Keatch and D Dollimore, 'An Introduction to Thermogravimetry', 2nd Edition, Heyden, London, 1975.
22. M A Tucker, C B Colvin and D S Martin, *Inorg Chem*, 1964, 2 1373.
23. K Nakamoto, 'Infrared Spectra of Inorganic and Coordination Compounds', 3rd Edition, Wiley, London.
24. T Osa, H Hino, S Fugieala, T Shio and T Kono, *Chem Pharm Bull*, 1986 34 (9), 3563.
25. S Arrhenius, *Z Physik, Chem*, 1889, 4 226.
26. H Eyring, *J Chem Phys*, 1935, 3 107.
27. J V Rund and F A Palocsey, *Inorg Chem*, 1969, 8 524.
28. D S Martin, T S Ellerman and L F Grantham, *J Am Chem Soc*, 1955, 77 2965.
29. R G Pearson, H B Gray and F Basalo, *J Am Chem Soc*, 1960, 82 787.
30. F Basalo and R G Pearson, 'Mechanisms of Inorganic Reactions', 2nd Edition, Wiley, New York, 1967.
31. M N Hughes, 'Inorganic Chemistry of Biological Processes', 2nd Edition, Wiley, 1981.
32. R G Pearson, *J Chem Phys*, 1952 20 1471.
33. R Van Eldik, D A Palmer and H Kelm, *Inorg Chem*, 1979 18 (3) 572.
34. D J Evans, M Green and R van Eldik, *Inorg Chim Acta*, 1987, 128 27.
35. S Lanza, D Minniti, P Moore, J Sachinidis, R Romeo and M L Tobe, *Inorg Chem*, 1984, 23, 4428.
36. G Alibrandi, D Minniti, L M Scolaro and R Romeo, *Inorg Chem* 1989, 28, 1939.
37. Le Chatelier (1885) - quoted in J R Partington, 'Thermodynamics' 4th Edition, Constable and Co, 1950.
38. Y N Kukushkin and V B Ukrainstev, *Russ J Inorg Chem*, 1968, 13, (10), 2886.
39. Y N Kukushkin and V B Ukrainstev, *Russ J Inorg Chem*, 1968, 13, (11), 3143.

40. S Miya, K Kashiarabara and K Saito, *Inorg Chem*, 1980, 19 98.
41. D J Evans and M Green, *J Chem Soc Chem, Comm*, 1987, 124.
42. Y N Kukushkin and V B Ukrainstev, *Russ J Inorg Chem*, 1970, 15, (9), 1270.
43. K H Tonge, *Thermochim, Acta*, 1984, 74 151.
44. E S Freeman and B Carroll, *J Phys Chem*, 1958, 62 394.
45. D C Doyle, *J Appl Polymer Sci*, 1961, 5 285.
46. A W Coates and J P Redfern, *Nature*, 1964, 4 161.
47. T R Ingraham and P Marrier, *Can J Chem*, 1964, 42 161.
48. S J Gentry, N W Hurst and A Jones, *J Chem Soc Faraday I*, 1979, 75.
49. L M Sverdlov, M A Kovnev and E P Krainor, 'Vibrational Spectra of Polyatomic Molecules'; 1970.
50. D W Clack and R D Gillard, *Inorg Chim Acta*, 1988, 141 37.
51. R D Gillard, *Co-ord Chem Revs*, 1983, 50 303.
52. A W Addison, K Dawson, R D Gillard, B T Heaton and H Shaw, *J Chem Soc, Dalton Trans*, 1972, 589.

Acknowledgement

The author would like to thank the Isle of Man Board of Education for generously providing the funding for this period of research. Thanks also to the School of Applied Science, Robert Gordons Institute of Technology, for the use of their facilities. The author extends sincere gratitude to Dr John Harper and especially Dr Ken Tonge for their continual guidance, encouragement, advice and expertise.

Thanks are also due to Dr S Bell, Dundee University, for carrying out Molecular Orbital calculations on the 2-amino-4-pyrimidine and purine systems, which were too large to be handled by the Honeywell computer.

A very special thanks to my immediate family for their patience and support.

Thanks must also go to Dr J Lusty for initiating this program of research.

Finally a very warm thanks to the Word Processing department of MMG Ltd for their excellent work in typing this thesis.

Appendix I

Solution Studies Raw Data

Initial Rate Results

Reaction between K_2PtCl_4 + 2-aminopyridine:

Time	Atomic Absorbance Values at Initial Molar Ratios K_2PtCl_4 :Ligand			
	0.2 : 0.4	0.4 : 0.4	0.2 : 0.8	0.2 : 0.3
5	0.097	0.180	0.091	0.093
10	0.092	0.168	0.083	0.090
15	0.089	0.160	0.081	0.088
20	0.084	0.150	0.074	0.086
30	0.078	0.140	0.070	0.081
40	0.068	0.130	0.065	0.077
50	0.063	0.128	0.063	0.073
60	0.060	0.124	0.061	0.071

Reaction between K_2PtCl_4 + 2-aminopyrimidine:

Time	Absorbance Values at Initial Molar Ratios K_2PtCl_4 :Ligand					
	0.2 : 0.4		0.4 : 0.4		0.2 : 0.8	
	AA	UV	AA	UV	AA	UV
1	0.130	1.001	0.359	1.120	0.158	2.216
5	0.121	0.933	0.339	0.991	0.130	2.095
7	0.116	0.905	0.329	0.938	0.124	2.005
10	0.107	0.860	0.314	0.841	0.113	1.942
15	0.096	0.785	0.288	0.681	0.089	1.787
18	0.089	0.735	0.276	0.600	0.079	1.730
20	0.084	0.698	0.264	0.549	0.064	1.640
25	0.072	0.627	0.240	0.472	0.054	1.493
30	0.069	0.547	0.226	0.420	0.046	1.356

Reaction between K_2PtCl_4 + Pyridine:

Time	Absorbance Values at Initial Molar Ratios K_2PtCl_4 :Ligand					
	0.2 : 0.4		0.4 : 0.4		0.2 : 0.8	
	AA	UV	AA	UV	AA	UV
1	0.303	0.910	0.536	0.961	0.402	1.916
5	0.257	0.810	0.450	0.722	0.310	1.709
7	0.235	0.750	0.402	0.615	0.244	1.532
10	0.200	0.672	0.335	0.457	0.200	1.419
12	0.173	0.605	0.312	0.393	0.156	1.335
15	0.143	0.543	0.303	0.345	0.140	1.282
20	0.125	0.406	0.293	0.321	0.122	1.189
25	0.115	0.350	0.291	0.298	0.098	1.140
30	0.110	0.331	0.290	0.296	0.086	1.105

Reaction between K_2PtCl_4 + 2-amino-4-methylpyrimidine:

Time	Absorbance Values at Initial Molar Ratios K_2PtCl_4 :Ligand					
	0.2 : 0.4		0.4 : 0.4		0.2 : 0.8	
	AA	UV	AA	UV	AA	UV
1	0.150	1.180	0.239	1.300	0.323	2.092
5	0.140	1.113	0.214	1.177	0.303	1.981
8	0.134	1.081	0.206	1.129	0.288	1.892
10	0.128	1.049	0.192	1.049	0.279	1.840
15	0.114	0.980	0.167	0.902	0.254	1.708
18	0.108	0.935	0.152	0.820	0.239	1.613
20	0.104	0.911	0.144	0.781	0.230	1.555
25	0.097	0.835	0.135	0.740	0.214	1.490
30	0.094	0.758	0.130	0.729	0.202	1.450

Reaction between K_2PtCl_4 + Purine:

Time	Absorbance Values at Initial Molar Ratios K_2PtCl_4 :Ligand					
	0.2 : 0.4		0.4 : 0.4		0.2 : 0.8	
	AA	UV	AA	UV	AA	UV
1	0.241	1.289	0.342	1.171	0.262	2.568
3	0.230	1.210	0.319	1.019	0.245	2.463
5	0.218	1.131	0.295	0.862	0.216	2.270
7	0.205	1.060	0.272	0.720	0.187	2.098
10	0.185	0.940	0.237	0.489	0.158	1.921
12	0.173	0.851	0.230	0.378	0.148	1.810
15	0.159	0.769	0.215	0.307	0.144	1.759
20	0.130	0.640	0.204	0.224	0.139	1.710
30	0.098	0.549	0.194	0.171	0.136	1.563

Integrated Rate Equation Results

Reaction between K_2PtCl_6 + 2-aminopyridine:

Atomic Absorbance Values

Time	Absorbance at each Temperature			
	303	306	308	310
5	0.2872	0.2557	0.2667	0.2381
10	0.2743	0.1575	0.2459	0.2339
15	0.2629	0.2542	0.2381	0.2115
20	0.2530	0.2356	0.2292	0.2195
30	0.2433	0.2271	0.2046	0.1738
45	0.2067	0.1999	0.1771	0.1414
60	0.1926	0.1703	0.1613	0.1231
75	0.1785	0.1504	0.1450	0.1156
90	0.1023	0.1481	0.1315	0.1028
120	0.1402	0.1221	0.1111	-

UV Absorbance Values

Time	Absorbance at each Temperature			
	303	306	308	310
5	1.6129	1.3889	1.311	1.4323
10	1.4706	1.2433	1.232	1.1905
15	1.3514	1.1128	1.111	0.9345
20	1.2500	1.0135	1.018	0.8628
30	1.0869	0.8625	0.904	0.6635
45	0.9091	0.7143	0.695	0.5183
60	0.7752	0.5988	0.592	0.4393
75	0.6757	0.5714	0.530	0.3770
90	0.6028	0.5181	0.453	0.3415
120	0.4903	0.3953	0.359	-

Reaction between K_2PtCl_6 + Pyridine:

AA Absorbance Readings

Time	Absorbance at each Temp(K)					
	298	301.5	306	308.5	313	316
5	.3576	.3400	.3448	.2458	.2571	.3239
10	.3572	.3109	.3088	.2003	.2003	.2528
15	.3324	.2737	.2735	.1798	.1722	.2041
20	.3045	.2482	.2449	.1593	.1556	.1736
30	.2688	.2143	.2142	.1305	.1256	.1380
40	.2273	.1956	.1751	.1240	.1122	-
45	.2133	.1767	.1665	.1005	.1029	.0957
50	.2059	.1744	.1535	.0956	.0816	-
60	.1938	.1576	.1338	.0815	.0796	.0791
75	.1703	.1288	.1194	.0713	.0668	-

UV Absorbance Reading

Time	Absorbance at each Temp (K)					
	294.5	298	306	308.5	313	316
5	1.214	1.022	0.920	0.801	0.869	0.874
10	1.096	0.972	0.776	0.784	0.653	0.653
15	0.891	0.878	0.941	0.643	0.543	0.481
20	0.864	0.787	0.674	0.530	0.426	0.403
30	0.684	0.676	0.525	0.432	0.343	0.289
45	0.801	0.555	0.373	0.309	0.249	0.205
60	0.521	0.479	0.306	0.265	0.200	0.154
75	0.496	0.384	0.254	0.204	0.161	0.126

Reaction between K_2PtCl_4 + 2-aminopyrimidine:

AA Absorbance Readings

Time	Absorbance at each Temp(K)					
	303	308	311	313	316	318
5	.2128	.4010	.2562	.2191	.3998	.2322
10	.2041	.3831	.2154	.1918	.3298	.1893
15	.2000	.3058	.1798	.1540	.2427	.1568
20	.1942	.2558	.1684	.1420	.1980	.1485
30	.1667	.1733	.1387	.1249	.1414	.1008
45	.1351	.1431	.1040	.0885	.0990	.0906
60	.1143	.1161	.0929	.0782	.0762	.0605
75	.0900	.0941	.0696	.0603	.0619	.0529
90	.0878	.0763	.0618	.0520	.0521	-

UV Absorbance Readings

Time	Absorbance at each Temp (K)					
	293	303	308	311	313	318
5	1.318	1.005	1.482	1.063	.9667	.9123
10	1.206	0.904	0.914	0.879	.8330	.7565
15	1.109	0.886	0.814	0.763	.6828	.6130
20	1.024	0.788	0.754	0.677	.6457	.5487
30	0.932	0.749	0.669	0.570	.5213	.4013
45	0.777	0.641	0.514	0.422	.3817	.2853
60	0.651	0.520	0.428	0.377	.3207	.2310
75	0.588	0.434	0.354	0.287	.2747	.2130
90	0.515	0.396	0.333	0.276	.2245	.2110

Reaction between K_2PtCl_4 + 2-amino-4-methylpyrimidine:

AA Absorbance Readings

Time	Absorbance at each Temp(K)					
	303	305.5	308	310	313	318
10	.2964	.3119	.3220	.3859	.3057	.2403
15	.2859	.2978	.3123	.3509	.3082	.2142
20	.2948	.3121	.3074	.3126	.3053	.1916
30	.2874	.2894	.2965	.2778	.2402	.1788
45	.2805	.2730	.2663	.2299	.1990	.1437
60	.2660	.2357	.2324	.1832	.1623	.1021
75	.2368	.2233	.2105	.1787	.1328	.0840
90	.2149	.2035	.1772	.1486	.1190	.0704
105	.2064	.1738	.1598	.1332	.1039	.0582
120	.1927	.1613	.1383	.1199	.0936	.0523
150	.1687	.1510	.1174	.1015	.0779	.0435

UV Absorbance Readings

Time	Absorbance at each Temp (K)					
	303	305.5	310	313	316	318
10	.9350	.8772	.9677	.9093	.7693	.848
15	.9220	.8696	.9547	.8242	.7465	.759
20	.9055	.8130	.9468	.8313	.7073	.6065
30	.8248	.7576	.7825	.6645	.5878	.488
45	.7853	.6897	.6800	.5393	.4490	.417
60	.7140	.6329	.5695	.4355	.3965	.294
75	.6685	.5850	.5278	.3668	.3228	.266
90	.6215	.5435	.4423	.3225	.2903	.2205
105	.5824	.5076	.3989	.2906	.2098	.206
120	.5479	.4757	.3720	.2900	.1914	.1836
150	.4825	.4219	.3005	.2390	.1629	.1508

Reaction between K_2PtCl_4 + Purine :

AA Absorbance Readings

Time	Absorbance at each Temp(K)					
	299	302	304	306	310	313
5	.2349	.2245	.1170	.2012	.2107	.2219
10	.1986	.2024	.1032	.1757	.1684	.1656
15	.1710	.1789	.0939	.1529	.1334	.1271
20	.1416	.1613	.0855	.1309	.1147	.1047
30	.1227	.1276	.0755	.1099	.0811	.0735
45	.0975	.1008	.0590	.0800	.0635	.0556
60	.0779	.0756	.0497	.0591	.0513	.0444
75	.0662	.0651	.0430	.0491	.0417	.0364

UV Absorbance Readings

Time	Absorbance at each Temp (K)					
	299	302	304	306	310	313
5	.2349	.2245	.1170	.2012	.2107	.2219
10	.1986	.2024	.1032	.1757	.1684	.1656
15	.1710	.1789	.0939	.1529	.1334	.1271
20	.1416	.1613	.0855	.1309	.1147	.1047
30	.1227	.1276	.0755	.1099	.0811	.0735
45	.0975	.1008	.0590	.0800	.0635	.0556
60	.0779	.0756	.0497	.0591	.0513	.0444
75	.0662	.0651	.0430	.0491	.0417	.0364

Appendix II

Typical Thermogravimetric Analysis Input and Output

Non-isothermal Input:

S T E P A N A L Y S I S

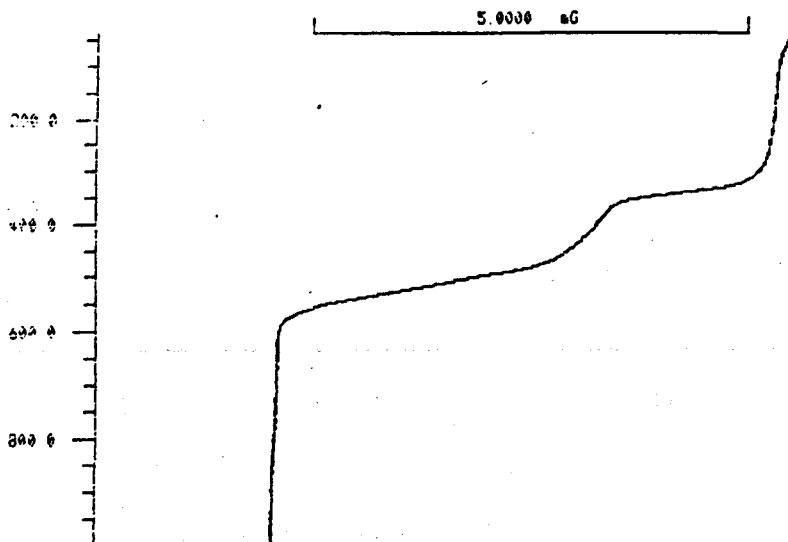
19-OCT-88 12:16

SCAN PARAMETERS

START TEMP. °C	40
RATE K/MIN.	10
END TEMP. °C	1000
TIME ISO. MIN.	0
FLOT CH	10
RANGE FS µG	10
OFFSET %G	80
VALUE T/1 1/2	0
STEP ANALYSIS	
DYN/ISO 1/2	1
AUTOLIMIT 0/1	1
START	50
END	800
BASELINE TYPE	1
FLOT CH	11
FLOT MODE	2031
MOL MASS GAS	0
MOL MASS INIT.	0
IDENT. NO.	1
WEIGHT µG	10.350

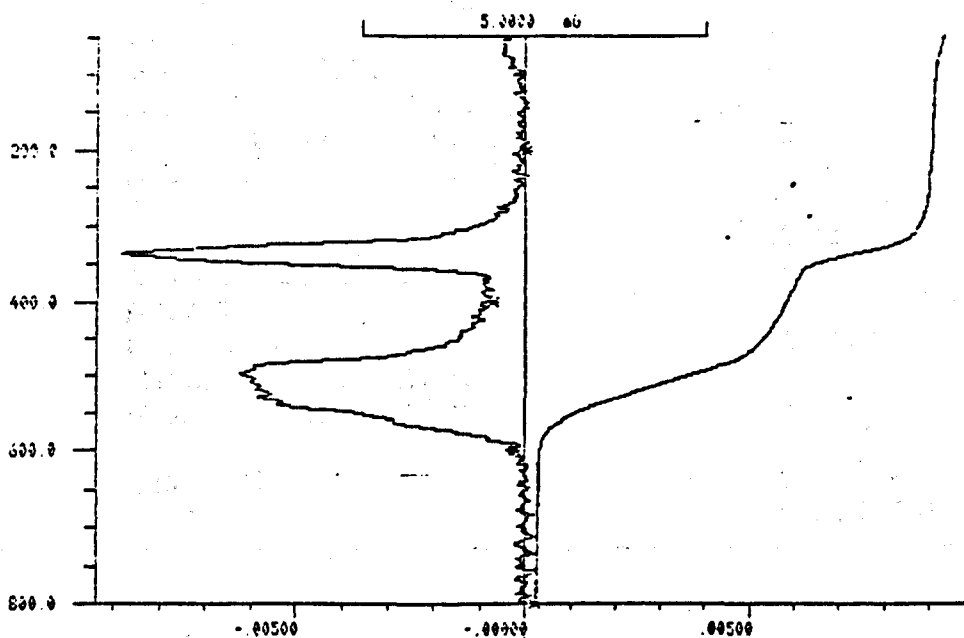
TEMPERATURE °C

WEIGHT GAIN----->



TEMPERATURE °C

WEIGHT GAIN----->



DTG μG/S

STEP		
START TEMP. °C		152.5
PEAK TEMP. °C		347.5
END TEMP. °C		410.0
▲B	μG	-2.1560
▲B	%	-19.663

STEP		
START TEMP. °C		410.0
PEAK TEMP. °C		552.5
END TEMP. °C		800.0
▲B	μG	-3.9410
▲B	%	-35.942

***** METTLER TA3000 SYSTEM *****

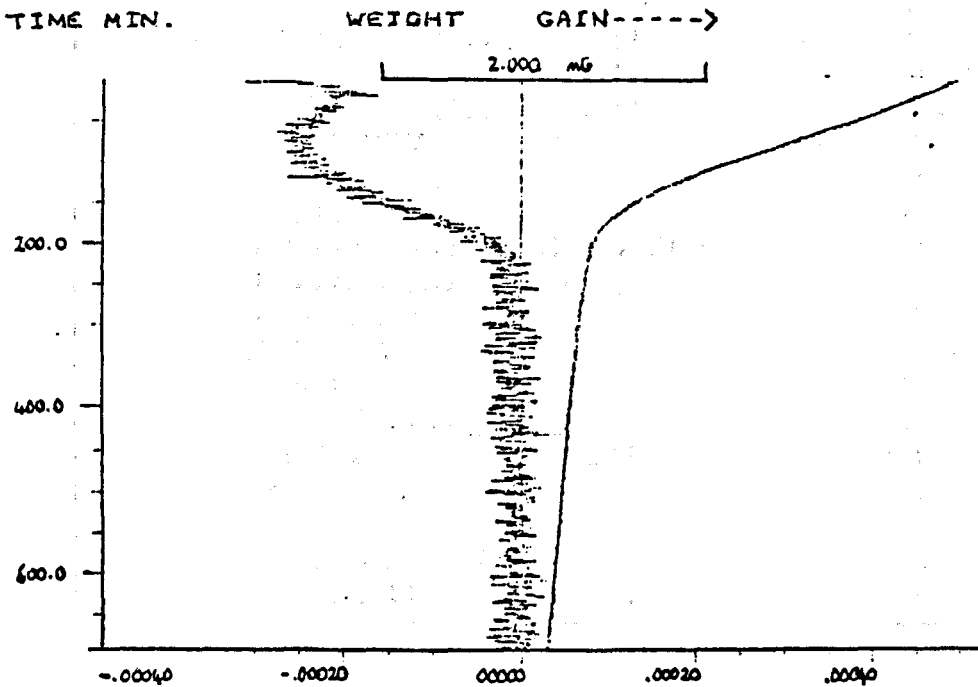
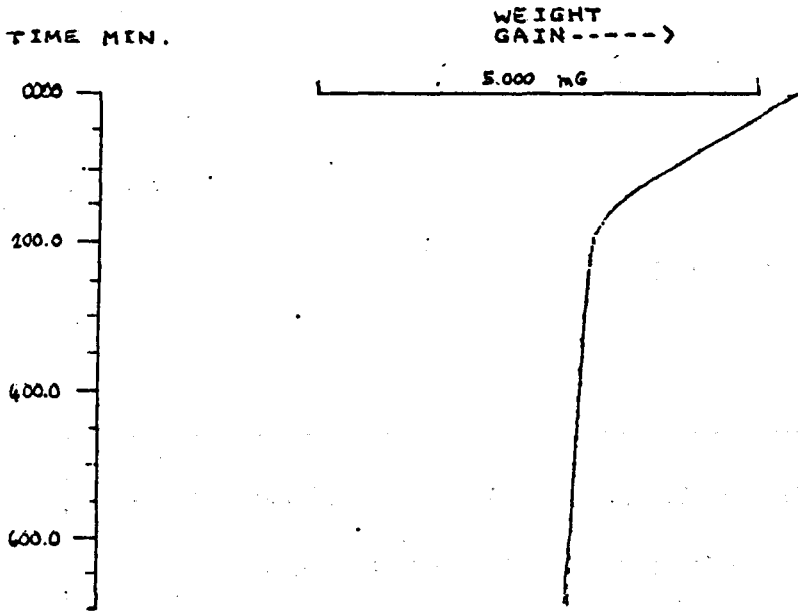
Non-isothermal Output

Isothermal Input:

S T E P A N A L Y S I S

31-JAN-87 17:06

SCAN PARAMETERS	
START TEMP. °C	285
RATE K/MIN.	0
TIME ISO. MIN.	700
PLOT CM	10
RANGE FS MG	10
OFFSET %	80
VALUE T/1 1/2	0
STEP ANALYSIS	
DYN/ISO 1/2	2
AUTOLIMIT 0/1	1
START	5
END	695
BASELINE TYPE	1
PLOT CM	11
PLOT MODE	2031
MOL MASS GAS	0
MOL MASS INIT.	0
IDENT. NO.	1
WEIGHT MG	10.394



DTG MG/S

STEP		
START T. MIN.		5.50
PEAK TIME MIN.		4.95
END TIME MIN.		168.30
ΔM	MG	-2.0870
ΔM	%	-20.079

Isothermal Output

DSC Input :

P E A K I N T E G R A T I O N

14-OCT-88 12:16

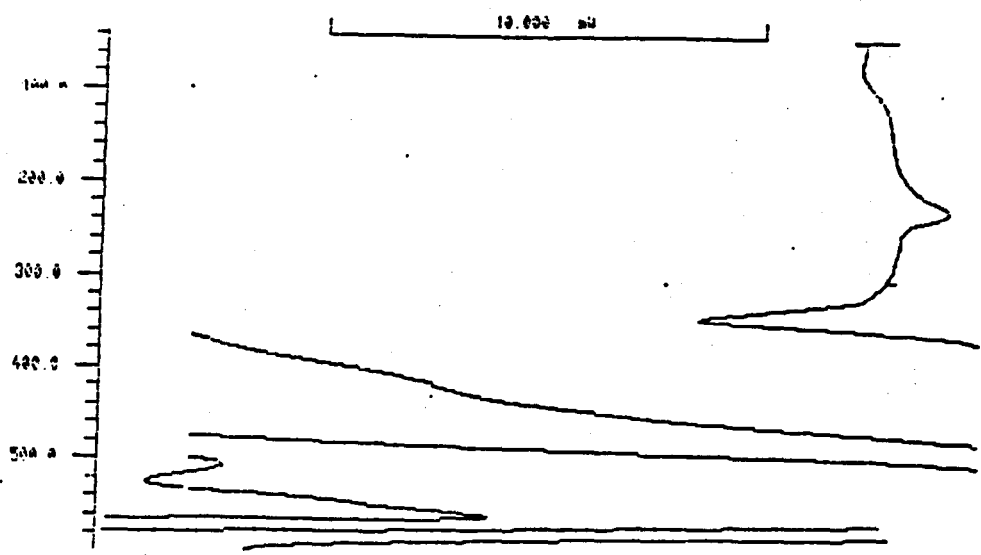
SCAN PARAMETERS

START TEMP. °C	40
RATE K/MIN.	5
END TEMP. °C	600
TIME ISO. MIN.	0
PLOT CM	10
RANGE FS mW	20
OFFSET %	90
PAN TYPE 1/2	1
LIMIT mW	0
PEAK INTEGRATION	
DYN/ISO 1/2	1
AUTOLIMIT 0/1	1
START	50
END	550
BASELINE TYPE	8
PLOT CM	10
PLOT MODE	101

IDENT. NO.	2
WEIGHT mg	9.018

TEMPERATURE °C

HEAT FLOW
EXOTHERMAL-->

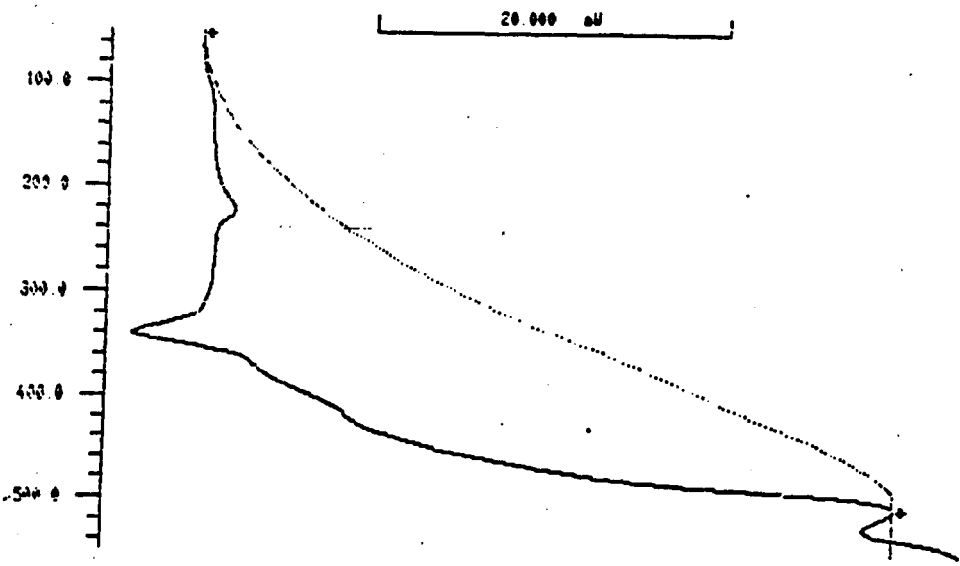


AUTOLIMITS
START TEMP. °C
END TEMP. °C

51.7
503.3

TEMPERATURE °C

HEAT FLOW
EXOTHERMAL-->



ΔH ENDC mJ
ΔH J/G
PEAK TEMP. °C

59413
6586.3
337.7

***** METTLER TA3000 SYSTEM *****

DSC Output

Appendix III

Z Matrices of Ligands

Z Matrix of Pyrimidine

ATOM NUMBER (I)	CHEMICAL SYMBOL	BOND LENGTH (ANGSTROMS)	BOND ANGLE (DEGREES)		TWIST ANGLE (DEGREES)			
		NA:I	NB:NA:I		NC:NB:NA:I	NA	NB	NC
1	N							
2	C	1.36300				1		
3	C	1.40500		120.11000		2	1	
4	C	1.40800		117.98000	.00000	3	2	1
5	N	1.36300		120.11000	.00000	4	3	2
6	C	1.36300		120.48000	.00000	5	4	3
7	H	1.09000		119.08000	180.00000	2	1	6
8	H	1.09100		121.01000	.00000	3	2	7
9	H	1.09000		120.82000	.00000	4	3	8
10	H	1.08900		119.57000	180.00000	6	5	4

Z Matrix of 2-aminopyridine

ATOM NUMBER (I)	CHEMICAL SYMBOL	BOND LENGTH (ANGSTROMS)	BOND ANGLE (DEGREES)		TWIST ANGLE (DEGREES)			
		NA:I	NB:NA:I		NC:NB:NA:I	NA	NB	NC
1	N							
2	C	1.36400				1		
3	C	1.41300		119.39000		2	1	
4	C	1.40800		119.60000	.00000	3	2	1
5	C	1.40700		119.55000	.00000	4	3	2
6	C	1.40800		119.55000	.00000	5	4	3
7	N	1.43600		117.90000	180.00000	2	1	6
8	H	1.09100		120.64000	180.00000	3	2	1
9	H	1.09100		120.29000	.00000	4	3	8
10	H	1.09100		120.56000	.00000	5	4	9
11	H	1.09100		120.75000	.00000	6	5	10
12	H	1.01100		109.86000	121.00000	7	2	1
13	H	1.01200		109.85000	59.00000	7	2	3

Z Matrix of 2-aminopyrimidine

ATOM NUMBER (I)	CHEMICAL SYMBOL	BOND LENGTH (ANGSTROMS) NA:I	BOND ANGLE (DEGREES) NB:NA:I	TWIST ANGLE (DEGREES) NC:NB:NA:I	NA	NB	NC
1	N						
2	C	1.36400			1		
3	N	1.36700	119.90000		2	1	
4	C	1.36200	121.05000	.00000	3	2	1
5	C	1.40700	119.99000	.00000	4	3	2
6	C	1.40700	117.94000	.00000	5	4	3
7	N	1.43500	118.63000	180.00000	2	1	6
8	H	1.09000	119.12000	180.00000	4	3	2
9	H	1.07100	121.02000	.00000	5	4	8
10	H	1.09000	120.87000	.00000	6	5	9
11	H	1.01100	109.65000	121.00000	7	2	1
12	H	1.01100	109.65000	59.00000	7	2	3

Z Matrix of 2-amino-4-methylpyrimidine

ATOM NUMBER (I)	CHEMICAL SYMBOL	BOND LENGTH (ANGSTROMS) NA:I	BOND ANGLE (DEGREES) NB:NA:I	TWIST ANGLE (DEGREES) NC:NB:NA:I	NA	NB	NC
1	N						
2	C	1.36100			1		
3	C	1.40700	119.92000		2	1	
4	C	1.41000	118.59000	0.00000	3	2	1
5	N	1.36500	118.91000	0.00000	4	3	2
6	C	1.36400	121.82000	0.00000	5	4	3
7	H	1.09000	119.11000	180.00000	2	1	6
8	H	1.09000	120.36000	180.00000	3	2	1
9	N	1.43500	118.74000	180.00000	6	5	4
10	C	1.52800	120.87000	180.00000	4	3	2
11	H	1.01100	109.65000	120.00000	9	6	5
12	H	1.01100	109.65000	-120.00000	9	6	5
13	H	1.07200	113.97000	180.00000	10	4	3
14	H	1.07200	111.57000	60.00000	10	4	3
15	H	1.07200	111.53000	-60.00000	10	4	3

Z Matrix of Purine

ATOM NUMBER (I)	CHEMICAL SYMBOL	BOND LENGTH (ANGSTROMS) NA:I	BOND ANGLE (DEGREES) NB:NA:I	TWIST ANGLE (DEGREES) NC:NB:NA:I	NA	NB	NC
1	H						
2	C	1.36500			1		
3	N	1.36700	121.42000		2	1	
4	C	1.36500	121.07000	0.00000	3	2	1
5	C	1.40700	118.81000	0.00000	4	3	2
6	N	1.35300	130.92000	180.00000	5	4	3
7	C	1.35500	107.38000	180.00000	6	5	4
8	N	1.42200	110.42000	0.00000	7	6	5
9	C	1.41600	104.98000	0.00000	8	7	6
10	H	1.08900	119.29000	180.00000	2	1	9
11	H	1.09000	119.84000	180.00000	4	3	2
12	H	1.09000	124.26000	180.00000	7	6	5
13	H	0.99100	127.47000	180.00000	8	7	6

Appendix IV

Typical AMPAC Output

INTERATOMIC DISTANCES

	N 1	C 2	C 3	C 4	C 5	C 6
N 1	.000000					
C 2	1.355000	.000000				
C 3	2.424994	1.378000	.000000			
C 4	2.823125	2.383386	1.397000	.000000		
C 5	2.424175	2.714987	2.399060	1.397000	.000000	
C 6	1.353605	2.281007	2.714987	2.383386	1.378000	.000000
H 7	2.060653	1.092000	2.150509	3.384528	3.806176	3.251069
H 8	3.387502	2.139150	1.080000	2.162767	3.390484	3.794295
H 9	3.903125	3.371519	2.159737	1.080000	2.159842	3.371583
H 10	3.386449	3.794295	3.390484	2.162767	1.080000	2.139150
H 11	2.059000	3.251069	3.806176	3.384528	2.150509	1.092000
H 12	1.011499	2.082376	3.341553	3.834624	3.341061	2.081626

	H 7	H 8	H 9	H 10	H 11	H 12
H 7	.000000					
H 8	2.482523	.000000				
H 9	4.292908	2.508672	.000000			
H 10	4.884885	4.305429	2.508834	.000000		
H 11	4.110897	4.884885	4.292998	2.482523	.000000	
H 12	2.353801	4.217524	4.914624	4.216825	2.352604	.000000

PETERS TEST WAS SATISFIED IN FLETCHER-POWELL OPTIMISATION
SCF FIELD WAS ACHIEVED

AM1 CALCULATION

VERSION 1.00

FINAL HEAT OF FORMATION = 46.479261 KCAL

ELECTRONIC ENERGY = -3530.009564 EV

CORE-CORE REPULSION = 2601.652128 EV

IONISATION POTENTIAL = 15.620600

NO. OF FILLED LEVELS = 15

MOLECULAR WEIGHT = 80.109

04/18/90

SCF CALCULATIONS = 16

COMPUTATION TIME = 138.31 SECONDS

EIGENVECTORS

		ROOT NO.	1	2	3	4	5	6
			-46.89275	-40.05085	-37.51424	-30.64694	-29.96146	-25.61383
S	N	1	.55861	-.51656	.00122	-.31791	.00100	-.04442
PX	N	1	.06767	.01510	.20836	.11739	.38114	.32364
PY	N	1	.10644	.02227	-.13356	.18240	-.24459	.50547
PZ	N	1	.00000	.00000	.00000	.00000	.00000	.00000
S	C	2	.39114	-.05028	.45933	.31392	.28119	-.02088
PX	C	2	-.12081	.18932	.06500	.18175	-.19608	-.25799
PY	C	2	.08532	.11484	.05220	.06915	-.19184	.20030
PZ	C	2	.00000	.00000	.00000	.00000	.00000	.00000
S	C	3	.28678	.36065	.41479	.09179	-.35547	-.14456
PX	C	3	-.11088	-.05690	-.04043	-.01778	-.08183	-.19994
PY	C	3	-.01122	.11220	-.10759	-.31595	-.09880	.08250
PZ	C	3	.00000	.00000	.00000	.00000	.00000	.00000
S	C	4	.26534	.49966	-.00080	-.46521	.00049	.05817
PX	C	4	-.03462	-.04670	.16239	-.05242	-.25079	-.04357
PY	C	4	-.08528	-.07342	-.10383	-.08106	.16057	-.06806
PZ	C	4	.00000	.00000	.00000	.00000	.00000	.00000
S	C	5	.28704	.35953	-.41566	.09294	.35509	-.14459
PX	C	5	.03619	.12599	.08027	-.27929	.05614	.15880
PY	C	5	-.10552	-.00432	.08159	-.14822	.11589	-.14710
PZ	C	5	.00000	.00000	.00000	.00000	.00000	.00000
S	C	6	.39202	-.05228	-.45851	.31308	-.28177	-.02098
PX	C	6	.12814	.02492	-.02002	-.01299	.09245	.29060
PY	C	6	-.07430	.22027	-.08172	.19494	.25765	-.15047
PZ	C	6	.00000	.00000	.00000	.00000	.00000	.00000
S	H	7	.09501	-.02563	.16349	.13397	.15634	-.17382
S	H	8	.06695	.10924	.14448	.03964	-.17774	-.17777
S	H	9	.06183	.15327	-.00027	-.23195	.00022	-.02091
S	H	10	.06701	.10887	-.14478	.04019	.17751	-.17787
S	H	11	.09528	-.02632	-.16324	.13347	-.15673	-.17428
S	H	12	.14319	-.17916	.00051	-.20899	.00071	-.39182
		ROOT NO.	7	8	9	10	11	12
			-22.67096	-22.43541	-21.08834	-20.86305	-19.95126	-18.01656
S	N	1	-.00142	-.15399	-.11469	.00000	-.00008	-.01929
PX	N	1	-.36547	.09922	-.16064	.00000	-.09619	.08137
PY	N	1	.23581	.14839	-.25053	.00000	.06084	.12878
PZ	N	1	.00000	.00000	.00000	.69479	.00000	.00000
S	C	2	.10587	.22600	.08115	.00000	-.03901	-.02968
PX	C	2	.37257	.01746	.13011	.00000	.12832	-.12072
PY	C	2	.08803	-.30884	-.04484	.00000	-.41632	-.32074
PZ	C	2	.00000	.00000	.00000	.42065	.00000	.00000
S	C	3	-.08302	-.20880	-.12155	.00000	-.02938	.05728
PX	C	3	-.07844	.02729	-.42412	.00000	.38234	.14002
PY	C	3	-.37468	.04891	.06197	.00000	.06349	.29348
PZ	C	3	.00000	.00000	.00000	.24806	.00000	.00000
S	C	4	.00211	.25093	.11026	.00000	.00007	-.03061
PX	C	4	-.33507	.20638	-.18069	.00000	-.04071	-.25771
PY	C	4	.21817	.31616	-.28209	.00000	.02532	-.40627
PZ	C	4	.00000	.00000	.00000	.19788	.00000	.00000
S	C	5	.07974	-.20999	-.12159	.00000	.02933	.05761
PX	C	5	.30778	.02765	.23407	.00000	.10312	.20426
PY	C	5	.22947	.04138	-.35818	.00000	-.37436	.25167
PZ	C	5	.00000	.00000	.00000	.24844	.00000	.00000
S	C	6	-.10226	.22738	.08107	.00000	.03899	-.03034
PX	C	6	.07097	-.28863	-.09645	.00000	.43122	-.23887
PY	C	6	-.37721	-.10687	.09896	.00000	.05822	-.24430
PZ	C	6	.00000	.00000	.00000	.42179	.00000	.00000
S	H	7	.09920	.29792	.11003	.00000	.29611	.18489

ROOT NO.		13	14	15	16	17	18
		-17.82121	-16.50138	-15.62060	-5.89239	-5.15382	-3.80863
S	N 1	.00008	.00000	.00000	.00000	.00000	.51522
PX	N 1	.21562	.00000	.00000	.00000	.00000	.02975
PY	N 1	-.13695	.00000	.00000	.00000	.00000	.04522
PZ	N 1	.00000	.48034	.00164	-.47571	-.00122	.00000
S	C 2	-.05434	.00000	.00000	.00000	.00000	-.25236
PX	C 2	-.17840	.00000	.00000	.00000	.00000	.35296
PY	C 2	.18375	.00000	.00000	.00000	.00000	-.06266
PZ	C 2	.00000	.00890	.92377	.44258	-.47524	.00000
S	C 3	.03881	.00000	.00000	.00000	.00000	.06394
PX	C 3	.31304	.00000	.00000	.00000	.00000	-.04109
PY	C 3	-.26619	.00000	.00000	.00000	.00000	-.11675
PZ	C 3	.00000	-.45063	.47469	.14651	.52358	.00000
S	C 4	-.00009	.00000	.00000	.00000	.00000	.05041
PX	C 4	-.34527	.00000	.00000	.00000	.00000	-.02244
PY	C 4	.21864	.00000	.00000	.00000	.00000	-.0352
PZ	C 4	.00000	-.60410	-.00191	-.58238	-.00082	.00000
S	C 5	-.03844	.00000	.00000	.00000	.00000	.06380
PX	C 5	.37462	.00000	.00000	.00000	.00000	-.08864
PY	C 5	-.17041	.00000	.00000	.00000	.00000	-.08608
PZ	C 5	.00000	-.44837	-.47681	.14879	-.52267	.00000
S	C 6	.05422	.00000	.00000	.00000	.00000	-.25200
PX	C 6	-.24367	.00000	.00000	.00000	.00000	-.20437
PY	C 6	.08277	.00000	.00000	.00000	.00000	.29376
PZ	C 6	.00000	.01241	-.92248	.44163	.47626	.00000
S	H 7	-.24223	.00000	.00000	.00000	.00000	.10113
S	H 8	.29264	.00000	.00000	.00000	.00000	-.10280
S	H 9	-.00165	.00000	.00000	.00000	.00000	.01346
S	H 10	-.29147	.00000	.00000	.00000	.00000	-.10255
S	H 11	.24403	.00000	.00000	.00000	.00000	.10104
S	H 12	-.00084	.00000	.00000	.00000	.00000	-.51297
ROOT NO.		19	20	21	22	23	24
		-2.87573	-1.73421	-1.58617	-1.45913	-1.27494	-.99792
S	N 1	.00000	.00017	-.00697	.00023	.07426	.03689
PX	N 1	.00000	-.37148	-.12443	-.06641	.07345	-.08195
PY	N 1	.00000	.23180	-.20631	.04460	.11682	-.12869
PZ	N 1	.24543	.00000	.00000	.00000	.00000	.00000
S	C 2	.00000	.34990	.17342	-.21083	.16852	.18767
PX	C 2	.00000	-.14885	-.05554	-.24737	.30074	.08219
PY	C 2	.00000	.27489	-.32593	.14638	.18201	-.03929
PZ	C 2	-.35625	.00000	.00000	.00000	.00000	.00000
S	C 3	.00000	-.26277	-.04907	.15820	-.31100	.22229
PX	C 3	.00000	.13243	-.02278	-.23914	.23906	.09348
PY	C 3	.00000	.25516	-.22974	.09537	.06598	.34517
PZ	C 3	.46311	.00000	.00000	.00000	.00000	.00000
S	C 4	.00000	.00179	.18868	-.00184	.39584	-.24862
PX	C 4	.00000	.02865	-.10675	-.34218	-.00351	.21100
PY	C 4	.00000	-.02143	-.16016	.22141	-.00600	.32878
PZ	C 4	-.50669	.00000	.00000	.00000	.00000	.00000
S	C 5	.00000	.26320	-.06051	-.15685	-.30913	.22188
PX	C 5	.00000	-.18202	-.19539	-.18278	-.04133	.27544
PY	C 5	.00000	-.23207	-.10651	.17956	.24328	.22935
PZ	C 5	.46321	.00000	.00000	.00000	.00000	.00000
S	C 6	.00000	-.34478	.18842	.20842	.16643	.18781
PX	C 6	.00000	-.32073	-.26608	-.23247	.03724	-.06885
PY	C 6	.00000	.01192	-.18408	.16666	.34894	.05823
PZ	C 6	-.35649	.00000	.00000	.00000	.00000	.00000

ROOT NO.	25	26	27	28	29	30
	-.49240	-.23865	-.00394	.10997	.19980	.44910
S N 1	-.00026	-.05399	-.06220	-.00006	-.00032	-.03816
PX N 1	.16853	.22362	-.09369	.10574	.38808	-.19118
PY N 1	-.10691	.34905	-.14528	-.06799	-.24877	-.30148
PZ N 1	.00000	.00000	.00000	.00000	.00000	.00000
S C 2	-.14112	-.10034	-.10210	.07413	-.06971	.07879
PX C 2	.02712	.03440	-.25240	.16688	.39851	-.16701
PY C 2	.33377	-.19350	-.00123	.07779	.16559	.23636
PZ C 2	.00000	.00000	.00000	.00000	.00000	.00000
S C 3	-.09053	.18680	.09064	.20552	-.21849	-.03234
PX C 3	.30165	.21405	-.03088	.22449	-.15903	.35919
PY C 3	-.14816	-.20039	-.23915	.35674	.19387	-.05847
PZ C 3	.00000	.00000	.00000	.00000	.00000	.00000
S C 4	-.00019	.11019	.33135	-.00002	.00010	.07409
PX C 4	.29407	-.05905	.21653	-.42532	-.01901	-.18352
PY C 4	-.18842	-.09059	.33808	.27231	.01453	-.28647
PZ C 4	.00000	.00000	.00000	.00000	.00000	.00000
S C 5	.09109	.18723	.08959	-.20590	.21885	-.03140
PX C 5	.26064	-.27370	-.20290	-.22944	-.24136	-.20484
PY C 5	-.21165	.11035	-.12845	-.35371	.06062	.30179
PZ C 5	.00000	.00000	.00000	.00000	.00000	.00000
S C 6	.14086	-.10120	-.10177	-.07382	.06984	.07962
PX C 6	-.29233	-.18990	.10456	-.00076	.01537	.28474
PY C 6	-.16455	-.05083	-.22818	-.18413	-.43232	-.05529
PZ C 6	.00000	.00000	.00000	.00000	.00000	.00000
S H 7	.33457	-.08782	.14166	-.04555	.02453	.14600
S H 8	-.23237	-.36750	-.05703	-.32071	.30283	-.26056
S H 9	.00035	.01433	-.59415	-.00008	-.00171	.21270
S H 10	.23162	-.36880	-.05551	.32152	-.30074	-.26181
S H 11	-.33468	-.08704	.14135	.04536	-.02530	.14560
S H 12	.00088	.41717	-.12779	-.00023	-.00024	-.27882

NET ATOMIC CHARGES AND DIPOLE CONTRIBUTIONS

ATOM NO.	TYPE	CHARGE	ATOM ELECTRON DENSITY
1	N	-.0678	5.0678
2	C	-.0035	4.0035
3	C	-.1278	4.1278
4	C	.0101	3.9899
5	C	-.1281	4.1281
6	C	-.0029	4.0029
7	H	.1995	.8005
8	H	.2054	.7946
9	H	.1938	.8062
10	H	.2053	.7947
11	H	.1993	.8007
12	H	.3168	.6832

CARTESIAN COORDINATES

NO.	ATOM	X	Y	Z
1	N	.0000	.0000	.0000
2	C	1.3550	.0000	.0000
3	C	2.1468	1.1278	.0000
4	C	1.5223	2.3775	.0000
5	C	.1260	2.4209	.0000
6	C	-.5663	1.2294	.0000
7	H	1.8044	-.9953	.0000
8	H	3.2233	1.0418	.0000
9	H	2.1045	3.2871	.0000
10	H	-.4032	3.3624	.0000
11	H	-1.6583	1.2205	.0000
12	H	-.5451	-.8521	.0000